

Long-Duration Energy
Storage in Reliable Wind
and Solar Electricity
Systems

Thesis by
Jacqueline A. Dowling

In Partial Fulfillment of the Requirements for
the Degree of
Doctor of Philosophy

The logo for the California Institute of Technology (Caltech), featuring the word "Caltech" in a bold, orange, sans-serif font.

CALIFORNIA INSTITUTE OF TECHNOLOGY
Pasadena, California

2023
Defended May 16, 2023

© 2023

Jacqueline A. Dowling

ORCID: 0000-0001-5642-8960

ACKNOWLEDGEMENTS

Success doesn't happen in a vacuum. I knew I wanted to help pave a path toward clean energy. I'm proud to say that work accomplished as part of this thesis has informed national, state, and city-level decarbonization plans by dissemination through various political networks: America's Zero Carbon Action Plan, U.S. Climate Alliance, Renewable Gas 360, California Council on Science and Technology, California Hydrogen Business Council, and Pasadena League of Women Voters. In discussions with stakeholders and decision-makers, I highlighted the benefits of national-scale seasonal energy storage as a renewable reserve for blackout prevention. I want to thank the village that made it possible.

I would like to thank my advisor Nate Lewis for giving me the opportunity to be part of the clean energy transition. Although there is always much more work to be done, the satisfaction of knowing I contributed will stay with me my whole life. Nate has infinite patience for the truth and embraces fun. A renaissance man himself, he provided expansive resources that allowed me to pursue a unique type of doctorate degree combining techno-economic and materials research which gave me a deep sense of purpose. I value being able to say that I've both "talked the talk" and "walked the walk" in energy systems and technology development, just as Nate has. When some advisors would give high profile talks themselves, Nate puts his students first and gave my groupmate Kat Rinaldi and I opportunities to talk to online audiences of 400+ members as well as gas company executive boards about fuel switching to hydrogen. I thank Nate for the lifelong friends I've made in the Lewis Group, they were a joy to work with and they made science worth doing. I will cherish all the friends I made at Caltech and the experiences I had exploring the beautiful state of California for life.

Ken Caldeira is an unofficial co-advisor on this thesis and has mentored me through close collaboration with the Lewis Group throughout my PhD. I was a first-year graduate student with no background in energy systems when I spent summer 2018 at Carnegie Science in Stanford, but nonetheless we talked about science and world-changing philosophies as if I had the same expansive background as him. Ken celebrated my ideas and was key in helping me grow confidence. I've always been driven by problems and applications, and not tools.

Ken shares this ethos, and he taught me that science is a playground, to follow my curiosity, and not be afraid of new skills. I'll always be grateful that Ken helped me find my dream vocation (however expansive, twisting, and turning it might be) and for giving me the means to succeed and make an impact. Steve Davis at UC Irvine has been a key collaborator throughout my PhD and a model for identifying high-impact questions and whipping a draft up into something salient and beautiful. Thank you, Steve, for all your interactions with CLab and the Lewis Group, for making us excited about what we do, and for encouraging everyone around you to shoot for the moon. I look forward to post-doctoral research co-advised by Steve and Ken with infinite interesting conversations.

I would like to thank world-renowned Harry Gray for chairing my thesis committee. During my candidacy exam, he said that one of my chemistry ideas was a “slam dunk” and those words of encouragement buoyed me for years. He supported me after my propositions exam and encouraged me to follow my dreams. To so many of us, the joy, charisma, and generosity that Harry brings to science represents the best of academia and I am a proud member of the Harry Gray Nation. To my committee member Julie Kornfield, it was a joy to develop new sustainable chemical engineering curriculum with you. By the end of my PhD, our pizza seminar evolved into a full 9-unit course. Julie taught me that if you care enough to learn new things, you can teach anything. I have been so grateful to my committee member Melany Hunt for supporting my peers and I in our quest to pursue joint chemistry and macro-energy systems degrees. I had the opportunity to act in an NSF-funded short film spearheaded by Melany on women in science and engineering. I'm grateful for this empowering experience and the supportive community Melany fosters at Caltech.

I want to thank my Iowa City West High school teacher Ms. Wikner (AP Chemistry) for teaching me to reject the notion of fixed intelligence and embrace a growth mindset, this lesson has stayed with me for over a decade. Atmospheric chemists including Maggie Tolbert, Vicki Grassian, Kim Prather, Deborah Gross, Brian Toon, and Paul Wennberg opened key doors for me in research, teaching, and graduate school. I worked in a chemistry lab for the first time in high school in my Aunt Maggie Tolbert's lab. I co-authored my first

publication with Vicki Grassian and Kim Prather as an undergraduate researcher. My first teaching assistant experience was in Deborah Gross's class as a freshman at Carleton College. My Uncle Brian Toon helped me work on a climate model at NCAR before I had coding experience. Paul Wennberg admitted me to Caltech even though I hadn't decided on a research field. All these atmospheric chemists took a chance on me before I had proven myself, and in giving me opportunities I rose to the challenge. In their honor, I will continue to open doors for others. I started Energy Club at Carleton College with Arjendu Pattanayak who led a pivotal off-campus trip to India where we studied interdisciplinary aspects of energy. Steven Drew supervised my senior thesis on Bruce Parkinson's research and exposed me to electrochemistry. Thank you to Maggie Tolbert, Bert Tolbert, Anne Tolbert, Cody Finke, and Owen Freed for encouraging and inspiring me to choose Caltech for graduate school.

I joined the Lewis Group at Caltech and entered a world of phenomenal co-workers and friends. I am proud of everything the alumni macro-energy modeling team, Kat Rinaldi and Kathleen Kennedy, accomplished and I know the future is bright with the current team, Natasha Reich and Dominic Covelli, tackling timely and powerful projects that I'm proud to be a part of. Kat and Natasha especially, you have helped me move mountains and science is so fun with you. You both have an incredible knack for storytelling, Barnard must be a special place. Thank you, Katie Hamann and Azhar Carim, for your moral support through all the hard times, editorial feedback, and celebration during all the great times, you improved both my writing and quality of life significantly. My Lewis Group cohort (JaMMZ) is the best: Zach Ifkovits, Madeline Meier, and Mo Morla. Thank you to Zach for making the chemistry project possible with countless experiments, and for bringing our workspaces to life with fidget toys in the office and music in lab. Thank you to Jake Evans, Alex Ye, and Sean Byrne for all the help in lab, for being true team players, and for the great meals and conversations we've shared. Thank you to my undergraduate mentees Anna Li and Maddie Swint for shaping my time at Caltech and for your dedication to pushing our projects forward. I'm so proud of you both and excited to see what you will do next in the clean-tech world and in graduate school. Anna, I'm in awe of your tenacity and self-reliance. Maddie, you

made work in the chemistry lab an absolute joy. Thank you to the Lewis Group as a whole and the alumni I overlapped with, I learned something from each of you and had a blast playing baseball and dancing at group retreat with you: Paul Kempler, Matthias Richter, Ivan Moreno Hernandez, Pai Buabthong, Weilai Yu, Harold Fu, Michael Mazza, Katie Chen, Kyra Lee, Jingjing Jiang, Xinghao Zhou, Dan Torelli, Michael Lichterman, Stefan Omelchenko, Sisir Yalamanchili, Annelise Thompson, Paul Nuñez, Ellen Yan, Ethan Simonoff, Carlos Read, Miguel Cabán-Acevedo, Birch Simpson, and Renata Balgley. I want to thank Paul Kempler and Kat Rinaldi for inspiring me in science and life and for singing to me in the backyard at my birthday and wedding—the best gift.

Thank you to all the members of the CLab group at Carnegie in Stanford I overlapped with during my PhD: Tyler Ruggles, Edgar Virgüez, Lei Duan, Enrico Antonini, Michael Dioha, Candise Henry, Rebecca Peer, David Farnham, Mengao Yuan, and Fan Tong. I want to thank my invaluable co-author Tyler Ruggles for tirelessly answering all my questions with a smile, for his endurance in getting projects to the finish line, and for welcoming me to Providence, RI as his neighbor. Thank you to inspirational faculty in macro-energy modeling I've met at conferences including Destenie Nock, Michael Craig, and Jesse Jenkins for their interactions that buoyed me. I look forward to collaborating with the new CLab members: Lyssa Freese, Alicia Wongel, Tresa Thomas, and Angelo Carlino.

I want to thank Caltech housing for all the celebrations we hosted in our backyard. Thank you to my housemates: Katie Hamann, Emma Sosa, Tina Seeger, Madison Douglas, and Eric Ewing for all the couch conversations, infinite compassion, and fun. Thank you to Mike O'Connell, Alex Welch, Jamie Goldfield, Madison Douglas, Cullen Quine, Anna Scott, and Eric Ewing for skiing at Mammoth with me for six incredible years. Thank you, Mike, for being my workout buddy at the gym and Caltech Alpine Club co-president. Thank you to all the past and future Caltech Alpine Club leaders (especially Cody Finke, Elle Chimiak, Emily de Jong, and Noel Csomay-Shanklin) for establishing and maintaining a thousand-person club that is a steadfast fountain of youth in the community. Thank you to David Millard and Azhar Carim for the countless airport rides, meals, and conversations; they made a huge

difference in getting me through this year bouncing between Providence and Pasadena. Thank you, Eva Scheller and Vishnu Sridhar, for relieving my LA homesickness out east and reminding me that Caltech friends are lifelong friends wherever we are in the world. Thank you to all my Caltech friends from the original Geology and Planetary Science (GPS) cohort, Alpine Club, and the Lewis Group for making my twenties amazing! Thank you to my childhood swimming friends, high school friends, Carleton friends, LA-to-Boston friends, and Providence friends for always welcoming me back for a fun time no matter how long I had been gone, especially Annie Foxen, Brittany Todd, Zoie Jordan, Danae Bowen, Mikako Harata, Lexie Finer, Newton Nguyen, Marty Schwarz, Freya Morris, Lily Xu, Jordan Mann, Jeanie Noto, Sam Butler, Arjun Prakash, and Ben Spiegel. To my French sister: Adélie Guerin and her parents Jean-Baptiste and Clémence Guerin, thank you for making my childhood summers amazing, teaching me the meaning of loyalty, and accepting me into your family since I was 15 years old—I cherish every adventure with you!

I want to thank my best friend and husband Eric Ewing, and Katie Hamann, my Caltech roommate and Lewis-groupmate of 5 years, for being the shadow co-authors of this thesis, and for being the real reason it got finished. Although there is always more to learn, Katie taught me to write, and Eric taught me to code. Thank you both for processing and working through the first draft of my brain before my thoughts go out into the real world. Katie, you defined my Caltech experience, and I wouldn't trade laughing with you for anything. Eric's hugs fueled this thesis. Thank you for moving to LA for me and staying in LA for me when your advisor moved. Thank you for your unconditional love for me, deeply compassionate realism toward everyone, and our giggles and adventures. Thank you to our sheltie dog Millie for waking me up in the morning, taking me on walks, and helping me write. Eric, I could not have finished this thesis without you. I'm so happy you're my life partner, I want to be with you everywhere!

Thank you to everyone in my family, Mom, Dad, Ed, Ev, my grandparents, and my aunts and uncles for inspiring me, believing in me, and being proud of me. Thank you, Mom and Dad, for giving me the most beautiful childhood, taking me on runs, to alpine lakes, and

talking to me about everything happening in the world at the dinner table. Dad (David Dowling), thank you for exemplifying self-respect by teaching me to nurture my brain, body, and heart; you always know what to say to keep me going, whether it be climbing a hill or pursuing a project or friendship. Mom (Caroline Tolbert), thank you for exemplifying self-confidence, teaching me the value of time with family in nature, and to be brave enough to make changes to improve my life. Thank you, Ev and Ed (Eveline and Edward Dowling), for being my best friends and goofy buddies for life. I cherish my siblings infinitely, and I'm excited for a million more trips together with our partners. Ed, thank you for exemplifying authenticity and thoughtfulness and for understanding me on a deep level and challenging me to grow and find myself. Ev, thank you for teaching me the meaning of self-love and for moving to Carleton and California with me, you are my sunshine soul sister. My Grandpa Oak (G.O.) Dowling is the origin of the exuberant and charismatic intellectual in our family that can light up a room and build a community—these features have been passed down with pride to the grandchildren. Grammy (Mary Dowling) and Aunt Julie Dowling, you taught me how sacred life and laughter is; thank you for encouraging me to be colorful and to never stop moving, learning, and feeding the soul. My aunts and uncles are all role models, and I love my cousins and all our family dogs so much. Sarah Tolbert and Ben Schwartz are amazing singers and give excellent career advice. Lizzie Tolbert is our backcountry ski partner and inspired me to climb the tallest mountains. Brian Toon and Maggie Tolbert have been a lifelong inspiration, they hold everyone together in Boulder, find hidden spots while traveling, and maintain the raspberry patch and mulberry tree. I want to thank the entire Ewing Family including Ray and Penelope for their love and support of me and Eric. Thank you, Greg and Sarah, for taking us skiing, hiking, canoeing, on dog walks, and giving us peace in New Hampshire. Steve, Rachel, and Baby Brie your family and home is an inspirational love nest.

Grandma Anne (Tolbert), you have the resilience of a Bristlecone pine tree, and I am proud to have inherited your name. Your infinite love and listening helped me complete this thesis. Thank you for helping everyone achieve their dreams and for making the American Dream happen for our family starting with Great Grandma Yetta Zweifler. I want to thank my

Grandpa Bert Tolbert—an apple picking chemist who grew up on a farm in Idaho, raised four daughters who became nature-loving professors, and greeted everyone he met on the trail in Colorado, California, and Switzerland. When I was a young girl, he removed bee stingers from my foot with pocket-watch tweezers and told me to choose a line of work that would matter in the world. At age 98, he gave me an article clipping from Chemical & Engineering News on hydrogen storage and told me I was doing good work. He skied in Aspen at age 90 with the “over the hill gang” and we celebrated his 100th birthday with an accordion block party among friends and loved ones. He knew how to make every day a good day, and cherish his family, friends, and nature. My thesis is dedicated to Grandpa Bert for inspiring my life dream and to Eric Ewing for living it with me.

Jacqueline A. Dowling

May 2023

Pasadena, CA

ABSTRACT

Several U.S. states mandate zero-carbon electricity systems based primarily on renewable technologies, such as wind and solar. Reliable and affordable electricity systems based on these variable resources may depend on the ability to store large quantities of low-cost energy over long timescales. Long-duration energy storage technologies (10 to 100s of hours) have much cheaper energy storage capital costs than lithium-ion batteries. Multi-decadal weather datasets reveal unique long-duration energy storage roles, such as seasonal and multi-year storage, that increase the affordability of electricity from variable renewable energy, informing technology investments and policy. This thesis combines techno-economic analysis with materials chemistry to advance long-duration energy storage in reliable wind and solar electricity systems. Given short-, mid-, and long-duration energy storage options in wind- and solar-based systems, the addition of long-duration energy storage (such as provided by underground hydrogen storage) reduced total system costs most compared to systems without storage. We analyzed the tradeoff between capital cost reductions and efficiency improvements of hydrogen conversion and storage in different electricity systems with varying levels of dispatchable fossil power and otherwise-curtailed wind and solar generation. In the systems featuring abundant zero-cost electricity (resulting from wind and solar generation exceeding mean demand), hydrogen storage systems were not highly sensitive to an efficient utilization of otherwise-curtailed power, but they were sensitive to capital cost reductions. Electrolyzers paired with seasonal or multi-year hydrogen storage in reliable wind and solar systems may operate infrequently and benefit from times of abundant, otherwise-curtailed, zero-cost electricity to drive electrolysis. The low abundance and price volatility of iridium represents a bottleneck for the scale-up of proton exchange membrane electrolyzers. We synthesized earth-abundant manganese antimony oxide catalysts via a new chemical vapor deposition route and assessed their long-term electrochemical durability. Earth-abundant oxygen evolution electrocatalysts may be suitable replacements for iridium, despite lower activity, in electrolyzers paired with hydrogen energy storage in reliable wind and solar systems.

PUBLISHED CONTENT AND CONTRIBUTIONS

Portions of this thesis have been drawn from the following publications:

Dowling, J. A.; Lewis, N. S. Long-Duration Energy Storage for Reliable Renewable Electricity: The Realistic Possibilities. *Bulletin of the Atomic Scientists* **2021**, 77 (6), 281–284. DOI: 10.1080/00963402.2021.1989191

J.A.D. prepared the manuscript.

Dowling, J. A.; Rinaldi, K. Z.; Ruggles, T. H.; Davis, S. J.; Yuan, M.; Tong, F.; Lewis, N. S.; Caldeira, K. Role of Long-Duration Energy Storage in Variable Renewable Electricity Systems. *Joule* **2020**, 4 (9), 1907–1928. DOI: 10.1016/j.joule.2020.07.007.

J.A.D. designed the experiments, analyzed the data, and prepared the manuscript.

Li, A. X.*; Dowling, J. A.*; Virguez, E.; Ruggles, T. H.; Caldeira, K.; Lewis, N. S. Relative Value of Short-, Mid-, and Long-Duration Storage Technologies in Reliable Wind and Solar Electricity Systems. *In Preparation*.

J.A.D. assisted in designing the experiments, analyzing the data, and preparing the manuscript. (**equal author contributions*)

Dowling, J. A.; Ruggles, T. H.; Reich, N. D.; Virguez, E. A.; Davis, S. J.; Li, A. X.; Rinaldi, K. Z.; Ifkovits, Z. P.; Kennedy, K. M.; Duan, L.; Caldeira, K.; Lewis, N. S. Techno-economic analysis of hydrogen storage in wind and solar electricity systems. *In Preparation*.

J.A.D. designed the experiments, analyzed the data, and prepared the manuscript.

Dowling, J. A.*; Ifkovits, Z. P.*; Carim, A. I.; Evans, J. M.; Swint, M. C.; Ye, A. Z.; Richter, M. H.; Li, A. X.; Lewis, N. S. Long-term durability of chemical vapor deposited $Mn_ySb_{1-y}O_x$ electrocatalysts for water oxidation in acidic media. *In Preparation*.

J.A.D. designed and helped perform the experiments, analyzed the data, and prepared the manuscript. (**equal author contributions*)

TABLE OF CONTENTS

Acknowledgments.....	iii
Abstract.....	x
Published Content and Contributions	xi
Table of Contents	xii
List of Figures	xiii
Chapter 1: Introduction and Background.....	1
1.1 Long-duration energy storage for reliable renewable electricity	1
1.2 Scope of This Thesis	7
Chapter 2: Role of long-duration energy storage in variable renewable electricity systems.....	9
2.1 Summary	9
2.2 Introduction	9
2.3 Results	16
2.4 Discussion	26
2.5 Conclusions	32
2.6 Methods.....	33
Chapter 3: Relative value of short-, mid-, and long-duration storage technologies in reliable wind and solar electricity systems	37
3.1 Introduction.....	37
3.2 Results.....	40
3.3 Discussion	45
3.4 Conclusions	50
3.5 Methods.....	51
Chapter 4: Techno-economic analysis of hydrogen storage cost and efficiency in deeply decarbonized wind and solar electricity systems ...	54
4.1 Summary	54
4.2 Introduction.....	55
4.3 Results.....	57

4.4 Discussion	65
4.5 Conclusions	68
4.6 Methods	69
Chapter 5: Long-term durability of chemical vapor deposited $Mn_ySb_{1-y}O_x$ electrocatalysts for water oxidation in acidic media	72
5.1 Summary	72
5.1 Introduction	72
5.1 Results and Discussion	74
5.2 Conclusions	82
5.3 Methods	83
Chapter 6: Supporting Information	88
6.1 Macro-Scale Electricity Model	89
6.2 Supporting Information for Chapter 2	91
6.3 Supporting Information for Chapter 3	115
6.4 Supporting Information for Chapter 4	125
6.5 Supporting Information for Chapter 5	129
Bibliography	135

LIST OF FIGURES

- **Figure 2.1** Long- and short-duration energy storage technology capital costs by capacities.
- **Figure 2.2** Base case dispatch schedule.
- **Figure 2.3** Energy storage during 1 year (2018) in the base case.
- **Figure 2.4** Effect of simulation length on energy in long-duration storage.
- **Figure 2.5** Distribution of results for various simulation lengths.
- **Figure 2.6** System costs with different technology combinations.
- **Figure 2.7** Sensitivity of system cost to LDS and battery costs.
- **Figure 3.1** Energy-capacity costs and power-capacity costs of energy storage technologies.
- **Figure 3.2** Electricity sources, sinks, and storage technologies within the macroscale energy model.
- **Figure 3.3** Different energy storage technologies have varying techno-economic characteristics.
- **Figure 3.4** System costs for combinations of short-, mid-, and long-duration storage.
- **Figure 3.5** Energy in storage over one year for individuals or combinations of storage technologies.
- **Figure 3.6** System cost reductions and storage technologies present in scenarios with up to three storage options available: short-duration storage (Li-ion), long duration storage (hydrogen), and a hypothetical *Storage X* technology with varying energy- and power-capacity costs.
- **Figure 4.1** Despite low round-trip efficiency, hydrogen storage systems were valuable in wind and solar electricity systems.
- **Figure 4.2** System costs were increasingly sensitive to efficiency improvements in hydrogen storage systems as their capital costs decreased.
- **Figure 4.3** Value of innovation in base case hydrogen energy storage and conversion.
- **Figure 4.4** Trade-off between improvements in efficiency and capital cost of Power-to-H₂ technologies hydrogen storage technologies and H₂-to-Power technologies.
- **Figure 4.5** System costs of various technology options for hydrogen energy storage and conversion.
- **Figure 4.6** Parametrized natural gas restrictions show the value of various Power-H₂-Power technologies in deeply decarbonized wind- and solar-dominated systems.
- **Figure 4.7** Modeled restrictions on underground capacity and deliverability based on historic natural gas usage.

- **Scheme 5.1** $\text{Mn}_{0.63}\text{Sb}_{0.37}\text{O}_x$ synthesis process via chemical vapor deposition and annealing.
- **Figure 5.1** Growth rates of MnO_x and SbO_x via CVD and ALD respectively derived from ellipsometry analysis.
- **Figure 5.2** Electrochemical activity, stability, and faradaic efficiency of $\text{Mn}_{0.63}\text{Sb}_{0.37}\text{O}_x$ during OER at $J = 10 \text{ mA cm}^{-2}$ for 7 days in 1 M H_2SO_4 acid.
- **Figure 5.3** Catalyst composition as determined by both EDX and ICP-MS techniques. Representative SEMs of $\text{Mn}_{0.63}\text{Sb}_{0.37}\text{O}_x$ before and after OER at $J = 10 \text{ mA cm}^{-2}$ for 168 h in 1 M H_2SO_4 .
- **Figure 5.4** XP spectra of $\text{Mn}_{0.63}\text{Sb}_{0.37}\text{O}_x$ before and after OER at $J = 10 \text{ mA cm}^{-2}$ for 168 h in 1 M H_2SO_4 .
- **Figure 5.5** Electrochemical activity and stability of $\text{Mn}_{0.63}\text{Sb}_{0.37}\text{O}_x$ during OER at $J = 100 \text{ mA cm}^{-2}$ for 9 h in 1 M H_2SO_4 acid.

Chapter 1

INTRODUCTION AND BACKGROUND

Adapted from: Dowling, J. A.; Lewis, N. S. Long-Duration Energy Storage for Reliable Renewable Electricity: The Realistic Possibilities. *Bulletin of the Atomic Scientists* **2021**, 77 (6), 281–284. DOI: 10.1080/00963402.2021.1989191

1.1 Long-Duration Energy Storage for Reliable Renewable Electricity

Because a very cold polar vortex swept through much of Texas in February of 2021, everything from dispatchable natural gas facilities to intermittent wind turbines froze.¹ The power outage produced food, water, and heat shortages that either directly or indirectly led to hundreds of deaths. During the same polar vortex, natural gas plants and wind farms in Minnesota—much farther north and much colder than Texas—continued to operate. Texas electricity operators had bet on warm weather and didn't spend the extra money to winterize equipment. Nature warned them—and us—how damaging electricity blackouts can be.

In a world of increasing climate variability, it pays to spend money on reliability. In electricity systems dominated by wind and solar generation, long-duration storage is a way to obtain it. In this new climatic world, the reliability of variable renewable energy sources—primarily wind and solar—will require consideration of extremes over decades. Without planning, *Dunkleflaute*—the German word for dark, windless times when wind and solar power are unavailable—could well undermine electricity systems of the future.

Several American states have adopted 100 percent clean electricity mandates with mid-century deadlines, requiring large amounts of wind and solar power to be deployed. Wind and solar energy can provide large amounts of cheap carbon-free electricity to many areas, but only on Mother Nature's terms. Wind and solar power can experience multi-day

resource “droughts” when the available electricity is far lower than expected.² In the United States, wind power is especially susceptible to a seasonal low during the summer doldrums. Long-duration storage may fill in for the variability of wind and solar resources and help meet demand during unexpected Dunkleflautes and expected seasonal lows.

Even with this inherent variability, about 80 percent of US decarbonization could likely be obtained with wind and solar power alone. But getting that last 20 percent or so of reliable electricity supply requires some form of technology that can provide multiple days or weeks of electricity at a time.³ American states that have access to geothermal, hydroelectric, or nuclear power could potentially use them as clean and reliable resources. For other parts of the United States, long-duration energy storage—in the form of stored hydrogen, pumped hydropower, compressed air, and other technologies—could be key to unlocking affordable and reliable clean electricity.

Needed: more than one type of storage

How long is long-duration energy storage? An energy storage technology’s duration is its energy capacity (in kilowatt hours) divided by its discharge power capacity (in kilowatts). The Energy Department’s Long Duration Storage Energy Earthshot aspires to cut long-duration energy storage costs by 90 percent below lithium-ion battery costs to about \$15 to \$30 per kilowatt-hour by 2030, defining “long-duration” as 10 hours or more. But multiple academic researchers find that hundreds of hours of long-duration storage are needed to ensure reliability over many years in least-cost wind-solar-battery systems.⁴⁻⁶

Energy storage technology will look entirely different, depending on scale. Battery storage is well-suited for a cell phone, whereas underground hydrogen storage in salt caverns or other geologic reservoirs may be more appropriate for an entire country for a whole summer. Think of an energy storage system as a sort of bathtub. Storage technologies can be characterized by their rate of charging (that, is, how quickly the faucet will fill the tub) and discharging (or how long it takes to drain the tub); in this metaphor, the volume of energy held in the storage reservoir is analogous to the size of the bathtub. Cell phones

have power capacities (faucet and drain rates) that are high relative to their energy capacities (tub size), facilitating quick charging. The opposite is true for seasonal storage technologies that have lower power capacities (faucet and drain), but much higher energy capacities (i.e. a larger tub).

Seasonal energy storage for a country's electricity grid can be charged up slowly over the off season but will need to store large amounts of energy. There is likely a need for at least two storage technologies, one for power and one for energy. The hybrid Prius automobile can serve as a familiar analogy. A hybrid car uses a battery to run an electric motor and a gasoline engine to provide energy when the battery runs low. Similarly, inter-storage transfer allows the electricity system to take advantage of the strongest characteristics of each storage type. Lithium-ion batteries can charge quickly to capture sharp peaks in wind and solar generation and then transfer energy to a large energy reservoir for long-term storage.

Storage technologies are defined by a variety of characteristics, including charge and discharge cost, charge and discharge efficiency, leakage rate, lifetime, and energy cost. But the most important parameter for competitive seasonal energy storage is the capital costs of energy capacity. Long-duration energy storage requires capital costs as low as \$50 per kilowatt-hour before utilities will begin to use it. And capital costs for long-duration energy storage may need to fall as low as \$10 or even \$1 per kilowatt-hour before a storage method becomes the dominant technology used in reliable, multi-year wind and solar electricity systems.⁶⁻⁸

If the capital cost of storage is \$200 per kilowatt-hour (about the cost of lithium-ion batteries) and the storage system lasts 10 years, spreading the cost over those years and allowing for one cycle (that is, one filling and emptying of the "tub") per year would require the owner of the system recover about \$20 per kilowatt-hour for electricity sold per annual cycle to break even. Thus, a customer would need to pay upwards of \$20 per kilowatt-hour when storage is powering the grid. This is an extremely high cost compared to the \$0.05-

0.20 per kilowatt-hour rates seen on utility bills in the US. Storage capital costs need to be very cheap if cycled infrequently. Lithium-ion batteries would need to come down about two orders of magnitude to be cost-effective for seasonal storage. In contrast, some long-duration energy storage technologies, such as hydrogen, have very low energy capacity costs.

Our research shows that using excess solar and wind electricity to produce hydrogen, and then storing that hydrogen in geologic repositories, would be valuable not just for seasonal but also for multi-year storage.⁴ In the past, grid operators could ensure reliability by simply dispatching more natural gas-fired electricity when demand increased. With variable renewables in the mix, grid operators will have to plan years in advance for unexpected lows in electricity generation to ensure reliability. We found that dependence on long-duration energy storage increases when reliable systems plan for more years.

What are the realistic options for long-duration energy storage?

Multiple proposed technologies for long-duration energy storage have achieved energy capacity costs lower than lithium-ion batteries, making them potentially competitive candidates for long-duration energy storage.

Underground hydrogen energy storage in salt caverns is the cheapest scalable energy storage available today, with capital costs of \$0.10 to \$1 per kilowatt-hour. The Utah Intermountain Power Plant is constructing the largest energy storage facility in the world in the form of a salt dome for hydrogen energy storage.⁹ Hydrogen may be piped in from Montana where renewable electricity is used to produce it via electrolysis of reclaimed water. Then, after storage in a salt dome, the hydrogen will be burned to power turbines in Utah that can provide summertime electricity to the project's largest customer: the Los Angeles Department of Water & Power (LADWP). The Advanced Clean Energy Storage Project in Utah will teach the United States a great deal about the value of long-duration storage via several technologies, including hydrogen stored in salt caverns, large flow batteries, and solid oxide fuel cells.¹⁰

Other forms of long-duration storage include pumped hydro storage and compressed air energy storage. Pumped-hydro accounts for over 90 percent of the United States' current grid energy storage, but major future cost reductions are not expected because it is a very mature technology. Pumped-hydro has capital costs from \$5 to \$100 per kilowatt-hour and is typically used for four- to 16-hour duration storage. Compressed air energy storage is another form of long-duration energy storage that relies on underground salt caverns and can be used for hundreds of hours of storage at costs from \$2 to \$50 per kilowatt-hour, although current diabatic designs are not carbon-free.

Compressed air, pumped hydro, and underground hydrogen storage technologies are geographically constrained to places with suitable geological features. The geographical constraints may be eased by cross-country electricity transmission or hydrogen pipelines. Other forms of storage are not geographically constrained and can be built anywhere. Form Energy recently announced its iron-air energy storage chemistry for approximately 100-hour duration batteries that are projected to have capital costs of around \$20 per kilowatt-hour.¹¹ Vanadium redox flow batteries have separately scalable power and energy components but cost \$300 to \$500 per kilowatt-hour and generally compete with lithium-ion batteries for short-duration storage.

Thermal energy storage—generally using molten salt as a medium—can be paired with concentrated solar power in suitable locations, typically in the desert. Although thermal energy storage is cheaper than lithium-ion batteries (\$30 to \$80 per kilowatt-hour), thermal energy storage tied to concentrated solar power still competes primarily with lithium-ion batteries for daily storage, and not with hydrogen for seasonal storage.¹² Cambridge, Mass.-based Malta Inc. uses pumped thermal energy for storage independent of generation source. Malta is currently aiming for 10- to 12- hour durations but claims it could build for durations up to 200 hours of storage.¹³ Energy Vault uses a gravitational storage idea in which robot arms stack heavy blocks in a tower to store energy and then let the blocks fall to release the energy. Energy Vault's projected energy capacity costs (approximately \$200

per kilowatt-hour) are similar to lithium-ion batteries and will possibly play a role in daily storage as opposed to providing cost-effective scalable seasonal storage.¹⁴

When will long-duration energy storage become important?

Long-duration energy storage is only needed when other sources of dispatchable electricity (like fossil fuels) are tightly constrained by policy. The state of California already requires 60 percent renewable electricity by 2030 and 100 percent clean electricity by 2045. That means the scale-up of long-duration energy storage may be necessary in California within a decade. In general, the more variable renewable energy that is installed, the larger the need for charge/discharge power capacity. As the share of renewable capacity increases and fossil emissions decrease, more energy storage capacity is needed.¹⁵

Of the long-duration technologies discussed, underground hydrogen may be best suited for seasonal energy storage. Incorporating hydrogen energy at scale may also require scaling up electrolyzers that take carbon-free electricity and produce “green” hydrogen from water. Earth-abundant catalysts could replace the scarce iridium used in commercial polymer-electrolyte-membrane (PEM) electrolyzers. Leveraging existing natural gas infrastructure may also be key for affordability of hydrogen transport and storage; repurposing depleted natural gas reservoirs for underground hydrogen energy storage and retrofitting natural gas pipes and fittings for use with hydrogen is less expensive than building new infrastructure. In addition to hydrogen, a portfolio of seasonal and long-duration energy storage technologies would facilitate an affordable transition to meet wind and solar mandates beyond 80 percent and open a path to 100 percent carbon-free electricity.¹⁵

Decarbonizing the last 20 percent of the U.S. electricity sector will likely require flexibility in generation, demand, and storage, probably in a combination of strategies.¹⁶ But nothing now available in terms of battery storage or demand shifting can compensate for seasonal variability of the wind and the sun—much less Texas-freeze style weather events and their associated blackouts. In this context, long-duration energy storage presents one way to build for reliability during the transition to clean electricity.

1.2 Scope of This Thesis

This thesis considers a holistic treatment of long-duration energy storage in wind and solar electricity systems, from both systems and materials perspectives. With a macro-scale energy model, I analyzed the roles and techno-economic innovation priorities of energy storage in deeply decarbonized electricity systems. In the laboratory, I developed earth-abundant catalytic materials with applications in electrolytic hydrogen production. My Ph.D. training in energy systems and technologies included basic science, engineering, and system-level economics.

Research in Chapters 2 and 3 used macro-scale energy models to understand the role of energy storage technologies in low-carbon electricity systems and decarbonization pathways. Chapter 2 focuses on the role of long-duration energy storage in variable renewable electricity systems. The results show that long-duration energy storage (e.g., hydrogen) can make reliable wind-solar-battery electricity systems more affordable. Long-duration storage meets demand during summertime lulls in wind power and fills in for interannual variations in wind and solar power. Chapter 3 focuses on the relative value of short-, mid-, and long-duration storage technologies in wind and solar electricity systems. Given short-, mid-, and long-duration energy storage options in wind- and solar-based systems, the addition of long-duration energy storage reduced total system costs most compared to systems without storage.

Long-duration energy storage technologies such as provided by underground hydrogen storage may improve reliability and affordability challenges of wind- and solar-based electricity systems. Research in Chapters 4 and 5 focus on innovations in hydrogen storage and conversion technology. Chapter 4 results showed that reducing current capital costs of hydrogen energy storage and conversion (such as fuel cell costs) reduced wind- and solar-based system costs more than round-trip efficiency improvements. Current hydrogen storage and conversion costs led to wind and solar generation in excess of demand and abundant curtailment in least-cost systems. In such systems, hydrogen energy storage was not highly sensitive to efficient utilization of abundant zero-cost electricity. This implies

that use of more earth-abundant, but lower efficiency catalysts in fuel cells and electrolyzers may not substantially increase costs of reliable wind- and solar-based electricity systems. My work in energy system modeling has directly motivated my laboratory efforts to improve green hydrogen conversion technologies such as electrolyzers. A less active electrocatalyst may be an economically acceptable replacement for active precious metal catalysts if it is used infrequently and if very low-cost electricity drives water splitting. Electrolyzers for hydrogen storage in reliable wind and solar electricity systems may be used at lower capacity factors compared to hydrogen for industrial applications and may additionally benefit from abundant times of zero-cost electricity due to wind and solar curtailment. In Chapter 5, results demonstrate the long-term durability of earth-abundant electrocatalyst materials such as antimony and manganese oxides that could be further developed as potential candidates to replace rare iridium in commercial proton exchange membrane electrolyzers.

Chapter 2

ROLE OF LONG-DURATION ENERGY STORAGE IN VARIABLE RENEWABLE ELECTRICITY SYSTEMS

Dowling, J. A.; Rinaldi, K. Z.; Ruggles, T. H.; Davis, S. J.; Yuan, M.; Tong, F.; Lewis, N. S.; Caldeira, K. Role of Long-Duration Energy Storage in Variable Renewable Electricity Systems. *Joule* **2020**, 4 (9), 1907–1928. DOI: 10.1016/j.joule.2020.07.007.

2.1 Summary

Reliable and affordable electricity systems based on variable energy sources, such as wind and solar may depend on the ability to store large quantities of low-cost energy over long timescales. Here, we use 39 years of hourly U.S. weather data, and a macro-scale energy model to evaluate capacities and dispatch in least cost, 100% reliable electricity systems with wind and solar generation supported by long-duration storage (LDS; 10 h or greater) and battery storage. We find that the introduction of LDS lowers total system costs relative to wind-solar-battery systems, and that system costs are twice as sensitive to reductions in LDS costs as to reductions in battery costs. In least-cost systems, batteries are used primarily for intra-day storage and LDS is used primarily for inter-season and multi-year storage. Moreover, dependence on LDS increases when the system is optimized over more years. LDS technologies could improve the affordability of renewable electricity.

2.2 Introduction

U.S. states and territories such as California, Maine, New Mexico, Washington, Hawaii, and Puerto Rico have enacted legislation specifying that by 2040–2050 all electricity must be generated by renewable or zero-carbon sources.^{17–22} Analogous policies are being contemplated, proposed, and/or enacted in other states, countries, and regions around the world.^{23–27} An even larger group of states have some form of renewable energy requirement

in place (e.g., renewable portfolio standards that specify the capacities of wind, solar, and energy storage to be deployed; Table S2).

However, reliable electricity systems based on variable energy sources, such as wind and solar, must accommodate the variability with, for example, energy storage or “firm” generators, such as hydroelectricity, nuclear, natural gas with carbon capture and storage (CCS), geothermal, and bioenergy. Indeed, a prominent study demonstrated that the addition of low- or zero-carbon “firm” generators lowers the overall costs of electricity systems with high fractions of variable renewable energy sources.²⁸ Geothermal energy and hydropower are severely constrained due to available sites suitable for expansion.²⁹ Moreover, state laws that specify that generation must come from zero-carbon resources legally preclude use of natural gas with or without CCS for generation (Table S2). Hourly averaged wind and solar resources within the contiguous U.S. (hereinafter “the U.S.”) over the 39-year period from 1980-2018 (Figure S1) reveal gaps in the availability of these resources that often span consecutive days and in some cases weeks (especially for wind).³ The combination of these longer-duration resource gaps and high reliability standards (e.g., >99.97%)³⁰ requires systems that rely solely on wind and solar generation to overbuild generation capacity and/or deploy prodigious amounts of energy storage.^{3,29,31–34}

Batteries are increasingly the focus of large-scale energy-storage projects; they made up 88% of new additions to grid-scale storage globally in 2016.^{35,36} Batteries can be readily deployed anywhere, have high (e.g., 90%) round-trip charge- discharge efficiencies, and their costs have steadily declined.^{37,38} In general, storage can add value to variable renewable energy systems (VRE).³⁹ As storage capital costs decrease, more storage is deployed, and system costs fall. However, the economics of battery storage are strongly dependent on the use scenario.⁴⁰ As more storage gets deployed, the marginal value per kWh of storage falls.⁴¹ In contrast to hourly backfilling of power or smoothing of the daily cycle, meeting multi-day or week-long gaps between supply and demand requires even larger quantities of storage capacity with much lower utilization rates.^{3,41} The levelized cost of battery-related energy storage sufficient to fill longer-duration gaps in solar and

wind generation thus remains high. Consequently, to achieve highly reliable wind and solar-only electricity systems, substantially “overbuilding” and distributing solar and wind capacity over large areas (perhaps facilitated by high voltage direct current, HVDC, transmission), may still be less costly than the required battery storage.^{3,42}

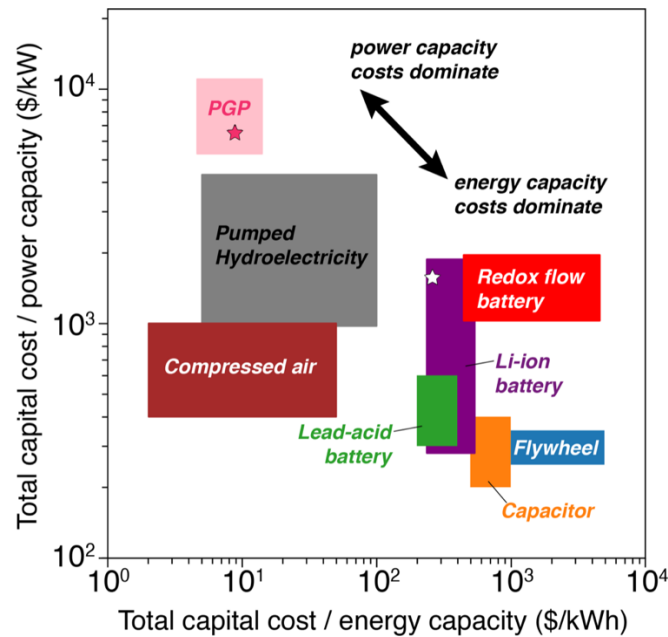


Figure 2.1 Long- and Short-Duration Energy Storage Technology Capital Costs by Capacities. Power-limited technologies are on the upper left, while energy-limited technologies are on the bottom right of the figure. The total capital cost by capacity for each storage technology is depicted with a box representing a range of values found in the literature (Tables S3 and S4). The height shows the range in capital costs divided by installed power capacities for typical systems and the width represents the range in capital costs divided by the usable energy storage capacities for typical systems. This figure does not show the impact of the different efficiencies and lifetimes for these storage options. The star in the Li-ion battery box (purple) is the base case cost for short- duration storage used in this analysis. The star in the PGP box (pink) reflects the base case cost for LDS divided by optimal power and energy capacities from the 2018 base case system. Base case cost and performance assumptions are in Table 2.1.

Here we assess the potential of long-duration energy storage (LDS) technologies to enable reliable and cost-effective VRE-dominated electricity systems.^{29,41,43} LDS technologies are characterized by high energy-to-power capacity ratios (e.g., the California Energy Commission, CEC, defines LDS as having at least 10 h of duration).⁴⁴ Unlike costs of conventional Li-ion batteries, LDS options are usually not limited by energy-capacity costs (x axis in Figure 2.1). Rather, power-capacity costs typically dominate total LDS costs (y

axis in Figure 2.1). The energy capacity times the energy-related capital costs is a small fraction of the total cost. For a variety of storage technologies, we provide the total capital cost divided by the power and again by the usable energy capacity of typical systems characterized in the literature (Figure 2.1; Table S3 includes additional performance metrics). Some technologies for long-duration applications, such as power-to-gas-to-power (PGP), pumped hydro storage (PHS), and compressed air energy storage (CAES), have additional flexibility in that the power and energy capacities for a given project can be sized independently (Table S4 provides energy and power specific capital costs). For comparison, short-duration storage technologies dominated by energy-capacity costs include flywheels, capacitors, and Li-ion and lead-acid batteries. Separating power and energy costs is more difficult for batteries. Most redox flow batteries have storage durations of 1–4 h, excluding them from the LDS category by CEC standards.⁴⁵ Redox flow batteries with 8–10 h durations exist, but are rare.⁴⁶ Other battery chemistries typically match short-term applications, but Form Energy’s pilot aqueous air battery system claims a 150 h duration at undisclosed costs.⁴⁷ All large-scale CAES designs demonstrated to date combust non-renewable natural gas,⁴⁸ and PHS is limited to certain geographical locations and has a high water footprint.⁴⁹ Technological options and viability of various LDS candidates including thermal energy storage (TES) are considered in more detail in the Discussion. Utility-scale PGP hydrogen energy-storage projects are currently expanding.^{6,50–52} For these reasons, we choose current costs for renewable PGP (with hydrogen for energy storage and fuel cells and electrolyzers for power conversion) to represent our base case for renewable LDS technology. As Li-ion batteries are commonplace, we set them as the base case short-duration storage technology (stars in Figure 2.1; Table 2.1 base case costs). By varying the costs of the base case across a wide range, we aim to characterize the broader grid role of LDS, and to determine the relationship between such costs and the systemwide value of LDS in power systems based primarily on variable renewable energy.

Many economy-wide deep decarbonization (80% carbon-emissions free) strategies do not include an LDS pathway, including the U.S. White House’s mid-century plan.^{29,53–55}

Generally, if low-cost dispatchable fossil fuels are included in the technology mix at about 20% or more of demand, LDS is minimized or not included.^{41,56-60} Although there have been some assessments of LDS in deeply decarbonized economy-wide systems, many deploy LDS within specific predetermined assumed use cases or scenarios.^{29,32,61} However, in an economy-wide deep decarbonization optimization for Europe, flexibility from LDS (PGP and TES) made a substantial contribution to the smoothing of variability from wind and solar and to the reduction of total system costs.⁶² In modeled least-cost 100% CO₂ emissions-free energy systems, fully decarbonized electricity is generally used for heating, synthesis of hydrogen and natural gas, and many other energy services, sometimes with minimal deployment of long-term energy storage.^{49,63,64}

	PGP Storage	To PGP	From PGP	Battery Storage		Wind	Solar
Assumptions from U.S. Energy Information Administration⁶⁵ unless otherwise noted.							
Technology description	Under-ground salt cavern ^a	PEM electrolysis, plus compression ^b	Molten carbonate fuel cell, CHP	Li-ion battery with coupled energy and power and a 6-hour charging time		Wind turbines, onshore	Solar PV, single axis tracking
Technology type	Storage	Conversion	Conversion	Storage	Conversion	Generation	Generation
Capacity (fixed) cost type	Energy capacity (\$/kWh)	Power capacity (\$/kW)	Power capacity (\$/kW)	Energy capacity (\$/kWh)	Power capacity (\$/kW)	Power capacity (\$/kW)	Power capacity (\$/kW)
Capacity (fixed) cost	0.16 ^{c,66}	1,058 ⁶⁷	5,854 ⁶⁸	261 ⁴⁰	1,568 ⁴⁰	1,657	2,105
Project life (years)	30 ⁶⁹	12.5 ^{67,69}	20 ⁶⁸	10 ⁷⁰	-	30	30
Discount rate	0.07	0.07	0.07	0.07	-	0.07	0.07
Capital recovery factor (%/yr)	8.06%	12.26%	9.44%	14.24%	-	8.06%	8.06%
Fixed O&M cost (\$/yr)	0	0	0	0	-	47.47	22.02
Round-trip efficiency	49% ^{d,67,68}			90% ³⁷		-	-

Loss rate	0.01 % per yr ⁷¹	-	-	1% per month ⁷²	(6 h duration) ⁴⁰	-	-
Annualized capital costs paid hourly							
Fixed cost	1.47 x 10 ⁻⁶ \$/kWh/h	0.0148 \$/kW/h	0.063 \$/kW/h	0.004 \$/kWh/h	0.021 \$/kW/h	0.022 \$/kW/h	
Variable cost	0.000 \$/kWh/h	0.000 \$/kW/h	0.000 \$/kW/h	0.000 \$/kWh/h	0.000 \$/kW/h	0.000 \$/kW/h	

Table 2.1. Base Case Costs and Assumptions. Assumptions from U.S. Energy Information Administration 96 except when otherwise noted. Annualized Capital Costs Paid Hourly. Economic and technological assumptions regarding wind, solar, LDS, and batteries used for the base case simulation. The base case LDS technology is modeled as PGP with renewable hydrogen. See model formulation in Chapter 6.1 for more detail. A) See Section S3; Table S9 for more detail on underground H₂ storage costs. B) See Section S3; Table S10 for more detail on fixed costs and lifetimes of polymer electrolyte membrane (PEM) electrolyzers and compressors. C) This cost is equivalent to \$6.3/kg H₂. The higher heating value (HHV) is 39.4 kWh/kg H₂. D) PEM electrolyzers and molten carbonate fuel cells with combined heat and power (CHP) are both modeled as 70% efficient.

State governmental agencies are specifically interested in studies focused on LDS interactions with zero-carbon and renewable electricity systems.⁴⁴ A data-driven optimization based on 5 years of European load and weather data and projected 2050 asset costs (without cost sensitivity studies) found that electricity system costs were reduced by 24% when LDS was included (as PGP with 10-fold lower power-capacity costs relative to current costs), when compared with a projected year 2050 scenario that involved only battery and PHS in conjunction with curtailed variable renewable generation.⁷³ Least-cost solutions for a modeled emissions-free, 99.9% reliable electricity system for the PJM (Pennsylvania, New Jersey, Maryland) load-balancing region, based on 4 years of load and weather data, contained substantially curtailed wind and solar generation relative to average load, and only 9–72 h of storage.⁴² Considering simplified generator profiles (without load data) and 20 years of wind and solar resource availability in four U.S. states, a study estimates with step-wise fixed capacities that meeting baseload demand (shaped as a constant flat line) 100% of the time requires storage energy-capacity costs below \$20/kWh.⁴³ A European power model based on 30 years of VRE data excluded both short- and long-term storage, but found that single-year studies can yield results that deviate by as much as 9% from the long-term average.⁷⁴ In contrast to previous studies that involve predetermined use-models or neglect cost sensitivity studies, in our work, we use real

resource and load data to assess what characteristics, in terms of power and energy costs, would be required for long-term storage technologies to make a substantive contribution to variable renewable electricity systems.

Here we comprehensively assess the roles and interactions of LDS and batteries for highly reliable wind-solar-storage electricity systems in the U.S. and several of its regional interconnects. Specifically, we use historical hourly averaged wind and solar resource data derived from a reanalysis weather dataset,⁷⁵ historical electricity demand data from all balancing authorities across the contiguous U.S.,⁷⁶ and a macro-scale energy model⁷⁷ to evaluate the relative merits and cost-effectiveness of LDS in conjunction with batteries for filling hourly, daily, weekly, seasonal, and inter-annual gaps in solar and wind generation in such systems, regions, and time periods. The large geographical areas and high temporal resolution require abstraction to make analyses tractable. Our model allows evaluation of system cost and performance, with 100% reliability as a strict constraint, over the U.S. during a multi-year time period (1980–2018), while maintaining a high temporal resolution (1 h). Insofar as comparisons can be made, our model is in qualitative agreement with more detailed multi-nodal electricity models.^{3,55,73,78–80} Hourly data were necessary and sufficient to assess compliance with existing resource adequacy planning regulations that require meeting hourly averaged demand for all but (at most) 1 h in a decade.³⁰ Inter-annual weather variability substantially impacted generation costs in a European power system.⁷⁴ The multi-decadal weather record is necessary to obtain a statistically significant description of infrequent weather-related events and inter-annual variability that affects seasonal and multi-year storage requirements and moreover facilitates assessment of system reliability over the comparable lifetimes of capital assets on an electricity grid.

We consider a limiting best case that minimizes variability of wind and solar generation by assuming lossless transmission from generation to load over all of the U.S., providing a lower bound for the minimum amount of storage required. The macro-scale electricity model thus represents an agglomerated single generation source at a given time, connected without any loss at that same time to a single agglomerated load (i.e., the load-balancing

region is the U.S.) We have also evaluated the robustness of our conclusions for smaller, regional geographic scales that confine both load balancing and resource availability to existing U.S. interconnect regions without assuming construction of new transmission. While it is important to explore a multitude of transition pathways due to various uncertainties in how these technologies will develop,²⁹ the current legal framework in a growing number of U.S. states requires the adoption of a renewables-dominated electricity system (Table S2). Therefore, we evaluate various possible end-states in a variety of asset cost scenarios that meet that requirement. Least-cost solutions were found for installed capacities and dispatch schedules (with perfect foresight and no assumed use-models) for wind and solar generation, battery storage, and LDS, subject to the constraint that hourly averaged demand must be met 100% of the time to comply with the existing regulatory framework for resource adequacy planning. A range of battery and LDS costs were considered, with cost and technical assumptions for the base case (PGP and Li-ion) presented in Table 2.1. Further details of our data sources and analytical approach are in the Methods. The base case exemplifies one LDS technology at current costs as a benchmark starting point. We then parameterize widely to determine the conditions and use cases under which long-term storage lowers system costs compared with curtailment and/or extensive deployment of short-term storage technologies.

2.3 Results

Long-Duration Storage Meets Summertime Demand and Coexists with Batteries

Figure 2.2 presents dispatch curves of the least-cost systems for 2018, assuming current costs (Table 2.1). Electricity sources in Figure 2.2 include both the generation technologies (wind and solar) and discharge of storage technologies (batteries and LDS) to the grid. Electricity sinks include both end-use demand and charging of storage technologies. Sources and sinks are balanced each hour (so that maximum positive values for any hour in Figure 2.2 mirror the most negative values in the corresponding hour). LDS (pink) and batteries (purple) are both present in the least-cost system.

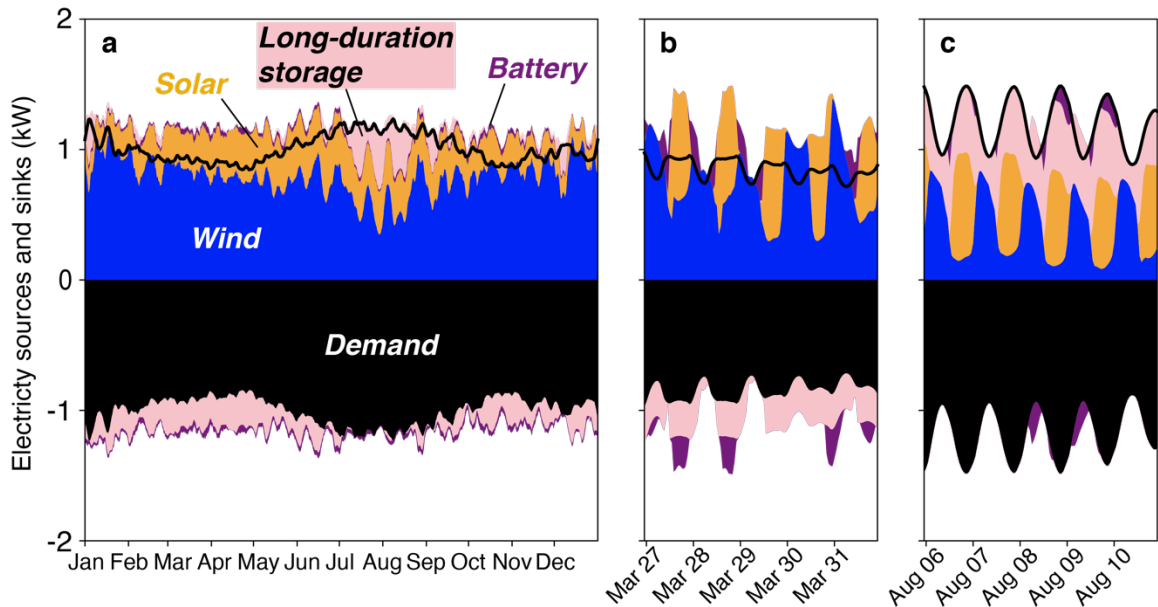


Figure 2.2. Base Case Dispatch Schedule. Electricity sources to the grid (positive values) and electricity sinks from the grid (negative values) are balanced at each hour of 2018. (A) Annual results with 5-day averaging. (B) 5-day period with maximum battery discharge (starting at 07:00 PM CST). (C) 5-day period with maximum LDS discharge (starting at 05:00 PM CST). The black area represents end-use demand (as does the black line). At each hour, generation from wind and solar plus dispatch from LDS and battery storage is balanced by end-use demand and charging of LDS and battery storage. LDS primarily provides inter-season storage whereas batteries provide intra-day storage.

The annual view of dispatch in this base case (Figure 2.2A, smoothed with a 5-day moving average) shows that when wind resources (blue) decrease during the summer months, the combined generation from wind and solar power are not sufficient to meet demand. A substantial amount of LDS (pink) is thus discharged to meet a substantial portion of demand during this low-resource period. In contrast to this large and seasonal discharge of LDS, batteries (purple) are routinely charged and discharged in small amounts throughout the year (Figure 2.2A). Curtailment is calculated in the model but not displayed in Figure 2.2. In the base case, wind and solar capacities are 2.5x and 1x average demand with average capacity factors of 0.36 and 0.27, respectively. VRE curtailment is on average 9% of VRE generation (i.e., 3% of VRE capacity).

Figures 2.2B and 2.2C show daily dispatch dynamics for the 5-day periods with the greatest battery and LDS discharge in March and August, respectively. In each case, solar peaks

correspond to noon. In this base case least-cost system, energy is sometimes transferred between batteries and LDS. Figure 2.2B shows simultaneous discharging of batteries and charging of LDS in the afternoon on March 28th and 29th, and in the morning on March 28th and April 1st. Conversely, Figure 2.2C shows simultaneous discharging of LDS and charging of batteries at night on August 8th and 9th. This phenomenon of inter-storage transfer is also observed in systems with only solar, LDS, and batteries (i.e., no wind; Figure S2), and wind, LDS, and batteries (i.e., no solar; Figure S3).

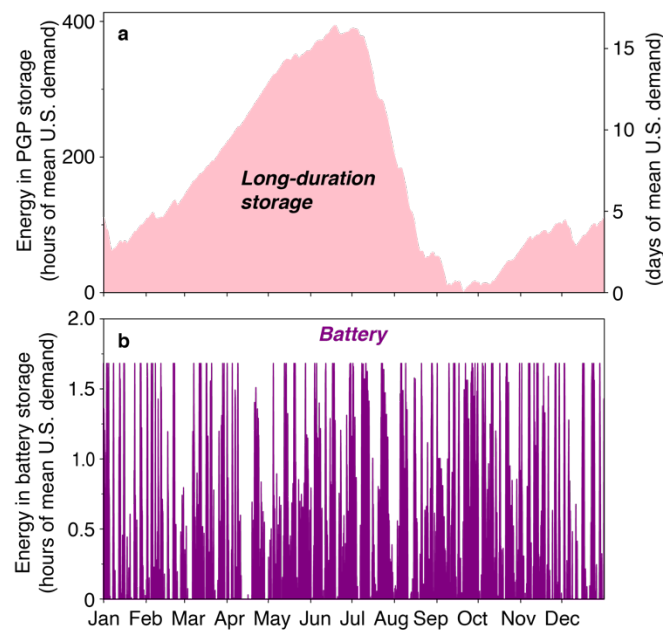


Figure 2.3 Energy Storage during 1 year (2018) in the Base Case. (A) LDS energy storage (B) battery energy storage. The maximum amount of available energy to meet demand with LDS (394 h, or 16 days of mean U.S. demand) and batteries (1.7 h of mean U.S. demand) is equal to the optimized energy-storage capacity for these technologies. The large LDS capacity is used primarily for inter-season storage. In contrast, the relatively small battery capacity is used primarily for intra-day storage.

As discussed, LDS is used primarily to provide large amounts of inter-season energy storage, mostly discharging in summer. While solar is most abundant during the summer months, wind availability decreases in summertime.⁸¹ Because least-cost optimizations of the base case include larger capacities of wind than solar, LDS is important for meeting summertime demand. Figure 2.3A highlights this behavior in the base case in 2018, showing that the amount of energy stored in LDS (as hydrogen fuel for PGP) increases

during winter, spring, and fall, when renewable resources (especially wind) are abundant, and is drawn down in the summer, when combined resources are relatively scarce. LDS thus cycles only once a year and has an energy capacity equivalent to 394 h (16 days) of mean U.S. demand. In contrast, Figure 2.3B shows that batteries are used to frequently provide small amounts of stored energy, cycle approximately once per day, and are frequently charged to their full installed energy capacity equivalent to 1.7 h of mean U.S. demand.

Multiple-Year Simulations Reveal the Role of Inter-annual Storage

Longer time periods are more likely to include large-scale weather events like wind droughts that require large reserves of stored energy. To examine long-term variations, simulations across the full 39 years of available wind and solar data (1980–2018) were modeled for 1-, 2-, 3-, 4-, 5- and 6-year periods, while still assuming current technology costs (Table 2.1; Figures 2.4 and 2.5). Indeed, longer simulation lengths typically resulted in larger deployed capacities of LDS to ensure system reliability during infrequent low-resource periods (Figure 2.4). Figure 4C highlights an example of multi-year storage dynamics in a 6-year simulation from 1980-1985, where substantial energy was in LDS during the first 3 years (1980– 1982), and energy then was depleted during the second 3 years (1983–1985). Overall, the median energy capacity of LDS assets in the 6-year simulations was 85% greater than the median energy capacity of LDS assets in the 1-year simulations (Figure 2.5). These substantial differences highlight the need for assessment of system performance over multiple years to meet resource adequacy planning standards for a reliable electricity system.

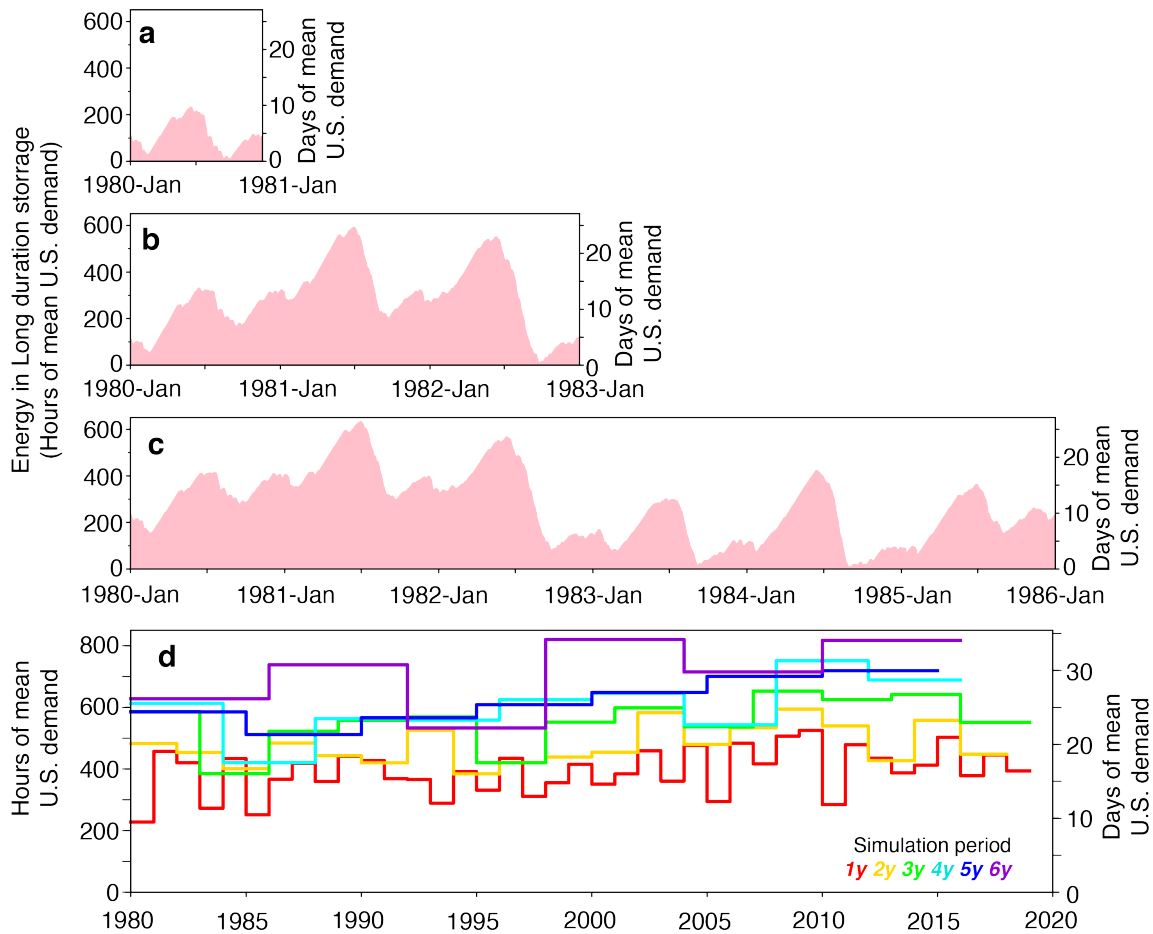


Figure 2.4 Effect of Simulation Length on Energy in Long-Duration Storage. (A–D) Energy in LDS over (A) 1 year (1980), (B) 3 years (1980–1982), and (C) 6 years (1980–1985). In (D) 1-, 2-, 3-, 4-, 5-, and 6-year simulations were performed across all 39 years of wind and solar data available (1980 to 2018). The horizontal sections of the lines represent the optimized LDS capacity for the periods simulated. Storage in the model is constrained to start and end with the same amount of energy. Dependence on LDS increases when the system is optimized over more years, as LDS is used for multi-year storage in addition to seasonal storage.

When least-cost optimizations were performed for single years of weather data from 1980 to 2018, the resulting installed capacities of LDS, batteries, wind, and solar were 29%–68% higher in some years than in other years (Figure 2.5). Asset builds based on a single year are not robust (i.e., do not reliably meet demand) for other years (Figure S4A). Specified asset capacities from simulations of varying lengths were applied to other years of data to assess the system reliability in other years (Figure S4B). While longer modeling horizons more accurately predicted needs (Figure S4B), 4-year simulations are not

necessarily enough to meet North American Reliability Corporation (NERC) resource adequacy planning standards.³⁰ Future analyses could explore how many simulation years are adequate to ensure that specified asset builds will meet regulatory resource adequacy standards over the lifetime of the capital asset stock on a typical grid.

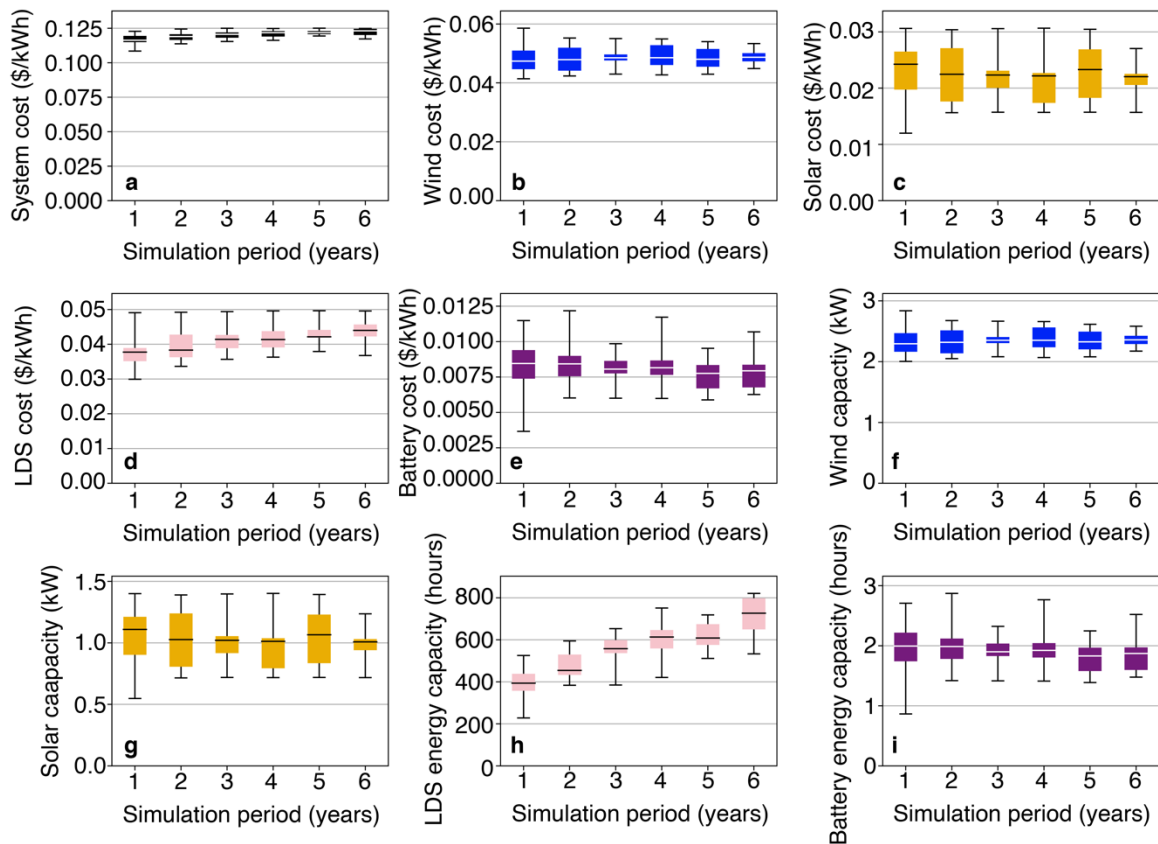


Figure 2.5 Distribution of Results for Various Simulation Lengths. Box and whisker plots show the distribution of total system cost, and individual technology capacities and contributions to system cost for various simulation lengths (1- to 6-year lengths). Whiskers represent the minimum and maximum of each dataset. With hourly resolution and many decision variables, the linear optimizer is computationally limited to 6-year simulation lengths for these systems. Power capacity is normalized such that 1 kW is mean U.S. demand and energy capacity is presented in hours of mean U.S. demand. Figures S5 and S6; Tables S5 and S6 provide supporting details and data for this figure. The impact of simulation length is strongest for LDS energy capacity where multi-year storage is a possibility. The median energy capacity of LDS deployed in the 6-year simulations was 85% greater than the median energy capacity of LDS deployed in the 1-year simulations.

Total system costs varied much less than the capacities of individual technologies (and their contributions to total system cost) (Figure 2.5). Total system costs were between

\$0.11/kWh and \$0.12/kWh across the 39 years studied (Figure 2.5), as different capacities of technologies trade off to maintain similar total system costs across the 39 years. LDS and wind dominated least-cost systems; together they made up about 75% of total system costs in all years 1980–2018 for all simulation lengths (Figure 2.5).

System Sensitivities to Region, Technology Mix, and Cost

In addition to the base case results already presented, we also performed a series of sensitivity analyses, varying the geographical area, available technologies, and technology costs. For example, to accommodate existing transmission constraints, we evaluated systems in smaller geographical regions corresponding to three largely independent interconnections in the U.S.: the Western Interconnection, the Eastern Interconnection, and the Texas Interconnection (Figure S7). Because our demand data is limited to the U.S., we exclude the contributions to the interconnections from Canada and Mexico. Using 2018 data, 100% reliable least-cost wind-solar- LDS-battery systems for each of these regions entailed technology mixes similar to the entire contiguous U.S. system, with investments in wind and LDS constituting two-thirds or more of total system costs.

To understand the relative benefits of using LDS and batteries individually and in combination, we performed a series of simulations in which some of the base case technologies (i.e., wind, solar, batteries, and LDS) were not available to the model. As shown in Figure 2.6, regardless of the mix of variable renewable generation technologies, introduction of LDS at current costs reduced total system costs relative to a battery only case. Indeed, in all cases in which LDS and batteries were included, the least-cost system was produced by spending more money on LDS than on batteries. The lowest system cost (\$0.12/kWh) corresponds to the wind-solar-LDS- battery base case, as compared with \$0.04/kWh for current U.S. system-averaged generation costs.⁸²

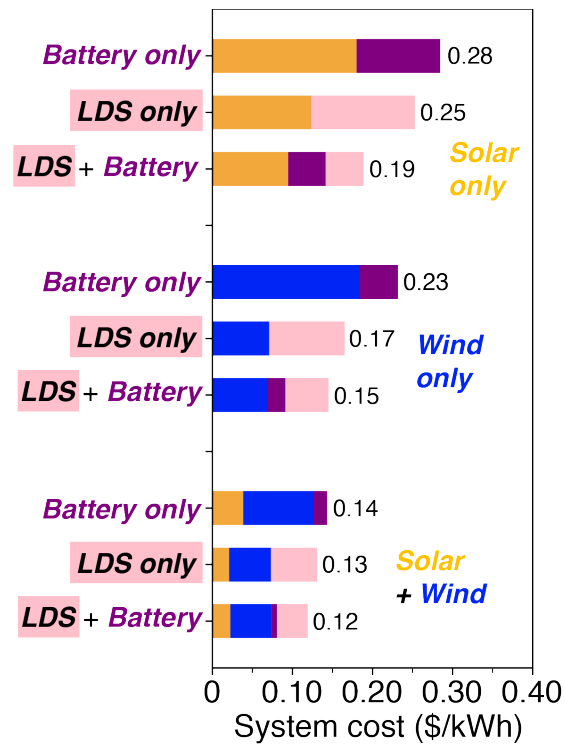


Figure 2.6 System Costs with Different Technology Combinations. In the top-most three bars, generation is obtained by solar only; in the middle three bars, by wind only; and in the bottom-most three bars generation is obtained by a combination of solar and wind. Within each group of three bars, the top-most bar represents a system with battery storage only, the middle bar represents a system with LDS storage only, and the bottom-most bar allows both storage technologies to be deployed. Stacked areas in each bar represent the cumulative contribution of each technology to total system cost over the optimization period (2018). The bottom-most bar represents the wind-solar-LDS-battery base case. Table S8 supports this figure. In all cases, introduction of LDS reduces overall system costs compared with a system with only batteries.

We also tested the sensitivity of system costs and configuration of the least-cost system to changes in storage costs for the wind-solar-LDS-battery base case using 2018 data. System costs are effectively only sensitive to reductions in LDS costs when compared with equivalent reductions in battery costs (Figure 7A). In Figure 7A, power-capacity (conversion) and energy-capacity (storage) costs of LDS are scaled by the same factor. Simulations in which power- and energy-capacity costs for LDS were varied independently are shown in Figures 7B and S8. We varied total cost for batteries, as separating power and energy costs is difficult for this technology. For LDS with PGP as the base case, total system costs are more sensitive to relative reductions in power-capacity costs (i.e., electrolyzer and fuel cell costs) than they are to reductions in energy-capacity costs (i.e.,

underground storage of hydrogen) (Figure 2.1 and S8). In contrast, for Li-ion batteries, energy-capacity costs dominate total costs (Figure 2.1). The PGP base case is compared with other LDS technologies including PHS and CAES in Figure 2.7B. The marked energy and power costs for both PHS and CAES represent annualized fixed costs for current technologies, where PHS and CAES are modeled with the same round-trip efficiency and self-discharge rate as PGP (costs in Table S4; lifetimes in Table S3). PGP at current costs is a competitive option for the LDS functional role while also meeting renewable requirements unlike current large-scale CAES demonstrations (Figure 2.7B); see the Discussion for further detail. Relative to other LDS technologies, PHS has high energy-capacity costs, which may limit its ability to compete in the LDS grid role.

We explored the sensitivity of least-cost asset builds and dispatch schedules to changes in storage costs. A 4-fold reduction in LDS costs entirely eliminated batteries from the least-cost system (Figures S9B and S10B). Conversely, eliminating LDS from the least-cost system required a 100-fold reduction in battery costs (Figures S9D and S10D). LDS also disappeared from the least-cost system with a 2x increase in LDS costs relative to current costs, whereas batteries remained until there was a 3.5x increase in current battery costs (Figures S9A, S9C, S10A, and S10C). In the system where battery costs were reduced by a factor of 100, and LDS at current PGP costs is eliminated, batteries fill the seasonal storage functional role (Figure S11). In contrast, in the case where LDS costs are reduced by a factor of 4, and batteries at current costs are eliminated, LDS is not used for high-frequency, intra-day storage (Figure S11). Less costly LDS resulted in an increased fraction of wind generation, whereas less costly batteries resulted in an increased fraction of solar generation in the least-cost system, highlighting the different needs to smooth out the qualitatively distinct variabilities in wind and solar resources (Figure S10).

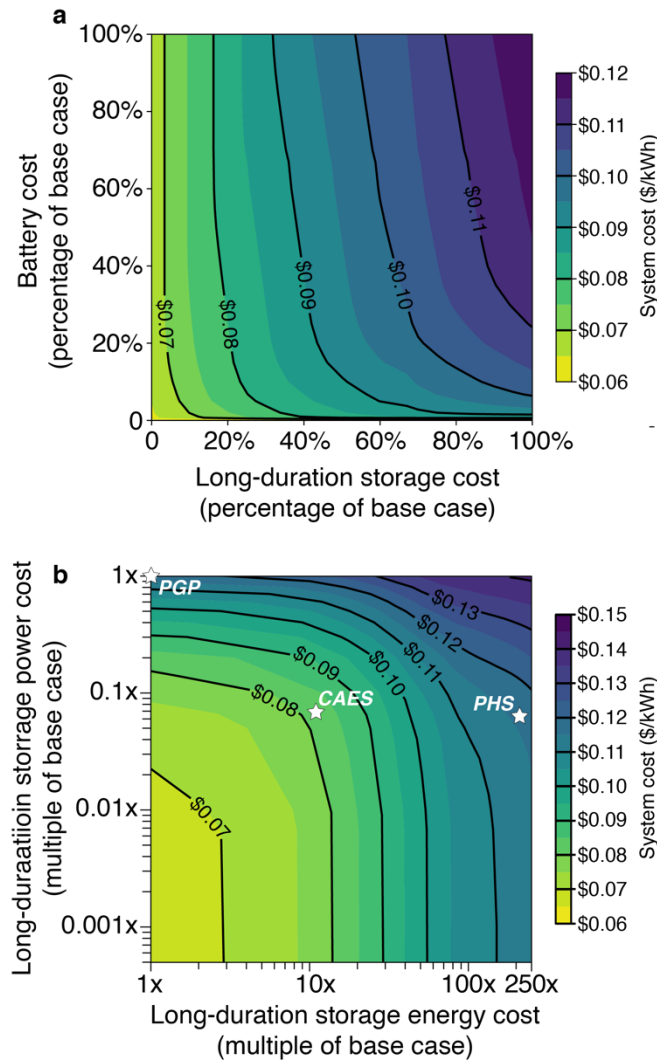


Figure 2.7 Sensitivity of System Cost to LDS and Battery Costs. (A) LDS and battery costs are independently reduced from base case assumptions (100% of base case costs) to free (0%), and total system costs for the optimization period (2018) are plotted as contour lines. Capacity and dispatch of each technology, including wind and solar, were optimized in response to each combination of LDS and storage costs. The system costs are much more sensitive to reductions in LDS costs than to reductions in battery costs. (B) LDS power and energy costs are scaled independently by multiples of base case costs. The base case system cost, with current PGP costs, is displayed with a star at 13. All system costs are generated using physical characteristics of PGP (round-trip efficiency, self-discharge rate), thus the CAES and PHS stars represent annualized fixed costs for these technologies and not system costs (costs in Table S4; lifetimes in Table S3). Note: CAES power costs are based on a carbon-emitting design; see Discussion for further detail. For PGP and CAES technologies, system costs are more sensitive to reductions in power costs than they are to similar reductions in energy costs. Figures 2.1 and S8 provide additional detail.

2.4 Discussion

Our results demonstrate that electricity systems that use only wind and/or solar generation and storage to reliably meet electricity demand cost substantially less if LDS is included as a storage option (Figure 2.6). The benefits of LDS are quite robust across single- and multi-year time periods, different spatial scales, and a wide range of modeled technology costs.

Implications of Changes in Energy Storage Costs

Because of uncertainty in future technology costs, it is essential to explore a wide spread of cost sensitivities when evaluating future electricity systems. Over a very wide range of battery costs, introduction of LDS leads to lower system costs—even at current PGP costs—provided that very high reliability (>99.97%) is a strict constraint on system design (Figure S9). For example, for a solar-battery only system at current costs, our model produces a system cost of \$0.28/kWh; adding LDS at current PGP costs decreases the system cost by 32% to \$0.19/kWh (Figure 2.6). Although still expensive when compared with current average U.S. electricity system costs of \$0.04/kWh,⁸² LDS minimizes expensive short-term storage that would otherwise be needed to compensate for the diurnal cycle of sunlight, and reduces and the overbuilding of generation that would otherwise be needed to compensate for the seasonal variation in insolation. System costs decrease further when there is a mix of wind and solar generation (at current asset costs), as least-cost systems optimize to avoid overbuild of generation and short-term energy storage (Figure 2.6). These system cost comparisons suggest that least-cost, reliable, emissions-free electricity systems benefit from the inclusion of complementary technologies, and that asset capacities will vary based on which technologies are allowed in the system. Deployment of LDS provides an expanded suite of low-cost options for building reliable, zero-carbon electricity systems with a variety of wind and/or solar asset mixes.

Less costly LDS led to higher penetration of wind power generation in reliable, least-cost electricity systems, whereas less costly batteries led to higher penetration of solar power generation (Figures S9 and S10). Because wind resources can be low for periods of several

weeks in the late summer, wind power penetration is facilitated by including an energy-storage technology that is capable of filling these extended gaps in which demand substantially exceeds generation. This characteristic occurs despite the relatively low PGP round-trip efficiency of 49%, which effectively increases costs associated with storing electricity for later dispatch (Table 2.1). In contrast, a major barrier to penetration of solar power is the ability to address diurnal variability. Electrochemical batteries are well-suited to this purpose due to their relatively low power conversion costs and high round-trip efficiencies. In the wind-solar-LDS-battery system, LDS and batteries coexist and fill complementary functional roles in the system (Figures 2.2 and 2.6). Including a wider range of technologies can lower system costs, but only if new technologies are less costly and physically similar to existing technologies, or physically different enough (in terms of cost structure, efficiency, lifetime, etc.) to complement existing technology by filling distinct functional roles.

Moreover, despite the recent focus on cost reductions and deployment of battery-based grid storage,^{35,36} reducing LDS costs results in a lower system cost than the same proportional reduction in battery costs. By varying costs widely from the PGP and Li-ion base case, we capture the impact of LDS costs on renewable electricity costs. For example, a 10% reduction in LDS costs would reduce system costs by nearly twice as much as would a 10% reduction in battery costs (Figure 2.7A). In particular, it is the power-capacity costs (i.e., electrolyzer and fuel cell for PGP) that matter; the main expenditure on PGP is for conversion between electricity and hydrogen fuel as opposed to energy-capacity (i.e., storage) costs (Table 2.1; Figures 2.7B and S8). Furthermore, while other technologies like CAES and PHS could fill the LDS functional role, PGP is both renewable (unlike current CAES designs) and has no partial energy-cost limitations (unlike PHS).

The importance of LDS power-capacity costs explains why the least-cost system often transfers energy between LDS storage and battery storage (Figures 2, S2, and S3). Inter-storage transfer allows the electricity system to take advantage of the strongest characteristics of each technology. Due to high capital costs of conversion technologies

associated with LDS, the use of a battery both during charging and discharging can reduce the amount of required LDS conversion capacity. Similarly, although batteries can dispatch electricity rapidly at low costs, their cost of energy storage is high. Therefore, costs can often be reduced if energy is stored in an LDS system and then slowly dispatched to a battery from which the energy can be rapidly dispatched when needed.

Technological Options for Long-Duration Storage

Although our base case reflects current cost and performance metrics of renewable PGP (Table 1), we explore LDS more generally by model runs, which vary these costs over a wide range of technology options. The results of this exercise suggest the potential for other LDS technologies with costs structures similar to PGP (Figure 2.1).

Large capacities of PHS exist worldwide, including 23 GW in the U.S., where it accounts for 95% of all utility-scale energy storage.^{83,84} DOE's hydropower vision estimates that 36 GW of new PHS capacity is possible in the U.S. by 2050, but recent growth rates point to more modest PHS increases—perhaps 0.5 GW of new capacity by 2050.⁸⁵ Key constraints include limited geographical locations and effects on the magnitude and timing of downstream water flows. It is usually used for storage times of less than 1 week.⁴⁹ The costs of PHS projects are highly site and project specific;⁸⁶ depending on the local topography, the same dam might store very different quantities of water depending on the shape and depth of its reservoir, necessitating caution when extrapolating PHS costs. Furthermore, most PHS in the U.S. was built in the 1970s.⁸⁴ Such a mature technology is less likely to experience large future cost reductions due to learning curves and economies of scale.

CAES technology uses electricity to compress, cool, and store air underground, followed by subsequent air expansion through a series of turbo-expanders producing electric power on demand. There are two large-scale CAES plants in operation worldwide: a 290 MW plant in Huntorf, Germany, and a 110 MW plant in McIntosh, Alabama, USA.⁸⁷ Both store compressed air in salt caverns. Future CAES projects could use renewable electricity for

the initial compression and cooling step without technological issues.⁴⁸ However, the Huntorf and McIntosh CAES plants both require supplemental heat when discharging and powering the grid. In both cases, the compressed air is preheated by burning natural gas before expansion.⁸⁷ There are conceptual adiabatic designs that preheat the expanding air with the stored heat of compression to avoid CO₂ emissions, but there have been no large-scale demonstrations of this approach.⁴⁸ Thus, regardless of the source of charging electricity, current CAES designs are inconsistent with goals of zero-carbon emissions and 100% renewable energy. Nonetheless, we include costs of current CAES designs in Figures 2.1 and 2.7 for comparison. Options for eliminating fossil CO₂ emissions from CAES (e.g., combusting fuel produced from a carbon neutral process or capturing and sequestering CO₂ from the exhaust) would increase the presented costs.

Utility-scale PGP projects are expanding at current costs.^{6,50-52} PGP is an energy-storage technology in which electricity is converted into fuel (e.g., hydrogen via electrolysis), followed by a subsequent conversion of the fuel back into electricity either thermally (combustion turbines) or electrochemically (fuel cells).^{49,88,89} In the future, substantial reductions in PGP power-capacity costs, and thus system costs, could be obtained if the costs of stationary fuel cells and electrolyzers were to decrease (Figure S8, current base case costs in Table 2.1). Current fixed costs of fuel cell and electrolyzer systems are about \$6,000/kW and \$1,100/kW, respectively (Table 2.1; with corroborating references).^{40,67,68,90} PGP power-capacity costs could also be reduced by the development and deployment of new gas turbines that operate with 100% H₂ and have costs of about \$1,000/kW, comparable to conventional gas turbines that operate on CH₄.⁹¹⁻⁹³ It is also possible to perform methanation using electrolytic H₂ and concentrated CO₂ with relatively little energy input,⁹⁴⁻⁹⁷ producing methane that could be stored as natural gas is routinely stored today, and later combusted in a turbine upon demand, with the CO₂ captured, concentrated, and recycled to form a closed loop. This alternative PGP process would replace the fuel cell or H₂-powered turbine⁹⁸ with a conventional methane-powered turbine, and allow geographically distributed, conventional methane gas storage, but would incur

costs associated with the capture, concentration, and purification of CO₂ from flue gas as well as conversion costs associated with methanation.

TES systems provide a range of services from temporally shifting heating and cooling loads in buildings and industry to smoothing the power delivered to the grid from concentrating solar power (CSP) plants.⁹⁹ TES systems store energy as either sensible heat, latent heat, or via thermochemical reactions. Because we focus on an electricity system only model in this paper, we neglect TES systems that do not provide electric power. Unlike other energy-storage technologies that convert electric power into stored energy and back to electric power, TES systems almost exclusively store heat from a direct heat source such as CSP.¹⁰⁰ While coupled CSP-TES systems may play a role in a future zero-emissions electricity system, simultaneous power generation and energy storage by heat input complicates comparisons with other LDS technologies.

Model Architecture Changes

In addition to costs, below we consider the implications of model architecture changes, such as region size, electricity demand, the availability of other technologies, and temporal range and resolution.

Wind and solar resources are less variable when aggregated over larger areas.³ Hence, confining the load-balancing region to individual states or independent system operator (ISO) regions generally requires more short-term and long-duration energy-storage capacity than the values obtained herein for the U.S. (Figure S7). Regardless of resource aggregation size, the addition of LDS leads to reductions in overall system costs because LDS storage is not limited by energy-capacity costs but rather the cost of power capacity (e.g., of electrolyzers and fuel cells for PGP; Figure S8B). This suggests that the system benefits of LDS that we find would occur in smaller regions, and that such benefits would be even more sensitive to changes in the cost of power capacity, than they would be to in the larger interconnects, or the entire contiguous U.S. Modeling additional transmission constraints would likely result in systems with higher required LDS capacities than our

base case.⁵⁷ Lossless transmission thus represents a best-case scenario and a lower bound for storage capacity reliability requirements.

Along the U.S. eastern coast, offshore wind has higher capacity factors than land-based wind, and may reduce overall renewable electricity costs by competing with land-based wind and solar generation.^{42,101} However, both land-based and offshore wind power technologies in the Eastern Interconnect have concurrent seasonal lows in the summer time.^{81,101} LDS is expected to benefit electricity systems based on both land-based and offshore wind generation by filling seasonal resource gaps. In most regions, the expansion of variable renewables into fossil fuel-based electricity systems can continue unabated for many years, but LDS may become increasingly valuable with lower fractions of natural gas. Indeed, LDS competes with natural gas in a 95% carbon-free electricity system, with system costs at \$0.09/kWh (Figure S12). With lossless transmission, the introduction of natural gas to the technology mix at 10% of demand minimizes or eliminates the need for storage (Figure S12). In some locations like Germany, LDS may be considered prior to 80% integration of renewables if there are transmission constraints.^{56,102}

Here we constrain our analysis to the electricity sector to specifically explore scenarios relevant to states that have adopted, or are considering adopting, 100% renewable power laws. Other energy system models have explored the use of electricity for heating, fuels, chemical feed-stocks, and battery storage in electric vehicle fleets.⁶² Although using electricity to satisfy the U.S. heating demand might substantially increase winter loads, it would not eliminate the need for LDS to compensate for inter-annual variability of solar and wind resources or reduced resource availability during different seasons or weather-related, multiple-day episodes in the electricity sector. Similarly, we would not expect our conclusions regarding the cost-effectiveness of adding LDS to wind-solar-battery electricity systems to be affected by whether deployed batteries are stationary or in battery electric vehicles; as discussed, changes in system costs are not very sensitive to changes in battery costs (Figure 2.7).

While the introduction of low- or zero-carbon “firm” generators, such as nuclear energy or natural gas with CCS would minimize or eliminate the need for storage technologies,^{28,29} these technologies are generally excluded or limited either by regulation or mandate from future electricity systems in many regions (Table S2; Figures S13 and S14). Regardless of the actual level of penetration, compensating for the variability of wind and solar will be required, and utilization of firm generators for this purpose will involve: use of firm generation technologies at low capacity factors, increasing costs, curtailment of VRE, or deployment of short-term and long-term grid storage technologies, with the trade space between the latter two options the focus of the work described herein.

The use of weather data from different years produces considerable differences in the capacities of technologies deployed in least-cost systems (up to 213% higher for one year compared with another for battery energy capacity), but due to offsetting changes in deployed capacities of different technologies, total system costs are not very sensitive to inter-annual differences in weather (Figure 2.5). The use of hourly time resolution explicitly assumes that load balancing and grid stabilization on more rapid timescales will be obtained using other, currently available technologies. Our approach notably allows quantification of the duration and energy required to obtain reliability from a system that relies exclusively on wind and solar generation resources, along with energy-storage technologies, over a timescale comparable to the lifetime of capital assets on an electricity grid. Although we assume that the notional electricity system is built instantaneously and do not account for cost reductions associated with increases in deployment, the conclusions are robust over a wide range of storage technology costs.

2.5 Conclusions

Our results indicate that introducing LDS technology reduces system costs of reliable electricity systems consisting of solely wind and solar electricity generation and battery storage. Examples of technologies that can provide long-duration energy storage include PGP, compressed air, and pumped hydro. Due to its low energy-storage capacity costs,

LDS provides seasonal and multi-year storage, substantially reducing the capacities of wind and solar generation that otherwise must be built to obtain high reliability over multi-year time periods. Indeed, we find that dependence on LDS increases when the system is optimized over more years. This is important because most grid planning tools used by utilities and regulators do not involve multi-year modeling horizons, and consequently may underestimate the value of LDS. Batteries are useful for hourly and daily storage because of their relatively low power-capacity costs, but do not provide cost-effective seasonal storage due to their high energy-storage capacity costs. Battery storage currently receives the vast majority of attention, investment, incentives, and mandates designed to promote zero-carbon grid storage technologies. However, relative to current costs, reductions in LDS costs would reduce system costs in a reliable wind and solar electricity system to a much greater extent than would equivalent reductions in battery costs. These results suggest that large-scale deployment of LDS and cost improvements in such technologies may greatly reduce the cost of future variable renewable electricity systems.

2.6 Methods

Data and Code Availability

The macro energy model (MEM) uses historical wind and solar input data with hourly resolution over the contiguous U.S. for a 39-year period (1980–2018) and hourly demand data for mid-2015 through mid-2019 from the U.S. Energy Information Administration (EIA) where mean demand was 457 GW (Figure S1).¹⁰³ In the interest of transparency, the model code, input data, and analytical results are publicly available on GitHub at https://github.com/carnegie/SEM_public/tree/Dowling_et_al_2020.

Wind and Solar Capacity Factors

The hourly based wind and solar capacity factors used in this study are estimated using the Modern-Era Retrospective analysis for Research and Application, Version 2 (MERRA-2) reanalysis satellite weather data, which has a horizontal resolution of 0.5 by latitude and 0.625 by longitude.⁷⁵ For solar capacity factors, we first calculate the solar zenith angle

and incidence angle based on the location and local hour,^{104,105} and then estimate the in-panel radiation.¹⁰⁶ We also separate the direct and diffuse solar components using an empirical piecewise model that takes into account both ratios of surface to top-of-atmosphere solar radiation (the clearness index) and the local time.¹⁰⁷ To improve the potential solar availability, we assume a horizontal single-axis tracking system with a tilt of solar panel to be 0 and a maximum tuning angle of 45. Power output from a given panel is calculated using a performance model, which considers both the surrounding temperature and the effect of irradiance.^{108,109}

For wind capacity factors, the raw wind speed data is first interpolated to 100 m by assuming a power law, based on wind speed at 10 and 50 m. The wind capacity factor calculation employed a piecewise function consisting of four parts: (1) below a cut-in speed (u_{ci}) of 3 m s⁻¹ the capacity factor is zero, (2) between a cut-in speed of 3 m s⁻¹ and rated speed (u_r) of 12 m s⁻¹ the capacity factor is u_{ci}^3/u_r^3 , (3) between a rated speed of 12 m s⁻¹ and cut-out speed (u_{co}) of 25 m s⁻¹ the capacity factor is set to 1, and (4) above a cut-out speed of 25 m s⁻¹ the capacity factor is zero.^{3,110}

The solar and wind capacities are first estimated for each grid cell in the U.S., with the same resolution as in MERRA-2. We then selected grid cells over land where the annual mean capacity factor is larger than 26% for both solar and wind. We chose this threshold such that our resulting average capacity factors over the 39-year time frame were comparable to the reported capacity factors for utility scale generation of wind and solar in the U.S.¹¹¹ This threshold includes about one-quarter and one-half of the total possible grid cells for solar and wind, respectively. The continental or interconnect scale resource data are then calculated as the average of these grid cells with grid area as weights.

EIA Demand Imputation

The EIA began collecting hourly electricity demand information from all balancing authorities (BAs) across the contiguous U.S. in July 2015. The collection process is based on form EIA-930 where values are calculated by each reporting BA individually.^{112,112} The

original EIA data were queried from their open data database on September 10, 2019 via an application programming interface.¹¹³ These data are the most temporally granular publicly available demand data that covers all of the contiguous United States. However, there are substantial quantities of missing and outlier values in the data. A data cleaning method was developed to remove outliers and replace missing and outlier values in order to create complete, usable data records.⁷⁶ 2.2% of the demand data were missing in the EIA's database. Additionally, some reported quantities are non-physical negative values or are extreme outliers. We developed an anomalous value screening process to flag the most extreme outliers for imputation. The screening algorithms are designed to respect the time series structure of the data and use excessive deviations as a reason to flag a value.

We used a multiple imputation by chained equations (MICE) technique for imputation.¹¹⁴ Each missing or anomalous demand value is predicted using a linear regression on the demand during that same hour for each other BA. This method leverages correlations to help fill in some 1,000 h or longer consecutive data gaps. Other predictors in the linear regression include the leading and lagging demand values surrounding the hour being predicted (to encourage time series continuity) and the site's average demand for that day of the year and hour of day.

The performance of the MICE technique was measured by intentionally marking good data as missing, imputing said data, and comparing these imputations against the true values. This comparison was performed via assessing the mean absolute percentage error (MAPE). The mean MAPE value across all the BAs was 3.5%. The imputation method exhibited only a small bias of 0.33% measured as the mean bias across all BAs. The cleaned data are publicly available.¹⁰³

Cost and Technological Assumptions

System costs in our model include fixed costs and variable costs. Variable costs were assumed to be zero for all technologies (wind, solar, PGP, and Li-ion batteries), and thus our system cost is primarily based on discounted fixed costs. Table 2.1 presents these costs

as well as power- and energy-capacity costs for PGP and batteries that were used in the base case. Wind and solar costs used for the base case were obtained from the U.S. EIA's 2018 Annual Energy Outlook.⁶⁵ Wind and solar capacity factors for the contiguous U.S. were calculated from the MERRA-2 reanalysis dataset as described above. Wind and solar capital costs are lower in the U.S. EIA's more recent 2020 Annual Energy Outlook and other references.¹¹⁵⁻¹¹⁷ We choose to retain the higher values to align our cost assumptions with previous analyses for easier comparison of results. This choice will not substantially alter any of the technical conclusions reached in this paper about the utility of LDS but may slightly overestimate resulting system costs.

Capacity costs (fixed costs), lifetimes, and efficiencies for PGP storage technologies were evaluated from the H2A model data compiled by the National Renewable Energy Laboratory (NREL).⁶⁶⁻⁶⁹ Battery storage capacity costs, efficiencies, and lifetimes were estimated from Lazard, a financial advisory and asset management firm.⁷⁰ The cost, energy capacity, and lifetime for Li-ion battery storage are based on usable energy capacity not nameplate capacity.⁷⁰ Specific values for battery storage characteristics were taken from Davis et al., and Pellow et al. and were within the ranges provided by Lazard.^{37,40} We assumed a 100% operational uptime for batteries and PGP systems, so results should be scaled proportionately in either the cost or the installed asset capacity to include a buffer against scheduled outages. In sensitivity studies, capacity costs for batteries and PGP (power and energy) were scaled from 13108 to 250, with 1 corresponding to Table 2.1 costs, and least-cost optimization was solved for each set of cost assumptions. For discussion of other storage costs besides PGP and batteries included in Figures 2.1 and 2.7, refer to Section S1.

Chapter 3

RELATIVE VALUE OF SHORT-, MID-, AND LONG-DURATION STORAGE TECHNOLOGIES IN RELIABLE WIND AND SOLAR ELECTRICITY SYSTEMS

Li, A. X.*; Dowling, J. A.*; Virguez, E.; Ruggles, T. H.; Caldeira, K.; Lewis, N. S. Relative Value of Short-, Mid-, and Long-Duration Storage Technologies in Reliable Wind and Solar Electricity Systems. *In Preparation*.

3.1 Introduction

Energy storage is an important component of reliable, cost-effective deeply-decarbonized electricity systems that rely on substantial generation from variable renewable energy resources, such as wind and solar energy.⁴¹ Energy storage technologies differ in their siting and supply chain constraints, socio-political challenges, and storage duration.^{15,118,119} Consequently, many modeled least-cost, deeply-decarbonized electricity systems contain multiple storage technologies.

Short-duration energy storage technologies have low power capacity costs, and thus are cost-effective for frequent (hourly) charging and discharging to smooth sharp peaks in electricity generation or demand. Currently, Li-ion batteries with durations of 1 - 4 h are the most widely deployed short-duration storage technology. In contrast, long-duration storage technologies such as pumped hydroelectric storage, compressed air energy storage, and electrolytic hydrogen have relatively high power capacity costs, but low energy-capacity costs. Long-duration energy storage compensates for sustained weather-related events lasting days or weeks, and buffers seasonal or interannual variability in renewable resource availability.^{4-6,120}

A third group of storage technologies has medium energy- and power-capacity costs and durations spanning wide ranges, potentially serving mid-duration roles (Figure 3.1). For

example, deployed redox-flow batteries have durations up to 10 h, and can theoretically be designed to provide storage for even longer durations. Thermal electricity storage can potentially provide durations between 8 and 192 h (8 days), whereas iron-air batteries are projected to provide durations of 100 and 150 h at a total cost of <\$20/kWh. Gravity-based energy storage has the potential to store energy for >12+ h.

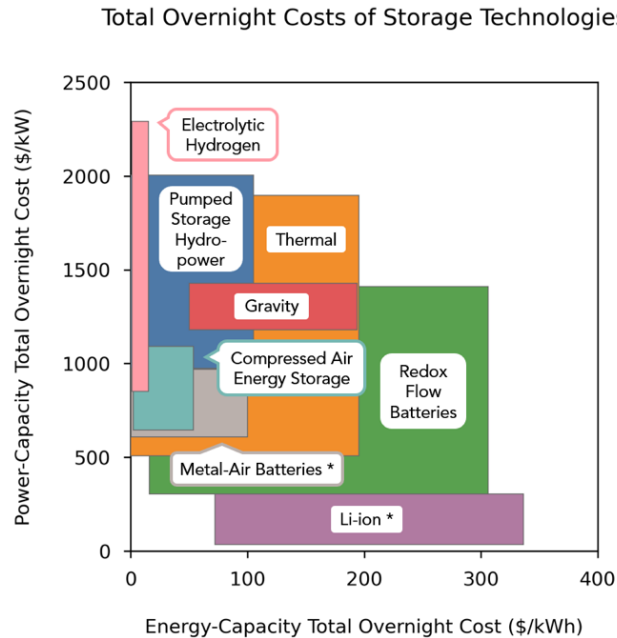


Figure 3.1. Energy-capacity costs and power-capacity costs of energy storage technologies. Ranges of total installed energy- and power-capacity costs of different storage technologies. Numerical values and sources are provided in Table S1. *Energy-capacity and power-capacity costs were combined to obtain the total cost of Li-ion battery or metal-air battery storage.

Previous studies demonstrate that introducing long-duration storage as a second storage technology alongside short-duration storage substantially lowers total system costs of reliable, wind and solar based electricity systems.^{120–123} However, studies that model deeply-decarbonized electricity sectors with 3 or more storage technologies differ in how many storage technologies are utilized. For a UK electricity system modeled with mainly wind and solar generation (and existing nuclear resources), in which demand flexibility was considered, almost all optimal storage portfolios consisted of only Li-ion batteries and electrolytic hydrogen.¹²⁴ Compressed air energy storage was only cost-competitive in

scenarios that required large oversupplies of energy. In another study modeling storage technologies at 2050 costs in seven independent U.S. system operators (with generation provided by wind, solar, nuclear, hydro, biomass, and geothermal sources), hydrogen and pumped hydro storage were included as third and fourth storage technologies alongside Li-ion batteries and compressed-air energy storage only when wind and solar shares exceeded 80-90% of generation.¹²⁵ In a report modeling storage technologies at 2050 costs in three different U.S. regions relying primarily on wind and solar generation, with constrained natural gas generation, low-cost Li-ion and redox-flow batteries displaced the need for longer duration storage provided by electrolytic hydrogen, thermal energy storage, or metal-air batteries.¹²⁶

Many different energy storage technologies are poised to compete for shares of the marketplace, and it is unclear which will be the most valuable to invest in and deploy. The objective of this study is to evaluate how many and which type of (short-, mid-, long-duration) storage technologies are necessary for reducing system costs and maintaining reliability in solar- and wind-based electricity systems. In doing so, this analysis aims to examine how techno-economic characteristics of storage technologies impact how much these storage technologies reduce total system costs. Furthermore, this study aims to elucidate what techno-economic characteristics advantage one storage technology over another for reducing total system costs.

In this study, portfolios of 1-3 storage technologies were modeled, consisting of various combinations of short-, mid-, and long-duration storage technologies (Figure 3.2). Then, to explore an expansive space of possible storage technology portfolios, a hypothetical storage technology (denoted *Storage X*) with energy- and power-costs parameterized across wide ranges, was modeled alongside short- and long-duration storage.

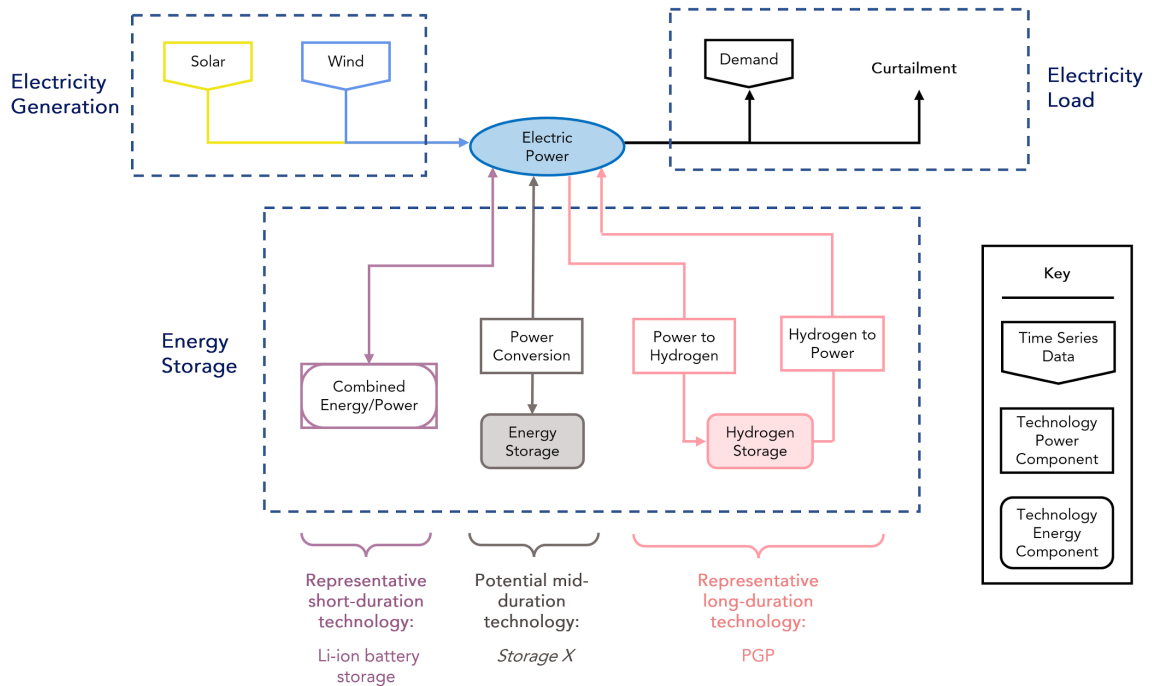


Figure 3.2 Electricity sources, sinks, and storage technologies within the macroscale energy model. Arrows indicate the direction of electricity flow, and shaded shapes represent nodes at which electricity can be stored. Conventional Li-ion batteries (Li-ion) are modeled with combined energy and power components and fixed to 4 hours of duration. *Storage X* is modeled with separate power and energy storage components. Electrolytic hydrogen storage is modeled with separate power and energy storage components, where charge and discharging can be built to different capacities.

3.2 Results

Modeled electricity systems relied only on wind and solar generation, along with various storage technologies, and were optimized for least-cost solutions subject to the constraint of 100% reliability. To frame this analysis, Li-ion batteries were used to represent a short-duration storage technology, whereas electrolytic hydrogen energy storage was used to represent a long-duration storage technology. Various technologies were used to represent mid-duration storage systems: RFB (redox-flow batteries), CAES (Compressed Air Energy Storage), PSH (Pumped Storage Hydropower), thermal energy storage, gravity energy storage, and metal-air battery storage. Figure 3.3 shows the base case costs for all storage technologies, which were taken from relatively recent references. Further description of parameters for each storage technology are included in text accompanying Table 3.2.

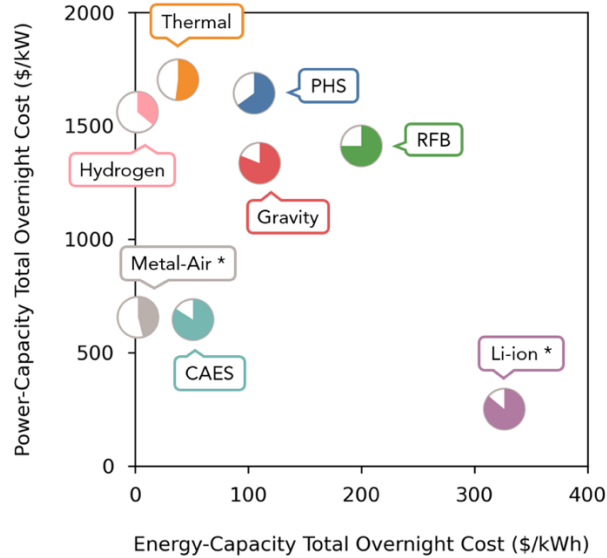


Figure 3.3 Different energy storage technologies have varying techno-economic characteristics. Base case energy-capacity costs, power-capacity costs, and round-trip efficiencies (designated by the colored area of pie charts) of different storage technologies modeled. Because electrolytic hydrogen storage and CAES have separate technologies for charging and discharging, their power-capacity cost was calculated by assuming equal charge and discharge capacities. In this work, we are considering electrolytic hydrogen as our long-duration storage technology, Li-ion batteries as our short-duration storage technology, and the other technologies as mid-duration storage technologies. See Table 3.1 and Table 3.2 for additional base case cost assumption details.* Total costs of Li-ion and metal-air battery technologies are based on additive energy- and power-capacity costs at fixed ratios of 4h and 100h, respectively.

Figure 3.4 shows cost contributions of generation and storage assets that were optimized de novo, in scenarios with different combinations of short-, mid-, and long-duration storage. At base case costs, the introduction of short-duration storage to systems with only mid-duration storage did not substantially reduce system costs (corresponding bars of Figure 3.4A vs. 3.4B). In contrast, system costs were reduced when mid-duration storage was introduced to a system with only short-duration storage (leftmost bar of Figure 3.4B). The use of metal-air batteries led to the largest reduction in system costs (33%), producing costs close to those of systems that included long-duration storage (rightmost bars of Figure 3.4A and 3.4B).

All systems with long-duration storage had mutually similar total system costs (Figure 3.4C and 3.4D). Most mid-duration storage options (with the exception of thermal energy

storage) were included as a second storage technology alongside long-duration storage (Figure 3.4C). However, only CAES and metal-air batteries were included as a third storage option alongside both short- and long-duration storage (Figure 3.4D). Note that at base case costs, the addition of short-duration storage to systems with long-duration storage as the sole storage technology, reduced system costs by approximately 1% (leftmost bars of Figure 3.4C and 3.4D).

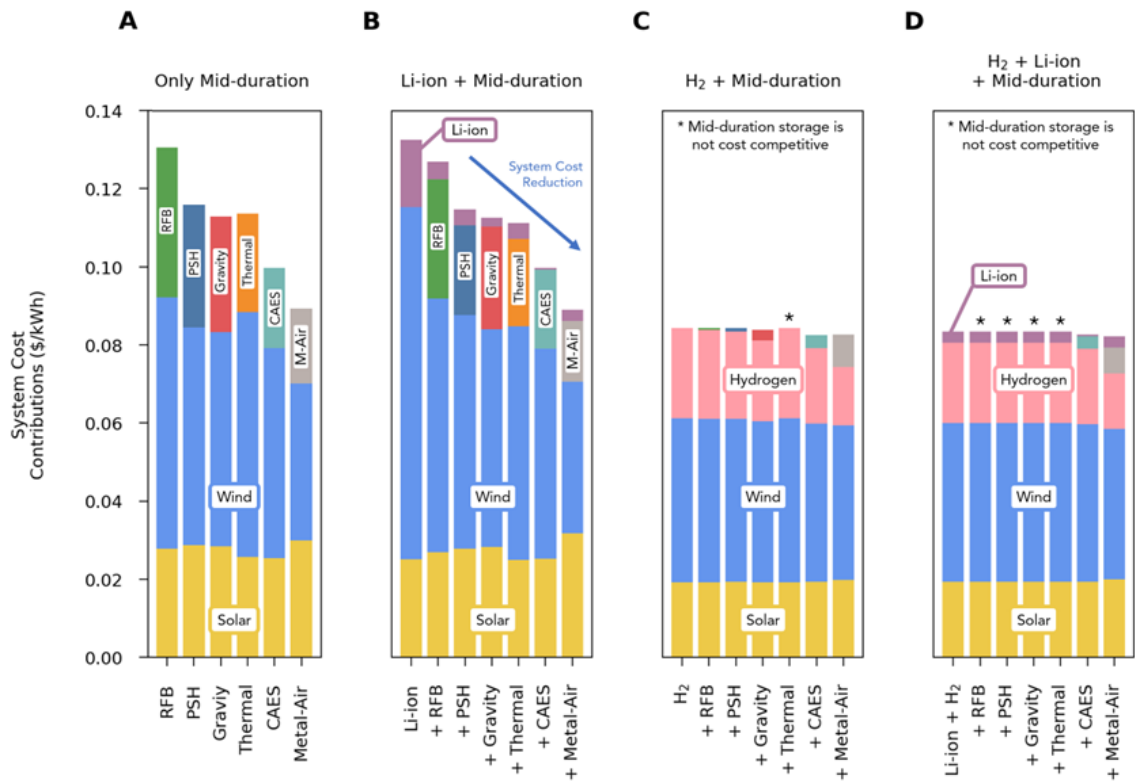


Figure 3.4 System costs for combinations of short-, mid-, and long-duration storage. Cost contributions of technologies in wind and solar generation based systems with one, two, and three storage technologies. System costs when: (A) Only mid-duration storage technologies were available, represented by *RFB* (redox-flow batteries), *CAES* (Compressed Air Energy Storage), *PSH* (Pumped Storage Hydropower), *Thermal* energy storage, *Gravity* energy storage, and *Metal-Air* battery storage. (B) Both short-duration (Li-ion) and mid-duration storage were available. (C) Both long-duration storage (electrolytic hydrogen storage) and mid-duration storage were available. (D) Short-, mid-, and long-duration storage were all available. As a benchmark, the leftmost bar in each panel shows cost contributions when mid-duration storage was omitted: (B) only short-duration storage was included (C) only long-duration storage was included (D) only short and long-duration storage were included.* Asterisks denote when mid-duration storage was not competitive.

The energy- to power-capacity ratio of storage technologies was used to characterize the “discharge time (hours)” of different storage technologies, whereas the total annual storage

discharge divided by the energy capacity was used to characterize the “equivalent annual discharge cycles (cycles per year)” of modeled storage technologies.

Figure 3.5 shows the timescale of each energy storage technology for systems that were constrained to have selected individual or combinations of storage technologies. Systems were optimized de novo for each scenario. When hydrogen was used as the sole storage technology, it was cycled 1.7 times a year and had a discharge time of 419 hours. When two storage technologies (Li-ion and hydrogen) were used, Li-ion cycled 232 times a year, while hydrogen cycled 1.5 times a year and had a discharge time of 522 hours. When three storage technologies (Li-ion, metal-air, and hydrogen) were used, Li-ion cycled 209 times a year, metal-air cycled 15 times a year, and hydrogen cycled 0.87 times a year with a discharge time of 823 hours.

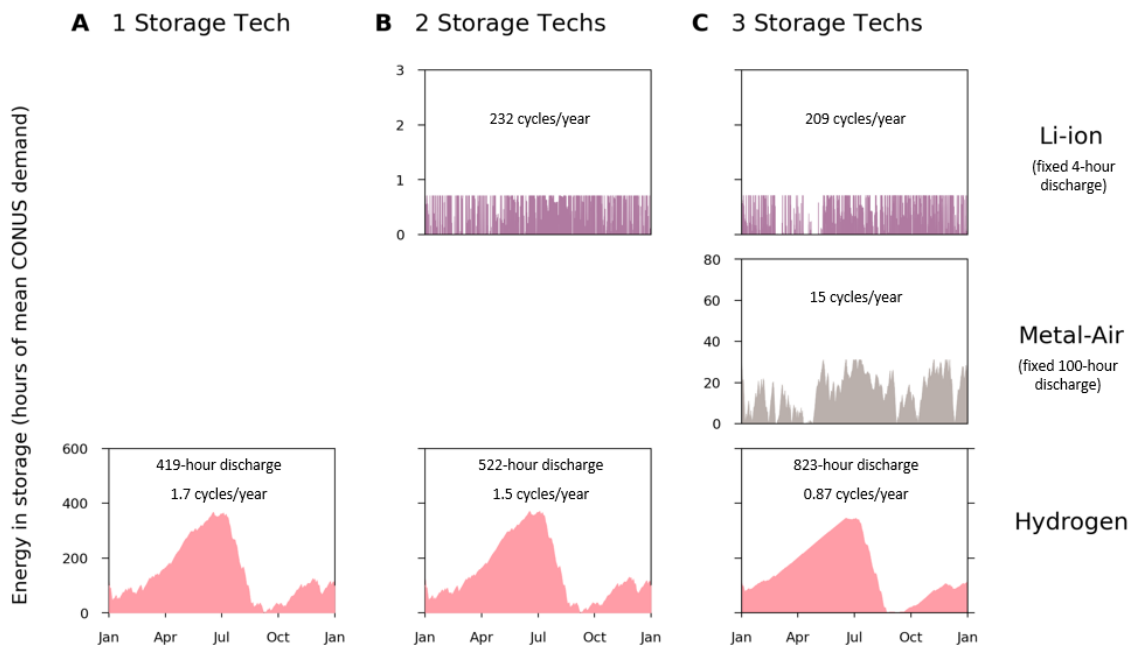


Figure 3.5 Energy in storage over one year for individuals or combinations of storage technologies. Storage technologies with different energy- and power-capacity costs were optimized to store energy on different timescale. Energy in storage over one year when: (A) One storage technology (hydrogen) was available. (B) Two storage technologies (Li-ion battery, metal-air battery, and hydrogen) were available. (C) Three storage technologies (Li-ion battery, metal-air battery, and hydrogen) were all available.

Figure 3.6 shows least-cost systems in which three storage technologies were available: short-duration storage, long-duration storage, and a hypothetical *Storage X* technology

with parameterized energy- and power costs. Energy- and power-capacity costs for Li-ion batteries and hydrogen were at base case costs across all systems (see the top and right of plots in Figure 3.6). The round-trip efficiency of *Storage X* was kept constant at 86%. (The Supporting Material describes results for analogous systems in which *Storage X* had a round-trip efficiency of 36%; Figure S3).

The introduction of *Storage X* as a third storage technology alongside short- and long-duration storage (gray dots in Figure 3.6A, blue in Figure 3.6B) led to system cost reductions of $< 0.5\%$. As *Storage X*'s energy and power costs decreased further, short-duration storage was eliminated, leaving only *Storage X* and long-duration storage (green in Figure 3.6B), but system costs were reduced by $< 5\%$ in the vast majority of cases (Figure 3.6A). Total system costs reductions were $> 5\%$ when *Storage X* energy-capacity costs were relatively low (< 80 \$/kWh). Long-duration storage was eliminated when *Storage X* energy-capacity costs were very low (< 10 \$/kWh).

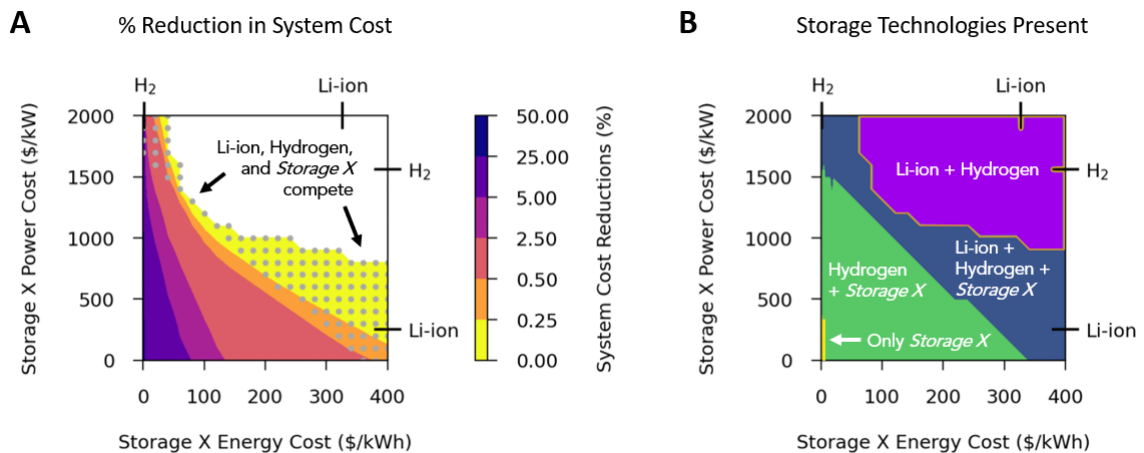


Figure 3.6 System cost reductions and storage technologies present in scenarios with up to three storage options available: short-duration storage (Li-ion), long duration storage (hydrogen), and a hypothetical *Storage X* technology with varying energy- and power-capacity costs. Energy- and power-capacity costs for Li-ion and hydrogen storage were kept constant at base-case values, marked on the top and right sides with values in Table 2. Note that the energy- and power-capacity ratio of Li-ion batteries are kept at a ratio of 4 hours. (A) Percent reductions in total system cost as compared to a least-cost system with only Li-ion and hydrogen storage at base case costs. (B) Types of storage technologies used in least-cost systems where *Storage X* energy- and power-capacity costs vary across wide ranges. The technologies that were present in each parameter range are written in white font.

3.3 Discussion

Long-term planning of future electricity systems requires analysis of which energy storage technologies will be the most valuable to invest in and deploy, given that many different energy storage technologies are poised to compete for shares of the marketplace. In this study, short-duration storage was represented with Li-ion batteries and long-duration storage was represented with a hydrogen storage system. Mid-duration storage was represented by redox-flow batteries, pumped-hydro storage, and gravity energy storage, thermal energy storage, compressed-air energy storage, and metal-air batteries. All storage technologies evaluated were not constrained in duration (energy-to-power capacity ratio), except for Li-ion batteries and metal-air batteries, which were constrained to durations of 4h and 100h respectively. Combinations of short-, mid-, and long-duration storage technologies were modeled in least-cost energy systems to evaluate how storage technologies compete and reduce system costs in reliable wind- and solar-based electricity systems.

Storage technologies with unconstrained durations outcompete Li-ion batteries at higher energy- and power-capacity costs than hydrogen storage.

In our analyses, a hypothetical storage technology (*Storage X*) with an unconstrained duration (i.e., separately sizable energy and power capacities) outcompeted Li-ion batteries at both higher energy-capacity costs and power-capacity costs than it outcompeted hydrogen storage. In Figure 3.6b, *Storage X* replaced Li-ion in least-cost systems once *Storage X* energy/power-capacity costs decreased past the diagonal border between the blue and green regions. In systems where Li-ion and *Storage X* were the only 2 allowed storage technologies, an analogous diagonal boundary defined costs at which *Storage X* replaced Li-ion (Figure S1). The stark diagonal boundary is a consequence of modeling Li-ion with a fixed duration. Individual Li-ion batteries have energy- and power-capacities that cannot be independently sized, meaning the 4-hour Li-ion battery considered here has an effective cost of 388.75 \$/kWh when sized for energy-capacity, but 1555 \$/kW when

sized for power-capacity (Figure S2). Thus, at energy-capacity costs near 0 \$/kWh, *Storage X* replaced Li-ion batteries below a power-capacity cost of ~1500 \$/kW, because it was competing based on power-capacity costs. At power-capacity costs near 0 \$/kW, *Storage X* replaced Li-ion batteries below an energy-capacity cost of ~330 \$/kWh, because it was competing based on energy-capacity costs.

Storage X eliminated hydrogen storage at very low energy-capacity costs below ~10 \$/kWh, and power-capacity costs below ~1600 \$/kW (transition from the green to yellow regions in Figure 3.6b, and more clearly shown in Figure S3 where hydrogen and *Storage X* were the only 2 allowed storage technologies). Hydrogen duration was unconstrained unlike Li-ion, and thus the boundary defining costs at which *Storage X* eliminated hydrogen was not linear (Figure 3.6b, Figure S3), unlike the diagonal boundary defining costs at which *Storage X* eliminated Li-ion. Hydrogen storage has separate energy and power components, consisting of electrolyzers to produce hydrogen (1706 \$/kW), underground hydrogen energy storage (2 \$/kWh), and fuel cells to consume hydrogen (1415 \$/kW). Thus, *Storage X* was able to compete with hydrogen separately on energy- and power-capacity costs.

At the base case costs considered, there was a relatively small range of energy- and power-capacity costs at which *Storage X* can compete with both Li-ion batteries and hydrogen storage in least-cost systems (blue region in Figure 3.6b).

Given short-, mid-, and long-duration energy storage options in wind- and solar-based systems, the addition of long-duration energy storage reduced total system costs most compared to systems without storage.

Total system costs were reduced when mid- and long-duration storage was added to a system with only Li-ion battery storage. In Figure 3.4, a least-cost system with only Li-ion battery storage is the system with the highest total costs (Figure 3.4b, leftmost bar). The introduction of mid- and long-duration storage options reduces the cost of this system with only Li-ion battery storage (Figure 3.4b). This is in part due to the generation profile used

representing the contiguous U.S., which had high wind capacity factors. Almost all mid- and long-duration storage options modeled had independently sizable energy- and power-capacities, as well low energy-capacity costs relative to Li-ion batteries, which allowed for large energy-to-power ratios to accommodate for the seasonal variation in wind energy generation. Although metal-air batteries had a constrained energy-to-power ratio (100 h duration), they were modeled with a low total capital cost (20 \$/kWh) which allowed them to play a longer-duration storage role.

Total wind- and solar-based system costs were not substantially reduced when Li-ion battery storage was added to systems with mid- or long-duration storage. The addition of Li-ion battery storage to systems that otherwise only had mid- or long-duration storage did not substantially reduce system costs (Figure 3.4a vs. 3.4b). Notably, the addition of Li-ion battery storage to systems that otherwise only had long-duration storage also did not substantially reduce system costs (Figure 3.4b and 3.4d, leftmost bars). This is in part due to the Li-ion cost assumed representing currently available technology. The effective total cost for Li-ion batteries and mid- and long-duration storage technologies were closely balanced (Figure S2). Mid- and long-duration storage technologies also served shorter-duration energy storage roles (such as rapid charging and discharging), due to assumed power capacity costs that were similar to those of Li-ion. When Li-ion batteries were modeled with 4x lower costs than assumed in the base case, power capacity costs between storage categories were no longer closely balanced and Li-ion batteries outcompeted RFB, PSH, and gravity energy storage (Figure S5), unlike in the base case (Figure 3.4b).

In solar-only systems (Figure S6), the addition of mid- and long-duration storage did not reduce system costs as much as in wind-heavy systems (Figure 3.4). In solar-heavy systems, the addition of Li-ion batteries to systems that otherwise only had mid- and long-duration storage reduced system costs more than our base case scenario. Generation profiles dominated by solar generation have more daily variation in generation. Thus, Li-ion's slight advantage in lower power-capacity costs was more valuable.

Given our assumptions, mid-duration storage primarily competed with short-duration storage in wind- and solar- based systems (Figure 3.4). The range of energy- and power-capacity costs for which a hypothetical storage technology (*Storage X*) outcompeted Li-ion was much larger than the range for which it outcompeted hydrogen storage (Figure 3.6). However, candidate mid-duration storage technologies reduced costs of wind-solar-battery systems in systems where hydrogen storage was not modeled (Figure 3.4b; Table S3). The cost of different systems that included hydrogen storage or metal-air batteries were quite similar (Figure 3.4a and 3.4c). Systems without hydrogen storage or metal-air batteries were 0.020 – 0.044 \$/kWh more costly (Figure 3.4b). Only metal-air batteries had an energy-capacity cost low enough to play the role of long duration storage nearly as cost-effectively as hydrogen storage did (0.083 \$/kWh with hydrogen storage versus 0.086 \$/kWh with metal-air batteries; rightmost bar of Figure 3.4b, compared to bars in Figures 3.4a and 3.4c; Tables S2, S3 and S4). Without long-duration storage, wind generation costs increased substantially, leading to much higher system costs in Figures 3.4a and Figure 3.4b.

In least-cost systems, the unconstrained energy-to-power ratio of mid-duration storage changed depending on what other storage and generation technologies were included.

In our stylized wind- and solar-based electricity systems, mid-duration storage technologies had different energy to power ratios in least-cost systems depending on whether short-duration (Li-ion) or long-duration (hydrogen) storage was available (Figure 3.5, Figure S7, Figure S8, Figure S9). When Li-ion battery storage was not modeled, mid-duration storage technologies played the role of short-duration energy storage, at relatively little additional cost. When hydrogen storage was not modeled, mid-duration storage technologies played the role of long-duration energy storage, but at substantially higher costs. These results for wind- and solar-based systems in the U.S. are summarized in Table S2, Table S3, Table S4.

Most mid-duration storage technologies considered in our analysis had independently sizable energy and power-capacities that allowed for free discharge duration adjustment

depending on techno-economic characteristics of other generation and storage technologies in the system. Thus, the complementary storage duration dynamics illustrated in stylized least-cost systems may provide insight for mid-duration storage companies selecting energy-to-power ratios of their storage systems to meet an unfilled storage niche in a specific market.

Limitations of our model and results

The capacity build of storage technologies may be constrained by geographic, material, legal, political, and social considerations that have not been included in our model. For example, PHS requires geographic areas with elevated locations for water reservoirs and water access that may be difficult to secure, due to competing fresh water needs from agricultural, industrial, and household needs. Similarly, CAES and hydrogen-based hydrogen storage require underground salt caverns for energy storage. Because hydrogen fuel has a higher energy density relative to compressed air, CAES may be unable to compete with hydrogen storage for geologically constrained underground storage resources. However, it should be noted that many geographic constraints could be alleviated by long-distance electricity transmission, which has its own set of legal constraints. Other energy storage technologies like redox-flow battery, gravitational, thermal, and metal-air battery storage are not necessarily constrained by geologic features, but still require open space for building facilities that may be scarce in urban environments. Furthermore, energy storage technologies have material requirements that may subject them to supply chain constraints. For example, Lithium-ion batteries require Cobalt and Lithium, and iron-air batteries require vanadium and iron, respectively, as well as other Storage technologies also face other constraints, including permitting by local, state, and federal agencies. Redox-flow battery, gravitational, thermal, and metal-air battery storage require open space for building facilities that may be scarce in urban environments, potentially favoring technologies with smaller footprints, such as Li-ion batteries.

We considered systems that were 100% reliant on wind and solar generation. In comparison, when firm generators such as natural gas are available, storage capacity

deployed in least-cost systems were vastly lower (Figure S10). We only considered the role of storage technologies in grid-scale bulk storage services for electricity sector balancing, and not in other energy storage services such as ancillary, or transmission and distribution infrastructure services. Furthermore, our electricity system was modeled with a specified electricity demand time-series and did not explicitly model end uses or demand flexibility. Our model assumed cost-optimal allocation of technology assets and lossless transmission of electricity across the contiguous United States. Constraining the load-balancing region to smaller geographic areas may change the least-cost technology mix, due to different local generation and demand profiles. Smaller geographic area constraints may also increase storage capacity builds due to the decreased capability of transmission to balance the variability of wind and solar resources. In real-world, non-optimal conditions, these limitations imply the need for more storage capabilities than our model calculates.

3.4 Conclusions

We have analyzed competition between short-, mid-, and long-duration storage in systems reliant on wind and solar generation. We found that given short-, mid-, and long-duration energy storage options in wind- and solar-based systems, the addition of long-duration energy storage reduced total system costs most compared to systems without storage. Furthermore, the storage role played by this mid-duration technology depended on what other storage and generation technologies are available in the system. When assembling energy storage capacity builds in a particular market, the goal of having a low-cost reliable net-zero-emissions electricity system may be advanced by considering the complementary and competitive roles of different energy storage technologies.

3.5 Methods

Wind and solar generation data

Hourly capacity factors for solar and wind data for 2018 were generated using reanalysis data with a grid-cell resolution of 0.5° latitude by 0.625° longitude from the Modern-Era Retrospective analysis for Research and Application, Version 2 (MERRA-2).⁷⁵ Solar capacities of utility-scale photovoltaics were calculated for a single-axis tracking system with 0° – 45° of tilt. Wind capacity factors for geographic regions with the top 25% generation potential of land-based wind turbines were calculated assuming a General Electric 1.6–100 turbine with a 1.6 MW nameplate capacity.^{110,127,128}

Electricity demand data

Electricity demand data for the contiguous US were obtained from hourly data for 2018 from the EIA.¹¹² The EIA data were cleaned, and missing values were replaced using the multiple imputation by chained equations (MICE) method.⁷⁶

Cost and Technological Assumptions

The model formulation and detailed technology cost calculations are specified in Chapter 6.1 of the supplemental materials. Base case costs for solar and wind generation were taken from the NREL ATB report (Table 3.1).

Generation Technology	Technology Description	Total overnight cost (\$/kW)	Fixed O&M (\$/kW-yr)	Lifetime (years)	Capital Recovery Factor (%/yr)	Fixed Hourly Cost (\$/kW/h)	Variable Cost (\$/MWh)
Solar	Utility photo-voltaics	1391	23	30	8.06	0.015	0
Wind	Land-based wind turbines	1436	43	30	8.06	0.018	0

Table 3.1 Base Case Costs and Assumptions of Generation Technologies

Table 3.2 presents the base case costs, efficiencies, and other characteristics for storage technologies used in the model. Parameters for Li-ion batteries, redox-flow batteries (RFB), pumped storage hydro (PSH), thermal energy storage, compressed air energy

storage (CAES), and hydrogen storage were taken from a 2021 NREL analysis of long-duration energy storage technologies. Gravity energy storage parameters were taken from the Pacific Northwest National Laboratory's 2020 Grid energy Storage Technology Cost and Performance Assessment, with energy- and power-capacity costs separated by linear regression, using cost estimates for 1000 MW storage systems at various durations. Energy- and power-capacity costs for metal-air batteries were taken from press releases by Form Energy.

Li-ion batteries and metal-air batteries were each modeled using one total cost, because the energy-and power-components of these batteries are non-separable. Li-ion batteries were modeled with a duration of 4 hours due to technological constraints. Metal-air batteries were assumed to be iron-air batteries with a duration of 100 h.

RFB, PSH, and thermal energy storage were modeled with separate energy- and power-capacity components. Charging and discharging these technologies depends on the same technological component so only one power-capacity cost was used for each system. RFB costs were based on a vanadium-based redox flow battery. PSH was assumed to be a closed loop pumped hydro storage system using upper and lower water reservoirs. Thermal energy storage was modeled after a pumped-thermal energy storage system, utilizing molten-salt technology for heat storage.

CAES and hydrogen storage were modeled with separate energy- and power-capacity components, but charging processes were assigned different power-capacity costs than discharging processes. An adiabatic CAES (A-CAES) system was assumed, with air compressed into a salt dome cavern, the heat of compression stored in thermal energy storage, and power generated by reheating air with stored thermal energy. For hydrogen storage, PEM electrolyzers were assumed to split water, hydrogen was assumed to be stored underground in salt caverns, and hydrogen was combusted in PEM fuel cells to generate power. Hydrogen storage was conservatively described using a leakage rate

characteristic of hydrogen stored in pipelines, as opposed to the lower leakage rate that is likely characteristic of leakage out of salt caverns.

Storage Technology		Total overnight cost	Fixed O&M	Fixed property tax, insurance, licensing, permitting	Life-time	Capital recovery factor	Fixed Hourly Costs	Variable O&M	Decay rate	Round-Trip Efficiency	
Units		\$/kWh for energy \$/kW for power	% of capital cost or \$/kW/yr	% of capital cost	yrs	%/yr	\$/kWh/h for energy \$/kW/h for power	\$/MWh	-	%	
Li-ion Battery Storage ¹²⁹	Energy	326	4.2%	-	30	8.06	3.957×10^{-3}	0.0031	1% per month	86%	
	Power	251	8.5	1.5%							
RFB (Redox Flow Batteries) ¹²⁹	Energy	200	1.5%	-	30	8.06	1.867×10^{-3}	-	-	75%	
	Power	1412	8.4	1.5%			0.01414	0.0269	-		
PHS (Pumped Hydro Storage) ¹²⁹	Energy	105	1.5%	-	30	8.06	9.820×10^{-4}	-	-	81%	
	Power	1644	12.8	1.5%			0.01681	0.0003	-		
Gravity ¹³⁰	Energy	117	0.5%	-	49	7.26	1.033×10^{-3}	-	-	84%	
	Power	1416	11.8	-			0.01309	0.5125	-		
Thermal ¹²⁹	Energy	38	1.5%	-	30	8.06	3.530×10^{-4}	-	1.5% per day	52%	
	Power	1703	13.9	1.5%			0.01749	0.0033			-
A-CAES (Adiabatic Compressed Air Energy Storage) ¹²⁹	Charge Power	517	13.8	1.5%	30	8.06	0.006405	0	-	65%	
	Energy	51	1.5%	-			4.770×10^{-4}	-	-		
	Discharge Power	774	13.8	1.5%			0.008805	0.0033	-		
Metal-Air Battery Storage ¹³¹	Energy	2.4	4.2%	-	30	8.06	3.420×10^{-5}	-	-	46%	
	Power	656	16.4	-			0.007908	0	-		
Hydrogen storage (hydrogen-based Power-to-gas-to-power) ¹²⁹	Charge Power	1706	13.1	1.5%	30	8.06	0.01742	0.0013	0.1% per day	36%	
	Energy	2.0	1.5%	-			1.870×10^{-5}	-			-
	Discharge Power	1415	13.1	1.5%			0.01470	0.0028			-
Storage X	Energy	0.01 - 400	1.5%	-	30	8.06	9.339×10^{-8} - 0.003736	0	-	86%	
	Power	0.01 - 2000	0	1.5%			9.339×10^{-8} - 0.01868	0	-		

Table 3.2 Base Case Costs and Assumptions for Storage Technologies. Values in the same row are taken from the same source.

Chapter 4

TECHNO-ECONOMIC ANALYSIS OF HYDROGEN STORAGE COST AND EFFICIENCY IN DEEPLY DECARBONIZED WIND AND SOLAR ELECTRICITY SYSTEMS

Dowling, J. A.; Ruggles, T. H.; Reich, N. D.; Virguez, E. A.; Davis, S. J.; Li, A. X.; Rinaldi, K. Z.; Ifkovits, Z. P.; Kennedy, K. M.; Duan, L.; Caldeira, K.; Lewis, N. S. Techno-economic analysis of hydrogen storage cost and efficiency in wind and solar electricity systems. *In Preparation*.

4.1 Summary

We identify hydrogen storage system innovation priorities during a theoretical transition from natural-gas fired electricity systems to wind and solar electricity systems given the availability of different system characteristics, such as dispatchable power and zero-cost otherwise curtailed power. Current costs and inefficiencies of currently available hydrogen storage and conversion technologies led to wind and solar generation in excess of demand in reliable least-cost systems. In these cases with abundant otherwise-curtailed electricity, hydrogen storage systems were not highly sensitive to an efficient utilization of zero-cost electricity. However, system costs became increasingly sensitive to efficiency improvements as hydrogen storage and conversion capital costs decreased. For example, at current costs of hydrogen technologies, efficiency improvements beyond 36% decreased wind- and solar-based system costs by a maximum of 7%, but the magnitude of this response increased to 21% when hydrogen storage and conversion were modeled with zero capital cost. When natural gas was restricted to 15% of the total dispatch, underground hydrogen storage (\$2/kWh) participated in the least-cost system alongside wind, solar and batteries. Our results suggest that innovation priorities for hydrogen storage technologies should differ depending on the characteristics of the electricity system in which the technology is utilized, with some cases placing greater value on technology cost reductions and in other cases efficiency improvements.

4.2 Introduction

Hydrogen storage may provide reliable and lower-cost electricity in systems relying principally on wind and solar generation.^{4,120,129,132–137} Utility-scale hydrogen energy storage and conversion projects are expanding globally.^{138,139} For example, in the U.S., the Intermountain Power Project is co-located with Advanced Clean Energy Storage in Delta, Utah and will be the largest energy storage project in the world in terms of energy capacity, at 150,000 MWh.⁹ Electrolyzers (220 MW) will capture excess renewable energy when most abundant and drive hydrogen production for underground storage in salt caverns. When the facility comes online in 2025, stored gas will be converted to electricity using hydrogen-ready natural gas turbines (840 MW) that can combust 30% hydrogen but are to transition to 100% hydrogen by 2045 as technology develops. The Intermountain Power Agency's largest customer is the Los Angeles Department of Water and Power (LADWP). NREL's study on paths toward a 100% clean Los Angeles include pathways that rely on electrolytic hydrogen.¹⁴⁰ Hydrogen energy storage may be used to fill in primarily for the summertime lull in wind power when electricity demand for air conditioning in L.A. will also be high.

Hydrogen storage systems or Power-H₂-Power technology can provide a scalable approach to long-duration grid storage, facilitating compensation for interannual, seasonal and weather-related variability in wind and solar electricity generation. In Power-H₂-Power technology, hydrogen fuel is generated by electrolysis. The hydrogen is then stored in either geologic reservoirs or in above-ground tanks, and the stored hydrogen fuel is converted on demand to electricity using either fuel cells or turbines. Techno-economic analyses have shown that in reliable electricity systems based entirely on wind and/or solar generation with short-term energy storage provided by batteries, addition of hydrogen as a long-duration energy storage (LDES) technology lowers electricity system costs even at current costs for electrolyzers, hydrogen storage, and fuel cells.⁴ Compared to other storage options, underground hydrogen storage has very low energy capacity costs—the most

important attribute of long-duration (> 100 hour discharge duration) energy storage technologies.^{5,6,8,49}

In this work, we have evaluated which hydrogen storage and conversion technology innovations would have the greatest impact on system-wide electricity costs in an idealized electricity system based on wind and solar generation with batteries for short-term storage and hydrogen for long-term storage. Previous work examined the LDES design space and the ability of a LDES option to displace firm low-carbon generation sources such as nuclear power.^{5,8} However, the influence of hydrogen storage system component costs and round-trip efficiency on the overall system cost has not been characterized in wind and solar systems with varying quantities of zero-cost, otherwise-curtailed electricity. Herein, we examine the LDES design space in wind and solar only scenarios as well as high natural gas scenarios to establish upper and lower bounds on the influence of scarce or abundant otherwise-curtailed electricity, respectively, on optimal LDES parameters. We illustrate the fundamental dynamics and value of hydrogen storage system cost and efficiency improvements in electricity systems with various quantities of zero-cost electricity from excess wind and solar power and various constraints on dispatchable power from natural gas.

Innovations in hydrogen storage and conversion include reductions in the cost and changes in efficiency of the electrolyzer; storing the hydrogen underground in repurposed natural gas storage reservoirs; and use of 100% hydrogen fed turbines or polymer electrolyte membrane (PEM) fuel cells instead of molten carbonate fuel cells. The base case includes commercially available technology in 100% reliable wind-solar-battery-H₂ electricity systems (Table S1). We also assessed changes in the optimal capacity mix of wind, solar, hydrogen and batteries that would result from these innovations in a least-cost reliable wind/solar electricity system. We used historical hourly averaged wind and solar availability data derived from the MERRA-2 reanalysis weather data. Wind, solar, and storage dispatch balanced hourly historical electricity demand in the continental U.S. over one year (2018). A macro-scale electricity model was used to determine least-cost asset

capacities and dispatch schedules for fully decarbonized electricity systems with reliability as a strict constraint.^{4,16,77,141} As a simple proxy for a theoretical transition to reliable wind and solar electricity, we included a sensitivity study with increasingly restricted natural gas dispatch to evaluate carbon emissions reductions levels where hydrogen storage systems would participate in the system. Finally, we imposed constraints on underground hydrogen energy storage capacity and deliverability based on historical natural gas usage in the U.S. and investigated the impact on system cost and least-cost technology mix.

4.3 Results

The base case included commercially available technology for wind, solar, battery, and hydrogen storage systems (cost and performance assumptions in Table 1). Polymer electrolyte membrane (PEM) electrolyzers were used to convert electrical energy to hydrogen, which was stored in newly constructed salt caverns. PEM fuel cells were used to convert the stored hydrogen back into electricity. Power-H₂-Power was modeled with 36% round-trip efficiency in the base case representing currently available technology (Hunter et al, 2021). Other hydrogen storage and conversion technologies, such as depleted oil and gas reservoirs and hydrogen turbines, are available for blends of hydrogen and natural gas and are actively being developed for 100% hydrogen applications at scale (Table 2).

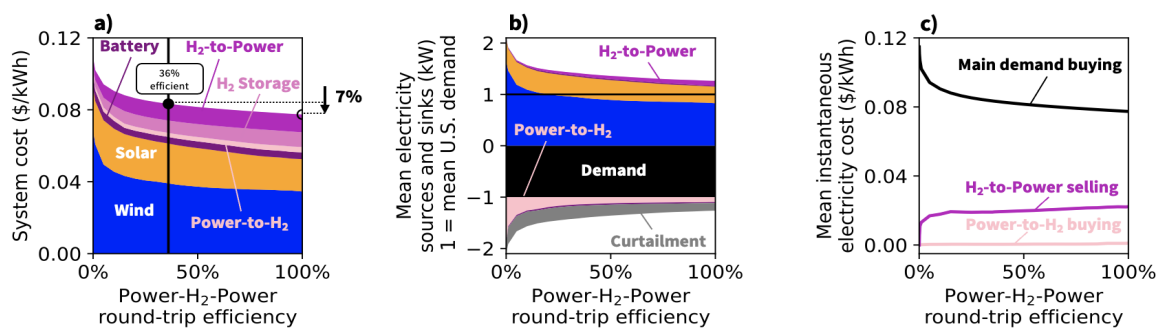


Figure 4.1 Despite low round-trip efficiency, hydrogen storage systems were valuable in wind and solar electricity systems. A) System cost contributions of each modeled technology (wind, solar, battery, H₂-to-Power, H₂ Storage, and Power-to-H₂) at base case costs for parameterized Power-H₂-Power round-trip efficiencies. Improvements in Power-H₂-Power efficiency from 36% to 100% would reduce the cost of wind- and solar-based systems by 7%. B) Mean annual dispatch of electricity sources to the grid (positive values) and electricity sinks from the grid (negative values) are balanced for parameterized Power-H₂-Power round-trip efficiencies. The black area represents end-use demand (as does the black line). Generation from wind and solar plus dispatch from hydrogen and battery storage is balanced by end-use demand, curtailment (gray

area), and charging of storage. Storage and conversion costs led to wind and solar generation in excess of demand and abundant curtailment in least-cost systems. C) Mean annual instantaneous electricity costs to hydrogen conversion technologies remained similar over widely parameterized Power-H₂-Power round-trip efficiencies. Hydrogen storage systems were not highly sensitive to efficient utilization of abundant zero-cost electricity.

Changes in hydrogen storage system round-trip efficiency on electricity system costs had little influence on overall system costs for least-cost systems optimized with base case assumptions (Figure 4.1). Hydrogen storage systems were valuable in wind and solar electricity systems, even under low round-trip efficiency assumptions. Improving the round-trip efficiency of hydrogen storage systems from 36% to 100% reduced wind-solar-battery-H₂ system costs only by about 7% (Figure 4.1A).

Wind and solar generation was substantially greater than mean demand in least-cost systems with currently available technology for hydrogen and batteries. In least-cost wind-solar-battery-H₂ systems, the cost of hydrogen storage systems (dominated by H₂-to-Power costs such as fuel cells) led to wind and solar generation that exceeded demand, even if hydrogen storage systems provided 100% round-trip efficiency (Figure 4.1B).

In all cases considered in Figure 4.1, wind and solar generation was substantially greater than mean demand, and there was curtailment of otherwise-wasted electricity in many hours. Power-to-H₂ technologies such as electrolyzers took advantage of abundant zero-cost electricity to drive hydrogen production (Figure 4.1C; Power-to-H₂ buying). H₂-to-Power technologies such as fuel cells sold electricity on demand at a higher cost than the electricity that produced hydrogen. To the extent that hydrogen storage systems were able to rely on available zero-cost electricity, the cost of electricity provided by hydrogen was not highly sensitive to efficiency of use of that zero-cost resource.

System costs became increasingly sensitive to Power-H₂-Power efficiency improvements as parameterized storage and conversion capital costs were decreased (Figure 4.2A). When Power-H₂-Power was modeled with zero capital cost, an efficiency improvement from 36% to 100% reduced system costs by 21%, driven by a reduction in wind and solar capacities

(Figure 4.2B, Figure 4.S1). Hydrogen storage system efficiency and cost improvements reduced wind and solar capacity and dispatch in excess of demand (Figure 4.2B). As hydrogen storage system capital costs decreased, therefore wind and solar generation was sized to mean demand in least-cost systems, the mean instantaneous cost of electricity driving electrolysis increased (Figure 4.2C). In most cases studied, hydrogen round-trip efficiency improvements beyond current (36%, white vertical lines Figure 4.2) led to substantially lower wind and solar dispatch and relatively constant capacities of hydrogen components (Figure 4.2B). In most cases, capital cost reductions increased hydrogen storage and conversion component capacities more than round-trip efficiency improvements beyond 36% (Figure 4.2D-F).

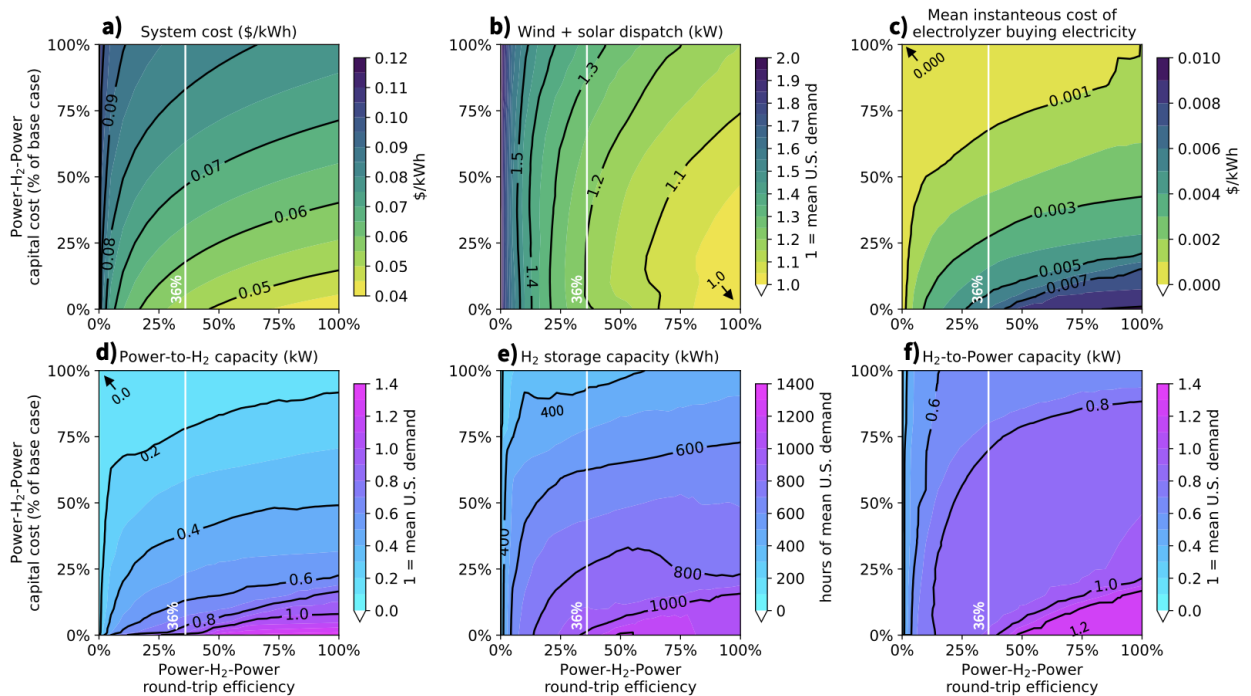


Figure 4.2 System costs were increasingly sensitive to efficiency improvements in hydrogen storage systems as their capital costs decreased. A) System cost for parameterized Power-H₂-Power round-trip efficiencies. When Power-H₂-Power was modeled with zero capital cost, improvements in hydrogen storage efficiency from 36% to 100% reduced the cost of wind- and solar-based systems by 21% (supported by Figure S1). B) Mean annual dispatch of wind and solar electricity sources to the grid per unit mean U.S. demand is plotted for parameterized Power-H₂-Power round-trip efficiencies. Hydrogen storage and conversion inefficiencies and costs led to wind and solar generation in excess of demand. C) Mean annual instantaneous electricity costs to Power-to-H₂ technologies such as electrolyzers increased as Power-H₂-Power capital costs decreased, but remained similarly low-cost over widely parameterized round-trip efficiencies. Hydrogen energy storage is not highly sensitive to efficient utilization of nearly zero-cost electricity especially in capital cost regimes where it is abundant. D-F) Displays capacities of Power-to-H₂, H₂ storage, and H₂-Power

technologies. Beyond 36% round-trip efficiency, corresponding to the efficiency, corresponding the efficiency in the base case (white vertical lines), Power-H₂-Power capacities increase more with capital cost reductions than efficiency improvements in wind and solar systems.

Under the assumption that deployed assets of least-cost systems are calculated de novo as a function of changes in either hydrogen capacity cost (Figure 4.3, left column) or hydrogen efficiency (Figure 4.3, right column) relative to the base case, the impact of various technology improvements on electricity system costs differ widely. Reductions in the cost of H₂-to-Power technologies had the largest impact on electricity system costs (Figure 4.3e). Relative to the base case, which assumed PEM fuel cells and storage in newly constructed salt caverns, the electricity system cost and asset mix in least-cost electricity systems was most sensitive to reductions in the cost of fuel cells and salt caverns. Base case electricity system costs were more sensitive to reductions in Power-H₂-Power capital costs (such as of PEM fuel cells and salt cavern storage) than to changes in efficiency (Figure 4.3, Figure 4.4). Hydrogen discharge efficiency improvements reduced system costs more than hydrogen charging efficiency improvements (Figure 4.4). However, hydrogen storage system innovation priorities were sensitive to base case cost and efficiency assumptions.

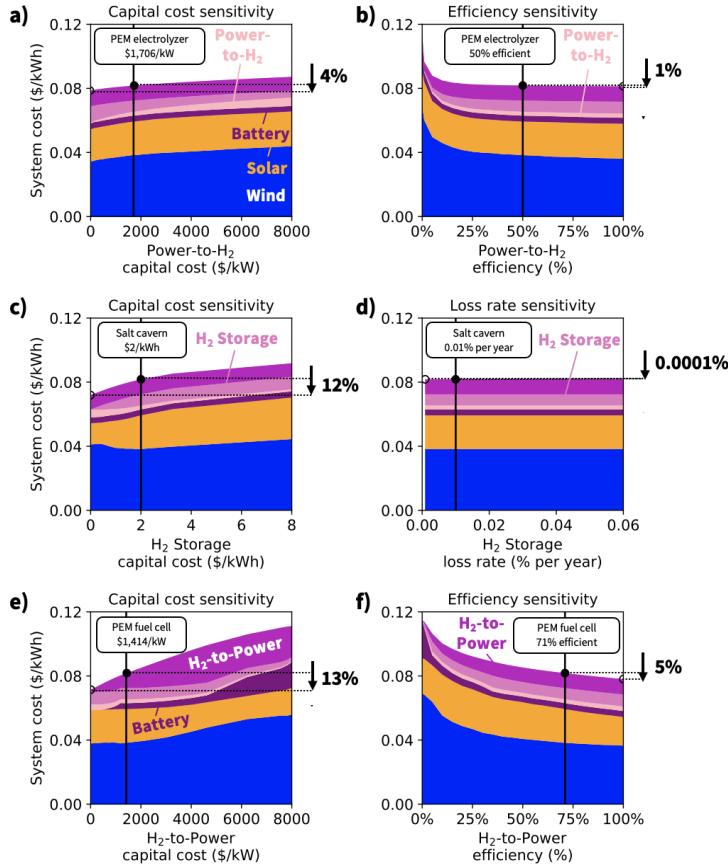


Figure 4.3 Value of innovation in base case hydrogen energy storage and conversion. Percentages show the system cost reduction from currently available hydrogen conversion and storage technologies (solid black line) to theoretical 100% efficient (right column) or zero capital cost technology (left column). The figure shows the system-wide impact of improvements or sacrifices in the cost or efficiency of hydrogen technologies (each row). Commercial technology compatible with 100% hydrogen includes energy stored in salt caverns and power conversion with polymer electrolyte membrane (PEM) electrolyzers and PEM fuel cells. System costs are disaggregated by contributions from modeled technologies including wind, solar, batteries, Power-to-H₂, H₂ storage, and H₂-to-Power (PEM fuel cell). Base case costs and efficiencies are listed in Table S1. System-wide electricity costs in the base case were more sensitive to hydrogen capital cost improvements (in panel c, energy capacity costs and in panel e, power capacity costs) than to efficiency improvements (panels b, d, f).

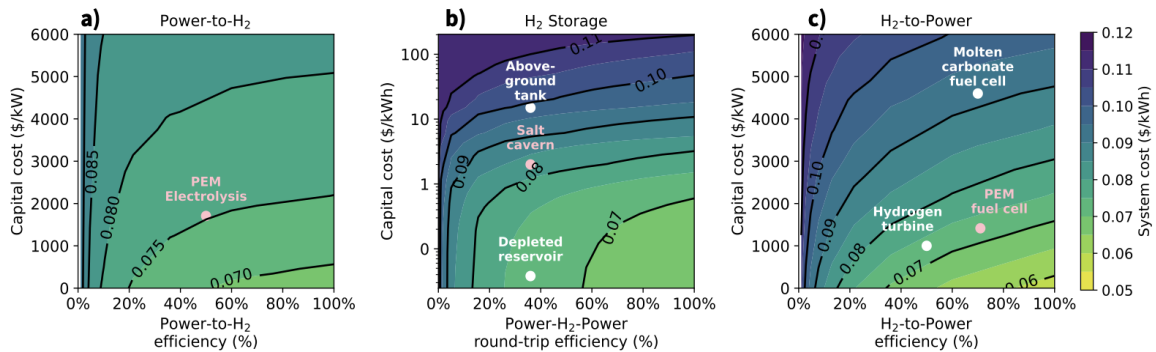


Figure 4.4 Trade-off between improvements in efficiency and capital cost of A) Power-to-H₂ technologies B) hydrogen storage technologies and C) H₂-to-Power technologies. Current costs and efficiencies of several technologies are shown for comparison. Contours of system costs show the total cost of a reliable wind-solar-battery-H₂, in panel A assuming that H₂-to-Power costs reflect current PEM fuel cells and in panel C assuming that Power-to-H₂ costs reflect current PEM electrolysis. Contours of system costs in panel B show the trade off between H₂ storage capital cost and Power-H₂-power round-trip efficiency assuming costs reflecting current PEM electrolysis and PEM fuel cells. In most cases considered, capital cost improvements were more important for reducing system cost than efficiency improvements.

The system costs of various technological options for hydrogen storage and conversion were lower relative to a system without hydrogen storage systems, and higher than a system with only natural gas (Figure 4.5). Compared to aboveground storage in tanks, underground hydrogen storage (i.e., depleted oil & gas reservoir) substantially reduced system costs compared to wind-solar-battery only systems as much as ~40%. Natural gas dispatch was increasingly restricted as a simple proxy for a theoretical transition from carbon-intensive to carbon-free electricity systems (Figure 4.6). Hydrogen with aboveground storage in tanks was deployed in least-cost systems when natural gas dispatch was limited to only 5% of total power. The most cost-effective hydrogen technologies utilized underground storage with PEM fuel cells or H₂-turbines. In these scenarios, hydrogen storage systems became a substantial part of electricity capacity, costs, and dispatch in the last 50-15% of power provided otherwise by natural gas (Figure 4.6). Hydrogen turbines were more valuable in systems with natural gas than PEM fuel cells because capital cost improvements were more important than roundtrip efficiency improvements under this regime (Figure 6d-f vs. Figure 4.6g-i). When natural gas dispatch was constrained to 5% of total dispatch in wind- and solar-based systems, hydrogen storage system efficiency improvements from 36% to 100% only improved system costs by about 4% (Figure S2). When natural gas capacity was available to provide dispatchable power (even in small portions of total dispatch), wind and solar system costs were not sensitive to improvements in hydrogen energy storage system efficiency relative to base case assumptions.

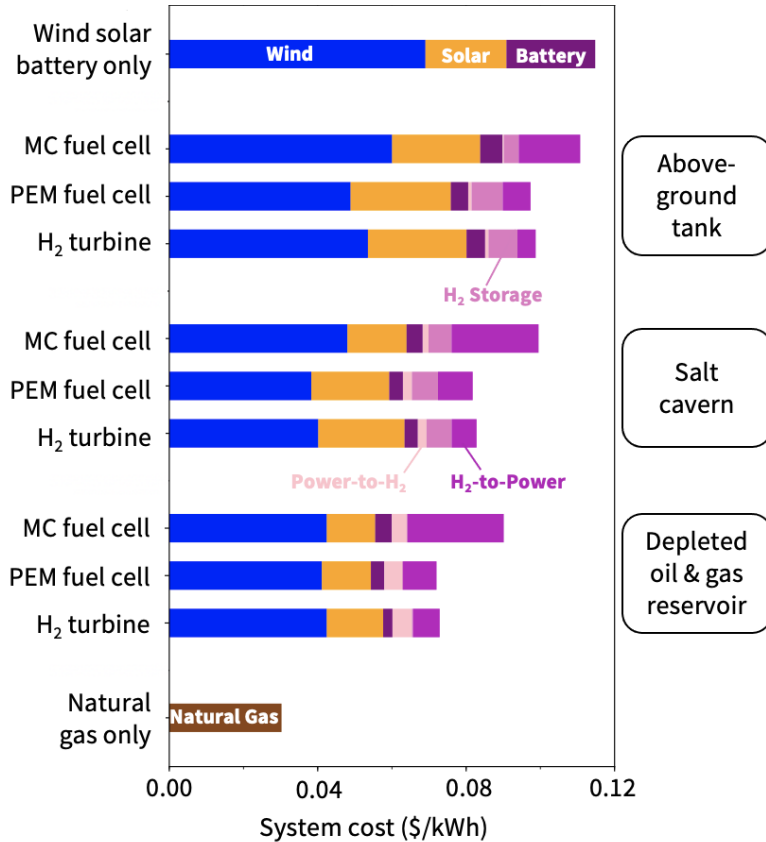


Figure 4.5 System costs of various technology options for hydrogen energy storage and conversion. Hydrogen can be stored above-ground in tanks or underground in salt caverns or depleted oil and gas reservoirs. H₂-to-Power technology options include molten carbonate (MC) fuel cells, polymer electrolyte membrane (PEM) fuel cells, and 100% H₂ turbines. The cost and efficiencies of hydrogen technology options are listed in Table S2. Compared to other hydrogen technology options, wind-solar-battery system costs improved most with underground hydrogen storage paired with either PEM fuel cells or 100% H₂ turbines.

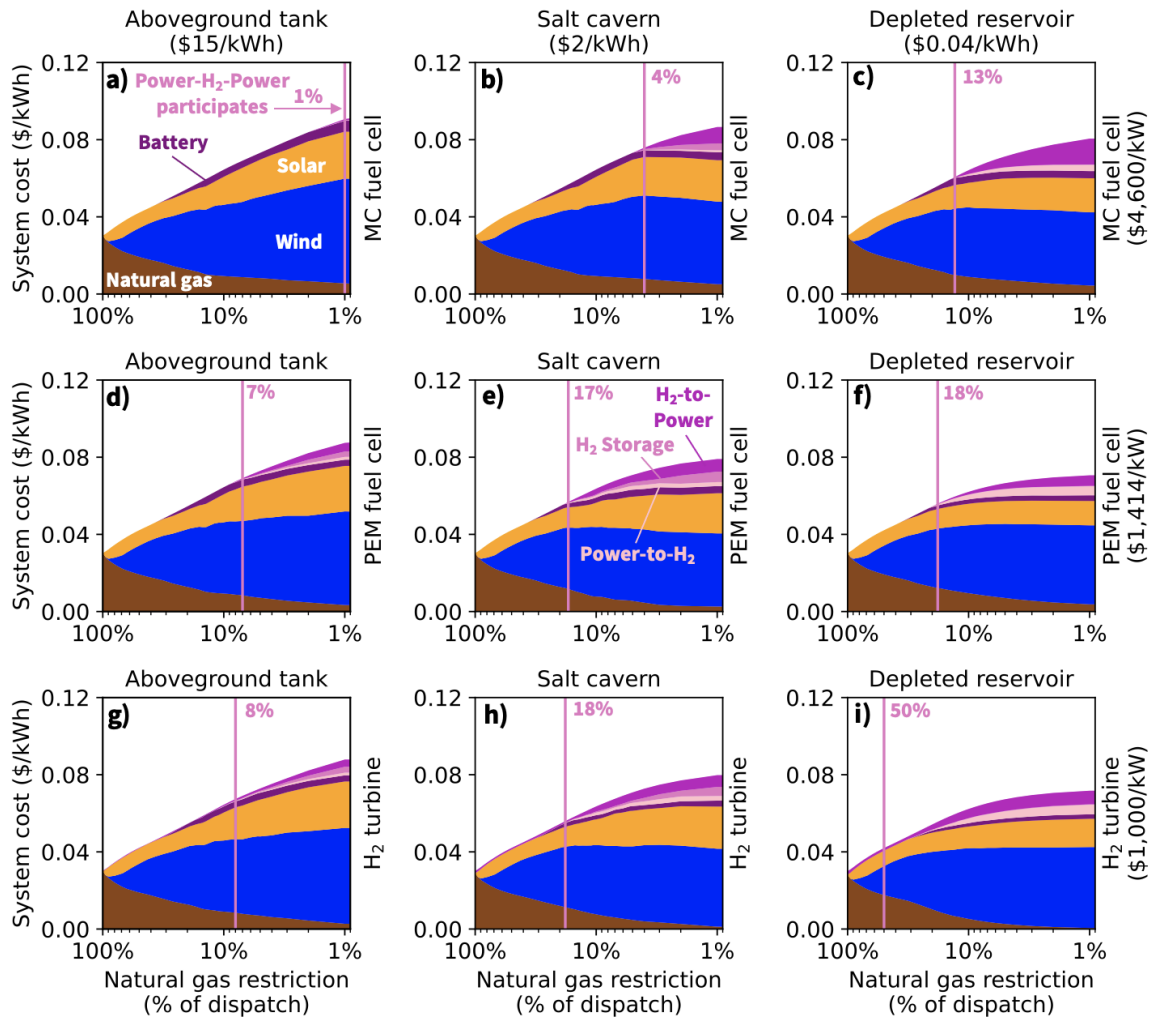


Figure 4.6 Parametrized natural gas restrictions show the value of various Power-H₂-Power technologies in deeply decarbonized wind- and solar-dominated systems. Natural gas total dispatch over the simulation period varied from unconstrained (100%) to partially restricted, to completely eliminated (0%) in wind-solar-battery-H₂ electricity systems. Pink vertical lines indicate the minimum natural gas restriction at which Power-H₂-Power technologies participated in least cost systems. Participation is defined here as when Power-H₂-Power comprised at least 2% of total system cost. The nine panels (a-j) show technology combinations of three hydrogen storage options (aboveground tanks, \$15/kWh; salt caverns, \$2/kWh; depleted oil and gas reservoirs, \$0.04/kWh) and three H₂-to-Power options (molten carbonate (MC) fuel cells, \$4,600/kW; polymer electrolyte membrane (PEM) fuel cells \$1,414/kW; and hydrogen turbines, \$1,000/kW). In the base case representing currently available technology (salt cavern + PEM fuel cell), Power-H₂-Power participated in least-cost systems when natural gas dispatch was restricted to 17% of total.

When underground hydrogen storage volume or deliverability was constrained based on historic natural gas usage, the capacity of hydrogen storage decreased substantially, but it remained valuable in wind-solar-battery-H₂ systems (Figure 4.7, Table S3).^{142–144} At 2018 demand levels in the U.S., repurposing for hydrogen storage 65% of depleted oil and gas

reservoirs currently in use for natural gas storage provided energy capacity for national-scale seasonal energy storage in a reliable 100% wind and solar system.

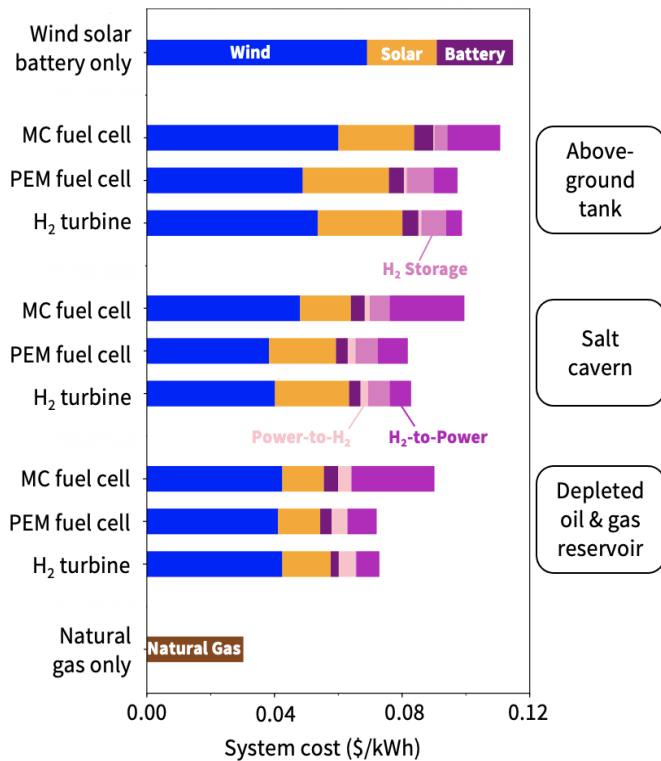


Figure 4.7 Modeled restrictions on underground capacity and deliverability based on historic natural gas usage. Underground hydrogen storage capacity available (based on current natural gas facilities) is 500 billion cubic feet (Bcf) in salt caverns, and 4,000 Bcf in depleted oil and gas reservoirs at normal conditions.¹⁴³ In a least-cost system modeled with 2018 demand in the U.S., 2,500 Bcf provided national-scale seasonal H₂ storage in 100% reliable wind and solar based systems. Deliverability of hydrogen storage was restricted based on historic natural gas max injection (132 Bcf/week) and withdrawal (359 Bcf/week) during 2010-2021. Table S3 shows modeled hydrogen restrictions. In least-cost systems with unconstrained injection/withdrawal, polymer electrolyte membrane (PEM) fuel cells, and the volume of hydrogen storage in depleted reservoirs restricted to historical natural gas values, only 65% of the maximum allowed storage capacity was used.

4.4 Discussion

Underground hydrogen energy storage may provide reliability beyond 85% emissions reduction in wind and solar based electricity systems.

Many states in the U.S. have recently adopted clean electricity mandates for the midcentury that require them to transition towards net-zero emissions electricity systems. Given the variable nature of solar and wind generation, and as policy constrains carbon emissions, other clean firm or dispatchable technologies, such as nuclear, hydrogen, or natural gas with carbon capture and storage, may be essential to provide reliability. Results herein show that unconstrained underground storage (e.g., depleted oil and gas reservoirs) with PEM fuel cells or hydrogen turbines allowed hydrogen storage systems to reduce the last

15% of carbon emissions. Hydrogen storage systems may be increasingly valuable for providing reliability in the years prior to mid-century.

When natural gas was restricted to 5% of the total dispatch in wind- and solar-based systems, fuel cell capital cost reductions were the highest innovation priority for hydrogen storage systems (Figure S3). Our results assume 100% efficient and unregulated markets. The economic incentives included in the Inflation Reduction Act (IRA) in the form of technology neutral investment tax credits (ITC) could accelerate capital costs reductions in hydrogen conversion and storage technologies such as electrolyzers and hydrogen storage.^{145–147} At base case assumptions, electrolyzer capital costs were not the system cost bottleneck for hydrogen storage applications in deeply decarbonized wind and solar dominated electricity systems.

Improvements in capital costs of commercially available hydrogen conversion and storage technologies were more valuable than round-trip efficiency improvements for applications in deeply decarbonized wind and solar electricity systems.

Hydrogen energy system technologies are rapidly improving.¹⁴⁸ Improvements in excess of 36% in the round-trip efficiency of hydrogen storage systems did not substantially impact electricity system costs in optimized least-cost wind-solar-battery electricity systems. This is important for design and selection of hydrogen conversion technologies such as electrolyzers, fuel cells, and turbines because in most cases, capital cost reductions are favored even if they come at the penalty of reductions in conversion efficiency. In wind and solar systems, electrolyzers can take advantage of otherwise curtailed zero-cost electricity, but fuel cells meet load during times of high cost electricity, such as during wind and solar droughts.^{2,16} In agreement with other analyses, we find that hydrogen discharge efficiency improvements reduce system costs more than hydrogen charging efficiency improvements.^{5,8} However, we found that hydrogen innovation priorities were sensitive to the cost and efficiency assumed in the base case as well as to the types of generation technologies included.

Electricity system costs were still relatively insensitive to hydrogen storage system round-trip efficiency improvements, even when 5% natural gas dispatch was allowed in the system alongside wind, solar, batteries, and hydrogen (Figure S1). However, if hydrogen energy storage and conversion were free, Power-H₂-Power efficiency improvements would substantially reduce the cost of wind and solar electricity systems, primarily due to cost savings from avoided wind and solar generation. In modeled simulations, wind and solar generation are optimized de novo for each change in hydrogen storage system efficiency. If wind and solar generation were not allowed to reoptimize, system cost would increase.

Underground hydrogen storage constraints indicate that depleted oil and gas reservoirs may beneficially be repurposed for hydrogen storage.

Given the limited capacity of existing salt caverns, hydrogen storage test sites in more abundant depleted oil and gas reservoirs could beneficially be investigated and developed. Fuel switching 65% of current underground natural gas storage capacity (in depleted oil and gas reservoirs) to hydrogen storage capacity provided adequate energy capacity for national-scale seasonal energy storage in a reliable wind and solar system based on 2018 demand in the US. However, hydrogen deliverability restrictions based on historical natural gas usage severely constrained energy capacity in least-cost systems (Figure 4.7). System costs were insensitive to leakage rates in storage reservoirs (Figure 4.3d). Additionally, increased hydrogen leakage associated with increasing underground storage injection/withdrawal rates did not increase system costs, so other policies or incentives beyond cost could discourage hydrogen leaks.

Our results indicated that injection and withdrawal rates were critically important to the value of underground hydrogen storage systems in low-carbon energy systems (Figure 4.6). Given that we used historical injection and withdrawal rates based on natural gas and that data for hydrogen systems of this size is not currently available, we leave a comprehensive techno-economic analysis of underground hydrogen storage injection and withdrawal rates to future studies.

Model architecture changes

Although this study focused primarily on an idealized electricity system, hydrogen fuel could also be coupled to other sectors and used for heating/air conditioning, or heavy-duty transportation such as shipping.⁶² Cross-sector couplings can substantially reduce the cost of delivered power in electricity systems with high contributions from renewable generation.¹⁴⁹ Deployment of other carbon-neutral firm generators such as nuclear, geothermal, or natural gas with carbon capture and storage is expected to reduce the amount of long-duration storage required for reliable systems.^{5,8} Electrification of other sectors such as heating and transportation could increase the demand for storage. Flexible loads such as hydrogen fuel production or electric vehicle charging with curtailed generation may reduce the availability of zero-cost electricity in wind and solar systems.¹⁶ In addition to other types of flexibility, long-duration storage with hydrogen is an option that would help facilitate an affordable transition to meet high wind and solar mandates, and reliable carbon-free electricity.¹⁴⁹

4.5 Conclusions

We analyzed the tradeoff between capital cost reductions and efficiency improvements of hydrogen conversion and storage in different electricity systems with varying levels of dispatchable fossil power and otherwise-curtailed wind and solar generation. In the systems featuring abundant zero-cost electricity (resulting from wind and solar generation exceeding mean demand), hydrogen storage systems were not highly sensitive to an efficient utilization of otherwise-curtailed power, but they were sensitive to capital cost reductions.

Hydrogen storage systems decreased costs of reliable wind and solar electricity systems, even at very low round-trip efficiencies. Reducing current capital costs of hydrogen energy storage and conversion reduced wind- and solar-based system costs more than round-trip efficiency improvements. Capital cost reductions (such as in underground storage and fuel cells) allowed hydrogen storage systems to complement reliable, wind- and solar-based systems.

4.6 Methods

Wind and solar generation data

Hourly capacity factors for solar and wind data in the U.S. for 2018 were generated using reanalysis data with a grid-cell resolution of 0.5° latitude by 0.625° longitude from the Modern-Era Retrospective analysis for Research and Application, Version 2 (MERRA-2).⁷⁵ Solar capacities of utility-scale photovoltaics were calculated for a single-axis tracking system with 0°–45° of tilt. Wind capacity factors for geographic regions with the top 25% generation potential of land-based wind turbines were calculated assuming a General Electric 1.6–100 turbine with a 1.6 MW nameplate capacity.^{110,127,128}

Electricity demand data

Electricity demand data for the contiguous US were obtained from hourly data for 2018 from the EIA.¹¹² The EIA data were cleaned, and missing values were replaced using the multiple imputation by chained equations (MICE) method.⁷⁶

Cost and technological assumptions

The macro-scale energy model formulation and detailed technology cost calculations are specified in Chapter 6.1 of the supplemental materials. Base case techno-economic assumptions are listed in Table 1. Various hydrogen energy storage and conversion technology cost and performance assumptions are in Table 2.

	Power-to-H ₂	H ₂ Storage	H ₂ -to-Power	Battery Storage		Wind	Solar
Assumptions from Hunter et al., 2021¹²⁹ unless otherwise noted.							
Technology description	PEM electrolysis	Under-ground salt cavern	Stationary PEM fuel cell	Li-ion battery with coupled energy and power and a 4-hour charging time		Wind turbines, onshore	Solar PV, single axis tracking
Technology type	Conversion	Storage	Conversion	Storage	Conversion	Generation	Generation
Capacity (fixed) cost type	Power capacity (\$/kW)	Energy capacity (\$/kWh)	Power capacity (\$/kW)	Energy capacity (\$/kWh)	Power capacity (\$/kW)	Power capacity (\$/kW)	Power capacity (\$/kW)
Capacity (fixed) cost	1706.46	1.9992	1414.74	326.4	250.92	1436	1391
Project life (years)	30	30	30	30	30	30	30
Discount rate	0.07	0.07	0.07	0.07	0.07	0.07	0.07
Capital recovery factor (%/yr)	8.06%	8.06%	8.06%	8.06%	8.06%	8.06%	8.06%
(\$/kW-yr, \$/kWh-yr)	13.056	0.0299	13.056	27.4187	28.9901	43	23
Efficiency	50%	-	70%	-		-	-
	36% round-trip efficiency			86% round-trip efficiency		-	-
Loss rate	-	0.01 % per yr (1.14e-8 fraction/hr)	-	12.1% per yr (1.38e-5 fraction/hr)		-	-
Annualized capital costs paid hourly							
Fixed cost	0.01742 \$/kW/h	0.00002 \$/kWh/h	0.00103 \$/kW/h	0.00395 \$/kWh/h		0.01812 \$/kW/h	0.01542 \$/kW/h
Variable cost	0.000 \$/kW/h	0.000 \$/kWh/h	0.000 \$/kW/h	0.000 \$/kWh/h		0.000 \$/kW/h	0.000 \$/kW/h

Table 1. Base case costs and efficiencies.

	Power-to-H ₂	H ₂ Storage	H ₂ Storage	H ₂ Storage	H ₂ -to-Power	H ₂ -to-Power	H ₂ -to-Power
Assumptions from Hunter et al., 2021¹²⁹ unless otherwise noted.							
Technology description	PEM electrolysis, compression	Under-ground salt cavern	Above-ground tank	Under-ground depleted reservoir	Stationary PEM fuel cell	Molten carbonate fuel cell	Combustion turbine, 100% H ₂ , (for 2050)
Technology type	Conversion (produce H ₂)	Storage (of H ₂)	Storage (of H ₂)	Storage (of H ₂)	Conversion (consume H ₂)	Conversion (consume H ₂)	Conversion (consume H ₂)
Capacity (fixed) cost type	Power capacity (\$/kW)	Energy capacity (\$/kWh)	Energy capacity (\$/kWh)	Energy capacity (\$/kWh)	Power capacity (\$/kW)	Power capacity (\$/kW)	Power capacity (\$/kW)
Capacity (fixed) cost	1706.46	1.9992	15	0.038	1414.74	4600	1000
Project life (years)	30	30	30	30	30	30	30
Discount rate	0.07	0.07	0.07	0.07	0.07	0.07	0.07
Capital recovery factor (%/yr)	8.06%	8.06%	8.06%	8.06%	8.06%	8.06%	8.06%
Fixed O&M cost (\$/kW-yr, \$/kWh-yr)	13.056	0.0299	0.018	27.4187	13.056	18.61	13.74
Efficiency	50%	-	-	-	71%	70%	50%
Loss rate (%/yr, fraction/h)	-	0.01 %/yr (1.14e-8 frac/h) ⁷¹	0.01 %/yr (1.14e-8 frac/h)	0.035 %/yr (3.99e-8 frac/h) ¹⁴⁴	-	-	-
Annualized capital costs paid hourly							
Fixed cost	0.01742 \$/kW/h	1.866e-5 \$/kWh/h	0.00014 \$/kWh/h	3.613e-7 \$/kWh/h	0.00103 \$/kW/h	0.0444 \$/kW/h	1.0768e-2 \$/kW/h
Variable cost	0.000 \$/kW/h	0.000 \$/kWh/h	0.000 \$/kWh/h	0.000 \$/kWh/h	0.000 \$/kW/h	0.000 \$/kW/h	0.000 \$/kW/h

Table 2. Hydrogen energy storage and conversion technology options.

Chapter 5

LONG-TERM DURABILITY OF CHEMICAL VAPOR DEPOSITED $Mn_ySb_{1-y}O_x$ ELECTROCATALYSTS FOR WATER OXIDATION IN ACIDIC MEDIA

Dowling, J. A.*; Ifkovits, Z. P.*; Carim, A. I.; Evans, J. M.; Swint, M. C.; Ye, A. Z.; Richter, M. H.; Li, A. X.; Lewis, N. S. Long-term durability of chemical vapor deposited $Mn_ySb_{1-y}O_x$ electrocatalysts for water oxidation in acidic media. *In Preparation*.

5.1 Summary

Earth-abundant oxygen evolution electrocatalysts may be suitable replacements for Ir, despite lower activity, in proton exchange membrane electrolyzers for H_2 for energy storage in reliable wind and solar systems. Manganese antimonate ($Mn_ySb_{1-y}O_x$) catalysts were synthesized via a new chemical vapor deposition route and the electrochemical stability and activity were assessed on fluorine-doped tin oxide (FTO). Multi-day durability of Mn-rich, rutile compositions of $Mn_ySb_{1-y}O_x$ catalysts were demonstrated. $Mn_{0.63}Sb_{0.37}O_x/FTO$ catalysts maintained steady oxygen-evolution reaction (OER) overpotential of 687 ± 9 mV for 168 h at 10 mA cm^{-2} in 1 M H_2SO_4 with $> 97\%$ Faradaic efficiency. Time-dependent anolyte composition analysis indicated steady dissolution of both Mn and Sb metals over time.

5.2 Introduction

The electrochemical oxygen-evolution reaction (OER) is an anodic process that oxidizes water, an abundant feedstock, and can supply electrons necessary to drive many fuel-forming cathodic processes including the production of H_2 from H_2O , NH_3 from N_2 , and hydrocarbons from CO_2 . Water electrolysis for H_2 generation specifically is of interest in the storage of energy from intermittent renewable sources. Carbon-free electricity can drive water electrolysis to generate green H_2 for use on demand. Proton exchange membrane (PEM) electrolyzers utilizing acidic electrolytes may complement wind and solar

electricity better than alkaline-based technologies because PEM electrolyzers can ramp-up faster to extract intermittent power from variable electricity.^{150–152} Commercial PEM electrolyzers utilize Ir-based catalysts to drive the oxygen-evolution reaction (OER) in acidic media which supplies the necessary electrons to drive H₂ generation. IrO_x exhibits high activity for the oxygen evolution reaction (OER) but corrodes in acid and degrades over time.¹⁵³ Furthermore, the low abundance of Ir represents a bottleneck for the scale-up of PEM electrolyzers.¹⁵⁴ An earth-abundant, but less-active PEM electrocatalyst may be an acceptable replacement for a more-active, precious metal catalyst in scenarios with infrequent electrolyzer use and low-cost electricity.¹⁵⁵ Compared to industrial chemical feedstock applications for H₂ that maintain high capacity factors (up times > 97%), electrolyzers paired with seasonal or multi-year H₂ storage in reliable wind and solar systems may operate at lower capacity factors (~ 50%) and benefit from times of abundant, otherwise-curtailed, zero-cost electricity to drive electrolysis.^{4,16,155} Earth-abundant catalysts that are less-active than IrO_x thus may be specifically valuable for long-duration H₂ storage applications in reliable wind and solar electricity systems.

A variety of earth-abundant catalysts have shown promise for acid-stable water-splitting including Mn-oxyhalides, arc melted Ni₂Ta electrodes, Co-doped Fe₂O₃ thin films, and N₂-doped W-carbide nanoarrays.^{156–159} Various Mn-oxides have shown promising activity for catalyzing water oxidation across a large range of electrolyte pH. However, in acidic electrolytes, Mn-oxides corrode, leading to poor long-term performance. Sb-oxides are stable in acidic electrolytes but do not effectively catalyze the OER. Earth abundant metal antimonates such as Mn_ySb_{1-y}O_x, have been recently demonstrated to catalyze the OER with promising activity and stability.^{160–164} Sb has been shown to stabilize other metals beyond Mn, such as in (Co, Mn, Ni, Fe, Ru)SbO_x oxides.¹⁶³ The (Mn-Co-Ta-Sb)O_x material family for acid-stable OER was initially discovered via high-throughput experiments, but initial unannealed candidates corroded in acid.¹⁶⁵ A high annealing temperature such as 700 °C effected rutile crystallinity in (Ni-Mn-Sb)O_x catalysts, and the catalysts maintained stable overpotential during weeklong galvanostatic operation at 10 mA cm⁻² in strong acid.¹⁶¹ Mn-rich catalysts within the rutile window of the Mn:Sb composition space in

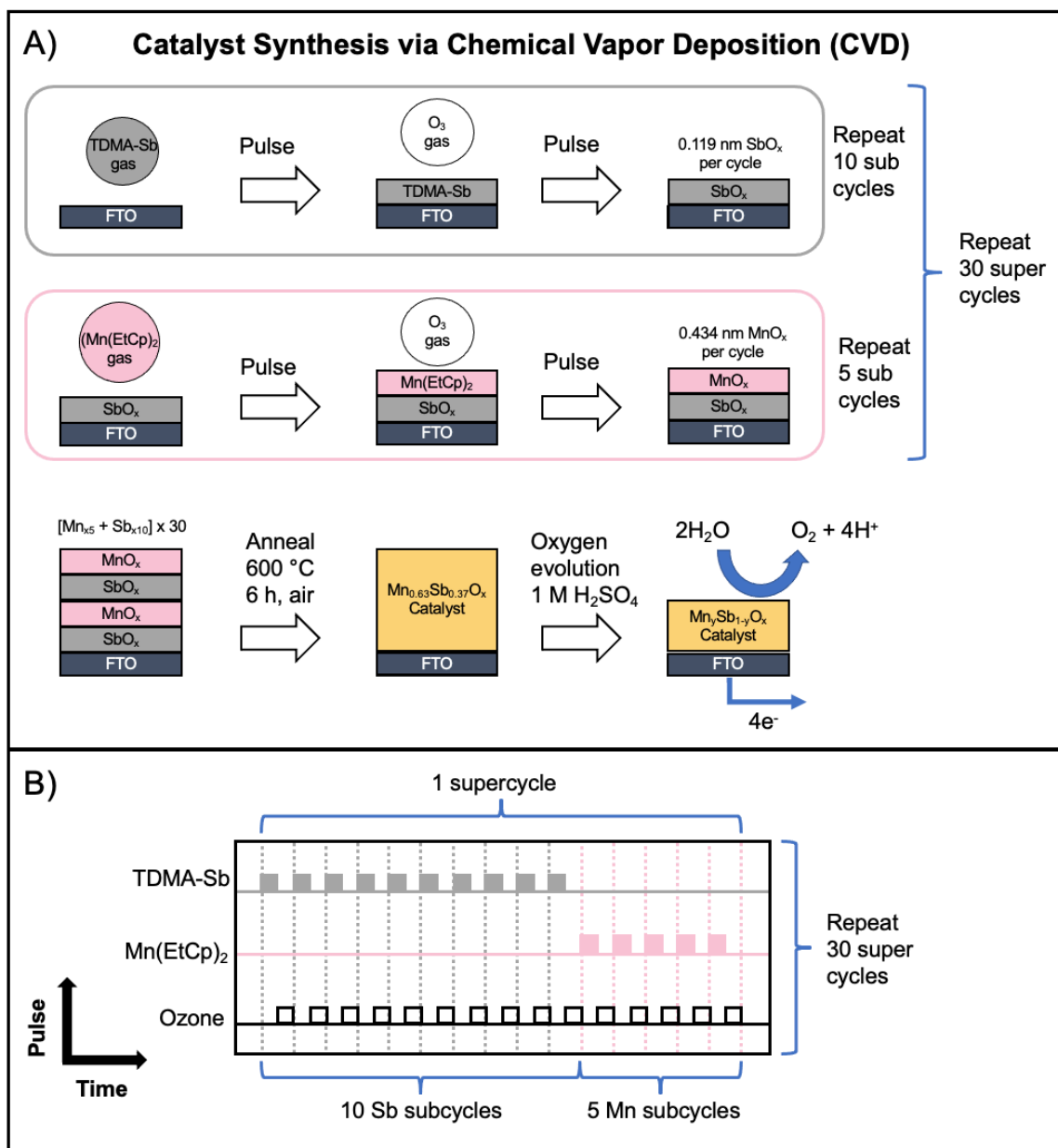
$\text{Mn}_y\text{Sb}_{1-y}\text{O}_x$ catalysts were more active and stable than Mn-poor catalysts with compositions outside the rutile window.¹⁶² Mn-rich, rutile $\text{Mn}_y\text{Sb}_{1-y}\text{O}_x$ powders were active in decoupled water-splitting had a $\sim\text{Mn}^{3+}$ oxidation state in the rest state.¹⁶⁴ Multi-day durability during continuous galvanostatic operation has not yet been evaluated for Mn-rich, rutile $\text{Mn}_y\text{Sb}_{1-y}\text{O}_x$ catalysts.

In this work, $\text{Mn}_{0.63}\text{Sb}_{0.37}\text{O}_x$ was synthesized via a chemical vapor deposition (CVD) method and the electrochemical performance and stability was benchmarked. CVD is a scalable method and may be an effective solution for coating high surface area carbon supports in the catalyst layers of a PEM electrolyzer. This method complements previous synthetic routes for generation of $\text{Mn}_y\text{Sb}_{1-y}\text{O}_x$ including sputtering, bulk powder-mixing, and electrodeposition.^{160–162,164} The specific material stoichiometry is Mn-rich and within the composition space that crystallizes in a rutile lattice. Multi-day durability during continuous galvanostatic operation has not yet been previously evaluated for such a composition. Long-term activity and stability compared to other established synthesis methods was evaluated via analysis of oxygen evolution for one week during continuous chronoamperometry in strong acid.

5.3 Results and Discussion

$\text{Mn}_y\text{Sb}_{1-y}\text{O}_x$ catalysts were synthesized via chemical vapor deposition (CVD) on fluorine-doped tin oxide (FTO) substrates, annealed in air for 6 h at 600 °C, and subsequently evaluated for the OER in 1 M H_2SO_4 (Scheme 5.1A). The ternary chemical vapor deposition process combined two single oxide deposition recipes (Scheme 5.1B).¹⁶⁶ Each chemical vapor deposition subcycle included one precursor pulse from either tris(dimethylamido)antimony(III) (TDMA-Sb) or bis(ethylcyclopentadienyl)-manganese ($\text{Mn}(\text{EtCp})_2$) and one ozone co-reactant pulse. $\text{Mn}_{0.63}\text{Sb}_{0.37}\text{O}_x$ thin films were deposited via 30 supercycles of 10 SbO_x subcycles and 5 MnO_x subcycles (Scheme 5.1B). Single oxide deposition growth rates of both MnO_x and SbO_x were measured via ellipsometry (Figure 5.1A). MnO_x thickness increased linearly with pulse duration indicating controlled chemical vapor deposition, whereas SbO_x thickness was constant and insensitive to pulse

duration indicating self-limiting atomic layer deposition.¹⁶⁷ A 0.33 sec pulse of $\text{Mn}(\text{EtCp})_2$, which corresponded to 0.434 nm MnO_x per cycle, and a 1 sec pulse of TDMA-Sb, which corresponded to 0.119 nm SbO_x per cycle, were utilized. The composition of as-deposited, unannealed catalyst was determined by dissolving it in 1 M H_2SO_4 acid for several days and analyzing it by inductively coupled plasma mass spectrometry (ICP-MS) was $\text{Mn}/(\text{Mn}+\text{Sb}) = 0.63 \pm 0.01$. The as-deposited catalyst composition was Mn-rich: $\text{Mn}/(\text{Mn}+\text{Sb}) > 0.5$ and within the pre-established rutile window: $\text{Mn}/(\text{Mn}+\text{Sb}) = 0.3$ - 0.7 .¹⁶² The as-deposited catalyst was annealed in air for 6 h at 600 °C, the maximum tolerable temperature for the TEC8 FTO substrate. In agreement with previous literature, a high temperature anneal allowed $\text{Mn}_{0.63}\text{Sb}_{0.37}\text{O}_x$ to crystallize.^{161,162} Grazing incidence X-ray diffraction (GIXRD) of annealed $\text{Mn}_{0.63}\text{Sb}_{0.37}\text{O}_x/\text{FTO}$ catalysts and FTO substrates indicated rutile crystallinity (Figure 5.1B). Reflections at $2\theta \approx 27, 35, 53,$ and 56° indicated rutile MnSb_2O_6 .^{161,162,164}



Scheme 5.1 (A) $\text{Mn}_{0.63}\text{Sb}_{0.37}\text{O}_x$ synthesis process via chemical vapor deposition and annealing. (B) Ternary chemical vapor deposition with TDMA-Sb and $\text{Mn}(\text{EtCp})_2$ precursors and ozone co-reactant.

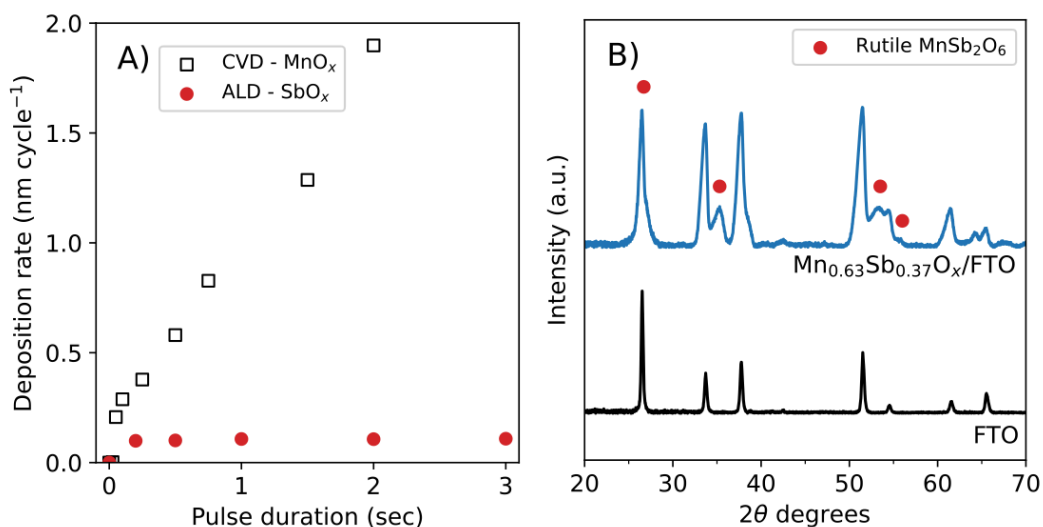


Figure 5.1 (A) Growth rates of MnO_x and SbO_x via CVD and ALD respectively derived from ellipsometry analysis. (B) GIXRD of Mn_{0.63}Sb_{0.37}O_x and XRD of the TEC8 FTO substrate after annealing both for 6 h in air at 600 °C. Reflections at $2\theta \approx 27, 35, 53,$ and 56° characteristic of rutile MnSb₂O₆ are indicated.

The long-term electrochemical activity and stability of Mn_{0.63}Sb_{0.37}O_x catalysts were evaluated with a 7-day durability test involving galvanostatic operation at $J = 10 \text{ mA cm}^{-2}$ in 1 M H₂SO₄. The average OER overpotential (η) during the 7-day durability test was 687 mV with a standard deviation of 9 mV (Figure 5.2A). Voltammetry and impedance data were collected at 24 h intervals following a 30 s hold at open circuit voltage (Figure 5.2B, Figure S1). In agreement with previous literature, the OER overpotential decreased and the catalyst “recovered” during short periods at open circuit voltage and between the first and second cyclic voltammograms collected in succession at each 24-hour interval (Figure 5.2A, Figure S1).^{161,162} Voltammetry data indicated that the initial OER overpotential was $\eta = 617 \text{ mV}$ at 10 mA cm^{-2} and the final OER overpotential at $t = 168 \text{ h}$ was $\eta = 618 \text{ mV}$ at 10 mA cm^{-2} (Figure 5.2B, Figure S1A). Measurements were corrected for uncompensated resistance and this value was approximately 14 mV at 10 mA cm^{-2} (Figure S1B). In agreement with previous literature on Mn_ySb_{1-y}O_x catalysts, redox peaks centered at 1.46 V vs. reversible hydrogen electrode (RHE) developed and increased in magnitude during the extended durability test (Figure 5.2B).¹⁶¹

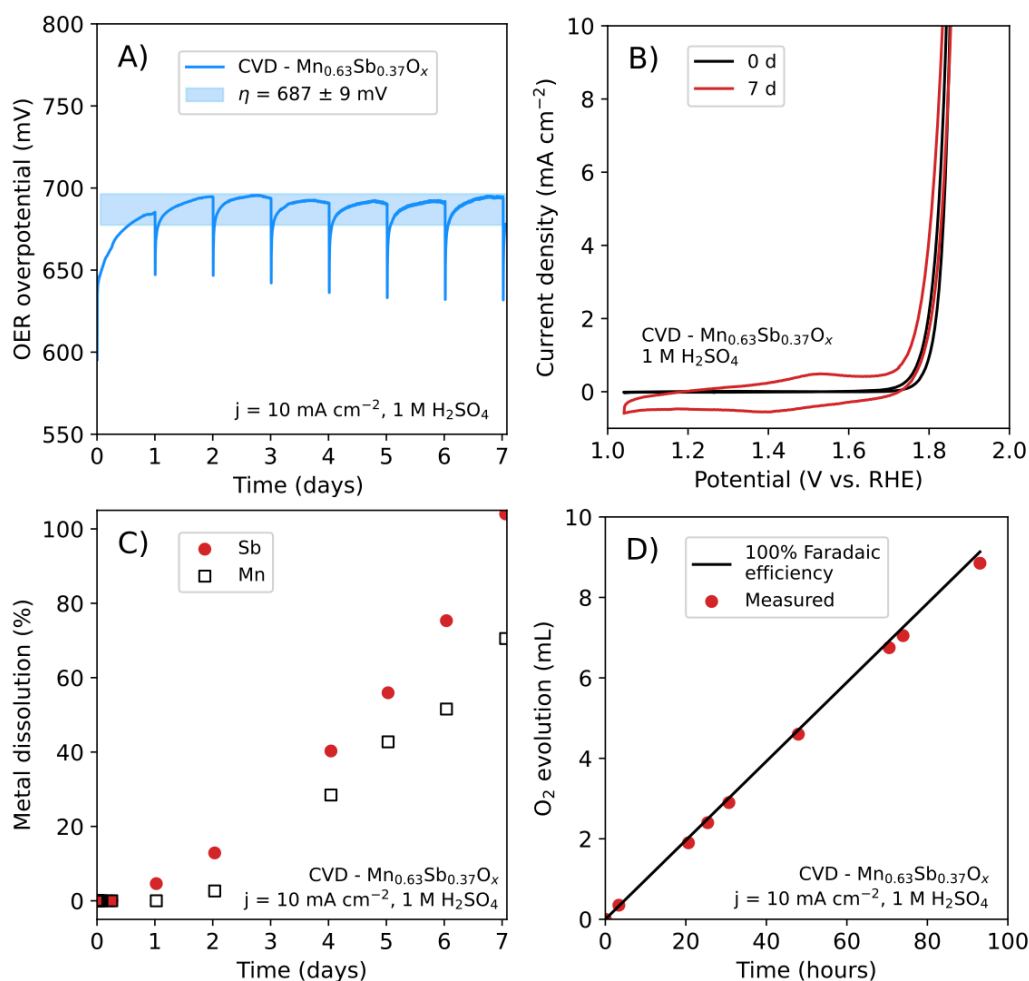


Figure 5.2 Electrochemical activity, stability, and faradaic efficiency of $\text{Mn}_{0.63}\text{Sb}_{0.37}\text{O}_x$ during OER at $J = 10 \text{ mA cm}^{-2}$ for 7 days in $1 \text{ M H}_2\text{SO}_4$ acid. (A) Chronopotentiometric response. (B) Cyclic voltammograms collected at 24 h intervals during the galvanostatic hold, initial and day 7 voltammogram displayed. (C) ICP-MS quantified corrosion products in the anolyte. (D) Faradaic efficiency of another $\text{Mn}_{0.63}\text{Sb}_{0.37}\text{O}_x$ electrode from the same deposition batch during 93 h of continuous operation at $J = 10 \text{ mA cm}^{-2}$.

Catalyst corrosion products were monitored during the 7-day durability test at 10 mA cm^{-2} in $1 \text{ M H}_2\text{SO}_4$. Aliquots of electrolyte solution were taken without replacement at approximately 24-hour intervals and ICP-MS quantified Sb and Mn metal dissolution during the 7-day durability test (Figure 5.2C). The average rate of Sb metal dissolution was comparable (11% per day, or $0.0013 \mu\text{mol cm}^{-2} \text{ h}^{-1}$) to the average rate of Mn metal dissolution (8% per day, or $0.0015 \mu\text{mol cm}^{-2} \text{ h}^{-1}$) during the 7-day test (Figure S2). The dissolution rate of both metals was lower during days 0-2 than during days 2-7 at 10 mA cm^{-2} in $1 \text{ M H}_2\text{SO}_4$. Faradaic efficiency measurements of another $\text{Mn}_{0.63}\text{Sb}_{0.37}\text{O}_x$ electrode from the same deposition batch showed 97.6% efficient oxygen evolution on average

during 93 h of continuous operation at 10 mA cm^{-2} in $1 \text{ M H}_2\text{SO}_4$ (Figure 5.2D). Despite high Faradaic efficiency and relatively stable OER overpotential at 10 mA cm^{-2} , significant fractions of the catalyst corroded during the durability test, consistent with other short-term durability tests of sputtered Mn-rich alloys.^{162,163} This indicates that a thin catalyst layer can evolve oxygen after the catalyst mass was reduced drastically. It is thus hypothesized that oxygen evolution on $\text{Mn}_{0.63}\text{Sb}_{0.37}\text{O}_x$ catalysts is predominantly an interfacial phenomenon. Analogous chronopotentiometry and ICP-MS measurements of a replicate electrode tested for 176 h (~ 7 days) at 10 mA cm^{-2} in $1 \text{ M H}_2\text{SO}_4$ showed OER overpotential and metal dissolution in agreement with the original $\text{Mn}_{0.63}\text{Sb}_{0.37}\text{O}_x$ electrode (Figure S2).

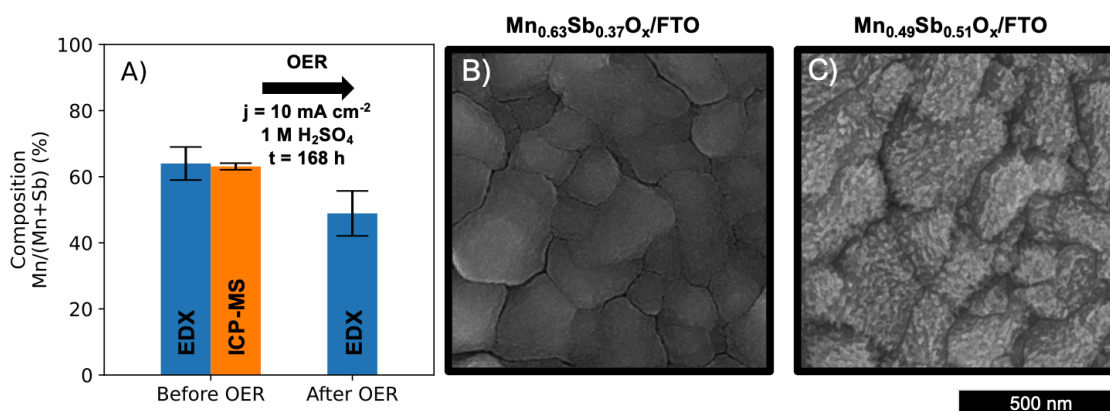


Figure 5.3 (A) Catalyst composition as determined by both EDX and ICP-MS techniques. Representative SEMs of $\text{Mn}_{0.63}\text{Sb}_{0.37}\text{O}_x$ (B) before and (C) after OER at $J = 10 \text{ mA cm}^{-2}$ for 168 h in $1 \text{ M H}_2\text{SO}_4$.

The $\text{Mn}_{0.63}\text{Sb}_{0.37}\text{O}_x$ electrode was characterized before and after the 7-day OER durability test at 10 mA cm^{-2} in $1 \text{ M H}_2\text{SO}_4$. Scanning electron microscopy (SEM) indicated conformal coating of the catalyst on the substrate prior to OER, and a roughened surface after the 7-day durability test (Figure 5.3 B and C, respectively). Capacitance data gathered with electrochemical impedance spectroscopy (EIS) at 24 h intervals indicated that the surface area roughened during the 7-day durability test (Figure 5.3, Figure S3). After the durability test, the roughness factor of as prepared $\text{Mn}_{0.63}\text{Sb}_{0.37}\text{O}_x$ increased by a factor of 22 (Figure S3). Energy-dispersive X-ray spectroscopy (EDX) indicated that the Mn metal fraction decreased from $64 \pm 5 \%$ before to $49 \pm 7 \%$ after the 7-day durability test (Figure 5.3A).

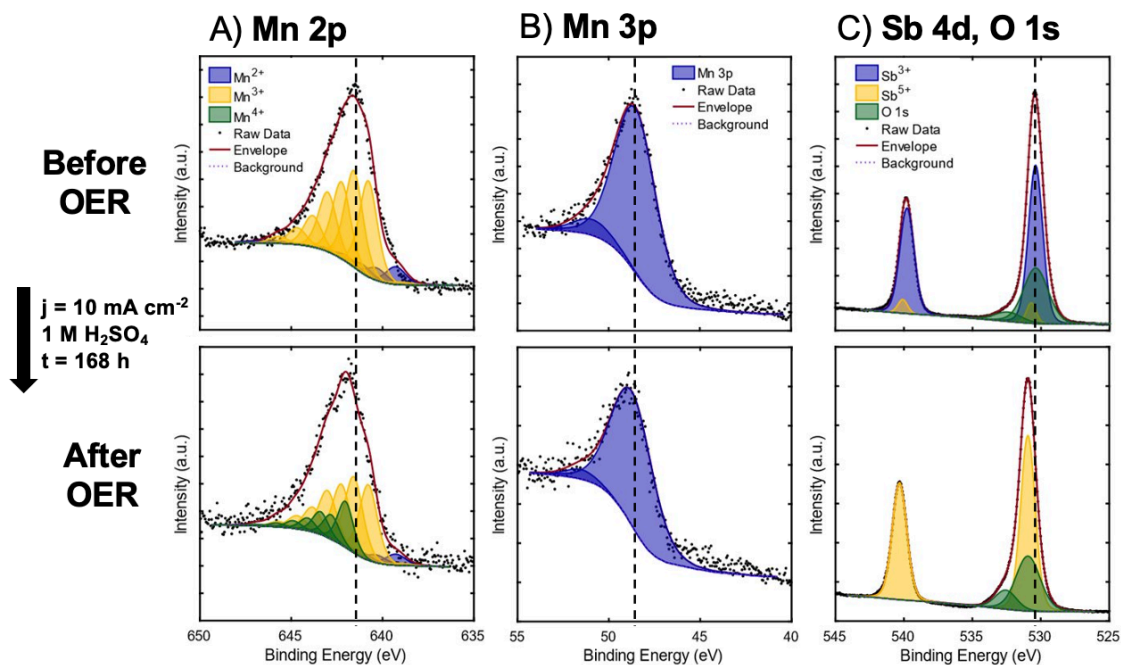


Figure 5.4 XPS spectra of $\text{Mn}_{0.63}\text{Sb}_{0.37}\text{O}_x$ before and after OER at $J = 10 \text{ mA cm}^{-2}$ for 168 h in 1 M H_2SO_4 . (A) Mn 2p spectra; (B) Mn 3p spectra; (C) Sb 3d, O 1s spectra.

To understand how the surface chemistry changed due to OER, X-ray photoelectron spectroscopy (XPS) was used to interrogate oxidation states of Mn and Sb before and after galvanostatic testing (Figure 5.4, Figure S4, Table S1). XP spectra of the Mn $2p_{3/2}$ peak indicated a shift in effective oxidation state from 2.9 before OER to 3.2 after OER and the Mn 3p peak indicated a shift in oxidation state from 2.8 to 3.4. Prior work has identified Mn^{3+} as the primary species present in stable $\text{Mn}_y\text{Sb}_{1-y}\text{O}_x$ alloys, aligning with the present observation.^{162,164} The observed oxidation of surface Mn is hypothesized to be due to irreversible electrochemical oxidation of some surface Mn^{3+} sites during OER. The small change in oxidation state is consistent with the high faradaic efficiency. Sb is expected to be electrochemically innocent, yet XP spectra of the Sb 3d region indicated a large oxidation state shift from 3.2 to 5.0.^{161,162,164} As Sb^{5+} has been previously reported to be the stabilizing species in $\text{Mn}_y\text{Sb}_{1-y}\text{O}_x$ alloys,^{160–162} it is hypothesized that surface Sb^{3+} originates from TDMA- Sb^{3+} ALD precursor forming Sb^{3+} oxides at the surface which then oxidize or dissolve under OER conditions to leave the stable, rutile Sb^{5+} state.

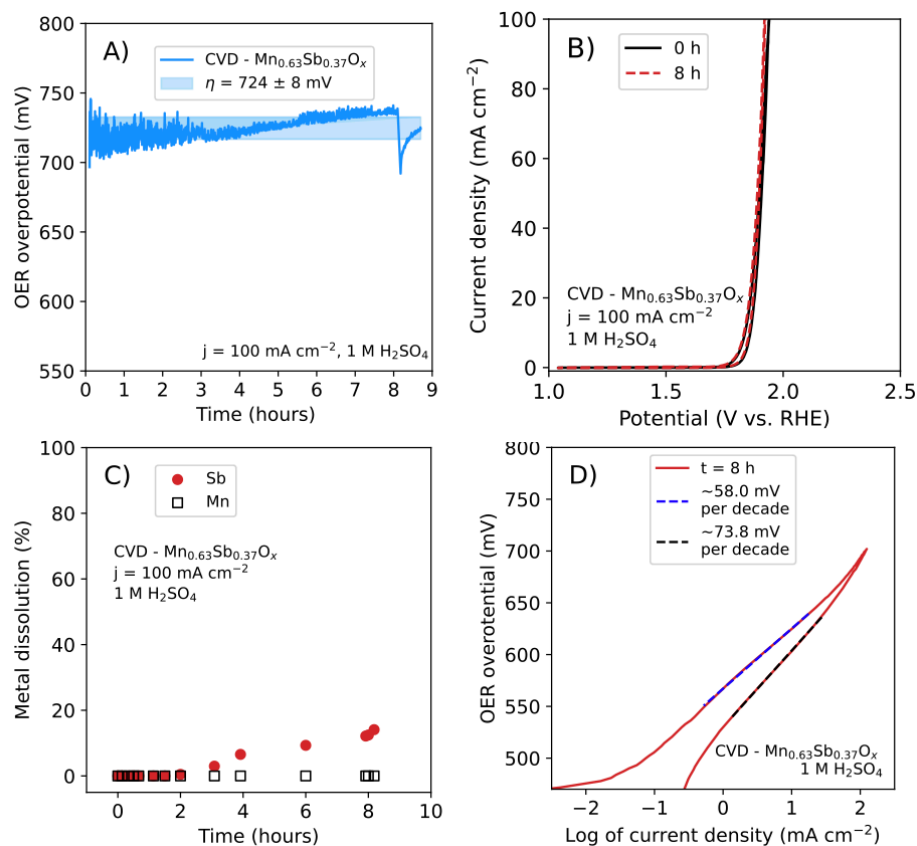


Figure 5.5 Electrochemical activity and stability of $\text{Mn}_{0.63}\text{Sb}_{0.37}\text{O}_x$ during OER at $J = 100 \text{ mA cm}^{-2}$ for 9 h in 1 M H_2SO_4 acid. (A) Chronopotentiometric response. (B) Cyclic voltammograms collected both initially and 8 h into the galvanostatic hold. (C) ICP-MS quantified corrosion products in the anolyte. (D) Tafel analysis of the voltametric data in (B).

Another $\text{Mn}_{0.63}\text{Sb}_{0.37}\text{O}_x$ electrode was evaluated at higher current densities. The initial OER overpotential at 350 mA cm^{-2} in 1 M H_2SO_4 was 819 mV (Figure S5). The average OER overpotential at 100 mA cm^{-2} was $724 \pm 8 \text{ mV}$ in 1 M H_2SO_4 for 8.5 h (Figure 5.5A). Voltammetry data indicated that the OER overpotential at 100 mA cm^{-2} was 709 mV at $t = 0 \text{ h}$ and 688 mV at $t = 8 \text{ h}$ (Figure 5.5B). Corrosion products were quantified over time with ICP-MS and indicated higher Sb leaching than Mn leaching in the first 8 h of $J = 100 \text{ mA cm}^{-2}$ in 1 M H_2SO_4 (Figure 5.5C). The Tafel plot showed an increase of $\sim 65 \text{ mV}$ OER overpotential per order of magnitude increase in current density (Figure 5.5D), lower than previous literature values of $\sim 75 \text{ mV/decade}$.¹⁶² The chronopotentiometry experiment at

100 mA cm⁻² in 1 M H₂SO₄ was conducted for a total of 26 hours with some interruptions due to bubble formation at the counter electrode (Figure S6).

5.4 Conclusions

Stability in mixed metal antimonates has been hypothesized to be a consequence of Sb stabilizing the trivalent Mn octahedra.¹⁶² Sb can induce enhanced hybridization of the O p- and Mn d-orbitals either by formation of an antimonate phase or by nanoscale intermixing of metal and antimony oxide crystallites.¹⁶³ Mn-rich alloys were thus hypothesized to be less stable than Sb-rich alloys, consistent with substantial metal dissolution of Mn_{0.63}Sb_{0.37}O_x catalysts observed during the multi-day durability test (Figure 5.2). The final Mn:Sb atomic ratio after the 168 h galvanostatic hold at $J = 10$ mA cm⁻² in 1 M H₂SO₄ was ~ 1:1 (Figure 5.3) with Mn^{~3+} and Sb⁵⁺ oxidation states (Figure 5.4), consistent with characterization of the more stable Sb-rich composition in other analyses.^{162,163} Notably, the overpotential required to drive $J = 10$ mA cm⁻² did not change substantially while the material actively dissolved. The increase in the electrochemically active surface area (Figure S3) during galvanostatic experiment due to interfacial roughening may have in part prevented the overpotential increase during the corrosion. The redox waves observed in the voltammetry data at ca. 1.46 V vs. RHE (Figure 5.2B) are consistent with behavior observed previously with MnO_x and other Mn_ySb_{1-y}O_x materials, but not in SbO_x materials.^{161,168} The oxidation of Mn sites may be a critical step in driving the OER. Moreover, Sb sites in binary oxide materials have been previously shown to be inactive for the OER reaction.¹⁶¹⁻¹⁶³ However, it is possible that Sb plays a role in electronically stabilizing Mn sites, thus providing the corrosion resistance observed here.

In summary, the multi-day durability of rutile Mn_{0.63}Sb_{0.37}O_x catalysts during galvanostatic operation at $J = 10$ and 100 mA cm⁻² in 1 M H₂SO₄ was assessed. A lower overpotential $J = 10$ mA cm⁻² was observed for Mn-rich alloy than previously demonstrated Sb-rich alloys.¹⁶¹ However, unlike the Sb-rich alloy, Mn_{0.63}Sb_{0.37}O_x catalysts corroded continuously during operation. This is consistent with the notion that Sb stabilizes Mn sites as well as with prior experiments using sputtered Mn-rich alloys.^{162,163} However, despite

this continuous corrosion of both Sb and Mn from the as-prepared material, the OER overpotential at $J = 10 \text{ mA cm}^{-2}$ did not substantially increase (Figure 5.5A), even at the point that $> 90 \%$ of the catalyst mass had been dissolved (Figure 5.2C).

5.5 Methods

Chemicals

Chemical vapor deposition (CVD) precursor bis(ethylcyclopentadienyl)manganese (98%-Mn, STREM) ($\text{Mn}(\text{EtCp})_2$) was used as received, preloaded in a CVD cylinder. Atomic layer deposition (ALD) precursor tris(dimethylamino)antimony (99.99%-Sb, STREM) (TDMA-Sb) was loaded into a new ALD cylinder under $\text{N}_{2(\text{g})}$ atmosphere in a glovebox. TEC 8 fluorine-doped tin oxide (FTO, Sigma Aldrich) substrates were used as received. The electrolyte, H_2SO_4 was diluted to 1 M using $18.2 \text{ M}\Omega\text{-cm}$ resistivity water obtained from a Thermo Scientific Nanopure deionized water system. In-Ga eutectic (99.99%, metals basis, Alfa Aesar) and PELCO conductive Ag paint (Ted Pella, Inc) were used as received for electrode preparation. Compressed $\text{O}_{2(\text{g})}$ (ultra-high purity grade, CGA-540, Airgas) was used to produce $\text{O}_{3(\text{g})}$ which was used as a co-reactant in chemical vapor deposition. Compressed $\text{O}_{2(\text{g})}$ (industrial purity, CGA-540, Airgas) purged the electrolyte solution during durability experiments.

Sample preparation

Chemical vapor deposition was performed using a Savannah S200 Atomic Layer Deposition (ALD) System by Cambridge Nanotech. After precursors and co-reactants were pulsed a waiting period allowed the ALD chamber (set at $150 \text{ }^\circ\text{C}$) to return to base vacuum pressure ($\sim 0.5 \text{ torr}$ at 20 sscm N_2 flow rate), and precursor cylinder jackets were heated as indicated in Table S2.

TEC8 fluorine-doped tin oxide (FTO) substrates were loaded into the ALD chamber after consecutive washing with iso-propyl alcohol (IPA), acetone, and H_2O and drying with $\text{N}_{2(\text{g})}$. Within the ALD chamber, prior to deposition, a glass slide was positioned on top of the

FTO substrate covering part of the surface, which allowed top-facing electrical contact directly to the substrate during electrode preparation (Figure S7). The as-deposited samples were annealed in a Thermolyne muffle furnace. Temperature was ramped from room temperature to 600 °C at a rate of 10 °C min⁻¹ and then held for 6 h before cooling to room temperature again.

The annealed Mn_{0.63}Sb_{0.37}O_x samples were cleaved such that In-Ga could be scribed directly onto the bare FTO substrate, that was previously covered by a glass slide in the ALD chamber (Figure S7a). A tinned Cu wire was placed on to the In-Ga area and coated with Pelco conductive silver paint (Ted Pella, Inc.). Ag paint dried in the oven at 95 °C for 1 h. Epoxy (Hysol 9460) encased the entire electrode except a small area where the catalyst was exposed. Electrodes encased in epoxy dried in the oven at 95 °C for approximately 8 h. The catalyst area not covered with epoxy (Figure S7d) was measured with an optical scanner (Epson perfection V360) and the surface area was quantified with ImageJ software (10-15 mm²).

Electrochemical activity and stability evaluation

Electrochemical analysis was performed using a Biologic SP-200 potentiostat using EC-Lab software. A 50 mL pyrex glass flask was used as the electrochemical cell. A two-compartment, three-electrode configuration was utilized (Figure S8). A calibrated CHI-150 saturated calomel electrode (SCE) was used as the reference electrode (0.241 V vs. RHE, CH Instruments, Inc.), which was referenced to RHE over a Pt mesh electrode with bubbling H_{2(g)}. A Ti-mesh counter electrode was isolated from the working and reference electrodes using a porous glass frit (porosity of 10-20 μm, Ace glass). All glassware was cleaned by immersing in a freshly-prepared 3 : 1 by volume ratio solution of HCl and HNO₃ for several hours and subsequently rinsed with H₂O before all electrochemical analysis. During all electrochemical experiments, the 1 M H₂SO₄ electrolyte solution (50 mL) was continuously stirred with a stir bar at room temperature and hydrated O_{2(g)} continuously bubbled into the electrolyte.

The electrochemical durability experiment was carried out under galvanostatic conditions (constant current, 10 mA cm^{-2}) for seven 24 h intervals (168 h total), and the working electrode potential was measured. Electrochemistry data was displayed in IUPAC convention. At 24 h intervals during durability tests at 10 mA cm^{-2} , three cyclic voltammetry cycles with $E_0 = 1.04 \text{ V vs. RHE}$ and $E_1 = 1.94 \text{ V vs. RHE}$ were acquired with $v = 40 \text{ mV s}^{-1}$. Impedance data were collected at open circuit potential ($\sim 1.4 \text{ V vs RHE}$), 10 data points were collected per decade at frequencies that ranged from 10 Hz to 10 kHz, and the amplitude of the single sinusoidal wave was 10 mV. Impedance data were fit to an equivalent circuit model ($R_1 + Q_2/R_2$) with EC-lab software to determine the solution resistance (R_1) and pseudo-capacitance (Q_2). Uncompensated resistance was corrected for 90% of the solution resistance (10-15 Ω) as determined by impedance. Pseudo-capacitance data (Q_2) derived from impedance spectroscopy was used to evaluate electrochemically active surface area (ECSA) and time-dependent roughness during the durability experiment. For ECSA calculations, the TEC 8 FTO substrate roughness factor was assumed to be equal to that of antimony-doped tin oxide (ATO) ($RF = 1.32$).¹⁶¹ According to preestablished methods, the geometric area-normalized capacitance of ATO ($0.0254 \text{ mF cm}^{-2}$) was divided by the roughness factor to determine the capacitance normalized to the electrochemical surface area ($0.0192 \text{ mF cm}^{-2}$).¹⁶¹

Aliquots of 0.2 mL of the electrolyte were taken during chronopotentiometry and were diluted by 5 mL of 5% nitric acid before analysis with inductively coupled plasma mass spectrometry (ICP-MS) using an Agilent 8800 Triple Quadrupole ICP-MS system. Standards of known concentration were prepared from purchased Mn and Sb standards, which were diluted into a range of concentration standards through serial dilution with 5% HNO_3 by mass.

Materials characterization

Growth rates of individual oxides on Si substrates were derived from ellipsometry with a J.A. Woolam Co., Inc. ellipsometry solutions system and thickness data were gathered at 65, 70, and 70 ° angles, scanned at 380-890 nm wavelengths, and analyzed with

CompleteEASE software. Material stoichiometry was obtained by dissolving the deposited unannealed metal films on Si substrates in 10 mL of 1.0 M H₂SO₄ for several days, followed by determination of the concentration of dissolved metals (Sb and Mn) using ICP-MS. Geometric area of the Si-substrates was measured with an optical scanner (using the same procedure used to define electrode area) to determine the area normalized mass-loading (23.53 μg Mn cm⁻², 32.3 μg Sb cm⁻²). A mass loading of 0.42 μmol Mn cm⁻² corresponded to oxides that were ~100 nm thick (Table S3).

Scanning-electron micrographs (SEMs) were obtained with a FEI Nova NanoSEM 450 at an accelerating voltage of 10.00 kV with a working distance of 5 mm and an in-lens secondary electron detector. Micrographs were acquired with a resolution of 688 pixels μm⁻¹ over ~ 2 μm² areas. Energy dispersive X-ray (EDX) spectroscopy was performed in the SEM using an accelerating voltage of 15.00 kV and a working distance of 5 mm. An Oxford Instruments X-Max silicon drift detector was utilized. Spectra were collected in the range of 0 to 10 keV and quantitative deposit compositions were derived from these spectra using the “INCA” software package (Oxford Instruments). Reported compositions are the average of n = 6 independent measurements from different locations on the sample. X-ray diffraction (XRD) data was collected using a Bruker D8 Discover diffractometer with a Cu Kα source and a two-dimensional Vantec detector. XRD data was acquired from the FTO substrate in a Bragg-Brentano geometry. Grazing incidence X-ray diffraction (GIXRD) was collected from Mn_ySb_{1-y}O_x on a FTO substrate with the X-rays directed at a grazing angle ω = 0.3 ° above the plane of the sample surface and the detector swept throughout the entire 2θ range.

X-ray photoelectron spectroscopy (XPS) was performed using a Kratos Axis Ultra system with a base pressure of 1 × 10⁻⁹ Torr in the analysis chamber. A 150 W monochromatic Al Kα source was used to irradiate the sample with X-rays (1486.6 eV). A hemispherical analyzer oriented for detection along the sample surface normal was used for maximum depth sensitivity. The data were analyzed using CasaXPS software. A Shirley background was used for Mn spectra and a U 2 Tougaard background was used for Sb, O, and C spectra

to more accurately capture the background signal. All peaks were referenced to adventitious C at a binding energy of 284.8 eV. The Mn 2p_{3/2} peak was fit to standards of pure oxides previously reported to estimate the Mn oxidation state and the contribution of multiple oxidation states to the peak.¹⁶⁹ Mn 3p spectra were used in concert with Mn 2p_{3/2} to more accurately determine the Mn oxidation state in accordance with literature methods.¹⁶⁹⁻¹⁷³ The Sb 3d_{5/2} peak overlaps with O 1s, so to determine Sb oxidation state, the Sb 3d_{3/2} peak, which has no overlap with O, was fit with literature standards for Sb oxidation state and the Sb 3d_{5/2} contribution was calculated by constraining the spin-orbit peak splitting ($\Delta\text{Sb } 3d = 9.38 \text{ eV}$), the full width at half max (FWHM) to be equivalent between the peaks, and area ratio ($3d_{5/2}:3d_{3/2} = 3:2$) and assuming remaining signal was due to O 1s.

Chapter 6

SUPPORTING INFORMATION

This chapter details supporting information referenced in the preceding chapters.

Chapter 6: Supporting Information	88
6.1 Macro-Scale Electricity Model	89
6.2 Supporting Information for Chapter 2	91
6.2.1 Supplemental Methods for Chapter 2.....	91
6.2.2 Supporting Figures and Tables.....	93
6.2.3 Supporting Cost Information.....	110
6.2.4 Supporting References within Chapter 6.2.....	113
6.3 Supporting Information for Chapter 3	115
6.4 Supporting Information for Chapter 4	125
6.5 Supporting Information for Chapter 5	129
Bibliography	135

6.1 Macro-Scale Electricity Model

This section presents the model formulation of the macro-scale electricity model (MEM) used in Chapters 2, 3, and 4.

Nomenclature

Symbol	Unit	Description
g (superscript)	-	Generation technology (wind, solar)
v (superscript)		Energy conversion (electrolyzer, fuel cell)
s (superscript)	-	Energy storage (PGP storage, battery storage)
from s (superscript)	-	Discharge from energy storage
to s (superscript)	-	Charge to energy storage
t (subscript)	-	Time step, starting from 1 and ending at T
c_{capital}	\$/kW for generation or conversion \$/kWh for storage	(Overnight) capital cost
c_{fixed}	\$/kW/h for generation or conversion \$/kWh/h for storage	Fixed cost
$c_{\text{fixed O\&M}}$	\$/kW/yr	Fixed operating and maintenance (O&M) cost
c_{var}	\$/kWh	Variable cost
f	-	Capacity factor (generation technology)
h	h/yr	Average number of hours per year
i	-	Discount rate
n	yrs	Project life
Δt	h	Time step size, i.e., 1 hour in the model
C	kW for generation or conversion kWh for storage	Capacity
D_t	kW	Dispatch at time step t
M_t	kWh	Demand at time step t
S_t	kWh	Energy remaining in storage at time step t
γ	1/yr	Capital recovery factor
δ	1/h	Storage decay rate, or energy loss per hour expressed as fraction of energy in storage
η	-	Storage charging efficiency
τ	h	Storage charging duration

Model formulation

Cost calculations

Fixed cost of generation and conversion technologies (wind, solar, electrolyzer, fuel cell):

$$c_{\text{fixed}}^{g,v} = \frac{\gamma c_{\text{capital}}^{g,v} + c_{\text{fixed O\&M}}^{g,v}}{h}$$

Fixed cost of energy storage (PGP storage, battery storage):

$$c_{\text{fixed}}^s = \frac{\gamma c_{\text{capital}}^s}{h}$$

Capital recovery factor:

$$\gamma = \frac{i(1+i)^n}{(1+i)^n - 1}$$

Constraints

Capacity:

$$0 \leq C^{g,v,s} \quad \forall g, v, s$$

Dispatch:

$$0 \leq D_t^g \leq C^g f_t^g \quad \forall g, t$$

$$0 \leq D_t^v \leq C^v \quad \forall v, t$$

$$0 \leq D_t^{\text{to } s} \leq \frac{C^s}{\tau^s} \quad s = \text{battery}, \forall t$$

$$0 \leq D_t^{\text{from } s} \leq \frac{C^s}{\tau^s} \quad s = \text{battery}, \forall t$$

$$0 \leq S_t^s \leq C^s \quad \forall s, t$$

$$0 \leq D_t^{\text{from } s} \leq S_t^s (1 - \delta^s) \quad \forall s, t$$

Storage energy balance:

$$\begin{aligned} S_1 &= (1 - \delta^s) S_T \Delta t + \eta^s D_T^{\text{to } s} \Delta t - D_T^{\text{from } s} \Delta t & \forall s \\ S_{t+1} &= (1 - \delta^s) S_t \Delta t + \eta^s D_t^{\text{to } s} \Delta t - D_t^{\text{from } s} \Delta t & \forall s, t \in 1, \dots, (T-1) \end{aligned}$$

System energy balance:

$$\sum_g D_t^g \Delta t + D_t^{\text{from } s} \Delta t = M_t + D_t^{\text{to } s} \Delta t \quad \forall g, t$$

Objective function

minimize(system cost)

system cost =

$$\begin{aligned} & \sum_g c_{\text{fixed}}^g C^g + \sum_g \left(\frac{\sum_t c_{\text{var}}^g D_t^g}{T} \right) + \sum_v c_{\text{fixed}}^v C^v + \\ & \sum_s c_{\text{fixed}}^s C^s + \frac{\sum_t c_{\text{var}}^{\text{to } s} D_t^s}{T} + \frac{\sum_t c_{\text{var}}^{\text{from } s} D_t^s}{T} \end{aligned}$$

6.2 Supporting Information for Chapter 2

Section 6.2.1: Supplemental Methods for Chapter 2

Model limitations

The linear model considers scenarios with perfect foresight, perfectly efficient markets, and no transmission losses. Despite these simplifications, key findings of our study are in accord with and build on a similar European electricity system that included transmission modeling.¹ Simulations for the West, East, and Texas Interconnects further show the robustness of our results (Figure S7). The system was confined solely to the electricity sector and did not consider conversion of electricity into fuel to serve other sectors such as transportation or heating. We did not include carbon capture with natural gas because the regulatory and legislative environment considered is confined to zero-carbon and renewable electricity sources (Table S2). We evaluate the system over an hourly timescale. Other technologies, including perhaps batteries, are assumed to provide short term (minutes to hours) smoothing of power variability. Additionally, although we include a project lifetime and self-discharge rate for batteries, we do not track battery deterioration due to cycling. Previous studies of electricity systems for the U.S. with high variable renewable penetration depend on future projections, consider shorter time periods, do not satisfy hourly demand with the statutorily required resource availability, and/or use highly complex models.

Storage technology costs:

In Table S3 we list cost and performance metrics for a variety of energy storage technologies. This table builds off of the compiled information in Luo et al.³ for the more mature technologies: pumped hydropower, compressed air energy storage, flywheels, capacitors, and lead-acid batteries; original works are cited in the table itself. More rapidly developing technologies, such as Li-ion batteries, redox flow batteries, and PGP cite more recent literature including references^{4,5} and those listed for the base case in Table 2.1. For some storage technologies (pumped hydropower, compressed air, redox flow, and PGP) the power and energy capacities for a given project can be sized independently. For these technologies, and all of the others, we provide the total capital cost divided by the power and again by the

energy capacity of typical systems characterized in the literature in Figure 2.1. In these cases, the flexibility of independently sizing power and energy capacities for a given project for the LDS candidates is not shown in this table. The values depicted in Figure 1 are shown in Table S3. The increased flexibility of the four LDS technologies: pumped hydropower storage (PHS), compressed air energy storage (CAES), redox flow batteries (potentially because of the ability to separate power and energy capacities), and PGP is shown in Table S3 where capital costs are split into power-related capital costs and energy-related capital costs. The costs of PHS projects are highly site and project specific;⁶ depending on the local geology, a dam capable of storing one quantity of water in one valley, could potentially store a very different quantity in another valley necessitating caution when extrapolating PHS costs. The conversion of pressurized air to power in a CAES systems relies on 4 multiple stages of air expansion with some involving gas turbines.⁷ This makes CAES inconsistent with the zero carbon emissions and 100% RE goal of this analysis. Despite this, we include CAES in Table S4. We emphasize that either gas produced from a carbon neutral process would be needed for the turbine or carbon capture and storage of the CO₂ from the exhaust. Either option would increase the presented CAES costs.

Section 6.2.2: Supplemental Figures and Tables

State	Max renewable requirement	Electricity sector end-state
Virginia ⁸	100% RE by 2050 ^a	100% RE-only by 2050 ^a
Maine ⁹	80% RE by 2030	100% RE-only by 2045
Hawaii ¹⁰	100% RE by 2050	100% RE-only by 2045
New Mexico ¹¹	80% RE by 2040	Zero-carbon by 2045
New York ¹²	70% RE by 2030	Zero-carbon by 2040 ^b
California ¹³	60% RE by 2030	Zero-carbon by 2045
Nevada ¹⁴	50% RE by 2030	Zero-carbon by 2045 ^c
Washington ¹⁵	only zero-carbon requirements	Zero-carbon by 2045
Puerto Rico ¹⁶	100% RE by 2050	100% RE-only by 2050
Washington D.C. ¹⁷	100% RE by 2032	100% RE-only by 2032

Table S2: 100% clean power state laws: renewable vs. zero-carbon requirements. Several states and jurisdictions have mandated the adoption of 100% clean electricity systems by 2030-2050. The term ‘zero-carbon’ is broader than renewable energy (RE), as it generally includes technologies like nuclear and large-scale hydropower, for example, that are not strictly renewable by policy definition in most state Renewable Portfolio Standards (RPS). RE technologies include wind, solar, batteries, renewable hydrogen, and others. Natural gas with CCS is currently not eligible as a “zero-carbon resource” for meeting clean energy mandates in states like California (although the CEC is actively discussing their eligibility for this purpose.)¹⁸ Natural gas with CCS may be permitted in net “zero-emissions” electricity systems in states like New York. Most states with 100% clean power laws have mandated the adoption of primarily RE technologies prior to zero-carbon or RE-only electricity system end-states. RPS are also used to specify the capacities of certain RE technologies such as wind, solar, and energy storage to be deployed. Iowa was the first state to establish an RPS and since then, more than half of states have established RE targets.¹⁹ While most state RE targets are between 10% and 45%, 14 states—California, Colorado, Hawaii, Maine, Maryland, Massachusetts, Nevada, New Mexico, New Jersey, New York, Oregon, Vermont, Virginia, Washington, as well as Washington, D.C., Puerto Rico, and the Virgin Islands—have requirements of 50% or greater.¹⁹

^aVirginia’s RE targets apply to ‘Phase I’ and ‘Phase II’ investor-owned utilities.

^bNew York’s goal involves reducing 100% of the electricity sector’s greenhouse gas emissions by 2040 as compared to 1990 levels.

^cNevada’s 50% RE by 2030 target is binding; its 100% zero-carbon by 2050 target is non-binding.

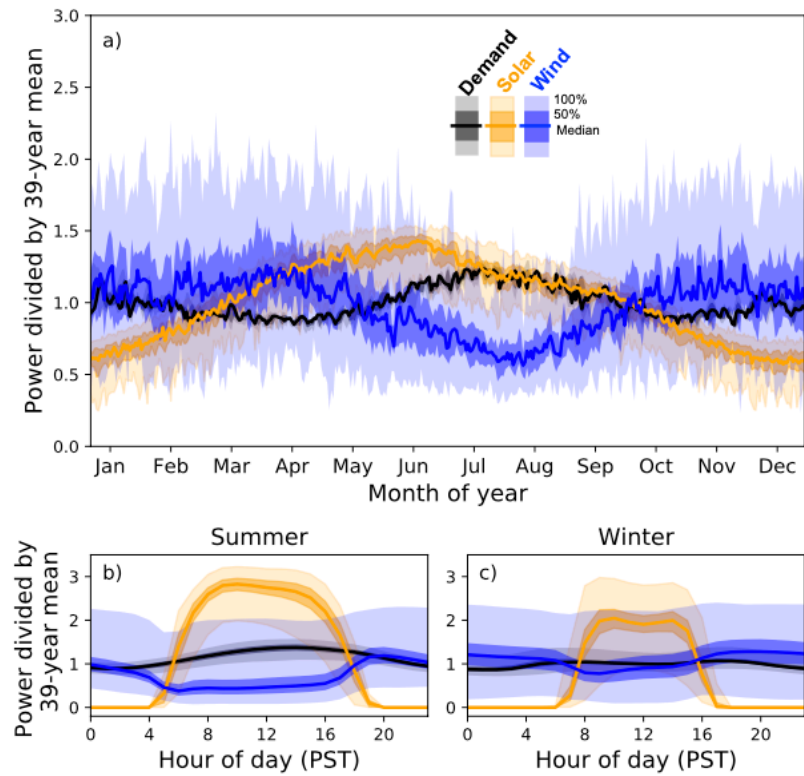


Figure S1: Resource and demand variability. The temporal variability of wind (blue) and solar (yellow) supply and electricity (black) demand over the contiguous United States from 1980-2018. Variability is shown over a) daily averaged, seasonal, b) hourly summer (June, July, and August), and c) hourly winter (December, January, February) timescales. The dark lines represent the median value, the darker shading represents the 25th to 75th percentile of data, and the lighter shading represents the 0th to 100th percentile of data. All data is normalized to its respective 39 year mean. See methods section on wind and solar capacity factors for more details. Data used in our analysis is displayed here. The plotting code is adapted. ²⁰

storage technology	total capital cost (\$/kW)	total capital cost (\$/kWh)	typical energy/power	typical round-trip efficiency RTE (%)	typical lifetime (years)
flywheel	250-350 ⁷	1,000-5,000 ⁷	≪1 ^{7,21}	~90-95 ⁷	~15 ⁷
capacitor	200-400 ⁷	500-1,000 ⁷	≪1-1 ⁷	~60-70 ⁷	~5 ⁷
lead-acid	300-600 ⁷	200-400 ⁷	<1-10 ^{7,22}	70-80, ⁷ 63-90, ²² 75-80 ²³	5-15 ⁷
Li-ion	280-513, 488-980, 898-1,874 ²⁴	295-540, ^e 257-517, ^e 237-494 ^e ²⁴	1, 2, 4 ²⁴	86-90 ²⁴	10 ²⁴
redox flow ^a (vanadium)	1,027-1,155, 1,788-1,956 ⁵	4,106-4,620, 447-489 ⁵	0.25, 4 ⁵	70-78, 76-79 ⁵	20 ⁵
pumped hydropower ^a	2,500-4,300, ²⁵ 2,000-4,000, ²¹ 975 ²⁶	5-100, ⁷ 97.5 ²⁶	1-24+, ⁷ 6-10, ²⁵ 10, ²¹ 10 ²⁶	70-85, ⁷ 70-80 ²¹	40-60, ⁷ 50 ^f
compressed air ^a	400-800, ⁷ 800-1,000, ²¹ 650 ²⁶	2-50, ⁷ 16 ²⁶	1-24, ⁷ 40 ²⁶	42, ⁷ 45-60 ²¹	20-40, ⁷ 30 ^f
power-to-gas-to-power ^a	6,500-6,600, ^b 5,300-11,000 ^c	5.6-8.8, ^b 4.6-14 ^c	740-1,200 ^b	electrolyzer 70, ^d fuel cell 70, ^d RTE 49 ^d	electrolyzer 12.5, ^d cavern 30, ^d fuel cell 20 ^d

Table S3: Technical characteristics of energy storage technologies with cost values reported as total capital costs divided by typical power and energy capacities.

^aTechnologies with more easily separated power and energy capacities and costs; values for the split costs for these technologies are include in Table S4.

^bCharacteristics for the specific PGP system used in this analysis and optimized using one year of 2018 demand and resource data and again with 6 years of 2013-2018 data.

^cThese values consider the two scenarios in the ^b note and the original uncertainty in fuel cell capital costs of 4,600-10,000\$/kW instead of using the base case value of 5,854 \$/kW. The PGP systems were not optimized based on the low and high fuel cell values.

^dReferences in Table 1.

^eValues originally reported based on nameplate energy storage, converted to usable energy by dividing by sqrt(0.9), where 90% is approximately the round-trip efficiency.

^f Exact values used in Figure 7b.

storage technology	power-related capital cost (\$/kW)	energy-related capital cost (\$/kWh)
redox flow (vanadium)	941-1,143 ⁵	196-356 ⁵
pumped hydropower	600, ^{c, 26} 1,200 ²⁷	37.5, ^{c, 26} 75 ²⁷
compressed air	580, ^{c, 26} 595 (€/kW), ^{a, 28} 700 ²⁷	1.75, ^{c, 26} 2 (€/kWh), ²⁸ 5 ²⁷
power-to-gas-to-power	6,380 ^b	0.16

Table S4: Technical characteristics of candidate long duration energy storage technologies. Costs are split into power-related capital costs and energy-related capital costs.

^aBased on 356.4 \$/kW for the properly sized turbine and compressor plus 238.8 \$/kW turbine for “other investment costs.”²⁸

^bBased on 1,058 \$/kW electrolyzer and 5,854 \$/kW fuel cell costs (Table 1) and a 1:2 electrolyzer-to-fuel cell capacity ratio (results of the 2018 base case).

^cExact values used in Figure 7b. All storage variable costs are modeled as zero \$/kWh.

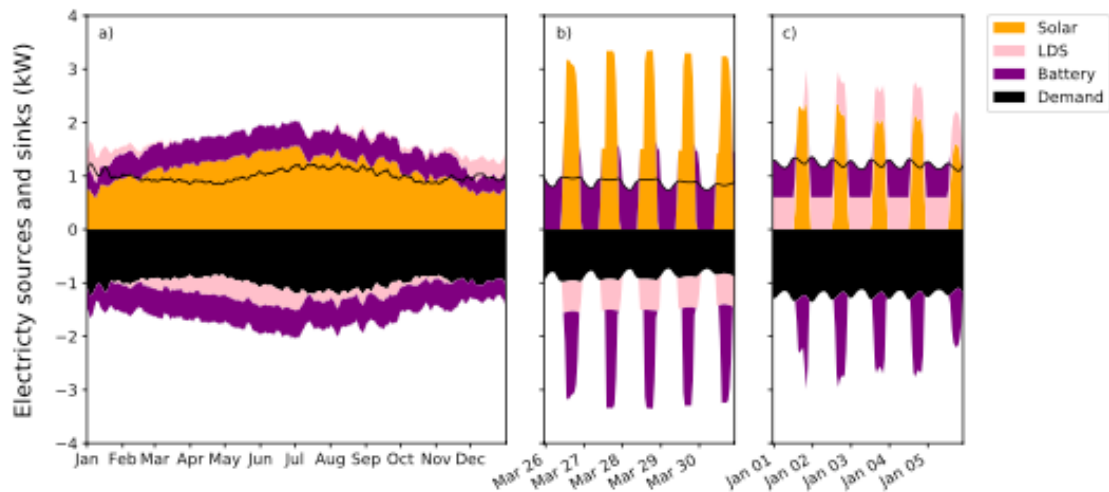


Figure S2: Dispatch curves: solar, LDS, batteries. a) Annual view of the solar only generation case for 2018. Batteries were charged and discharged on the daily cycle. LDS was charged during daily solar peaks and was used in wintertime during the seasonal low. b) 5-day period of maximum battery dispatch (starting at 08:00PM CST). Batteries were discharged, and LDS was simultaneously charged each day. c) 5-day period of maximum LDS dispatch (starting at 06:00PM CST). At peak daytime, excess solar and dispatched LDS were used to charge batteries. LDS and batteries met demand at night.

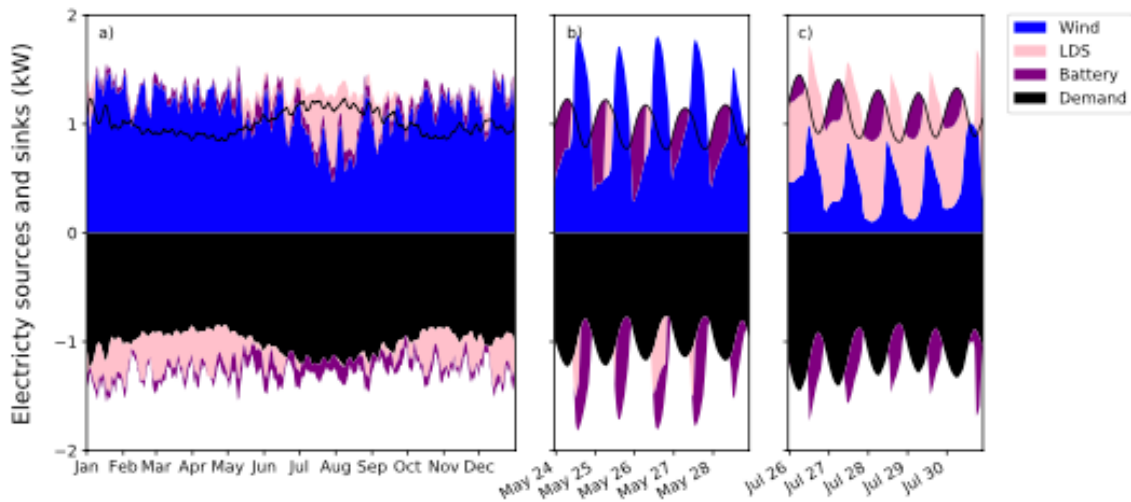


Figure S3: Dispatch curves: wind, LDS, batteries. a) Annual view of the wind only generation case for 2018. LDS was discharged primarily in the summer when the wind resource is least abundant. b) 5-day period of maximum battery electricity source (starting at 07:00AM CST). Batteries and LDS capture nighttime wind resource peaks. Both LDS and batteries meet demand during the day. c) 5-day period of maximum LDS electricity source (starting at 11:00AM CST). Simultaneous LDS discharge and battery charge occurred each night.

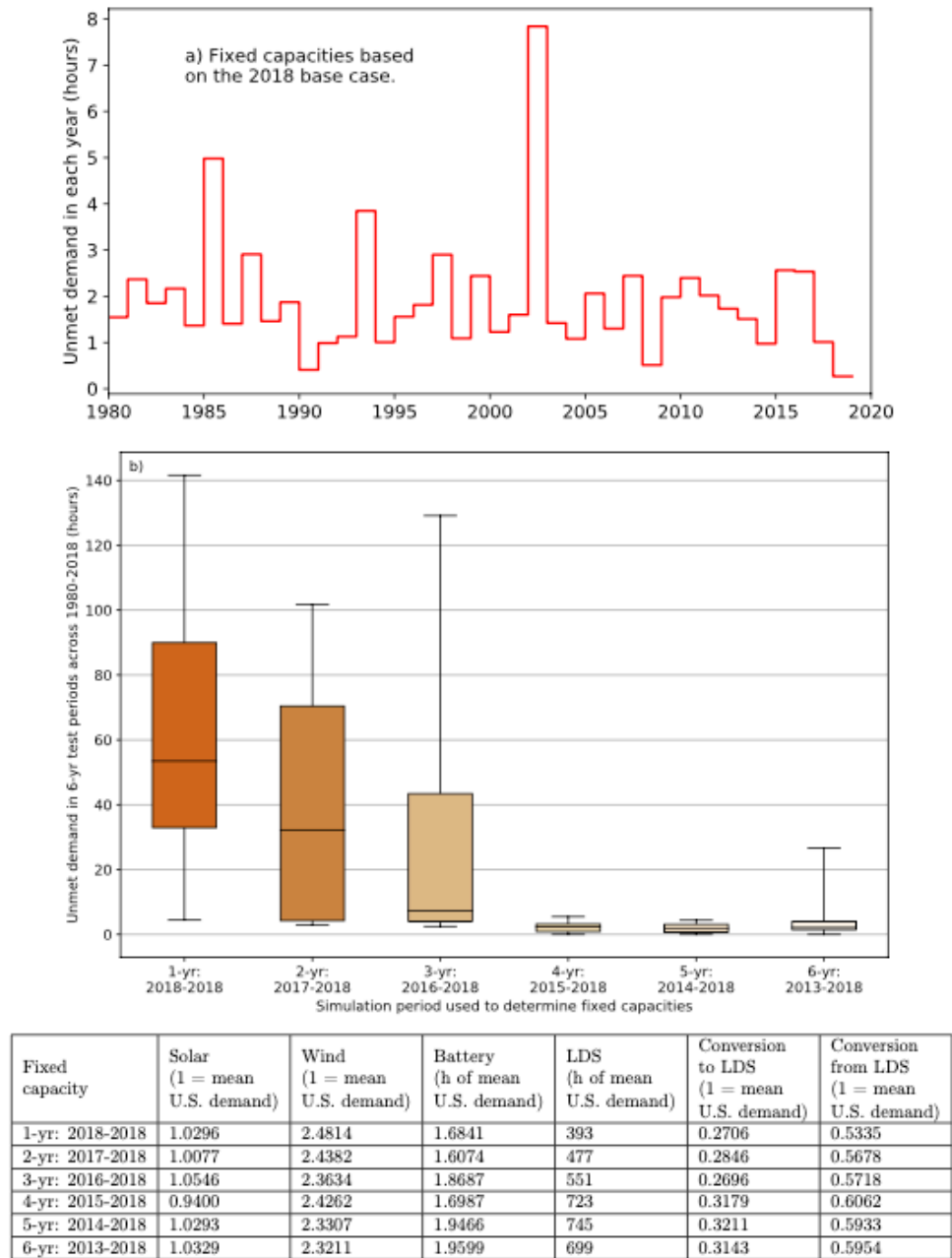


Figure S4: Fixed capacities based on asset builds from various simulations. The cost of unmet demand was set to \$10/kWh. a) Hours of unmet demand in each year over the 39 year period when specifying capacities based on results from the 2018 base case. Asset builds based on a single year are not always robust for other years. b) Fixed capacities based on 1-, 2-, 3-, 4-, 5-, and 6-yr asset builds from the 2010s (capacities shown in the table where mean demand over the full data set was 457 GW). Unmet demand met (hours) based on these capacities is shown for 6-year test periods across the data set 1980-2018 (7 data points per box). While longer horizon modeling more accurately predicts needs, four-year simulations are not necessarily enough to meet NERC reliability standards.²⁹ More detailed studies are needed to determine how many simulation years are enough.

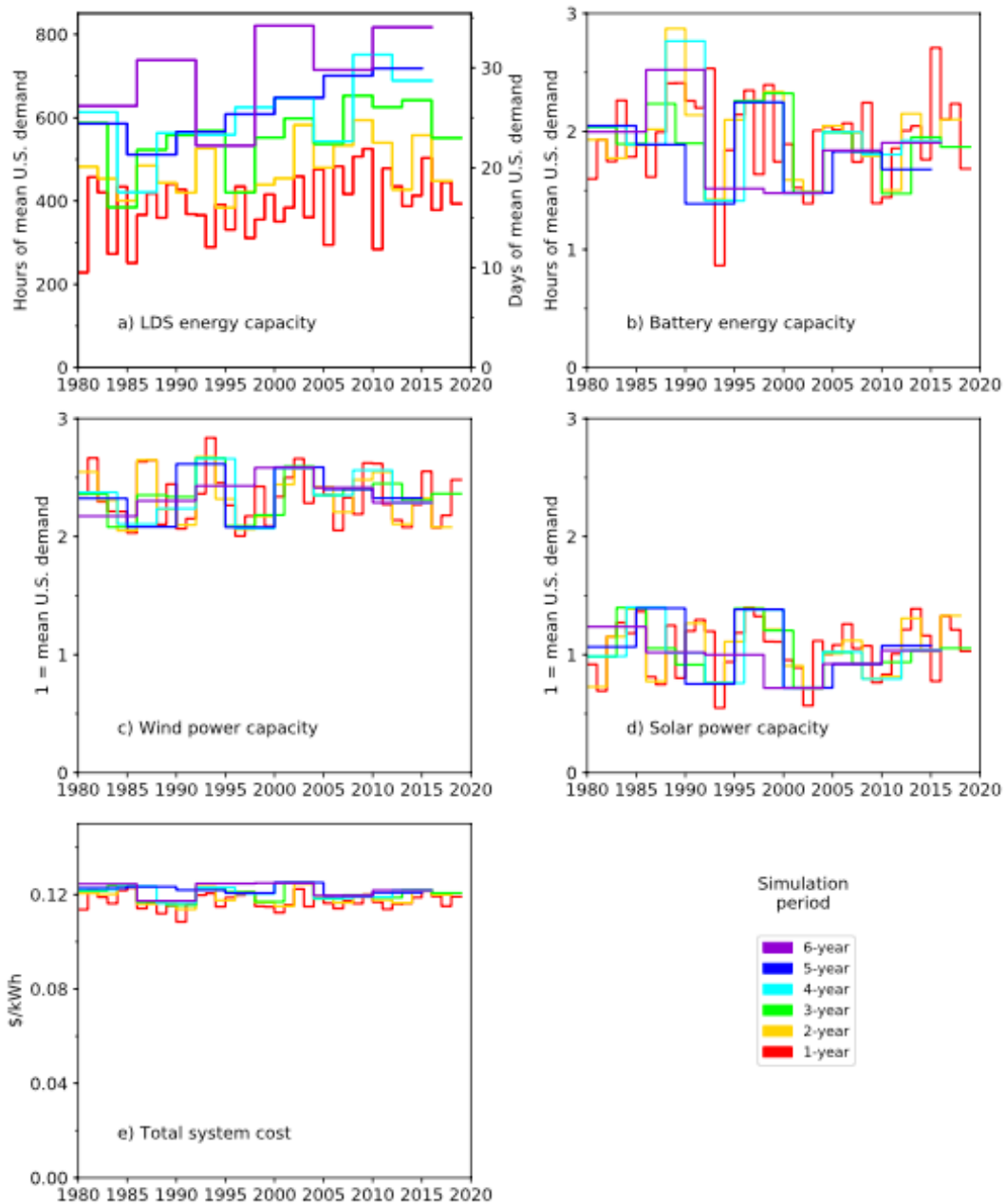


Figure S5: Multiple year simulations: capacities. 1-, 2-, 3-, 4-, 5-, and 6-year simulations were performed across all 39 years of wind and solar data available (1980 to 2018) for the contiguous U.S. The horizontal sections of the lines represent the optimized capacity for the periods simulated. Presented here are results for a) LDS energy capacity, b) battery energy capacity, c) wind power capacity, d) solar power capacity e) total system costs. In least-cost systems, longer simulation lengths resulted in larger installed storage capacities for LDS. System costs were ~ 0.12 \$/kWh for all simulation lengths.

Simulation length (across 39 years, 1980-2018)	Data type	Total system cost (\$/kWh)	LDS energy capacity (hours of mean U.S. demand)	Battery energy capacity (hours of mean U.S. demand)	Wind power capacity (1 kW = mean U.S. demand)	Solar power capacity (1 kW = mean U.S. demand)
1-yr periods (start years: 1980, 1981, 1982, 1983, 1984, 1985, 1986, 1987, 1988, 1989, 1990, 1991, 1992, 1993, 1994, 1995, 1996, 1997, 1998, 1999, 2000, 2001, 2002, 2003, 2004, 2005, 2006, 2007, 2008, 2009, 2010, 2011, 2012, 2013, 2014, 2015, 2016, 2018)	max Q3 median Q1 min spread	0.123 0.119 0.116 0.115 0.108 13.0 %	525.28 438.12 393.53 357.45 228.1 130.0 %	2.71 2.22 1.99 1.74 0.86 213.0 %	2.84 2.47 2.3 2.16 2.0 41.0 %	1.4 1.21 1.11 0.9 0.55 155.0 %
2-yr periods (start years: 1980, 1982, 1984, 1986, 1988, 1990, 1992, 1994, 1996, 1998, 2000, 2002, 2004, 2006, 2008, 2010, 2012, 2014, 2016)	max Q3 median Q1 min spread	0.124 0.121 0.119 0.117 0.114 9.0 %	594.35 529.7 454.44 433.0 383.73 55.0 %	2.87 2.12 1.99 1.78 1.42 102.0 %	2.68 2.51 2.32 2.14 2.05 30.0 %	1.39 1.24 1.03 0.81 0.72 94.0 %
3-yr periods (start years: 1980, 1983, 1986, 1989, 1992, 1995, 1998, 2001, 2004, 2007, 2010, 2013, 2016)	max Q3 median Q1 min spread	0.125 0.122 0.121 0.118 0.115 8.0 %	653.02 598.4 557.8 536.79 384.76 70.0 %	2.32 2.04 1.9 1.83 1.42 64.0 %	2.67 2.4 2.35 2.31 2.08 28.0 %	1.4 1.05 1.02 0.92 0.72 94.0 %
4-yr periods (start years: 1980, 1984, 1988, 1992, 1996, 2000, 2004, 2008, 2012, 2016)	max Q3 median Q1 min spread	0.125 0.123 0.122 0.119 0.116 7.0 %	751.28 646.51 613.24 558.93 420.82 79.0 %	2.77 2.04 1.92 1.8 1.41 96.0 %	2.66 2.56 2.35 2.24 2.07 29.0 %	1.4 1.04 1.01 0.79 0.72 95.0 %
5-yr periods (start years: 1980, 1985, 1990, 1995, 2000, 2005, 2010, 2015)	max Q3 median Q1 min spread	0.125 0.123 0.122 0.121 0.119 5.0 %	718.57 674.43 608.48 575.92 511.4 41.0 %	2.25 1.97 1.83 1.58 1.39 62.0 %	2.62 2.49 2.33 2.2 2.08 26.0 %	1.39 1.23 1.07 0.84 0.72 94.0 %
6-yr periods (start years: 1980, 1986, 1992, 1998, 2004, 2010, 2016)	max Q3 median Q1 min spread	0.125 0.125 0.123 0.12 0.117 6.0 %	820.78 797.47 726.43 649.74 532.92 54.0 %	2.52 1.97 1.87 1.6 1.48 71.0 %	2.58 2.43 2.36 2.29 2.17 19.0 %	1.24 1.03 1.01 0.94 0.72 72.0 %

Table S5: Distribution of capacities for various simulation lengths. This data table supports Figure S5 and 5. Spread is defined as the relative difference between the max and the min: $(\text{max}-\text{min})/\text{min} \times 100$. The maximum is "spread" % greater than the minimum.

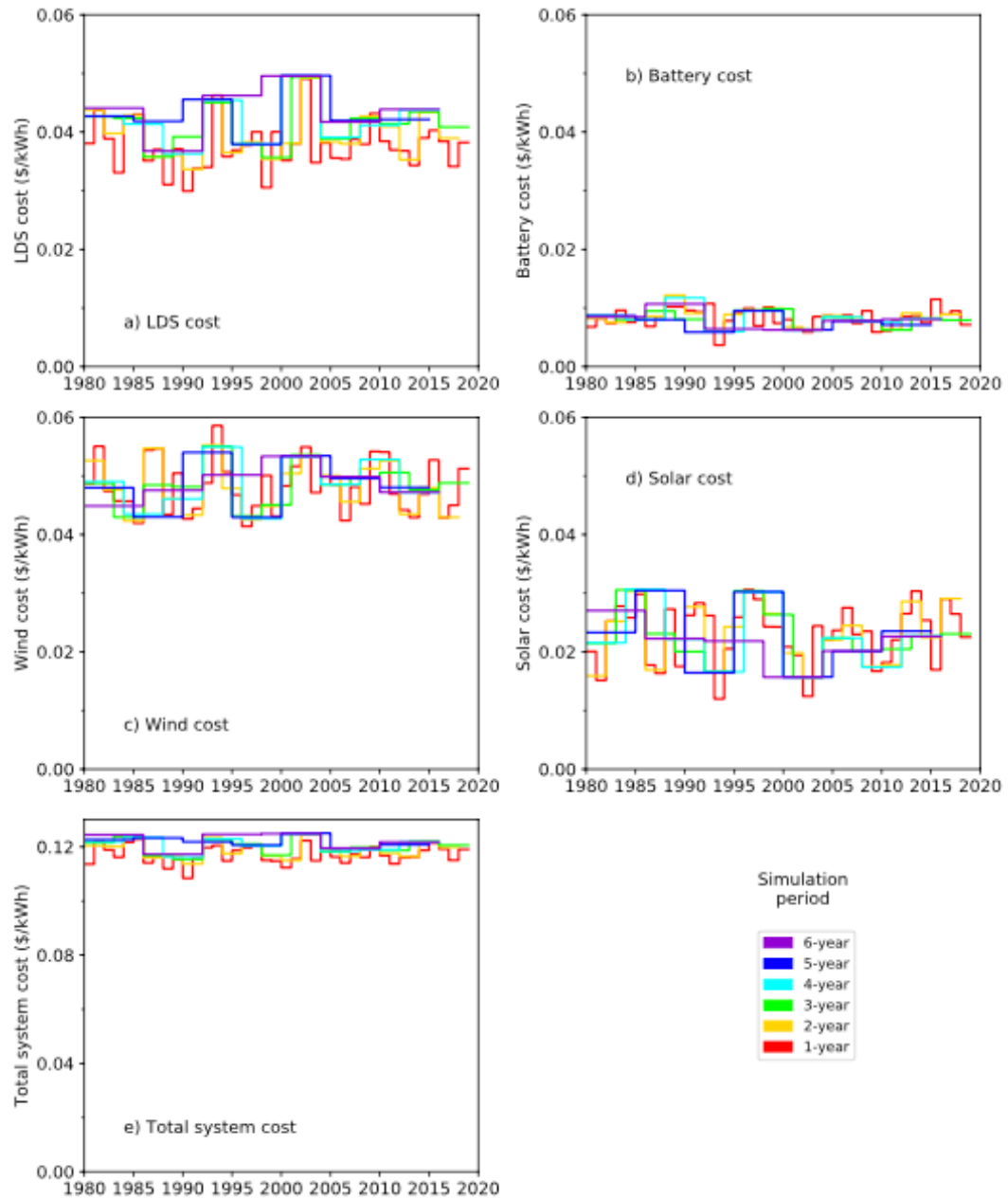


Figure S6: Multiple year simulations: costs. 1-, 2-, 3-, 4-, 5-, and 6-year simulations were performed across all 39 years of wind and solar data available (1980 to 2018) for the contiguous U.S. The horizontal sections of the lines represent the optimized investment in each technology for the periods simulated. Presented here are results for a) LDS cost, b) battery cost, c) wind cost, d) solar cost, and e) total system costs. LDS and wind technologies dominate system investments in all simulations periods across 1980-2018.

Simulation length (across 39 years, 1980-2018)	Data type	Total system cost (\$/kWh)	LDS cost (\$/kWh)	Battery cost (\$/kWh)	Wind cost (\$/kWh)	Solar cost (\$/kWh)
1-yr periods (start years: 1980, 1981, 1982, 1983, 1984, 1985, 1986, 1987, 1988, 1989, 1990, 1991, 1992, 1993, 1994, 1995, 1996, 1997, 1998, 1999, 2000, 2001, 2002, 2003, 2004, 2005, 2006, 2007, 2008, 2009, 2010, 2011, 2012, 2013, 2014, 2015, 2016, 2018)	max	0.123	0.049	0.011	0.059	0.031
	Q3	0.119	0.039	0.009	0.051	0.026
	median	0.116	0.038	0.008	0.047	0.024
	Q1	0.115	0.035	0.007	0.045	0.02
	min	0.108	0.03	0.004	0.041	0.012
	spread	12.0 %	64.0 %	213.0 %	41.0 %	155.0 %
2-yr periods (start years: 1980, 1982, 1984, 1986, 1988, 1990, 1992, 1994, 1996, 1998, 2000, 2002, 2004, 2006, 2008, 2010, 2012, 2014, 2016)	max	0.124	0.049	0.012	0.055	0.03
	Q3	0.121	0.043	0.009	0.052	0.027
	median	0.119	0.038	0.008	0.048	0.022
	Q1	0.117	0.036	0.008	0.044	0.018
	min	0.114	0.034	0.006	0.042	0.016
	spread	9.0 %	46.0 %	102.0 %	30.0 %	94.0 %
3-yr periods (start years: 1980, 1983, 1986, 1989, 1992, 1995, 1998, 2001, 2004, 2007, 2010, 2013, 2016)	max	0.125	0.049	0.01	0.055	0.031
	Q3	0.122	0.043	0.009	0.05	0.023
	median	0.121	0.041	0.008	0.049	0.022
	Q1	0.118	0.039	0.008	0.048	0.02
	min	0.115	0.036	0.006	0.043	0.016
	spread	8.0 %	39.0 %	64.0 %	28.0 %	94.0 %
4-yr periods (start years: 1980, 1984, 1988, 1992, 1996, 2000, 2004, 2008, 2012, 2016)	max	0.125	0.05	0.012	0.055	0.031
	Q3	0.123	0.044	0.009	0.053	0.023
	median	0.122	0.041	0.008	0.049	0.022
	Q1	0.119	0.039	0.008	0.046	0.017
	min	0.116	0.036	0.006	0.043	0.016
	spread	7.0 %	37.0 %	96.0 %	29.0 %	95.0 %
5-yr periods (start years: 1980, 1985, 1990, 1995, 2000, 2005, 2010, 2015)	max	0.125	0.05	0.01	0.054	0.03
	Q3	0.123	0.044	0.008	0.052	0.027
	median	0.122	0.042	0.008	0.048	0.023
	Q1	0.121	0.042	0.007	0.045	0.018
	min	0.119	0.038	0.006	0.043	0.016
	spread	5.0 %	31.0 %	62.0 %	26.0 %	94.0 %
6-yr periods (start years: 1980, 1986, 1992, 1998, 2004, 2010, 2016)	max	0.125	0.05	0.011	0.053	0.027
	Q3	0.125	0.046	0.008	0.05	0.023
	median	0.123	0.044	0.008	0.049	0.022
	Q1	0.12	0.042	0.007	0.047	0.021
	min	0.117	0.037	0.006	0.045	0.016
	spread	6.0 %	35.0 %	71.0 %	19.0 %	72.0 %

Table S6: Distribution of costs for various simulation lengths. This data table supports Figure S6 and Figure 5. Spread is defined as the relative difference between the max and the min: $(\text{max}-\text{min})/\text{min} \times 100$. The maximum is "spread" % greater than the minimum.

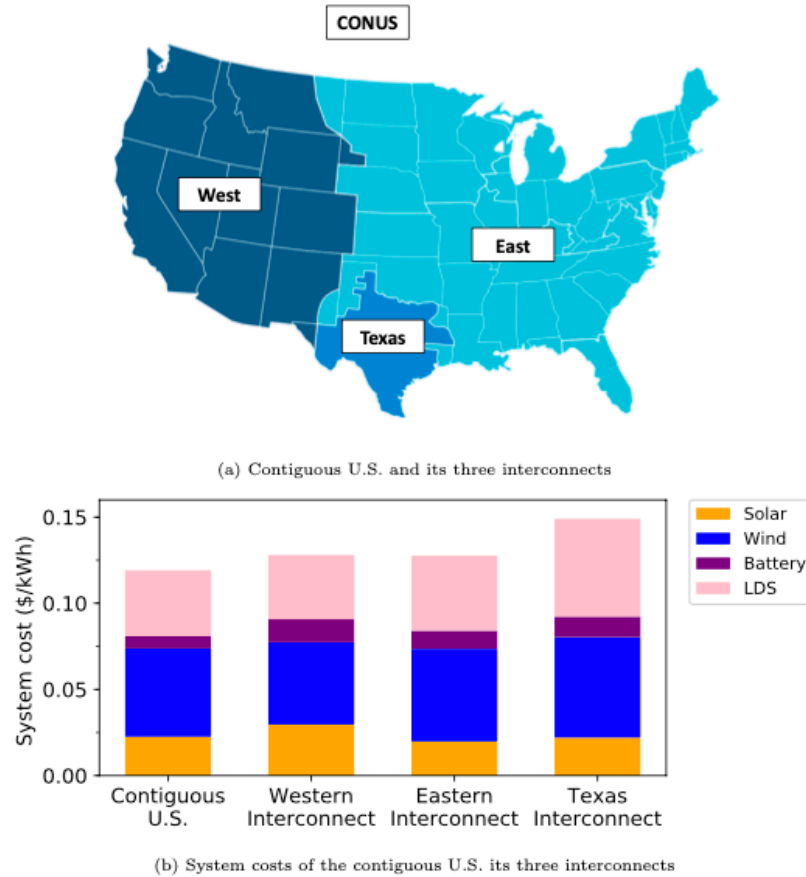


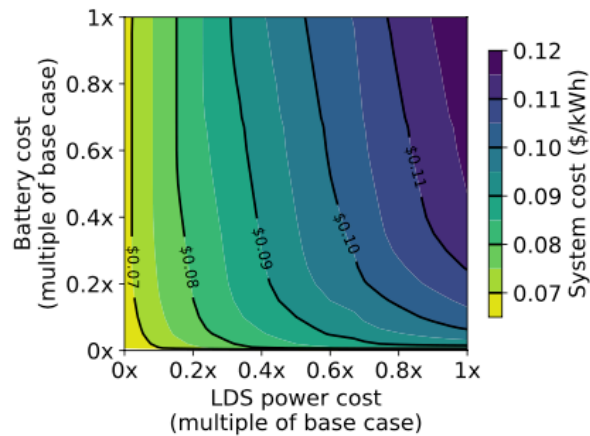
Figure S7: System costs of different geographical regions. System costs for the contiguous U.S. are compared to costs for systems confined to three largely independent interconnects: West, East, and Texas. Stacked areas in each bar represent the cumulative contribution of each technology to total system cost over the optimization period (2018). For each interconnect, the least-cost system includes substantial LDS and wind investment (66%, 76%, and 77% of total system cost for West, East, and Texas, respectively). The increased variability of wind and solar in small regions (such as Texas) requires compensation with more storage from both LDS and batteries. The map of the interconnects is adapted.³⁰ Table S7 supports this figure.

Region	Wind	Solar	LDS	Battery	Total system cost (\$/kWh)
Contiguous U.S.	0.05	0.02	0.04	0.01	0.12
Western Interconnect	0.05	0.03	0.04	0.01	0.13
Eastern Interconnect	0.05	0.02	0.04	0.01	0.13
Texas Interconnect	0.06	0.02	0.06	0.01	0.15

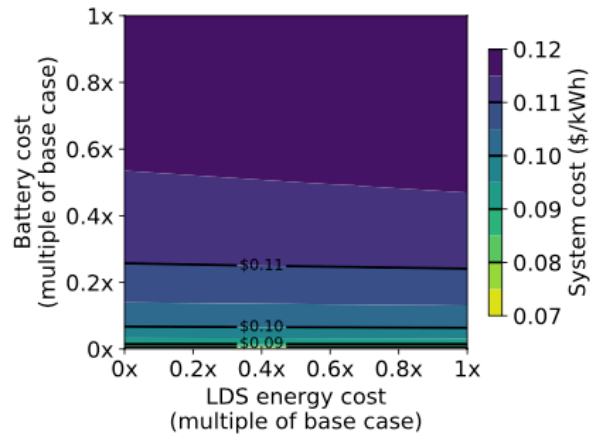
Table S7: System costs of different geographical regions. This data table supports Figure S7. Costs in \$/kWh represent each technology's contribution to the total system cost. Costs for LDS include both power-related and energy-related costs. While rounded results are displayed in the table, exact values were used for secondary calculations.

Technology mix	Wind	Solar	LDS	Battery	Total system cost (\$/kWh)
solar-battery	-	0.18	-	0.10	0.28
solar-LDS	-	0.12	0.13	-	0.25
solar-LDS-battery	-	0.09	0.05	0.05	0.19
wind-battery	0.18	-	-	0.05	0.23
wind-LDS	0.07	-	0.09	-	0.17
wind-LDS-battery	0.07	-	0.05	0.02	0.15
solar-wind-battery	0.09	0.04	-	0.02	0.14
solar-wind-LDS	0.05	0.02	0.06	-	0.13
solar-wind-LDS-battery	0.05	0.02	0.04	0.01	0.12

Table S8: System costs with different technology combinations. This data table supports Figure 6. Costs in \$/kWh represent each technology's contribution to the total system cost. Costs for LDS include both power-related and energy-related costs. While rounded results are displayed in the table, exact values were used for secondary calculations.



(a) LDS power-capacity cost and battery total cost reductions



(b) LDS energy-capacity cost and battery total cost reductions

Figure S8: Limiting factors of LDS and batteries. Battery costs are varied as a total capacity cost while LDS energy capacity and power capacity costs are varied independently. a) Power-capacity and b) energy-capacity costs were reduced from base case assumptions (1x) to free (0x), and total system costs were plotted as contour lines (\$/kWh). Each data point was a new simulation in which capacity and dispatch of each

technology, including wind and solar generation, were reoptimized in response to each value of the conversion and storage costs. For batteries, we varied the total costs and maintained a 6 hour charging duration. Total electricity system costs in a least-cost system decreased substantially with reductions in LDS conversion costs and, to a lesser extent, battery storage costs. This behavior occurs because the use of LDS in the least-cost system is limited by power capacity, whereas the use of batteries is limited by their energy capacity.

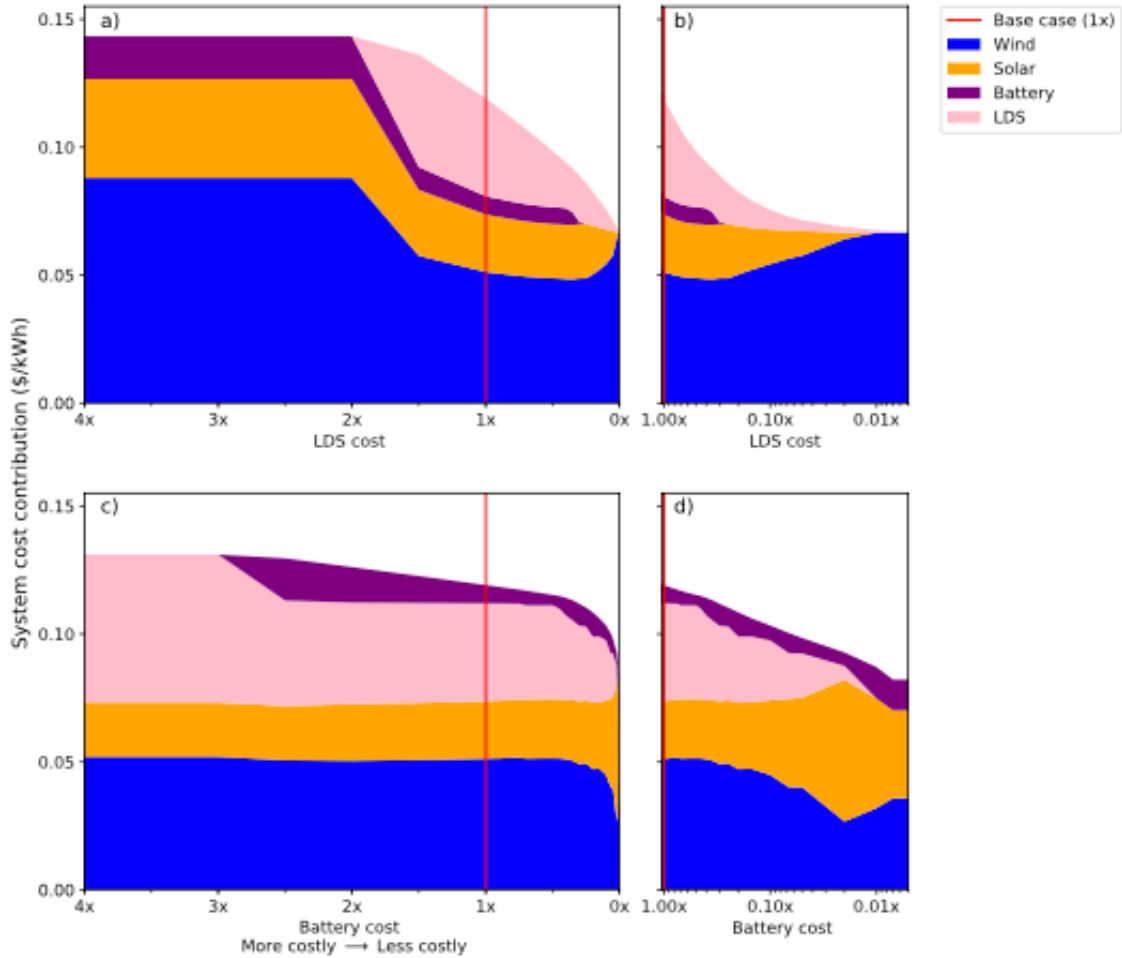


Figure S9: System cost contributions vs. LDS and battery costs. a, b) LDS and c, d) battery costs were varied from four times (4x) more costly than base case assumptions (1x) to free (0x). The contributions of each technology to the system cost for year 2018 are presented. Linear scale plots (a, c) showed that eliminating LDS from a least-cost electricity system required a $\sim 2x$ increase in costs relative to current costs, and batteries required a $\sim 3.5x$ increase in costs. The log scale plot of LDS cost reduction (b) showed that a ~ 4 -fold decrease in LDS costs (0.25x) eliminated batteries and reduced solar generation cost contribution. The log scale plot of battery cost reduction (d), showed that a ~ 100 -fold (0.01x) decrease in battery costs led to elimination of LDS and reduced cost contribution associated with wind generation.

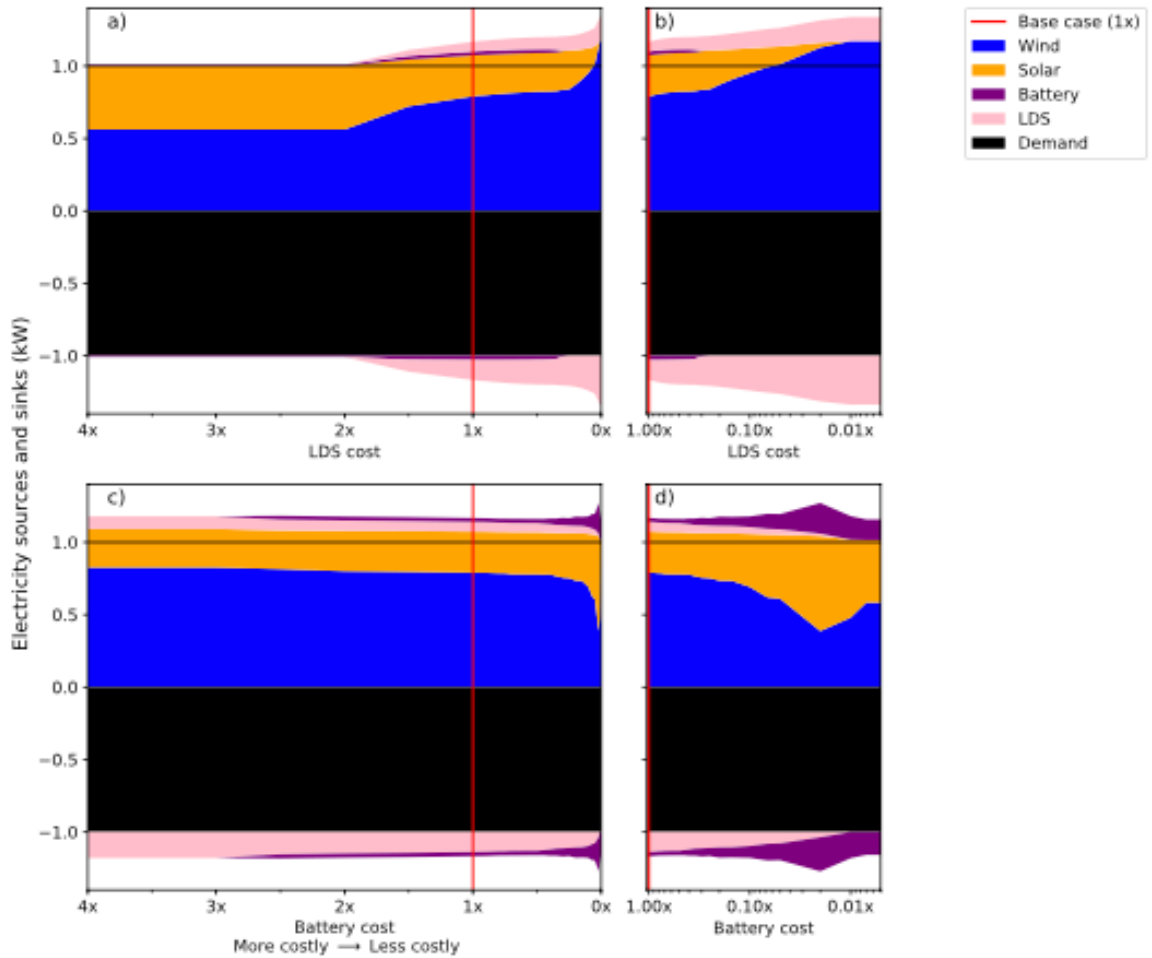
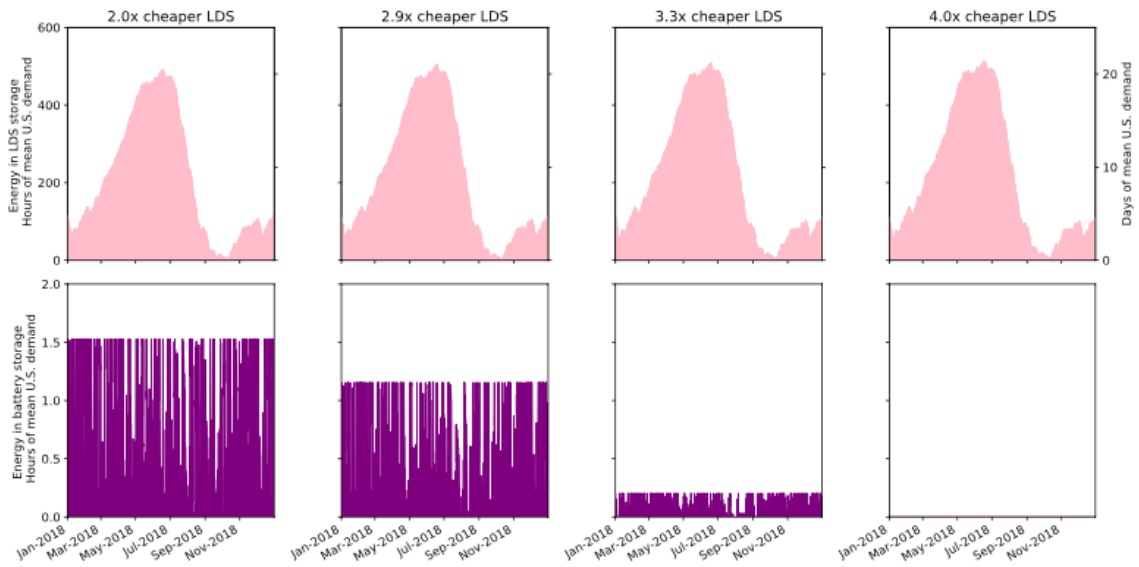
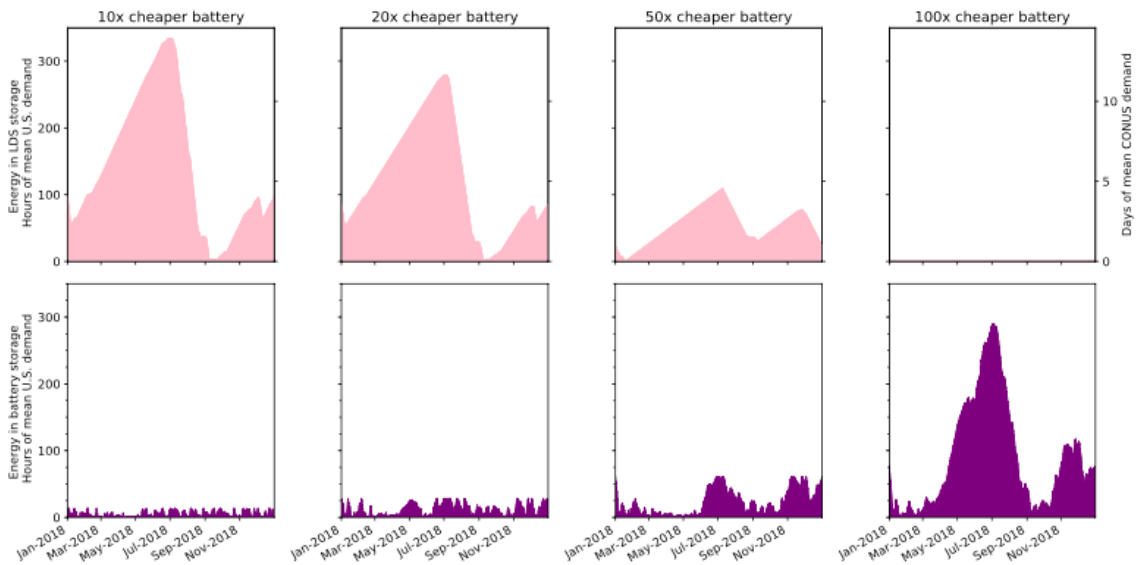


Figure S10: Dispatched electricity as a function of LDS and battery costs. a, b) LDS and c, d) battery costs were varied from four times (4x) more costly than base case assumptions (1x) to free (0x). Shares of electricity dispatched by each technology are shown on the y-axis. Total shares of electricity sources to the grid and those of electricity sinks from the grid are balanced for any hour in each simulation. The 49% round-trip efficiency of LDS is visually depicted in a, b) because the average power used for charging LDS was much larger than that obtained in discharging. This behavior can be compared to c, d) in which the 90% round-trip efficiency for batteries is evident. Cost contribution plots (Figure S9) in combination with power dispatch plots (Figure S10) allow determination of whether LDS's contribution to total system cost decreased because less LDS capacity was built or because LDS costs decreased.



(a) Less costly LDS



(b) Less costly batteries

Figure S11: Cost-driven functional role dynamics. This set of figures show energy stored in LDS and batteries at various costs. The top two rows of panels show that when LDS costs decrease at a factor of 4x, batteries disappear in the least-cost system. Despite lower LDS costs, LDS maintained its inter-season functional role, whereas batteries maintained their intra-day functional role. The bottom two rows of panels show that when battery cost is 100x cheaper, it is used more for inter-season storage than for purely intra-day storage, with the maximum energy stored in batteries reaching ~ 300 h of mean contiguous U.S. demand.

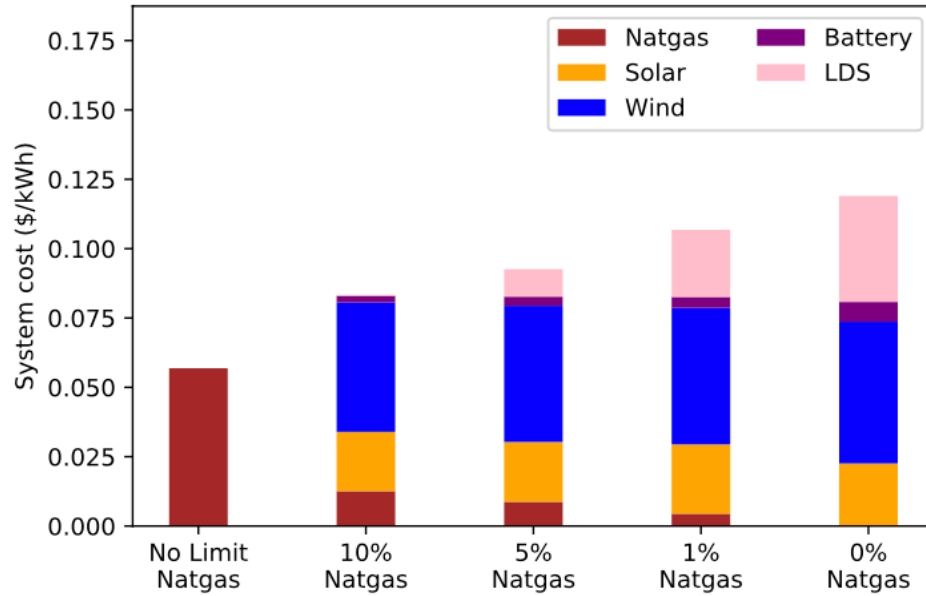


Figure S12: Natural gas: System costs approaching a 100% decarbonized system. A number of studies have shown that decarbonizing the electricity system becomes increasingly costly the close to 100% carbon-neutral the system is. We briefly explore these questions by allowing natural gas generators in our model but limit their annual dispatch to a fraction of total demand. We model 1) a system with current cost assumptions for natural gas with no limits on dispatch, 2) the same system with natural gas dispatch limited to 10% of annual demand, 3) natural gas limited to serving 5%, then 4) natural gas limited to 1% of demand. A reference bar is added that is the baseline no natural gas case modeled in the rest of this analysis. Stacked areas in each bar represent the cumulative contribution of each technology to total system cost over the optimization period (2018). Introduction of natural gas to the technology mix at 10% of demand minimizes or eliminates the need for storage. The system costs are: 1) 0.057 \$/kWh, 2) 0.083 \$/kWh, 3) 0.093 \$/kWh, 4) 0.107 \$/kWh, and 0.119 \$/kWh for the reference case. Technical and economic inputs for natural gas are in Table S11.

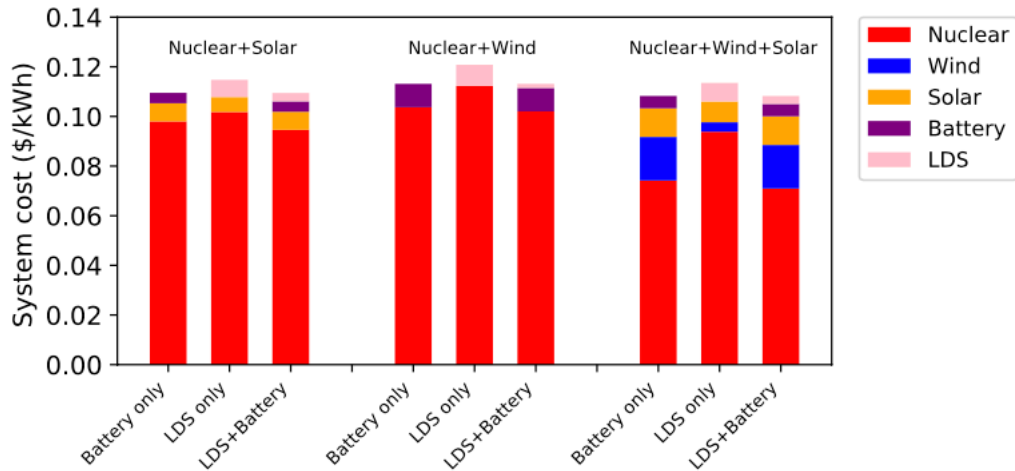


Figure S13: Nuclear: System costs for different technology combinations. In the left- most three bars, generation is provided only by solar energy and nuclear; in the middle three bars, by only wind energy and nuclear; and, in the right-most three bars, by a combination of solar, wind, and nuclear resources. Within each grouping of three bars, the left-most bar represents a system with only LDS storage, the middle bar represents a system with only battery storage, and the right-most bar allows both storage technologies to

compete. Stacked areas in each bar represent the cumulative contribution of each technology to total system cost over the optimization period (2018). Introduction of nuclear to the technology mix minimizes, but does not eliminate, the need for storage. Technical and economic inputs for nuclear are in Table S11.

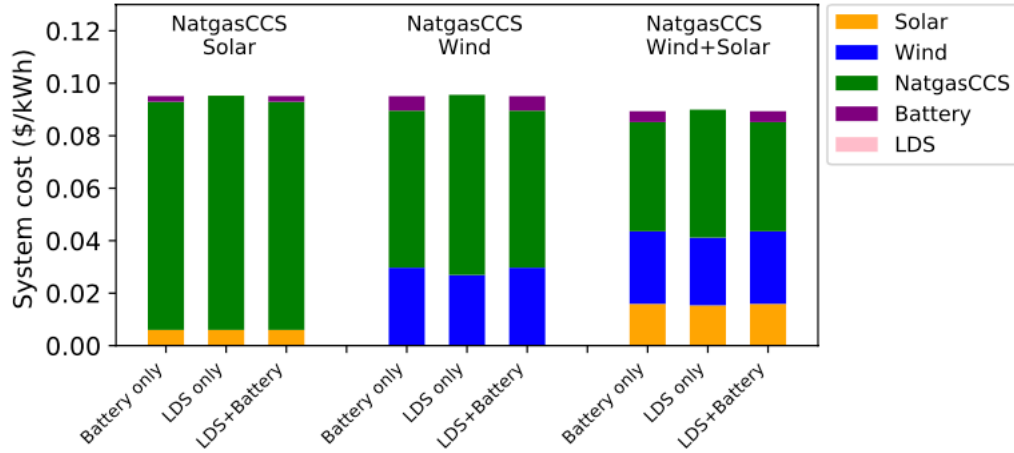


Figure S14: Natural gas with carbon capture and storage (natgas CCS): System costs for different technology combinations. In the left-most three bars, generation is provided only by solar energy and natgas CCS; in the middle three bars, by only wind energy and natgas CCS; and, in the right-most three bars, by a combination of solar, wind and natgas CCS resources. Within each grouping of three bars, the left-most bar represents a system with only LDS storage, the middle bar represents a system with only battery storage, and the right-most bar allows both storage technologies to compete. Stacked areas in each bar represent the cumulative contribution of each technology to total system cost over the optimization period (2018). Introduction of natgas CCS to the technology mix minimizes or eliminates the need for storage (especially LDS). Technical and economic inputs for natgas CCS are in Table S11.

Section 6.2.3 Supplementary Cost Information:

Base case long-duration storage technology: Power-to-Gas-to-Power (PGP) with renewable hydrogen

PGP underground storage

	Salt cavern (base case)	Reference and comments
Fixed capital cost (\$)	7,434,940	Capital cost plus land costs for just the cavern (not compressor) H2A tab "Gaseous H ₂ Geologic Storage" cell C217
Size (usable kg H ₂)	1,159,831	Default value in H2A model tab "Gaseous H ₂ Geologic Storage" cell B103
Size (Energy rating, kWh)	45,697,341.40	Calculated here using the higher heating value (H ₂): 39.4 kWh/kg. From Hydrogen Delivery Scenario Model (HDSAM) V 3.1.
Fixed cost (\$/kWh for storage)	0.16	Hydrogen Delivery Scenario Model (HDSAM) V 3.1. Note: Steward et al NREL report, (Table 3) quotes 0.16 \$/kWh for dry mined salt caverns.
Lifetime (yrs)	30	Hydrogen Delivery Scenario Model (HDSAM) V 3.1.

Table S9: Economic and technical assumptions for underground hydrogen storage. Models and reports referenced.^{31,32} This table supports Table 1. Figure 7b and Figure S8b show that results are not very sensitive to PGP energy capacity costs.

PGP electrolyzer + compressor combined fixed cost

Because electrolyzers and compressors are both power-rated conversion devices involved in the H₂ production step of PGP, we combined their fixed costs into one input variable for the model. To combine the fixed costs of electrolyzer and compressor devices, we determined the ratio of their system efficiencies as shown below.

Electrolyzer

$$\text{Electrolyzer system efficiency} = 67 \text{ kWh/kg}^{33}$$

Compressor

$$\text{Design Flow to Each Compressor} = 57,991 \text{ (kg/day)}$$

$$\text{Motor Rating per Compressor} = 1,487 \text{ kW}$$

Reference,³¹ tab "Gaseous H₂ Geologic Storage", cell B138 and B145 Electricity required to compress 57,991 kg of H₂:

$$(1,487 \text{ kW}) \times 24 \text{ (h/day)} = 35,688 \text{ kWh}$$

Compressor system efficiency:

$$(35,688 \text{ kWh}) / (57,991 \text{ kg H}_2) = 0.6154 \text{ kWh/kg H}_2$$

Electrolyzer / Compressor Ratio

Ratio of power consumption:

$$(67 \text{ kWh/kg}) / (0.6154 \text{ kWh/kg}) = 109$$

The electrolyzer consumes 109 times more power than the compressor for a given kg of H₂ that goes through the system. Thus, to combine the electrolyzer and compressor costs and put them into the units of the electrolyzer, we divide the fixed cost of the compressor by 109.

Combined fixed cost (\$/kW for conversion)

Costs for electrolyzers and compressors in \$/kW are in Table S10.

$$(1,045 \text{ \$/kW}) + (1392.2 \text{ \$/kW})/109 = 1,058 \text{ \$/kW}$$

The combined electrolyzer + compressor fixed cost is represented as the H₂ production conversion cost in Table 1.

	Electrolyzer (PEM)	Reference and comments	Compressor (Isentropic reciprocating)	Reference and comments
Fixed capital cost (\$)	118,258,606	Capital costs including O&M costs like labor PEM spreadsheet, tab "Capital costs", cell F36	2,070,236	H2A spreadsheet tab "Gaseous H ₂ Geologic Storage" cell C182
Size (Power rating, kW)	113,125	Capital costs including O&M costs like labor PEM spreadsheet, tab "Capital costs", cell C41	1,487	H2A spreadsheet tab "Gaseous H ₂ Geologic Storage" cell B182
Fixed cost (\$/kW for conversion)	1,045 input into the electrolyzer ¹	Current Central Hydrogen Production from Grid PEM Electrolysis V3 2018	1392.2 used to compress ^a	Hydrogen Delivery Scenario Model (HDSAM) V 3.1
Lifetime (yrs)	10	Schmit, 2017 ³⁴	15	H2A spreadsheet tab "Gaseous H ₂ Geologic Storage" cell B160
Efficiency	70%	Current Central Hydrogen Production from Grid PEM Electrolysis V3 2018 tab "Process Flow" cell G12	100%	Assume no hydrogen leaks during compression.

Table S10: Economic and technical assumptions for electrolyzers and compressors. Models referenced include.^{31,35} This table supports Table 1. Electrolyzer and compressor lifetime detail is available at the following link: https://docs.google.com/spreadsheets/d/1nmrfp_s-C8Pqtqgyp3kgou2Pi80tcXTFXiO-qWCvx9Q/edit?usp=sharing.

^aSee electrolyzer + compressor combined fixed cost calculation. The electrolyzer consumes 109 times more power than the compressor for a given kg of H₂ that goes through the system. Thus, to combine the electrolyzer and compressor costs and put them into the units of the electrolyzer, we divide the fixed cost of the compressor by 109.

Firm generator technology costs

	Natural gas	Natural gas with CCS	Nuclear
Technology description	Conventional gas/oil combined cycle	Advanced combined cycle with carbon capture and storage	Advanced nuclear
Total overnight capital cost [\$/W]	982	2175	5946
Fuel cost [\$/MMBtu]	3	3	-
Fuel cost [mills/kWh]	-	-	7.45
nth-of-a-kind heat rate [Btu/kWh]	6350	7494	10460
Fixed O&M cost [\$/kW/yr]	11.11	33.75	101.28
Variable O&M cost [\$/MWh]	3.54	7.20	2.32
Project life [yrs]	20	20	40
Calculated levelized costs			
Fixed cost [\$/kWh]	0.012	0.027	0.065
Variable cost [\$/kWh]	0.039	0.056	0.007

Table S11: Economic and technical assumptions for natural gas, natural gas with CCS, and nuclear. References included.³⁶⁻³⁸ This table supports Figure S12, Figure S13, and Figure S14. An example

calculation of fixed and variable costs for natural gas with CCS is in Table S12. Note: For nuclear we include only fuel costs as (in units of per kWh electricity not per kWh thermal) as variable costs and add all other non-fuel costs to the fixed cost.

Example calculation: natural gas with CCS fixed and variable cost

Variable cost calculation of natural gas with carbon capture and storage (NatgasCCS). This calculation supports Figure S14, Table S11, and Table S12.

Efficiency

Heat rate = 7493 (Btu/kWh)³⁶

Heat content of electricity = 3412.14 (Btu/kWh)³⁹ Efficiency: (1/7493) x 3412.14 = 0.4554

Fuel Cost

Fuel cost = 3 (\$/MMBtu-thermal)³⁸

Fuel cost = 0 (mills/kWh-electric)³⁸

Heat content of electricity = 0.293 (MWh/MMBtu)³⁹

Efficiency = 0.4554

Fuel cost (\$/kWh-electric): (3/0.293/1000)/0.4554 + 0/1000 = 0.0225

Variable cost

Fuel cost (\$/kWh-electric) = 0.0225

Efficiency = 0.4554

Variable O&M cost(\$/MWh) = 7.2³⁶

Variable cost: (0.0225/ 0.4554) + (7.2/1000) = 0.0566

NatgasCCS: Fixed cost calculations	Value	Reference and comments	NatgasCCS: Variable cost calculations	Value	Reference and comments
Capital cost (\$/kW)	2175	EIA, AEO2018, Electricity Market Module, Table 2	Fuel cost (\$/MMBtu-thermal)	3	EIA, EPA2016, Table 7.20
Assumed lifetime (yrs)	20	EIA, AEO2018, Commercial Demand Module, Table 3	Fuel cost (mills/kWh-electric)	0	EIA, EPA2016, Table 7.20
Capital recovery factor (% per year)	9.44%	Calculated with a discount rate of 0.07	Heat rate (Btu/kWh)	7493	EIA, AEO2018, Electricity Market Module, Table 2
Fixed O&M cost (\$/kW-yr)	33.75	EIA, AEO2018, Electricity Market Module, Table 2	Efficiency	0.4554	Calculated here
Fixed cost (\$/kW-yr)	239.05	(capital cost * capital recovery factor) + fixed O&M cost	Fuel cost (\$/kWh-electric)	0.0225	Calculated here
Fixed cost (\$/kWh)	0.02727	Divide the cell above by hours in a year	Variable O&M cost (\$/MWh)	7.2000	EIA, AEO2018, Electricity Market Module, Table 2
			Variable cost (\$/kWh)	0.0566	Calculated here

Table S12: Economic and technical assumptions for natural gas with carbon capture and storage (NatgasCCS). References included.³⁶⁻³⁸ This table supports Figure S14 and Table S11.

Section 6.2.4: Supporting Information References within Chapter 6.2:

1. Bussar, C., Stöcker, P., Cai, Z., Moraes Jr, L., Magnor, D., Wiernes, P., van Bracht, N., Moser, A., Sauer, D. U. (2016). Large-scale integration of renewable energies and impact on storage demand in a European renewable power system of 2050—Sensitivity study. *Journal of Energy Storage* 6, 1–10.
2. Ringkjøb, H.-K., Haugan, P. M., Solbrekke, I. M. (2018). A review of modelling tools for energy and electricity systems with large shares of variable renewables. *Renewable Sustainable Energy Rev.* 96, 440–459.
3. Luo, X., Wang, J., Dooner, M., Clarke, J. (2015). Overview of current development in electrical energy storage technologies and the application potential in power system operation. *Appl. Energy* 137, 511–536.
4. Lazard, New York (2019). Lazard’s Levelized Cost of Energy Analysis—Version 13.0, Tech. rep.
5. Viswanathan, V., Crawford, A., Stephenson, D., Kim, S., Wang, W., Li, B., Coffey, G., Thomsen, E., Graff, G., Balducci, P., Kintner-Meyer, M., Sprenkle, V. (2014). Cost and performance model for redox flow batteries. *J. Power Sources* 247, 1040–1051.
6. Deane, J. P., Ó Gallachóir, B. P., McKeogh, E. J. (2010). Techno-economic review of existing and new pumped hydro energy storage plant. *Renewable Sustainable Energy Rev.* 14, 1293–1302.
7. Chen, H., Cong, T. N., Yang, W., Tan, C., Li, Y., Ding, Y. (2009). Progress in electrical energy storage system: A critical review. *Prog. Nat. Sci.* 19, 291–312.
8. Virginia’s Legislative Information System (2020). House Bill 1526 Virginia Clean Economy Act, Legislation.
9. Maine Legislature (2019). Legislative Document 1494: An Act to Reform Maine’s Renewable Portfolio Standard, Legislation, <http://www.mainelegislature.org>.
10. Hawaii State Legislature (2015). House Bill 623 Relating to Renewable Standards, Legislation, <https://www.capitol.hawaii.gov>.
11. New Mexico Legislature (2019). Senate Bill 489 Energy Transition Act, Legislation, <https://www.nmlegis.gov>.
12. New York State Senate (2019). Senate Bill S6599, Legislation, <https://www.nysenate.gov>.
13. California Legislative Information (2018). Senate Bill 100 California Renewables Portfolio Standard Program: Emissions of Greenhouse Gases, Legislation, <https://leginfo.legislature.ca.gov>.
14. Nevada Legislature (2019). Senate Bill 358 Revises provisions relating to the renewable energy portfolio standard, Legislation, <https://www.leg.state.nv.us>.
15. Washington State Legislature (2019). Senate Bill 5116 Supporting Washington’s clean energy economy and transitioning to a clean, affordable, and reliable energy future, Legislation, <http://leg.wa.gov>.
16. Legislative Assembly of Puerto Rico (2019). Senate Bill 1121 Puerto Rico Energy Public Policy Act, Legislation, <https://aeepr.com>.
17. DC Legislature (2019). Clean Energy DC Omnibus Amendment Act of 2018, Legislation, <https://code.dccouncil.us>.
18. California Energy Commission (2020). Senate Bill 100 Modeling Inputs and Assumptions Workshop, Tech. rep., SB 100 Joint-agency report overview and analytical approach - Staff presentation. Slide 28. <https://www.energy.ca.gov/event/workshop/2020-02/senate-bill-100-modeling-inputs-and-assumptions-workshop>.
19. National Conference of State Legislatures (2020). State Renewable Portfolio Standards and Goals, Online, <https://www.ncsl.org>.
20. Shaner, M. R., Davis, S. J., Lewis, N. S., Caldeira, K. (2018). Geophysical constraints on the reliability of solar and wind power in the United States. *Energy Environ. Sci.* 11, 914–925.
21. International Renewable Energy Agency (2012). Electricity storage: technology brief, Tech. rep., Technology Policy Brief, Energy Technology Systems Analysis Programme. <https://www.irena.org>.
22. Beaudin, M., Zareipour, H., Schellenberglabe, A., Rosehart, W. (2010). Energy storage for mitigating the variability of renewable electricity sources: An updated review. *Energy for Sustainable Development* 14, 302–314.

23. Kaldellis, J. K., Zafirakis, D. (2007). Optimum energy storage techniques for the improvement of renewable energy sources-based electricity generation economic efficiency. *Energy* 32, 2295–2305.
24. Lazard, New York (2019). Lazard’s Levelized Cost of Storage Analysis– Version 5.0, Tech. rep.
25. Electric Power Research Institute (EPRI (2010). Electricity Energy Storage Technology Options: A White Paper Primer on Applications, Costs, and Benefits, Tech. rep.
26. Succar, S., Williams, R. H., Others, (2008). Compressed air energy storage: Theory, resources, and applications for wind power. Princeton Environmental Institute Report 8, 81.
27. Sandia National Laboratories (2011). Energy storage systems cost update: A study for the DOE Energy Storage Systems Program., Tech. rep., Sandia Report: SAND2011-2730.
28. Madlener, R., Latz, J. (2013). Economics of centralized and decentralized compressed air energy storage for enhanced grid integration of wind power. *Appl. Energy* 101, 299–309.
29. North American Electric Reliability Corporation. (NERC), Atlanta, GA (United States) (2012). 2012 State of Reliability, Tech. rep.
30. Duke Energy (2014). The Regional Grid - Duke Energy Electricity 101, Tech. rep., <https://datacache.duke-energy.com>.
31. Argonne National Laboratory, Centre for Transportation Research (2015). H2A Delivery Scenario Analysis Model Version 3.0*(HDSAM 3.0) User’s Manual, Tech. rep.
32. National Renewable Energy Lab (NREL), Golden, CO (United States) (2009). Lifecycle cost analysis of hydrogen versus other technologies for electrical energy storage.
33. Proton Onsite (2017). Technical Specifications: C Series Hydrogen Generation Systems, Tech. rep., <http://www.protonenergy.com>.
34. Schmidt, O., Gambhir, A., Staffell, I., Hawkes, A., Nelson, J., Few, S. (2017). Future cost and performance of water electrolysis: An expert elicitation study. *Int. J. Hydrogen Energy* 42, 30470–30492.
35. National Renewable Energy Lab (NREL), Golden, CO (United States) (2013). PEM Electrolysis H2A Production Case Study Documentation.
36. United States Energy Information (2018). Assumptions to the Annual Energy Outlook 2018: Electricity Market Module, Tech. rep., <https://www.eia.gov>.
37. United States Energy Information (2018). Assumptions to the Annual Energy Outlook 2018: Commercial Demand Module, Tech. rep., <https://www.eia.gov>.
38. United States Energy Information (2016). EIA Electric Power Annual 2016, Tech. rep., Table 7.20. Average Cost of Natural Gas Delivered for Electricity Generation by State, 2016 and 2015 <https://www.eia.gov/electricity/annual>.
39. United States Energy Information (2020). EIA Monthly Energy Review, Tech. rep., Table A6. Approximate Heat Rates for Electricity, and Heat Content of Electricity <https://www.eia.gov/totalenergy/data/monthly>.

6.3 Supporting Information for Chapter 3

Supporting Figures:

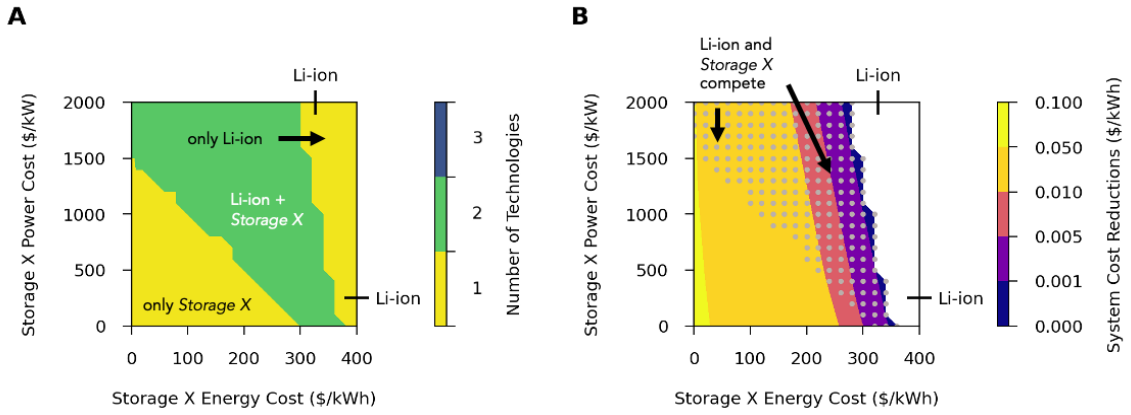


Figure S1. System cost reductions and storage technologies present in scenarios with up to two storage options available: short-duration storage (Li-ion) and a hypothetical Storage X technology with varying energy- and power-capacity costs. Total costs for Li-ion batteries were kept constant at base-case values, marked on the top and right sides with values in Table 2. Note that the energy- and power-capacity ratio of Li-ion batteries are kept at a ratio of 4 hours. (A) Types of storage technologies used in least-cost systems where Storage X energy- and power-capacity costs vary across wide ranges. The technologies that were present in each parameter range are written in black and white font. (B) Percent reductions in total system cost as compared to a least-cost system with only Li-ion battery storage at base case costs.

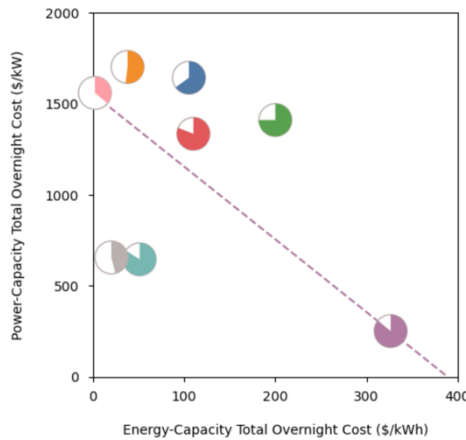


Figure S2. Base case energy- and power-capacity total overnight costs of energy storage technologies modeled, where Li-ion total costs are shown as a dashed-line. Although Li-ion costs have been divided by the source into an energy-capacity cost of 326 \$/kWh and power-capacity cost of 251 \$/kW, individual Li-ion batteries have energy and power capacities that cannot be independently sized. Thus, for the 4-hour Li-ion battery considered here, if the battery is sized based on energy capacity, then the effective energy-capacity cost is 326 \$/kWh+251 \$/kW4h=388.75 \$/kWh and the effective power-capacity cost is 0 \$/kW. In contrast, if the battery is sized based on power capacity, then the effective energy-capacity cost is 0 \$/kWh and the effective power-capacity cost is 388.75 \$/kWh4h=1555 \$/kW. The dashed line that intersects these two points describe the cost of Li-ion batteries when they are partially sized for power-capacity, and partially sized for energy-capacity.

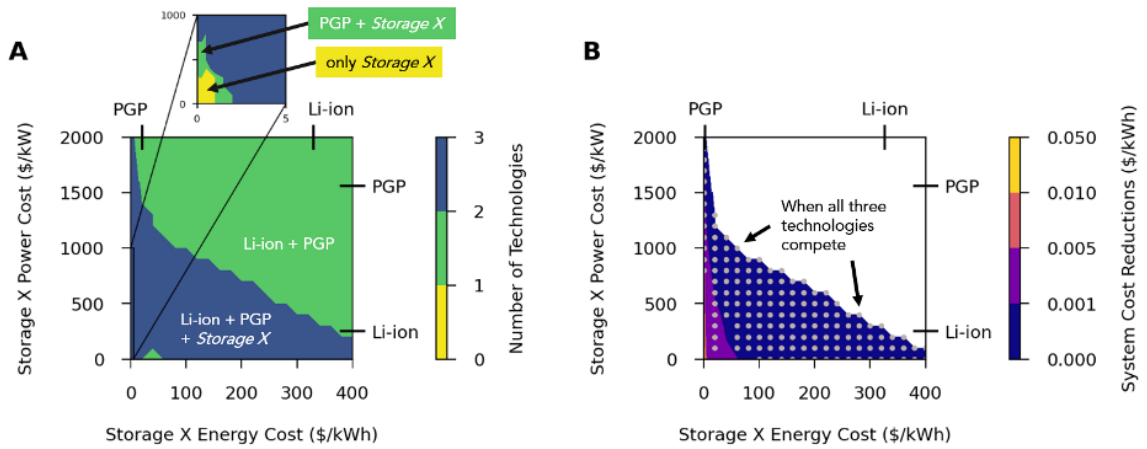


Figure S3. Competitive behavior of storage technologies remained consistent even at different efficiencies for *Storage X*. (A) Number and types of technologies present and (B) system cost reductions when *Storage X* has an efficiency of 36%. Results are qualitatively similar to those when *Storage X* has an efficiency of 86%.

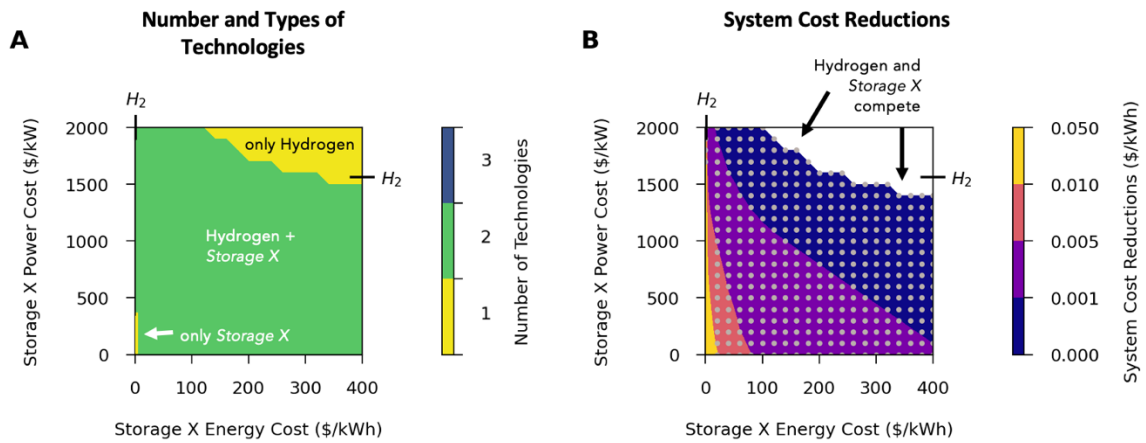


Figure S4. System cost reductions and storage technologies present in scenarios with up to two storage options available: long duration storage (hydrogen) and a hypothetical Storage X technology with varying energy- and power-capacity costs. Energy- and power-capacity costs for hydrogen storage were kept constant at base-case values, marked on the top and right sides with values in Table 2. (A) Types of storage technologies used in least-cost systems where Storage X energy- and power-capacity costs vary across wide ranges. The technologies that were present in each parameter range are written in black and white font. (B) Percent reductions in total system cost as compared to a least-cost system with only hydrogen storage at base case costs.

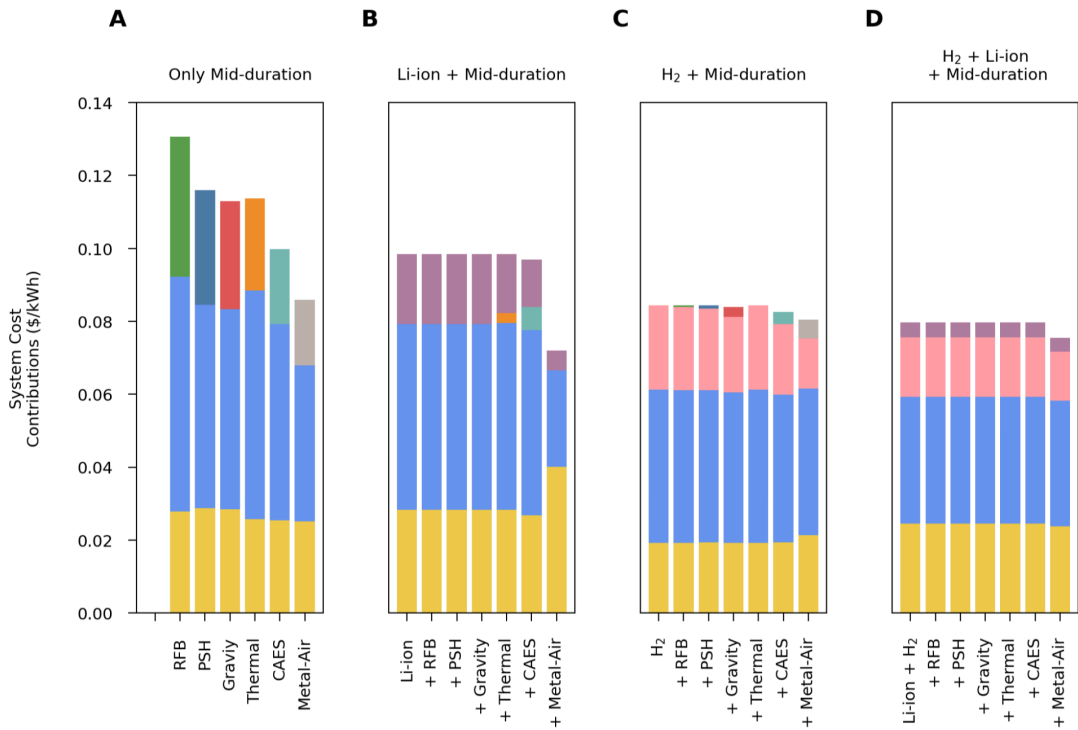


Figure S5. System costs for combinations of short-, mid-, and long-duration storage. Same conditions as Figure 3.4, except Li-ion batteries have a cost of 100 \$/kWh (instead of base case cost of 350 \$/kWh).

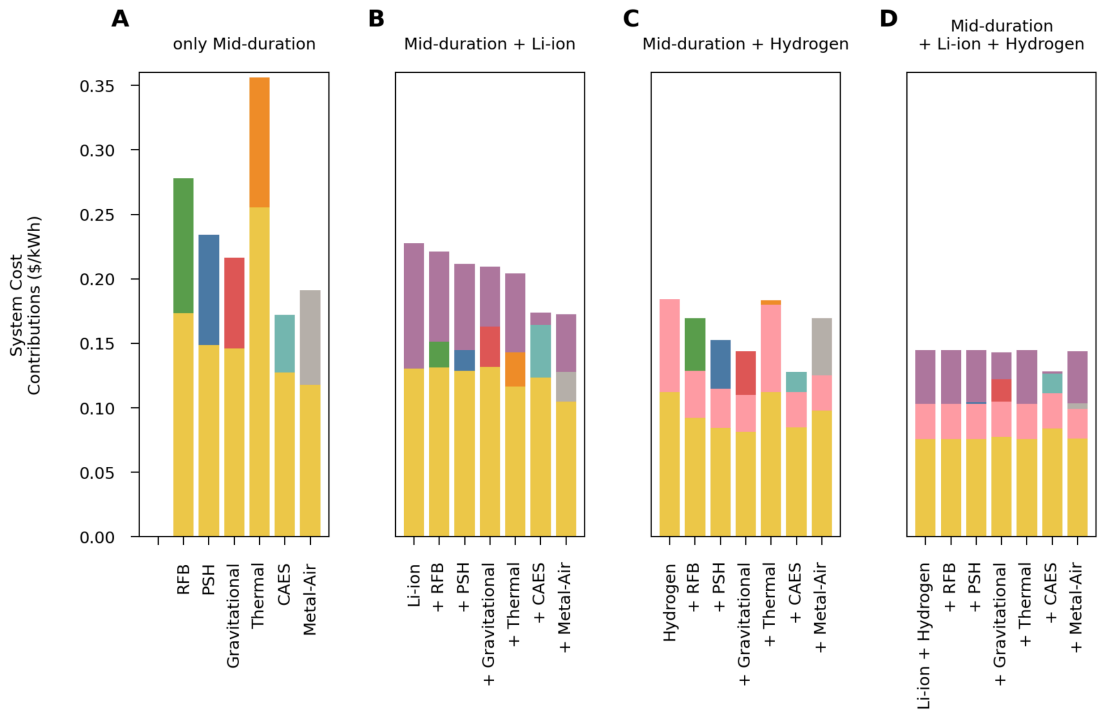


Figure S6. System costs for combinations of short-, mid-, and long-duration storage with only solar generation. Same conditions as Figure 3.4, but only solar generation.

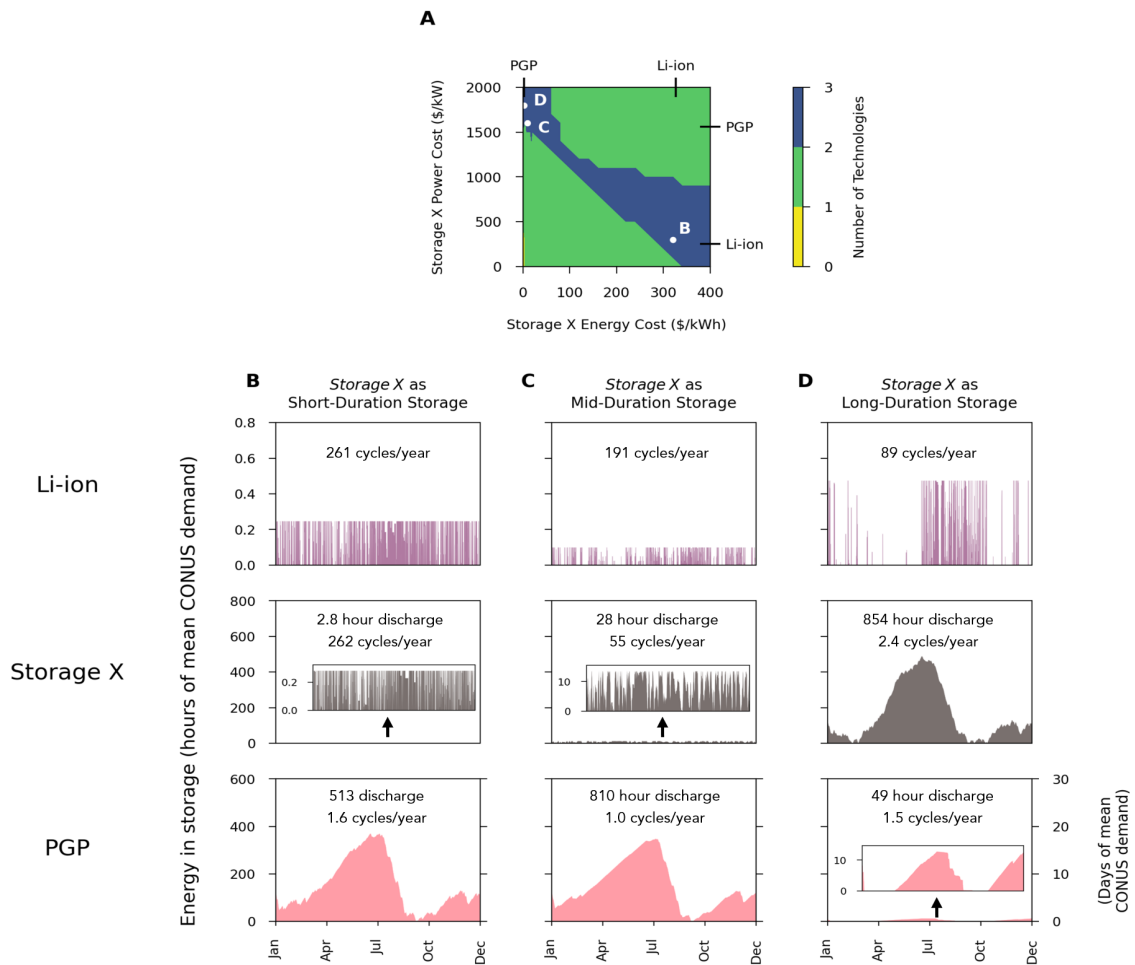


Figure S7. A hypothetical *Storage X* stores energy on different timescales, based on its energy- and power-capacities relative to those of Li-ion battery storage and hydrogen storage. Energy in storage over the period of one year when all three storage technologies (Li-ion, *Storage X*, and hydrogen storage) play a role. The energy- and power-capacity costs of this hypothetical *Storage X* technology are denoted in panel (A). (B) When *Storage X* had power-capacity costs comparable with those of Li-ion, but energy-capacity costs much higher than those of hydrogen storage, it competed with Li-ion batteries for the role of short-duration storage, storing energy on daily timescales. (C) When *Storage X* had costs still competitive with Li-ion batteries, and energy-capacity costs approaching those with hydrogen storage, it played the role of mid-duration storage, storing energy on weekly timescales. (D) When *Storage X* had costs still competitive with Li-ion batteries, and energy-capacity costs low enough to be competitive with those of hydrogen storage, it competed for hydrogen storage for the role of long-duration storage, storing energy on a seasonal timescale and substantially reducing the capacity build of hydrogen storage.

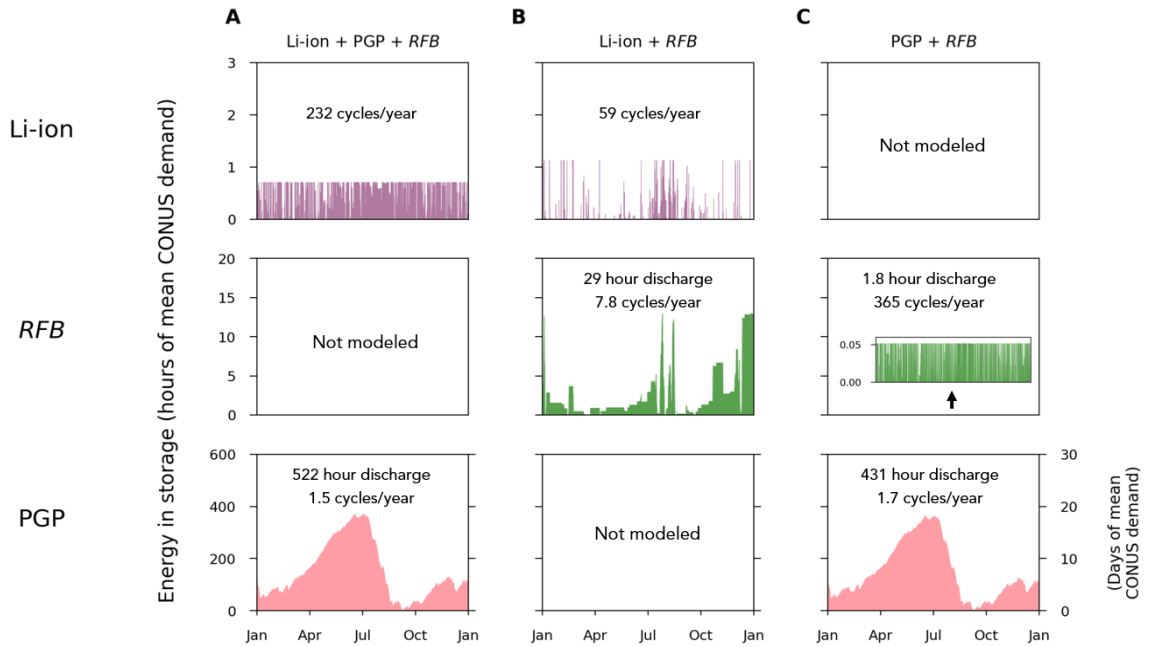


Figure S8. The energy storage role of RFB depends on the presence of other storage technologies in the system. (A) When both Li-ion batteries and hydrogen storage were available as storage technologies, RFB was not cost-competitive. (B) When RFB only competed against Li-ion, it played the role of long duration storage. (C) When RFB only competed against hydrogen storage, it played the role of short duration storage.

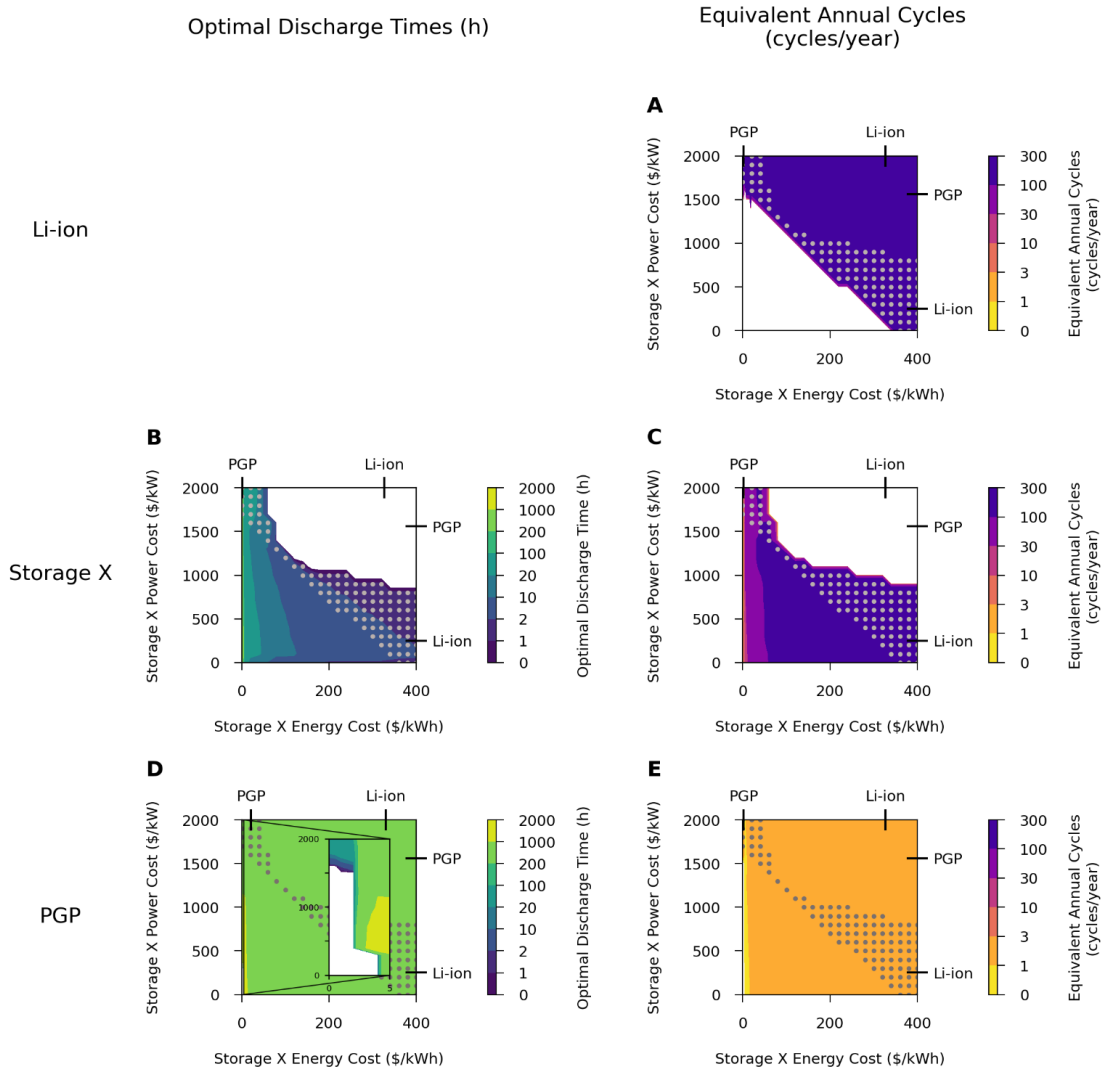


Figure S9. A hypothetical *Storage X* plays different energy storage roles depending on its energy- and power-capacity costs compared to those of Li-ion and hydrogen storage. Optimal discharge times in hours of (B) *Storage X* and (C) hydrogen storage, and equivalent annual cycles in cycles per year of (A) Li-ion battery storage, (C) *Storage X*, and (E) hydrogen storage.

Result	Units	Case Without <i>Storage X</i>	Storage X Options					
		Only Li-ion + hydrogen	+ RFB	+ PSH	+ Gravitational	+ Thermal	+ CAES	+ Metal-Air
System Cost	\$/kWh	0.083	0.083	0.083	0.083	0.083	0.083	0.080
Li-ion Capacity	kWh	0.714	0.714	0.714	0.714	0.714	0.114	0.252
To Storage X Power Capacity	kW	Not modeled	0	0	0	0	0.0085	0.456
Storage X Energy Storage Capacity	kWh	Not modeled	0	0	0	0	2.435	39.531
From Storage X Out Power Capacity	kW	Not modeled	-	-	-	-	0.221	-
To hydrogen storage Power Capacity	kW	0.179	0.179	0.179	0.179	0.179	0.165	0.092
hydrogen storage Energy Storage Capacity	kWh	371.949	371.949	371.949	371.949	371.949	375.528	320.149
From hydrogen storage Power Capacity	kW	0.712	0.712	0.712	0.712	0.712	0.644	0.384
Storage X Optimal Discharge	h	Not modeled	0	0	0	0	11.027	86.72
hydrogen storage Optimal Discharge	h	522.204	522.204	522.204	522.204	522.204	582.806	833.433
Li-ion Equivalent Annual Cycles	Cycles/yr	232.375	232.375	232.375	232.375	232.375	293.762	295.319
Storage X Equivalent Annual Cycles	Cycles/yr	Not modeled	0	0	0	0	83.906	19.558
hydrogen storage Equivalent Annual Cycles	Cycles/yr	1.545	1.545	1.545	1.545	1.545	1.39	1.102

Table S2. Least-cost system results when various *Storage X* technologies are the third storage technology alongside Li-ion battery storage and hydrogen storage. A column with results for a system with only two storage technologies (Li-ion and hydrogen storage) is shown for comparison. Results correspond to the cases shown in Figure 4a.

Result	Units	Case Without <i>Storage X</i>	Storage X Options					
		Only Li-ion	+ RFB	+ PSH	+ Gravitational	+ Thermal	+ CAES	+ Metal-Air
System Cost	\$/kWh	0.133	0.127	0.115	0.113	0.111	0.103	0.086
Li-ion Capacity	kWh	4.381	1.136	1.005	0.558	1.009	0.096	0.52
To Storage X Power Capacity	kW	Not modeled	0.454	0.510	0.641	0.511	0.546	0.754
Storage X Energy Storage Capacity	kWh	Not modeled	12.991	14.654	17.376	37.952	28.403	296.53
From Storage X Out Power Capacity	kW	Not modeled	-	-	-	-	0.768	-
Storage X Optimal Discharge	h	Not modeled	28.605	28.746	27.123	74.278	37.004	393.42
Li-ion Equivalent Annual Cycles	Cycles/yr	11.744	59.342	8.776	104.236	73.47	141.344	177.697
Storage X Equivalent Annual Cycles	Cycles/yr	Not modeled	7.838	14.226	10.957	6.247	8.843	3.166

Table S3. Least-cost system results when various *Storage X* technologies are the second storage technology alongside Li-ion battery storage. A column with results for a system with only Li-ion battery storage is shown for comparison. Results correspond to the cases shown in Figure 4b.

Result	Units	Case without <i>Storage X</i>	Storage X Options					
		Only hydrogen storage	+ RFB	+ PSH	+ Gravita- tional	+ Thermal	+ CAES	+ Metal- Air
System Cost	\$/kWh	0.084	0.084	0.084	0.084	0.084	0.083	0.081
To Storage X Power Capacity	kW	Not modeled	0.029	0.043	0.163	0	0.095	0.487
Storage X Energy Storage Capacity	kWh	Not modeled	0.052	0.191	0.583	0	2.641	41.479
From Storage X Out Power Capacity	kW	Not modeled	-	-	-	-	0.25	-
To hydrogen storage Power Capacity	kW	0.198	0.195	0.189	0.181	0.198	0.165	0.093
hydrogen storage Energy Storage Capacity	kWh	368.036	366.558	362.759	367.673	368.036	375.212	324.302
From hydrogen storage Power Capacity	kW	0.879	0.851	0.839	0.723	0.879	0.643	0.409
Storage X Optimal Discharge	h	Not modeled	1.807	4.424	3.567	0	10.577	85.164
hydrogen storage Optimal Discharge	h	418.765	430.835	432.587	508.812	418.765	583.293	792.791
Storage X Equivalent Annual Cycles	Cycles /yr	Not modeled	365.081	294.149	258.548	0	88.039	20.041
hydrogen storage Equivalent Annual Cycles	Cycles /yr	1.74	1.724	1.698	1.584	1.74	1.387	1.097

Table S4. Least-cost system results when various *Storage X* technologies are the second storage technology alongside hydrogen storage. A column with results for a system with only hydrogen storage is shown for comparison. Results correspond to the cases shown in Figure 4c.

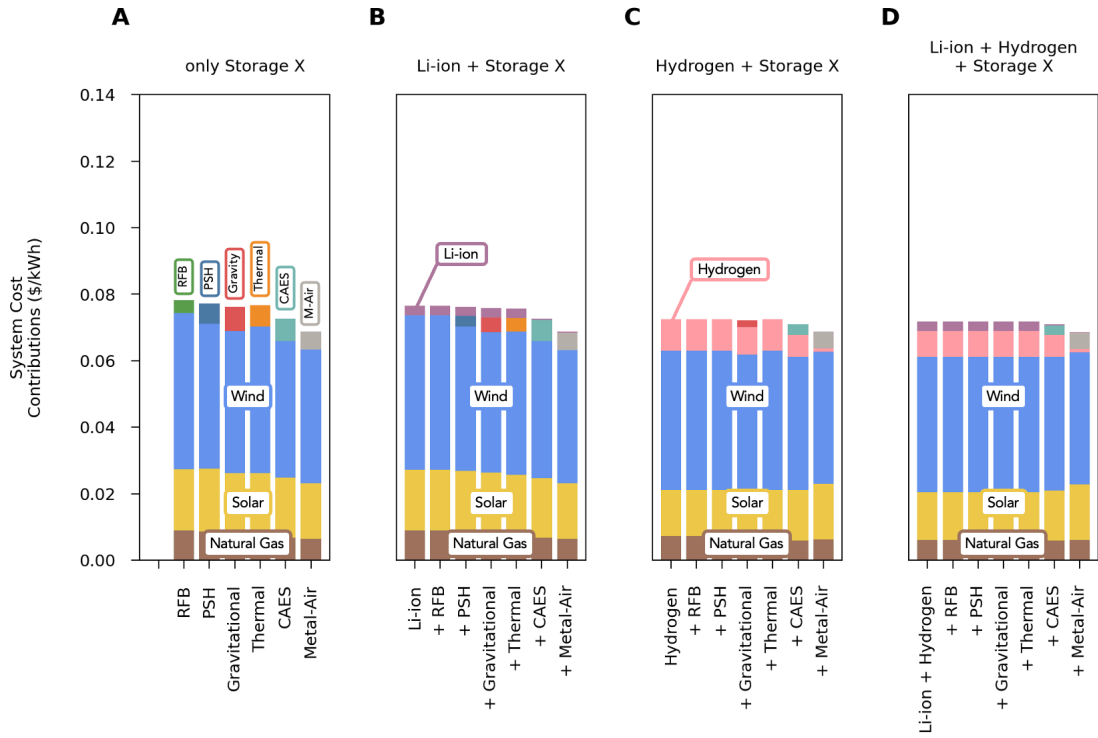


Figure S10. System costs for combinations of short-, mid-, and long-duration storage with constrained natural gas generation. Same conditions as Figure 3.4, but with natural gas constrained to 5% of total dispatch.

6.4 Supporting Information for Chapter 4

Supporting Figures and Tables:

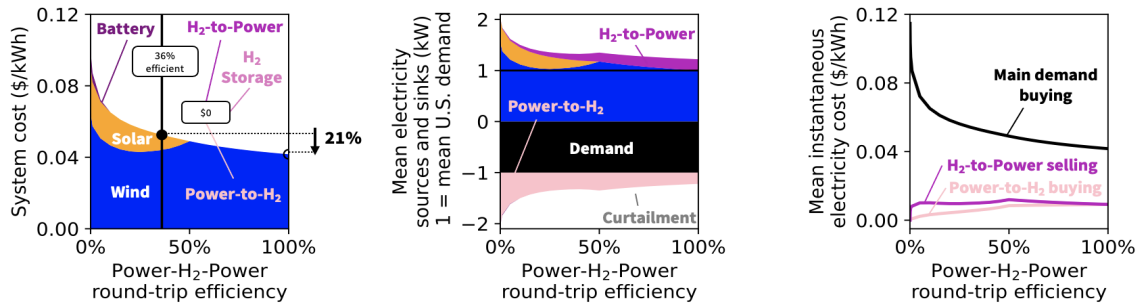


Figure S1. If hydrogen energy storage and conversion were free, Power-H₂-Power efficiency improvements would substantially reduce the cost of wind and solar electricity systems. A) System cost contributions of each modeled technology (wind, solar, battery, with zero-cost H₂-to-Power, zero-cost H₂ Storage, and zero-cost Power-to-H₂) for parameterized Power-H₂-Power round-trip efficiencies. Improvements in hydrogen storage system efficiency from 36% to 100% reduced the cost of wind- and solar-based systems by 21%. B) Mean annual dispatch of electricity sources to the grid (positive values) and electricity sinks from the grid (negative values) were balanced for parameterized Power-H₂-Power round-trip efficiencies. The black area represents end-use demand (as does the black line). Generation from wind and solar plus dispatch from hydrogen and battery storage was balanced by end-use demand, curtailment (gray area, not present here), and charging of storage. When hydrogen storage systems were modeled with zero capital cost and 100% round-trip efficiency, mean wind and solar generation was equal to mean electricity demand. Hydrogen storage and conversion inefficiencies led to wind and solar generation in excess of demand, but zero-cost storage and conversion eliminated nearly all curtailment in least-cost systems. C) In these systems, other-wise curtailed electricity was scarce, thus mean annual instantaneous electricity costs to hydrogen conversion technologies was sensitive to widely parameterized Power-H₂-Power round-trip efficiencies. When modeled with zero-capital cost, hydrogen storage systems were sensitive to efficient utilization of abundant zero-cost electricity.

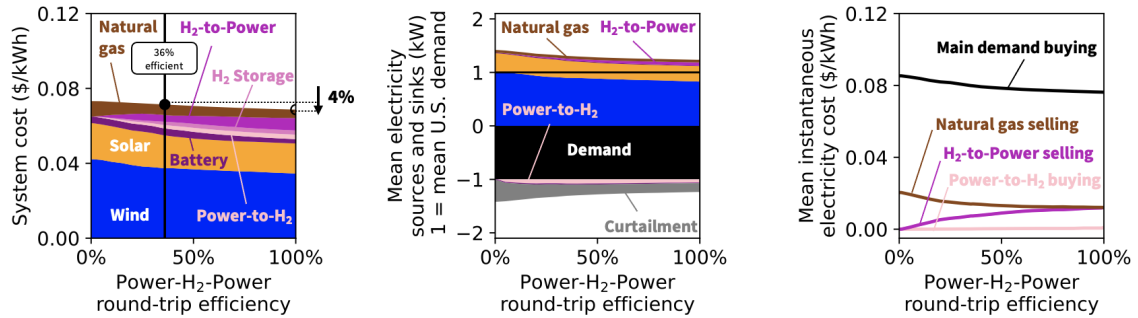


Figure S2. Despite low round-trip efficiency, hydrogen storage systems are valuable in deeply decarbonized electricity systems. A) System cost contributions of each modeled technology (wind, solar, battery, H₂-to-Power, H₂ Storage, Power-to-H₂, and natural gas constrained to 5% of dispatch) for parameterized Power-H₂-Power round-trip efficiencies. Improvements in hydrogen storage efficiency from 36% to 100% would reduce the cost of wind- and solar-based systems by 4%. B) Mean annual dispatch of electricity sources to the grid (positive values) and electricity sinks from the grid (negative values) are balanced for parameterized Power-H₂-Power round-trip efficiencies. The black area represents end-use demand (as does the black line). Generation from wind and solar plus dispatch from hydrogen and battery storage is balanced by end-use demand, curtailment (gray area), and charging of storage. Storage and conversion costs led to wind and solar generation in excess of demand and abundant curtailment in least-cost systems. C) Mean annual instantaneous electricity costs to hydrogen conversion technologies remains similar over widely parameterized Power-H₂-Power round-trip efficiencies. In wind and solar systems with natural gas restricted to 5% of dispatch, hydrogen energy storage was not highly sensitive to efficient utilization of abundant zero-cost electricity.

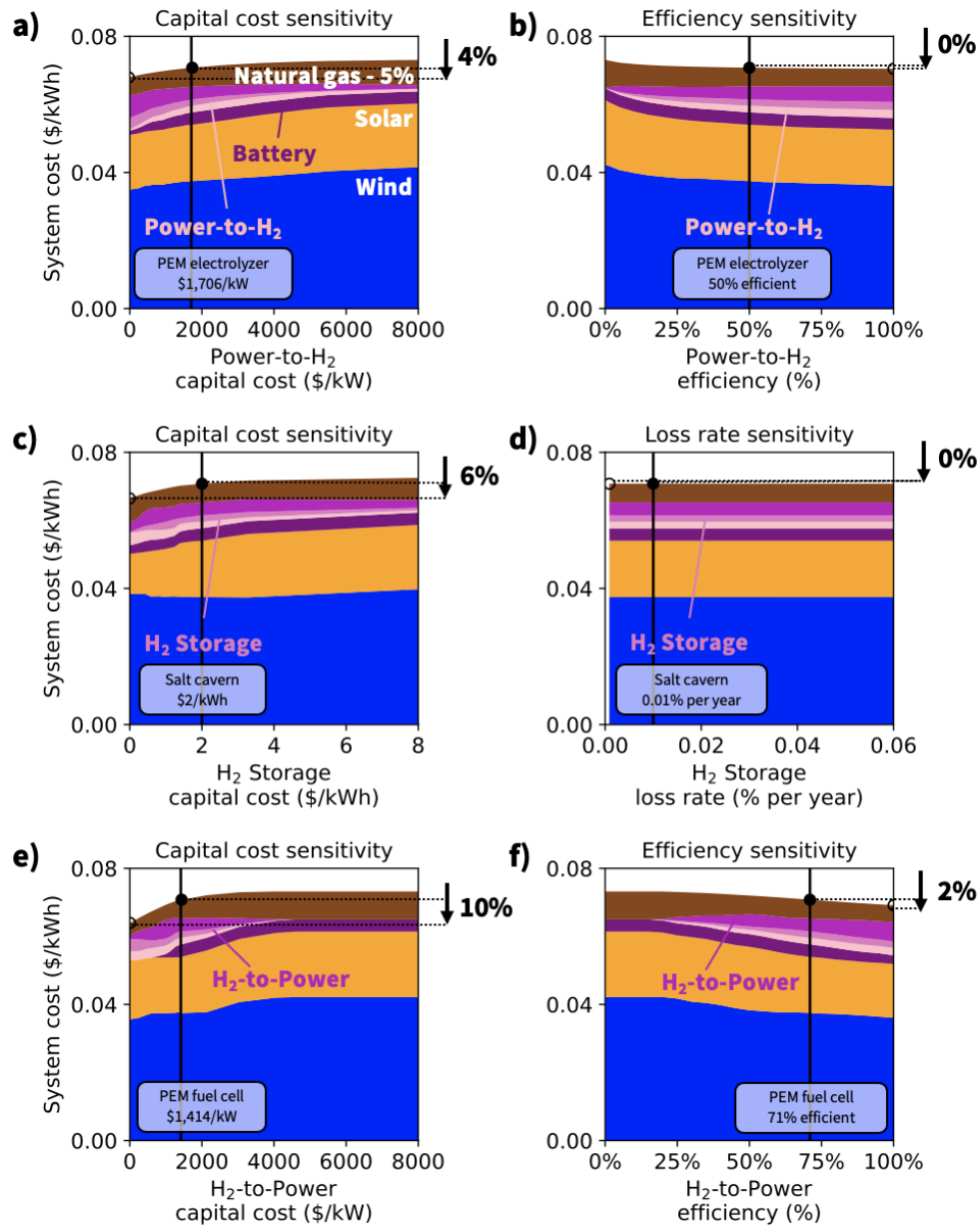


Figure S3. Value of innovation in hydrogen storage systems when natural gas was restricted to 5% of the total. Percentages show the system cost improvement from currently available hydrogen conversion and storage technologies (solid black line) to theoretical 100% efficient or zero capital cost technology. The figure shows the system-wide impact of improvements or sacrifices in the cost (left column) or efficiency (right column) of hydrogen technologies (each row). Commercial technology compatible with 100% hydrogen includes energy stored in salt caverns and power conversion with PEM electrolyzers and PEM fuel cells. System costs are disaggregated by contributions from modeled technologies including wind, solar, batteries, Power-to-H₂, H₂ storage, and H₂-to-Power. Base case costs and efficiencies are listed in Table S1. System-wide electricity costs in the base case were more sensitive to hydrogen capital cost improvements (in panel c, energy capacity costs and in panel e, power capacity costs) than to efficiency improvements (panels b, d, f). When natural gas dispatch was restricted to 5% of the total, improvements in PEM fuel cell capital costs (panel e) decreased system costs substantially.

	Unrestricted hydrogen usage in least-cost systems (Figure 5)	Historic natural gas usage with volume and deliverability data from refs. ^{142,143}	Restricted hydrogen usage (Figure 7) using deliverability ratio from ref. ¹⁴⁴
Salt cavern volume (Bcf) (h of mean U.S. demand in 2018)	<u>Salt caverns + PEMFC:</u> 2,429 Bcf (376 h of mean U.S. energy demand in 2018)	488 Bcf natural gas	500 Bcf hydrogen MEM input constraint: 77 h of mean U.S. energy demand in 2018
Depleted reservoir volume (Bcf) (h of mean U.S. demand in 2018)	<u>Depleted reservoirs + PEMFC:</u> 4,237 Bcf (656 h of mean U.S. energy demand in 2018)	3,912 Bcf natural gas	3,912 Bcf hydrogen MEM input constraint: 605 h of mean U.S. energy demand in 2018
Maximum injection in depleted reservoir (Bcf/week) (fraction of mean U.S. power demand in 2018)	<u>Salt caverns + PEMFC:</u> 105 Bcf/week (0.138 of mean U.S. power demand in 2018) <u>Depleted reservoirs + PEMFC:</u> 212 Bcf/week (0.277 of mean U.S. power demand in 2018)	132 Bcf/week natural gas	132*0.4 = 52.8 Bcf/week hydrogen MEM input constraint: 0.069 of mean U.S. power demand in 2018
Maximum withdrawal in depleted reservoir (Bcf/week) (fraction of mean U.S. power demand in 2018)	<u>Salt caverns + PEMFC:</u> 484 Bcf/week (0.636 of mean U.S. power demand in 2018) <u>Depleted reservoirs + PEMFC:</u> 468 Bcf/week (0.613 of mean U.S. power demand in 2018)	359 Bcf/week natural gas	359*0.4 = 143.6Bcf/week hydrogen MEM input constraint: 0.19 of mean U.S. power demand in 2018

Table S3. Modeled restrictions on underground hydrogen storage capacity and deliverability. Historic natural gas usage data from EIA (volume, deliverability).^{142,143} Hydrogen has 40% of the deliverability of natural gas.¹⁴⁴

6.5 Supporting Information for Chapter 5

Supporting Figures and Tables:

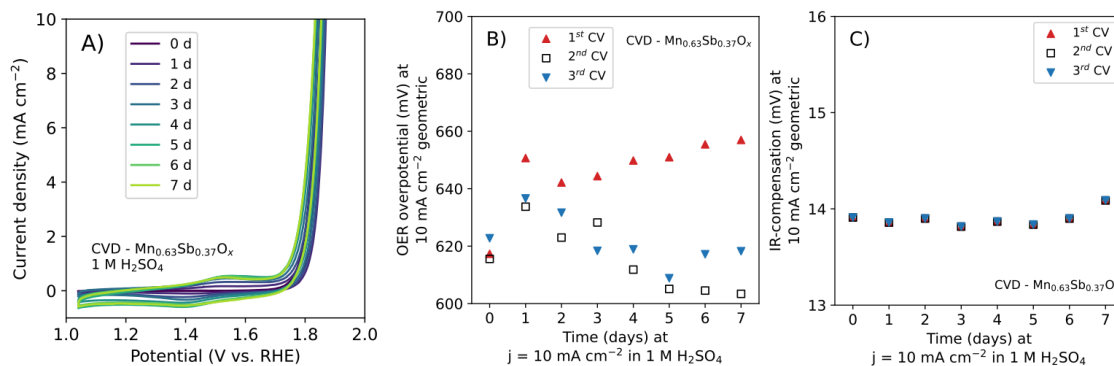


Figure S1. (A) Cyclic voltammetry (CV) data of Mn_{0.63}Sb_{0.37}O_x was taken at 24 h intervals during OER at $j = 10 \text{ mA cm}^{-2}$ for 7 days in 1 M H₂SO₄. Three CVs were scanned at 1-day intervals. (B) OER overpotential at 10 mA cm⁻² (geometric) and (C) the corresponding IR-compensation ($\sim 14 \text{ mV}$). The OER overpotential of the 1st CV on each day was higher than the 2nd and 3rd CV of the same day, and this phenomenon was most pronounced on day 7. CVs indicate that the catalyst activity regenerates substantially between the 1st and 2nd CVs.

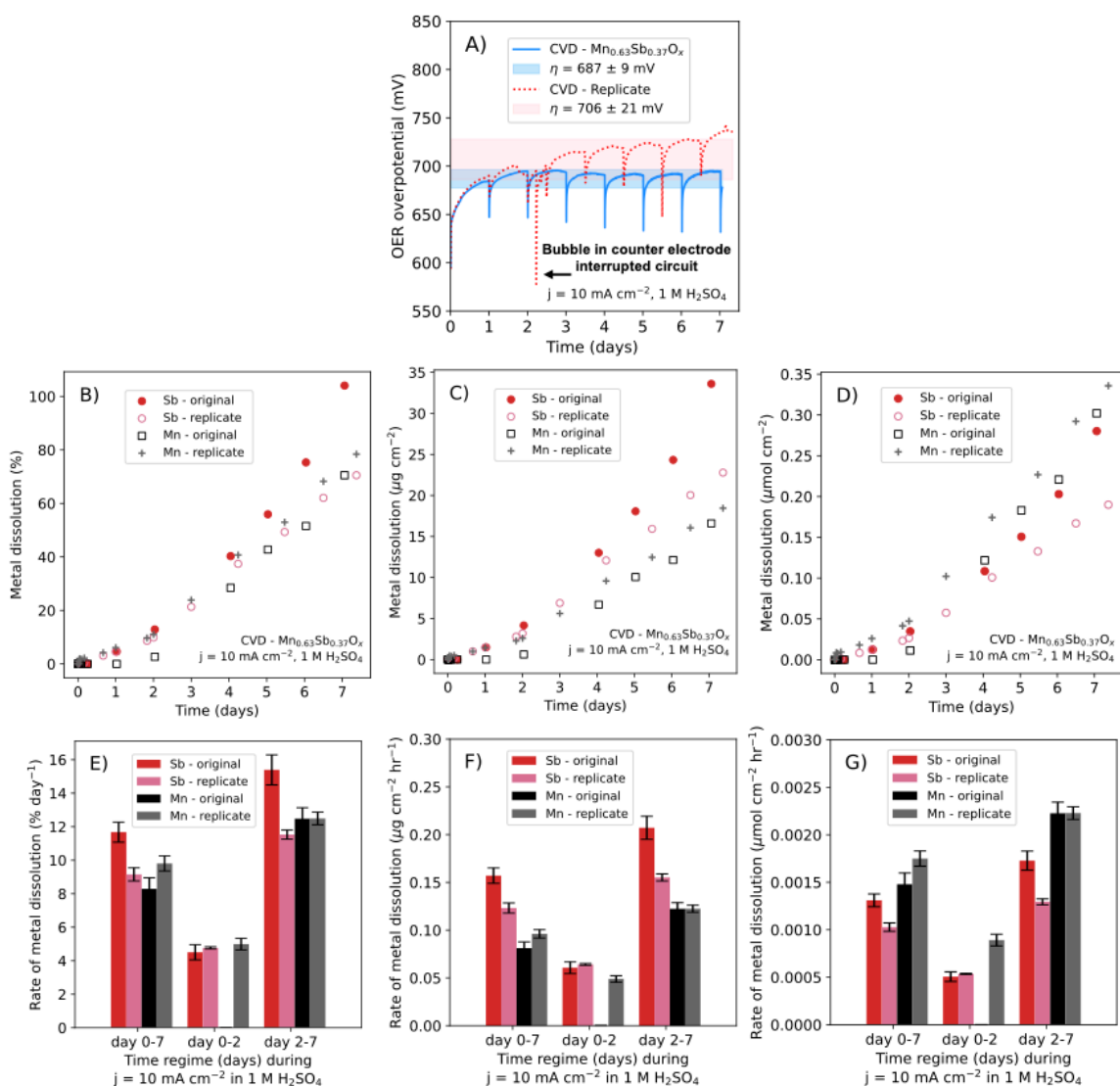


Figure S2. Replicate of Mn_{0.63}Sb_{0.37}O_x during analogous OER durability test. (A) OER overpotential was $\eta = 706 \pm 21$ mV on average at $j = 10$ mA cm⁻² for 176 h in 1 M H₂SO₄. ICP-MS quantified corrosion products in the electrolyte during the analogous 176-h durability test in relative (B) and absolute terms (C, D). The corresponding bar graphs in panels (E-G) compare metal dissolution rates in various regimes: day 0-7, day 0-2, and day 2-7. Error bars represent the standard error of the dissolution rate given by linear regression over the specified time regime.

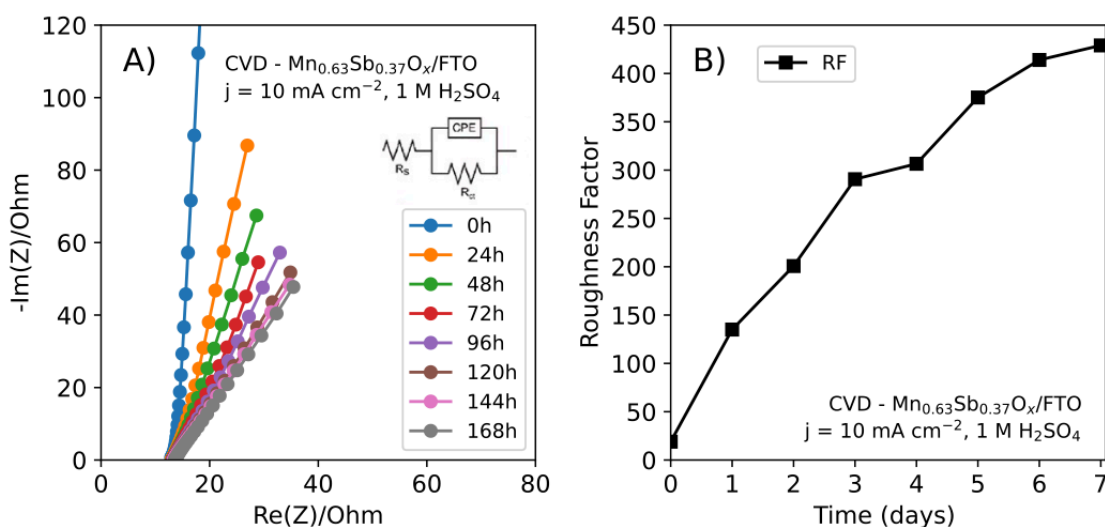


Figure S3. (A) Impedance and (B) roughness factor $\text{Mn}_{0.63}\text{Sb}_{0.37}\text{O}_x$ taken at 24-h intervals during OER at $j = 10 \text{ mA cm}^{-2}$ for 168 h in 1 M H_2SO_4 . TEC 8 FTO substrate roughness factor was assumed to be equal to ATO ($\text{RF} = 1.32$).¹⁶¹ According to preestablished methods, the geometric area-normalized capacitance of ATO ($0.0254 \text{ mF cm}^{-2}$) was divided by the roughness factor to determine the capacitance normalized to the electrochemical surface area ($0.0192 \text{ mF cm}^{-2}$).¹⁶¹

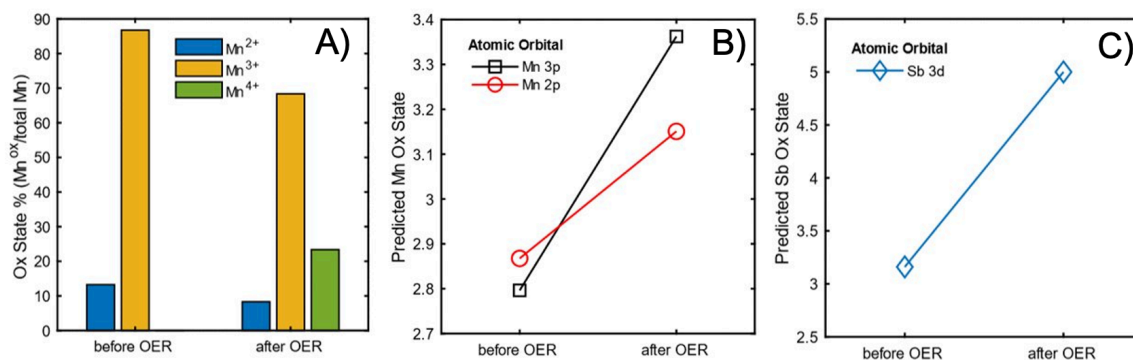


Figure S4. XP spectra predicted oxidation state of $\text{Mn}_{0.63}\text{Sb}_{0.37}\text{O}_x$ before and after OER at $j = 10 \text{ mA cm}^{-2}$ for 168 h in 1 M H_2SO_4 . (A) Mn oxidation states (B) predicted Mn oxidation states from 3p and 2p peaks. (C) Predicted Sb oxidation state from 3d peak.

OER $j = 10 \text{ mA cm}^{-2}$, 1 M H_2SO_4			
	Predicted Oxidation State by XP Spectra		
	Mn 2p	Mn 3p	Sb 3d
Before OER	2.9	2.8	3.2
After OER	3.2	3.4	5.0

Table S1. XP spectra predicted effective oxidation state of $\text{Mn}_{0.64}\text{Sb}_{0.36}\text{O}_x$ before and after OER at $j = 10 \text{ mA cm}^{-2}$ for 168 h in 1 M H_2SO_4 .

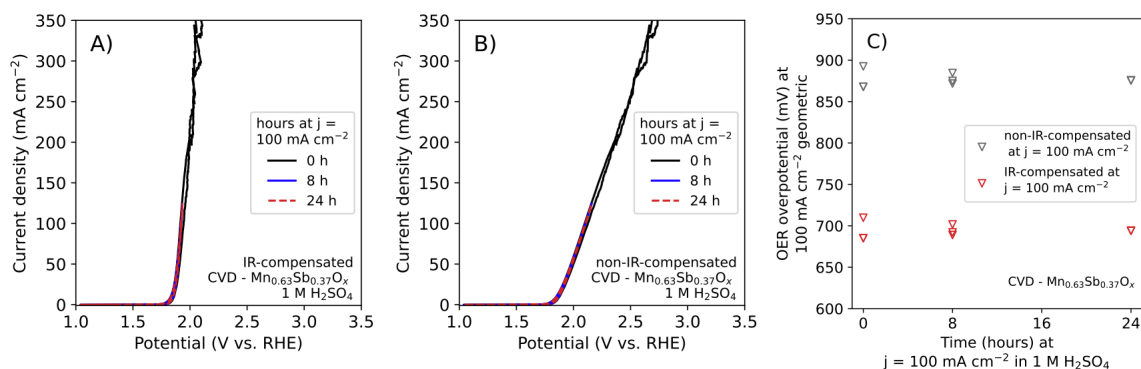


Figure S5. Cyclic voltammetry of $\text{Mn}_{0.63}\text{Sb}_{0.37}\text{O}_x$ (A) IR-compensated and (B) non-IR-compensated reaching current densities of 350 mA cm^{-2} at $t = 0 \text{ h}$. Figure S6 shows additional data from the 26-h durability test at $j = 100 \text{ mA cm}^{-2}$ in 1 M H_2SO_4 . Voltammetry data at $t = 8$ and $t = 24$ showed that the OER overpotential at 100 mA cm^{-2} matched the OER overpotential at $t = 0 \text{ h}$. At $t = 0 \text{ h}$, $\eta = 819 \text{ mV}$ at 350 mA cm^{-2} with an IR-compensation of 639 mV . Panel (C) shows OER overpotential (η) at $j = 100 \text{ mA cm}^{-2}$ in 1 M H_2SO_4 throughout the durability test. At $t = 0 \text{ h}$ in 1 M H_2SO_4 , $\eta = 709 \text{ mV}$ at 100 mA cm^{-2} with an IR-compensation of 183 mV . At $t = 8 \text{ h}$ in 1 M H_2SO_4 , $\eta = 688 \text{ mV}$ at 100 mA cm^{-2} with an IR-compensation of 183 mV . At $t = 24 \text{ h}$ in 1 M H_2SO_4 , $\eta = 694 \text{ mV}$ at 100 mA cm^{-2} with an IR-compensation of 181 mV .

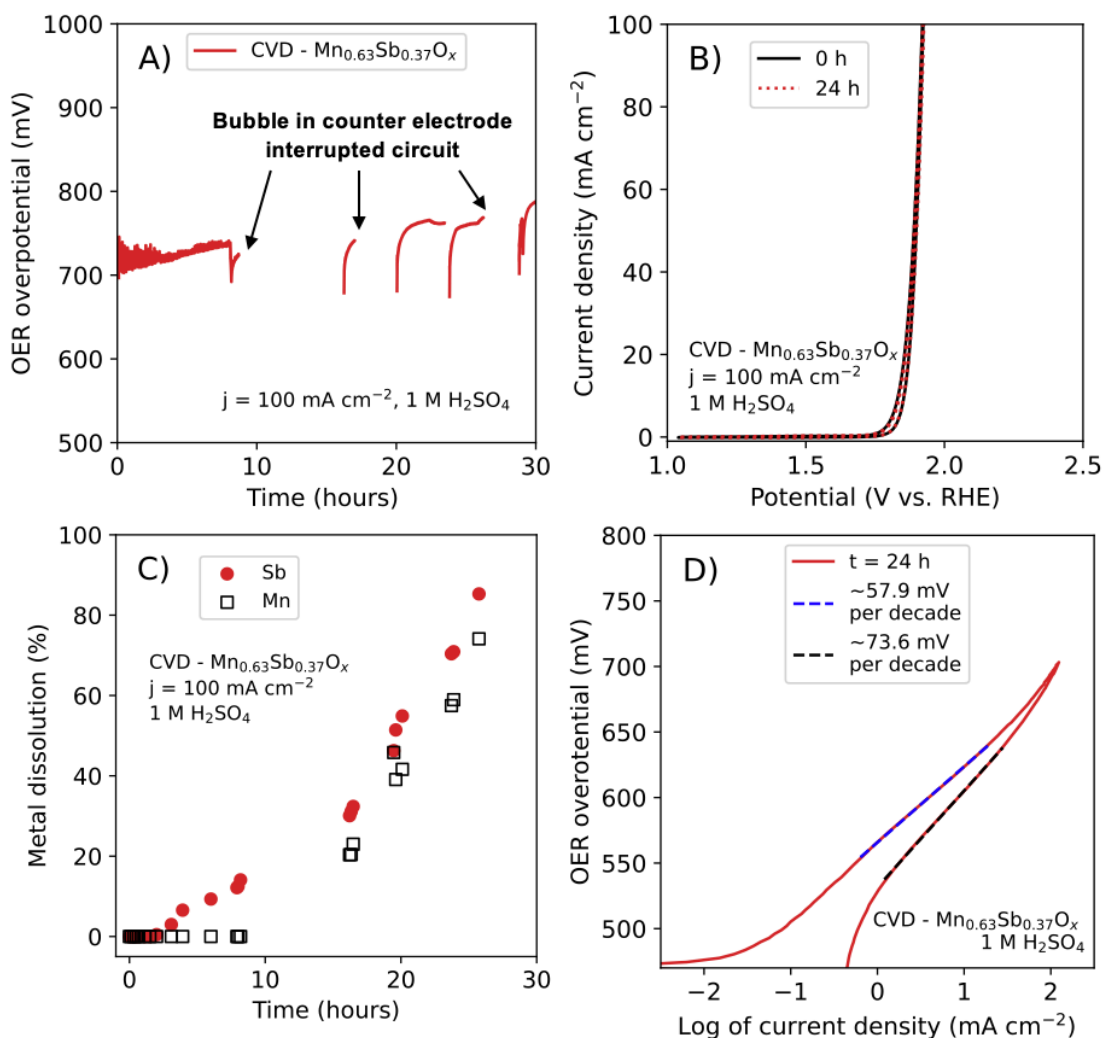


Figure S6. Electrochemical activity and stability of $\text{Mn}_{0.63}\text{Sb}_{0.37}\text{O}_x$ during OER between 100 mA cm^{-2} and open circuit voltage for 30 h in $1 \text{ M H}_2\text{SO}_4$ acid during which (A) chronopotentiometry (B) and voltammetry data were collected. The sample was in acid for a total of 26 h and at 100 mA cm^{-2} for 16 h. (C) ICP-MS quantified corrosion products in the electrolyte during the 30 h test. (D) Tafel slope of a CV taken at $t = 24 \text{ h}$ was $\sim 65 \text{ mV/decade}$. During circuit interruptions due to bubbles in the counter electrode, ICP-MS showed that Sb and Mn continued to leach into the electrolyte while at open circuit voltage in $1 \text{ M H}_2\text{SO}_4$. This may indicate reduced acid-stability of $\text{Mn}_{0.63}\text{Sb}_{0.37}\text{O}_x$ electrodes that were annealed for 6 h at $600 \text{ }^\circ\text{C}$ compared to other $\text{Mn}_y\text{Sb}_{1-y}\text{O}_x$ catalysts annealed at higher temperatures.^{161,162}

CVD subcycle		SbO_x subcycle		MnO_x subcycle	
Precursor	Co-reactant	TDMA-Sb	O_3	$Mn(EtCp)_2$	O_3
Pulse time	Pulse time	1 sec	0.09 sec	0.33 sec	0.06 sec
Wait time	Wait time	25 sec	25 sec	15 sec	15 sec
Jacket temp	Jacket temp	55 °C	25 °C	100 °C	25 °C
Number of subcycles		Repeat for 10 subcycles		Repeat for 5 subcycles	

Repeat for 30 supercycles

Table S2. Chemical vapor deposition recipe for $Mn_{0.63}Sb_{0.37}O_x$.

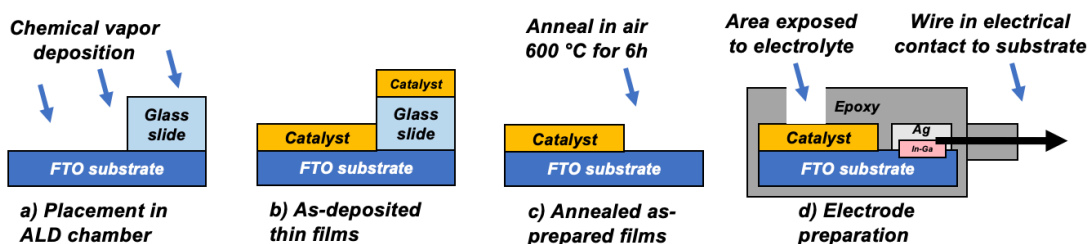


Figure S7. Cross-sectional of sample preparation. Placement of a glass slide partially covering the FTO substrate allowed for front facing electrical contact directly to FTO substrate.

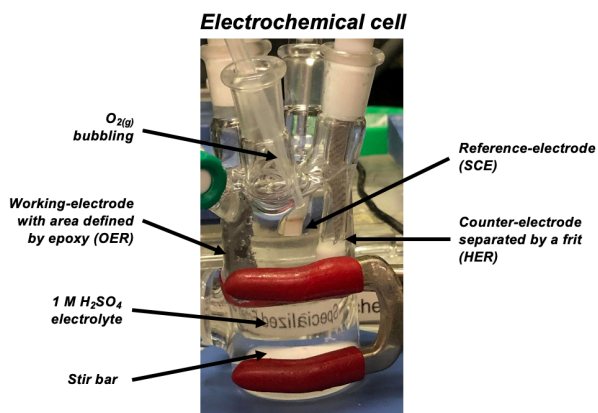


Figure S8. Image of electrochemical cell experimental set up.

Metal	Metal fraction (%)	Mass loading ($\mu\text{g cm}^{-2}$)	Mass loading ($\mu\text{mol cm}^{-2}$)	Oxide thickness (nm)
Sb	63%	32.3	0.27	35.7
Mn	37%	23.53	0.43	65.1
Total metal	100%	55.83	0.70	~100

Table S3. As-prepared $Mn_{0.63}Sb_{0.37}O_x$ catalysts mass loading, and metal fraction determined by ICP-MS analysis of unannealed films digested in acid. Oxide thickness based on individual oxide growth rates and total subcycles (Scheme 1).

BIBLIOGRAPHY

- (1) Searcey, D. No, Wind Farms Aren't the Main Cause of the Texas Blackouts. *The New York Times*. February 17, 2021. <https://www.nytimes.com/2021/02/17/climate/texas-blackouts-disinformation.html> (accessed 2023-05-04).
- (2) Rinaldi, K. Z.; Dowling, J. A.; Ruggles, T. H.; Caldeira, K.; Lewis, N. S. Wind and Solar Resource Droughts in California Highlight the Benefits of Long-Term Storage and Integration with the Western Interconnect. *Environ. Sci. Technol.* **2021**, *55* (9), 6214–6226. <https://doi.org/10.1021/acs.est.0c07848>.
- (3) Shaner, M. R.; Davis, S. J.; Lewis, N. S.; Caldeira, K. Geophysical Constraints on the Reliability of Solar and Wind Power in the United States. *Energy Environ. Sci.* **2018**, *11* (4), 914–925. <https://doi.org/10.1039/C7EE03029K>.
- (4) Dowling, J. A.; Rinaldi, K. Z.; Ruggles, T. H.; Davis, S. J.; Yuan, M.; Tong, F.; Lewis, N. S.; Caldeira, K. Role of Long-Duration Energy Storage in Variable Renewable Electricity Systems. *Joule* **2020**, *4* (9), 1907–1928. <https://doi.org/10.1016/j.joule.2020.07.007>.
- (5) Sepulveda, N. A.; Jenkins, J. D.; Edington, A.; Mallapragada, D. S.; Lester, R. K. The Design Space for Long-Duration Energy Storage in Decarbonized Power Systems. *Nat Energy* **2021**, *6* (5), 506–516. <https://doi.org/10.1038/s41560-021-00796-8>.
- (6) Albertus, P.; Manser, J. S.; Litzelman, S. Long-Duration Electricity Storage Applications, Economics, and Technologies. *Joule* **2020**, *4* (1), 21–32. <https://doi.org/10.1016/j.joule.2019.11.009>.
- (7) Plumer, B. Energy Department Targets Vastly Cheaper Batteries to Clean Up the Grid. *The New York Times*. July 14, 2021. <https://www.nytimes.com/2021/07/14/climate/renewable-energy-batteries.html> (accessed 2023-05-04).
- (8) Jenkins, J. D.; Sepulveda, N. A. Long-Duration Energy Storage: A Blueprint for Research and Innovation. *Joule* **2021**, *5* (9), 2241–2246. <https://doi.org/10.1016/j.joule.2021.08.002>.
- (9) St. John, J. *How to Build a Green Hydrogen Economy for the US West*. Greentech Media. www.greentechmedia.com (accessed 2021-06-01).
- (10) *Utah Aims to Shatter Records With 1,000MW Energy Storage Plant*. <https://www.greentechmedia.com/articles/read/utah-aims-to-shatter-records-with-1000-mw-energy-storage-plant> (accessed 2023-05-04).
- (11) *Startup Claims Breakthrough in Long-Duration Batteries - WSJ*. <https://www.wsj.com/articles/startup-claims-breakthrough-in-long-duration-batteries-11626946330> (accessed 2023-05-04).
- (12) Kennedy, K. M.; Ruggles, T. H.; Rinaldi, K.; Dowling, J. A.; Duan, L.; Caldeira, K.; Lewis, N. S. The Role of Concentrated Solar Power with Thermal Energy Storage in Least-Cost Highly Reliable Electricity Systems Fully Powered by Variable Renewable Energy. *Advances in Applied Energy* **2022**, *6*, 100091. <https://doi.org/10.1016/j.adapen.2022.100091>.
- (13) Colthorpe, A. Long-duration 'pumped heat energy storage' startup Malta raises US\$50 million in Series B round. Energy Storage News. <https://www.energy-storage.news/long-duration-pumped-heat-energy-storage-startup-malta-raises-us50-million-in-series-b-round/> (accessed 2023-05-04).
- (14) *Energy Vault Lands \$110M From SoftBank's Vision Fund for Gravity Storage*. <https://www.greentechmedia.com/articles/read/energy-vault-lands-110m-from-softbanks-vision-fund-for-gravity-energy-stora> (accessed 2023-05-04).
- (15) Guerra, O. J.; Eichman, J.; Denholm, P. Optimal Energy Storage Portfolio for High and Ultrahigh Carbon-Free and Renewable Power Systems. *Energy Environ. Sci.* **2021**, *14* (10), 5132–5146. <https://doi.org/10.1039/D1EE01835C>.
- (16) Ruggles, T. H.; Dowling, J. A.; Lewis, N. S.; Caldeira, K. Opportunities for Flexible Electricity Loads Such as Hydrogen Production from Curtailed Generation. *Advances in Applied Energy* **2021**, *3*, 100051. <https://doi.org/10.1016/j.adapen.2021.100051>.
- (17) *Senate Bill 100 California Renewables Portfolio Standard Program: Emissions of Greenhouse Gases*; Tech Report; California Legislative Information, 2018.
- (18) *An Act to Reform Maine's Renewable Portfolio Standard*; Tech Report; Maine Legislature, 2019.

- (19) *Senate Bill 489 Energy Transition Act*; Tech Report; New Mexico Legislature, 2019.
- (20) *Senate Bill 5116 Supporting Washington's Clean Energy Economy and Transitioning to a Clean, Affordable, and Reliable Energy Future*; Tech Report; Washington State Legislature, 2019.
- (21) *House Bill 623 Relating to Renewable Standards*; Tech Report; Hawaii State Legislature, 2015.
- (22) *Senate Bill 1121 Puerto Rico Energy Public Policy Act*; Tech Report; Legislative Assembly of Puerto Rico, 2019.
- (23) *100% Commitments in Cities, Counties, and States*; Tech Report; Sierra Club.
- (24) *The European Green Deal*; Tech Report; European Energy Commission, 2019.
- (25) *Renewable Energy Target Setting*; International Renewable Energy Agency, 2015.
- (26) *States March toward 100% Clean Energy—Who's Next?*; Tech Report; Union of Concerned Scientists, 2019.
- (27) *Tracking Progress on 100% Clean Energy Targets | Greentech Media*. <https://www.greentechmedia.com/articles/read/tracking-progress-on-100-clean-energy-targets> (accessed 2023-05-04).
- (28) Sepulveda, N. A.; Jenkins, J. D.; de Sisternes, F. J.; Lester, R. K. The Role of Firm Low-Carbon Electricity Resources in Deep Decarbonization of Power Generation. *Joule* **2018**, 2 (11), 2403–2420.
- (29) Jenkins, J. D.; Luke, M.; Thernstrom, S. Getting to Zero Carbon Emissions in the Electric Power Sector. *Joule* **2018**, 2 (12), 2498–2510.
- (30) *2012 State of Reliability*; North American Electric Reliability Corporation. (NERC), Atlanta, GA (United States), 2012.
- (31) Steinberg, D.; Bielen, D.; Eichman, J.; Eurek, K.; Logan, J.; Mai, T.; McMillan, C.; Parker, A.; Vimmerstedt, L.; Wilson, E. *Electrification and Decarbonization: Exploring US Energy Use and Greenhouse Gas Emissions in Scenarios with Widespread Electrification and Power Sector Decarbonization*; National Renewable Energy Lab.(NREL), Golden, CO (United States), 2017.
- (32) Jacobson, M. Z.; Delucchi, M. A.; Bazouin, G.; Bauer, Z. A. F.; Heavey, C. C.; Fisher, E.; Morris, S. B.; Piekutowski, D. J. Y.; Vencill, T. A.; Yeskoo, T. W. 100% Clean and Renewable Wind, Water, and Sunlight (WWS) All-Sector Energy Roadmaps for the 50 United States. *Energy Environ. Sci.* **2015**, 8 (7), 2093–2117. <https://doi.org/10.1039/C5EE01283J>.
- (33) Clack, C. T. M.; Qvist, S. A.; Apt, J.; Bazilian, M.; Brandt, A. R.; Caldeira, K.; Davis, S. J.; Diakov, V.; Handschy, M. A.; Hines, P. D. H.; Jaramillo, P.; Kammen, D. M.; Long, J. C. S.; Morgan, M. G.; Reed, A.; Sivaram, V.; Sweeney, J.; Tynan, G. R.; Victor, D. G.; Weyant, J. P.; Whitacre, J. F. Evaluation of a Proposal for Reliable Low-Cost Grid Power with 100% Wind, Water, and Solar. *Proceedings of the National Academy of Sciences* **2017**, 114 (26), 6722–6727. <https://doi.org/10.1073/pnas.1610381114>.
- (34) Heard, B. P.; Brook, B. W.; Wigley, T. M.; Bradshaw, C. J. Burden of Proof: A Comprehensive Review of the Feasibility of 100% Renewable-Electricity Systems. *Renewable and Sustainable Energy Reviews* **2017**, 76, 1122–1133.
- (35) Sivaram, V.; Dabiri, J. O.; Hart, D. M. The Need for Continued Innovation in Solar, Wind, and Energy Storage. *Joule* **2018**, 2 (9), 1639–1642.
- (36) Dunn, B.; Kamath, H.; Tarascon, J.-M. Electrical Energy Storage for the Grid: A Battery of Choices. *Science* **2011**, 334 (6058), 928–935.
- (37) Pellow, M. A.; Emmott, C. J.; Barnhart, C. J.; Benson, S. M. Hydrogen or Batteries for Grid Storage? A Net Energy Analysis. *Energy & Environmental Science* **2015**, 8 (7), 1938–1952.
- (38) *2019 Annual Technology Baseline (ATB): Electricity - Battery Storage*; Tech Report; National Renewable Energy Lab, 2019.
- (39) Braff, W. A.; Mueller, J. M.; Trancik, J. E. Value of Storage Technologies for Wind and Solar Energy. *Nature Climate Change* **2016**, 6 (10), 964.
- (40) Davis, S. J.; Lewis, N. S.; Shaner, M.; Aggarwal, S.; Arent, D.; Azevedo, I. L.; Benson, S. M.; Bradley, T.; Brouwer, J.; Chiang, Y.-M.; Clack, C. T. M.; Cohen, A.; Doig, S.; Edmonds, J.; Fennell, P.; Field, C. B.; Hannegan, B.; Hodge, B.-M.; Hoffert, M. I.; Ingersoll, E.; Jaramillo, P.; Lackner, K. S.; Mach, K. J.; Mastrandrea, M.; Ogden, J.; Peterson, P. F.; Sanchez, D. L.; Sperling, D.; Stagner, J.; Trancik, J. E.; Yang, C.-J.; Caldeira, K. Net-Zero Emissions Energy Systems. *Science* **2018**, 360 (6396), eaas9793. <https://doi.org/10.1126/science.aas9793>.
- (41) De Sisternes, F. J.; Jenkins, J. D.; Botterud, A. The Value of Energy Storage in Decarbonizing the Electricity Sector. *Applied Energy* **2016**, 175, 368–379.

- (42) Budischak, C.; Sewell, D.; Thomson, H.; Mach, L.; Veron, D. E.; Kempton, W. Cost-Minimized Combinations of Wind Power, Solar Power and Electrochemical Storage, Powering the Grid up to 99.9% of the Time. *Journal of Power Sources* **2013**, *225*, 60–74.
- (43) Ziegler, M. S.; Mueller, J. M.; Pereira, G. D.; Song, J.; Ferrara, M.; Chiang, Y.-M.; Trancik, J. E. Storage Requirements and Costs of Shaping Renewable Energy Toward Grid Decarbonization. *Joule* **2019**, *3* (9), 2134–2153. <https://doi.org/10.1016/j.joule.2019.06.012>.
- (44) *GFO-19-308 - Assessing Long-Duration Energy Storage Deployment Scenarios to Meet California's Energy Goals*; Tech Report; California Energy Commission, 2020.
- (45) Viswanathan, V.; Crawford, A.; Stephenson, D.; Kim, S.; Wang, W.; Li, B.; Coffey, G.; Thomsen, E.; Graff, G.; Balducci, P.; Kintner-Meyer, M.; Sprengle, V. Cost and Performance Model for Redox Flow Batteries. *J. Power Sources* **2014**, *247*, 1040–1051.
- (46) Kenning, T. *SDG&E and Sumitomo unveil largest vanadium redox flow battery in the US*. Energy Storage News. <https://www.energy-storage.news/sdge-and-sumitomo-unveil-largest-vanadium-redox-flow-battery-in-the-us/> (accessed 2022-09-18).
- (47) *Long Duration Breakthrough? Form Energy's First Project Tries Pushing Storage to 150 Hours*. <https://www.greentechmedia.com/articles/read/form-energys-first-project-pushes-long-duration-storage-to-new-heights-150-hour-duration> (accessed 2022-06-30).
- (48) Fertig, E.; Apt, J. Economics of Compressed Air Energy Storage to Integrate Wind Power: A Case Study in ERCOT. *Energy Policy* **2011**, *39* (5), 2330–2342. <https://doi.org/10.1016/j.enpol.2011.01.049>.
- (49) Blanco, H.; Faaij, A. A Review at the Role of Storage in Energy Systems with a Focus on Power to Gas and Long-Term Storage. *Renewable and Sustainable Energy Reviews* **2018**, *81*, 1049–1086.
- (50) Trabish, H. K. Green Hydrogen Gets Real as Utility Business Models and Delivery Solutions Emerge. *Utility Dive* **2020**.
- (51) *Projects Proliferate*; Tech Report; Modern Power Systems, 2019.
- (52) *USA: Air Liquide Operates the World's Largest Hydrogen Storage Facility*; Press Release; Air Liquide, 2017.
- (53) United States Mid-Century Strategy for Deep Decarbonization. *White, House, and Washington* **2016**, No. United Nations Framework Convention on Climate Change, Washington, DC.
- (54) Williams, D. J. H.; Haley, B.; Kahrl, D. F.; Moore, J.; Jones, D. A. D.; McJeon, D. H.; Borgeson, D. S.; Farbes, J.; Hart, D. E.; Kwok, G.; Jones, R.; Mahone, A. Pathways to Deep Decarbonization in the United States. *Technical report, The US report of the deep decarbonization pathways project of the sustainable development solutions network and the institute for sustainable development and international relations, Revision with technical supplement, Nov 16, 2015*.
- (55) MacDonald, A. E.; Clack, C. T.; Alexander, A.; Dunbar, A.; Wilczak, J.; Xie, Y. Future Cost-Competitive Electricity Systems and Their Impact on US CO₂ Emissions. *Nature Climate Change* **2016**, *6* (5), 526.
- (56) Weitemeyer, S.; Kleinhans, D.; Wienholt, L.; Vogt, T.; Agert, C. A European Perspective: Potential of Grid and Storage for Balancing Renewable Power Systems. *Energy Technology* **2016**, *4* (1), 114–122.
- (57) Steinke, F.; Wolfrum, P.; Hoffmann, C. Grid vs. Storage in a 100% Renewable Europe. *Renewable Energy* **2013**, *50*, 826–832.
- (58) Scholz, Y.; Gils, H. C.; Pietzcker, R. C. Application of a High-Detail Energy System Model to Derive Power Sector Characteristics at High Wind and Solar Shares. *Energy Economics* **2017**, *64*, 568–582.
- (59) Schill, W.-P.; Zerrahn, A. Long-Run Power Storage Requirements for High Shares of Renewables: Results and Sensitivities. *Renewable and Sustainable Energy Reviews* **2018**, *83*, 156–171.
- (60) Victoria, M.; Zhu, K.; Brown, T.; Andresen, G. B.; Greiner, M. The Role of Storage Technologies throughout the Decarbonisation of the Sector-Coupled European Energy System. *Energy Conversion and Management* **2019**, *201*, 111977.
- (61) Connolly, D.; Lund, H.; Mathiesen, B. Smart Energy Europe: The Technical and Economic Impact of One Potential 100% Renewable Energy Scenario for the European Union. *Renewable and Sustainable Energy Reviews* **2016**, *60*, 1634–1653.
- (62) Brown, T.; Schlachtberger, D.; Kies, A.; Schramm, S.; Greiner, M. Synergies of Sector Coupling and Transmission Reinforcement in a Cost-Optimised, Highly Renewable European Energy System. *Energy* **2018**, *160*, 720–739.

- (63) Schaber, K. Integration of Variable Renewable Energies in the European Power System: A Model-Based Analysis of Transmission Grid Extensions and Energy Sector Coupling. PhD Thesis, Technische Universität München, 2014.
- (64) Ram, M.; Bogdanov, D.; Aghahosseini, A.; Gulagi, A.; Oyewo, A.; Child, M.; Caldera, U.; Sadovskaia, K.; Farfan, J.; Barbosa, L.; others. Global Energy System Based on 100% Renewable Energy—Power, Heat, Transport and Desalination Sectors. *Study by Lappeenranta University of Technology and Energy Watch Group, Lappeenranta, Berlin* **2019**.
- (65) *Annual Energy Outlook 2018*; U. S. Energy Information Administration, 2018.
- (66) Steward, D.; Saur, G.; Penev, M.; Ramsden, T. *Lifecycle Cost Analysis of Hydrogen versus Other Technologies for Electrical Energy Storage*; National Renewable Energy Lab.(NREL), Golden, CO (United States), 2009.
- (67) James, B.; Colella, W.; Moton, J.; Saur, G.; Ramsden, T. *PEM Electrolysis H₂A Production Case Study Documentation*; National Renewable Energy Lab.(NREL), Golden, CO (United States), 2013.
- (68) Steward, D.; Penev, M.; Saur, G.; Becker, W.; Zuboy, J. *Fuel Cell Power Model Version 2: Startup Guide, System Designs, and Case Studies. Modeling Electricity, Heat, and Hydrogen Generation from Fuel Cell-Based Distributed Energy Systems*; National Renewable Energy Lab.(NREL), Golden, CO (United States), 2013.
- (69) Elgowainy, A.; Reddi, K.; Mintz, M.; Brown, D. *H₂A Delivery Scenario Analysis Model Version 3.0*(HDSAM 3.0) User's Manual*; Tech Report; Argonne National Laboratory, Centre for Transportation Research, 2015.
- (70) Lazard. Lazard's Levelized Cost of Storage Analysis—Version 5.0, 2019.
- (71) Crotagino, F.; Donadei, S.; Bünger, U.; Landinger, H. Large-Scale Hydrogen Underground Storage for Securing Future Energy Supplies. **2010**.
- (72) Buchmann, I. BU-802b: What Does Elevated Self-Discharge Do?, 2020.
- (73) Bussar, C.; Stöcker, P.; Cai, Z.; Moraes Jr, L.; Magnor, D.; Wiernes, P.; van Bracht, N.; Moser, A.; Sauer, D. U. Large-Scale Integration of Renewable Energies and Impact on Storage Demand in a European Renewable Power System of 2050—Sensitivity Study. *Journal of Energy Storage* **2016**, *6*, 1–10.
- (74) Collins, S.; Deane, P.; Gallachóir, B. Ó.; Pfenninger, S.; Staffell, I. Impacts of Inter-Annual Wind and Solar Variations on the European Power System. *Joule* **2018**, *2* (10), 2076–2090.
- (75) Gelaro, R.; McCarty, W.; Suárez, M. J.; Todling, R.; Molod, A.; Takacs, L.; Randles, C. A.; Darmenov, A.; Bosilovich, M. G.; Reichle, R.; Wargan, K.; Coy, L.; Cullather, R.; Draper, C.; Akella, S.; Buchard, V.; Conaty, A.; Silva, A. M. da; Gu, W.; Kim, G.-K.; Koster, R.; Lucchesi, R.; Merkova, D.; Nielsen, J. E.; Partyka, G.; Pawson, S.; Putman, W.; Rienecker, M.; Schubert, S. D.; Sienkiewicz, M.; Zhao, B. The Modern-Era Retrospective Analysis for Research and Applications, Version 2 (MERRA-2). *Journal of Climate* **2017**, *30* (14), 5419–5454. <https://doi.org/10.1175/JCLI-D-16-0758.1>.
- (76) Ruggles, T. H.; Farnham, D. J.; Tong, D.; Caldeira, K. Developing Reliable Hourly Electricity Demand Data through Screening and Imputation. *Sci Data* **2020**, *7* (1), 155. <https://doi.org/10.1038/s41597-020-0483-x>.
- (77) Levi, P. J.; Kurland, S. D.; Carbajales-Dale, M.; Weyant, J. P.; Brandt, A. R.; Benson, S. M. Macro-Energy Systems: Toward a New Discipline. *Joule* **2019**, *3* (10), 2282–2286.
- (78) *The National Energy Modeling System (NEMS): An Overview*; Report DOE/EIA-0581; Energy Information Administration (EIA), U.S. Department of Energy, Washington, DC (United States), 2009.
- (79) Hand, M. M.; Baldwin, S.; DeMeo, E.; Reilly, J.; Mai, T.; Arent, D.; Porro, G.; Meshek, M.; Sandor, D. *Renewable Electricity Futures Study. Volume 1. Exploration of High-Penetration Renewable Electricity Futures*; National Renewable Energy Lab.(NREL), Golden, CO (United States), 2012.
- (80) Cebulla, F.; Naegler, T.; Pohl, M. Electrical Energy Storage in Highly Renewable European Energy Systems: Capacity Requirements, Spatial Distribution, and Storage Dispatch. *Journal of Energy Storage* **2017**, *14*, 211–223.
- (81) *Wind generation seasonal patterns vary across the United States*. <https://www.eia.gov/todayinenergy/detail.php?id=20112> (accessed 2023-05-04).
- (82) *Electricity Explained: Factors Affecting Electricity Prices*; Energy Information Administration (EIA), U.S. Department of Energy, Washington, DC (United States), 2018.
- (83) *Pumped Storage Hydropower*. Energy.gov. <https://www.energy.gov/eere/water/pumped-storage-hydropower> (accessed 2023-05-04).

- (84) *Most pumped storage electricity generators in the U.S. were built in the 1970s.* <https://www.eia.gov/todayinenergy/detail.php?id=41833> (accessed 2023-05-04).
- (85) *Hydropower Vision: A New Chapter for America's 1st Renewable Electricity Source.* Energy.gov. <https://www.energy.gov/eere/water/articles/hydropower-vision-new-chapter-americas-1st-renewable-electricity-source> (accessed 2023-05-04).
- (86) Deane, J. P.; Gallachóir, B. Ó.; McKeogh, E. Techno-Economic Review of Existing and New Pumped Hydro Energy Storage Plant. *Renewable and Sustainable Energy Reviews* **2010**, *14* (4), 1293–1302.
- (87) Budt, M.; Wolf, D.; Span, R.; Yan, J. A Review on Compressed Air Energy Storage: Basic Principles, Past Milestones and Recent Developments. *Applied Energy* **2016**, *170*, 250–268. <https://doi.org/10.1016/j.apenergy.2016.02.108>.
- (88) Colbertaldo, P.; Agustin, S. B.; Campanari, S.; Brouwer, J. Impact of Hydrogen Energy Storage on California Electric Power System: Towards 100% Renewable Electricity. *International Journal of Hydrogen Energy* **2019**, *44* (19), 9558–9576.
- (89) Maroufmashat, A.; Fowler, M. Transition of Future Energy System Infrastructure; through Power-to-Gas Pathways. *Energies* **2017**, *10* (8), 1089.
- (90) Darrow, K.; Tidball, R.; Wang, J.; Hampson, A. Catalog of CHP Technologies. *US Environmental Protection Agency, Washington, DC* **2015**, 5–6.
- (91) York, W. D.; Ziminsky, W. S.; Yilmaz, E. Development and Testing of a Low NOx Hydrogen Combustion System for Heavy-Duty Gas Turbines. *Journal of Engineering for Gas Turbines and Power* **2013**, *135* (2).
- (92) *Gas Turbine World 2019 GTW Handbook*; Handbook; Pequot Publishing Inc, 2019; Vol. 34.
- (93) *Annual Energy Outlook 2017: With Projections to 2040*; Tech Report; United States Energy Information Administration, 2017.
- (94) Götz, M.; Lefebvre, J.; Mörs, F.; Koch, A. M.; Graf, F.; Bajohr, S.; Reimert, R.; Kolb, T. Renewable Power-to-Gas: A Technological and Economic Review. *Renewable energy* **2016**, *85*, 1371–1390.
- (95) Iaquaniello, G.; Setini, S.; Salladini, A.; De Falco, M. CO₂ Valorization through Direct Methanation of Flue Gas and Renewable Hydrogen: A Technical and Economic Assessment. *International Journal of Hydrogen Energy* **2018**, *43* (36), 17069–17081.
- (96) Schaaf, T.; Grunig, J.; Schuster, M.; Orth, A. Storage of Electrical Energy in a Gas Distribution System-Methanation of CO₂-Containing Gases. *Chemie Ingenieur Technik* **2014**, *86* (4), 476–485.
- (97) Fasihi, M.; Bogdanov, D.; Breyer, C. Techno-Economic Assessment of Power-to-Liquids (PtL) Fuels Production and Global Trading Based on Hybrid PV-Wind Power Plants. *Energy Procedia* **2016**, *99*, 243–268.
- (98) Goldmeer, D. J. *Power to Gas: Hydrogen for Power Generation. Fuel Flexible Gas Turbines as Enablers for a Low or Reduced Carbon Energy Ecosystem*; General Electric Power, 2019.
- (99) Luo, X.; Wang, J.; Dooner, M.; Clarke, J. Overview of Current Development in Electrical Energy Storage Technologies and the Application Potential in Power System Operation. *Appl. Energy* **2015**, *137*, 511–536.
- (100) Murphy, C.; Sun, Y.; Cole, W. J.; Maclaurin, G. J.; Mehos, M. S.; Turchi, C. S. *The Potential Role of Concentrating Solar Power within the Context of DOE's 2030 Solar Cost Targets*; National Renewable Energy Lab.(NREL), Golden, CO (United States), 2019.
- (101) Mills, A. D.; Millstein, D.; Jeong, S.; Lavin, L.; Wiser, R.; Bolinger, M. Estimating the Value of Offshore Wind along the United States' Eastern Coast. *Environmental Research Letters* **2018**, *13* (9), 094013.
- (102) Deign, J. Germany's Maxed-Out Grid Is Causing Trouble Across Europe.
- (103) Ruggles, T.; Farnham, D. EIA Cleaned Hourly Electricity Demand Data, 2019. <https://doi.org/10.5281/zenodo.3517197>.
- (104) Braun, J.; Mitchell, J. Solar Geometry for Fixed and Tracking Surfaces. *Solar energy* **1983**, *31* (5), 439–444.
- (105) Meeus, J. H. *Astronomical Algorithms*; Willmann-Bell, Incorporated, 1991.
- (106) Perez, R.; Ineichen, P.; Seals, R.; Michalsky, J.; Stewart, R. Modeling Daylight Availability and Irradiance Components from Direct and Global Irradiance. *Solar energy* **1990**, *44* (5), 271–289.
- (107) Reindl, D. T.; Beckman, W. A.; Duffie, J. A. Diffuse Fraction Correlations. *Solar energy* **1990**, *45* (1), 1–7.

- (108) Huld, T.; Gottschalg, R.; Beyer, H. G.; Topič, M. Mapping the Performance of PV Modules, Effects of Module Type and Data Averaging. *Solar Energy* **2010**, *84* (2), 324–338.
- (109) Pfenninger, S.; Staffell, I. Long-Term Patterns of European PV Output Using 30 Years of Validated Hourly Reanalysis and Satellite Data. *Energy* **2016**, *114*, 1251–1265.
- (110) Bett, P. E.; Thornton, H. E. The Climatological Relationships between Wind and Solar Energy Supply in Britain. *Renewable Energy* **2016**, *87*, 96–110. <https://doi.org/10.1016/j.renene.2015.10.006>.
- (111) *Capacity Factors for Utility Scale Generators Primarily Using Non-Fossil Fuels*; Tech Report; U.S. Energy Information Administration, 2018.
- (112) *Hourly and Daily Balancing Authority Operations Report Data Format and Transmittal Instructions ELA-930*; Tech Report; U.S. Energy Information Administration.
- (113) *Open Data*; Tech Report; U.S. Energy Information Administration, 2019.
- (114) van Buuren, S.; Boshuizen, H. C.; Knook, D. L. Multiple Imputation of Missing Blood Pressure Covariates in Survival Analysis. *Statistics in Medicine* **1999**, *18* (6), 681–694. [https://doi.org/10.1002/\(SICI\)1097-0258\(19990330\)18:6<681::AID-SIM71>3.0.CO;2-R](https://doi.org/10.1002/(SICI)1097-0258(19990330)18:6<681::AID-SIM71>3.0.CO;2-R).
- (115) *Annual Energy Outlook 2020*; U. S. Energy Information Administration, 2020.
- (116) *Annual Technology Baseline: Electricity*; U. S. National Renewable Energy Laboratory, 2019.
- (117) Lazard. Lazard's Levelized Cost of Energy Analysis–Version 13.0, 2019.
- (118) Beaudin, M.; Zareipour, H.; Schellenberglobe, A.; Rosehart, W. Energy Storage for Mitigating the Variability of Renewable Electricity Sources: An Updated Review. *Energy for Sustainable Development*, 2010, *14*, 302–314.
- (119) Caldeira, K.; Dowling, J. A. Portfolios All the Way down *Joule* **2021**, *5* (10), 2545–2548. <https://doi.org/10.1016/j.joule.2021.10.008>.
- (120) Guerra, O. J.; Zhang, J.; Eichman, J.; Denholm, P.; Kurtz, J.; Hodge, B.-M. The Value of Seasonal Energy Storage Technologies for the Integration of Wind and Solar Power. *Energy Environ. Sci.* **2020**, *13* (7), 1909–1922. <https://doi.org/10.1039/D0EE00771D>.
- (121) Dowling, J. A.; Rinaldi, K. Z.; Ruggles, T. H.; Davis, S. J.; Yuan, M.; Tong, F.; Lewis, N. S.; Caldeira, K. Role of Long-Duration Energy Storage in Variable Renewable Electricity Systems. *Joule* **2020**, *4* (9), 1907–1928. <https://doi.org/10.1016/j.joule.2020.07.007>.
- (122) Sepulveda, N. A.; Jenkins, J. D.; Edington, A.; Mallapragada, D. S.; Lester, R. K. The Design Space for Long-Duration Energy Storage in Decarbonized Power Systems. *Nat Energy* **2021**, *6* (5), 506–516. <https://doi.org/10.1038/s41560-021-00796-8>.
- (123) Albertus, P.; Manser, J. S.; Litzelman, S. Long-Duration Electricity Storage Applications, Economics, and Technologies. *Joule* **2020**, *4* (1), 21–32. <https://doi.org/10.1016/j.joule.2019.11.009>.
- (124) Crozier, C.; Baker, K. Optimal Sizing of an Energy Storage Portfolio Considering Multiple Timescales. In *2021 IEEE Power & Energy Society General Meeting (PESGM)*; 2021; pp 01–05. <https://doi.org/10.1109/PESGM46819.2021.9637953>.
- (125) Guerra, O. J.; Eichman, J.; Denholm, P. Optimal Energy Storage Portfolio for High and Ultrahigh Carbon-Free and Renewable Power Systems. *Energy Environ. Sci.* **2021**, *14* (10), 5132–5146. <https://doi.org/10.1039/D1EE01835C>.
- (126) MIT Energy Initiative. *The Future of Energy Storage*; 2022. <https://energy.mit.edu/research/future-of-energy-storage/> (accessed 2022-07-30).
- (127) Clack, C. T. M.; Alexander, A.; Choukulkar, A.; MacDonald, A. E. Demonstrating the Effect of Vertical and Directional Shear for Resource Mapping of Wind Power. *Wind Energy* **2016**, *19* (9), 1687–1697. <https://doi.org/10.1002/we.1944>.
- (128) Sedaghat, A.; Hassanzadeh, A.; Jamali, J.; Mostafaeipour, A.; Chen, W.-H. Determination of Rated Wind Speed for Maximum Annual Energy Production of Variable Speed Wind Turbines. *Applied Energy* **2017**, *205*, 781–789. <https://doi.org/10.1016/j.apenergy.2017.08.079>.
- (129) Hunter, C. A.; Penev, M. M.; Reznicek, E. P.; Eichman, J.; Rustagi, N.; Baldwin, S. F. Techno-Economic Analysis of Long-Duration Energy Storage and Flexible Power Generation Technologies to Support High-Variable Renewable Energy Grids. *Joule* **2021**, *5* (8), 2077–2101. <https://doi.org/10.1016/j.joule.2021.06.018>.
- (130) Mongird, K.; Viswanathan, V.; Alam, J.; Vartanian, C.; Sprenkle, V.; Baxter, R. 2020 Grid Energy Storage Technology Cost and Performance Assessment. **2020**, *12*.

- (131) MIT Energy Initiative. *The Future of Energy Storage*; 2022. <https://energy.mit.edu/research/future-of-energy-storage/> (accessed 2022-07-30).
- (132) Egeland-Eriksen, T.; Hajizadeh, A.; Sartori, S. Hydrogen-Based Systems for Integration of Renewable Energy in Power Systems: Achievements and Perspectives. *International Journal of Hydrogen Energy* **2021**, *46* (63), 31963–31983. <https://doi.org/10.1016/j.ijhydene.2021.06.218>.
- (133) Hargreaves, J. J.; Jones, R. A. Long Term Energy Storage in Highly Renewable Systems. *Frontiers in Energy Research* **2020**, *8*.
- (134) Dowling, J. A.; Lewis, N. S. Long-Duration Energy Storage for Reliable Renewable Electricity: The Realistic Possibilities. *Bulletin of the Atomic Scientists* **2021**, *77* (6), 281–284. <https://doi.org/10.1080/00963402.2021.1989191>.
- (135) Ruhna, O.; Qvist, S. Storage Requirements in a 100% Renewable Electricity System: Extreme Events and Inter-Annual Variability. *Environ. Res. Lett.* **2022**, *17* (4), 044018. <https://doi.org/10.1088/1748-9326/ac4dc8>.
- (136) Zhang, J.; Guerra, O. J.; Eichman, J.; Pellow, M. A. Benefit Analysis of Long-Duration Energy Storage in Power Systems with High Renewable Energy Shares. *Front. Energy Res.* **2020**, *8*, 527910. <https://doi.org/10.3389/fenrg.2020.527910>.
- (137) Neumann, F.; Brown, T. The Near-Optimal Feasible Space of a Renewable Power System Model. *Electric Power Systems Research* **2021**, *190*, 106690. <https://doi.org/10.1016/j.epsr.2020.106690>.
- (138) *Hydrogen Projects in the US*. Clean Energy Group. <https://www.cleanenergygroup.org/initiatives/hydrogen/projects-in-the-us/> (accessed 2023-05-05).
- (139) *Large scale Hydrogen Storage in German salt caverns*. Hydrogen Newsletter. <https://www.hydrogennewsletter.com/large-scale-hydrogen-storage-in-german-salt-caverns/> (accessed 2023-05-05).
- (140) *LA100: The Los Angeles 100% Renewable Energy Study | Energy Analysis | NREL*. <https://www.nrel.gov/analysis/los-angeles-100-percent-renewable-study.html> (accessed 2023-05-05).
- (141) Yuan, M.; Tong, F.; Duan, L.; Dowling, J. A.; Davis, S. J.; Lewis, N. S.; Caldeira, K. Would Firm Generators Facilitate or Deter Variable Renewable Energy in a Carbon-Free Electricity System? *Applied Energy* **2020**, *279*, 115789. <https://doi.org/10.1016/j.apenergy.2020.115789>.
- (142) *Weekly Natural Gas Storage Report - EIA*. <https://ir.eia.gov/ngs/ngs.html> (accessed 2023-05-05).
- (143) *U.S. Underground Natural Gas Storage Capacity*. https://www.eia.gov/dnav/ng/ng_stor_cap_dc_u_nus_a.htm (accessed 2023-05-05).
- (144) Amid, A.; Mignard, D.; Wilkinson, M. Seasonal Storage of Hydrogen in a Depleted Natural Gas Reservoir. *International journal of hydrogen energy* **2016**, *41* (12), 5549–5558.
- (145) *Financial Incentives for Hydrogen and Fuel Cell Projects*. Energy.gov. <https://www.energy.gov/eere/fuelcells/financial-incentives-hydrogen-and-fuel-cell-projects> (accessed 2023-05-05).
- (146) *Building on the Inflation Reduction Act Framework: Hydrogen and the Energy Transition*. Reuters Events: Hydrogen North America (2023). <https://1.reutersevents.com/LP=34636> (accessed 2023-05-05).
- (147) *Hydrogen tax credits in the U.S. Inflation Reduction Act*. Canadian Climate Institute. <https://climateinstitute.ca/publications/hydrogen-tax-credits-in-the-u-s-inflation-reduction-act/> (accessed 2023-05-05).
- (148) Yue, M.; Lambert, H.; Pahon, E.; Roche, R.; Jemei, S.; Hissel, D. Hydrogen Energy Systems: A Critical Review of Technologies, Applications, Trends and Challenges. *Renewable and Sustainable Energy Reviews* **2021**, *146*, 111180. <https://doi.org/10.1016/j.rser.2021.111180>.
- (149) He, G.; Mallapragada, D. S.; Bose, A.; Heuberger-Austin, C. F.; Gençer, E. Sector Coupling via Hydrogen to Lower the Cost of Energy System Decarbonization. *Energy Environ. Sci.* **2021**, *14* (9), 4635–4646. <https://doi.org/10.1039/D1EE00627D>.
- (150) Eichman, J.; Harrison, K.; Peters, M. *Novel Electrolyzer Applications: Providing More Than Just Hydrogen*; NREL/TP-5400-61758; National Renewable Energy Lab. (NREL), Golden, CO (United States), 2014. <https://doi.org/10.2172/1159377>.
- (151) Varela, C.; Mostafa, M.; Zondervan, E. Modeling Alkaline Water Electrolysis for Power-to-x Applications: A Scheduling Approach. *International Journal of Hydrogen Energy* **2021**, *46* (14), 9303–9313. <https://doi.org/10.1016/j.ijhydene.2020.12.111>.

- (152) Buttler, A.; Spliethoff, H. Current Status of Water Electrolysis for Energy Storage, Grid Balancing and Sector Coupling via Power-to-Gas and Power-to-Liquids: A Review. *Renewable and Sustainable Energy Reviews* **2018**, *82*, 2440–2454. <https://doi.org/10.1016/j.rser.2017.09.003>.
- (153) Cherevko, S.; Geiger, S.; Kasian, O.; Kulyk, N.; Grote, J.-P.; Savan, A.; Shrestha, B. R.; Merzlikin, S.; Breitbach, B.; Ludwig, A.; Mayrhofer, K. J. J. Oxygen and Hydrogen Evolution Reactions on Ru, RuO₂, Ir, and IrO₂ Thin Film Electrodes in Acidic and Alkaline Electrolytes: A Comparative Study on Activity and Stability. *Catalysis Today* **2016**, *262*, 170–180. <https://doi.org/10.1016/j.cattod.2015.08.014>.
- (154) Minke, C.; Suermann, M.; Bensmann, B.; Hanke-Rauschenbach, R. Is Iridium Demand a Potential Bottleneck in the Realization of Large-Scale PEM Water Electrolysis? *International Journal of Hydrogen Energy* **2021**, *46* (46), 23581–23590. <https://doi.org/10.1016/j.ijhydene.2021.04.174>.
- (155) Hubert, M. A.; King, L. A.; Jaramillo, T. F. Evaluating the Case for Reduced Precious Metal Catalysts in Proton Exchange Membrane Electrolyzers. *ACS Energy Lett.* **2022**, *7* (1), 17–23. <https://doi.org/10.1021/acseenergylett.1c01869>.
- (156) Han, N.; Yang, K. R.; Lu, Z.; Li, Y.; Xu, W.; Gao, T.; Cai, Z.; Zhang, Y.; Batista, V. S.; Liu, W.; Sun, X. Nitrogen-Doped Tungsten Carbide Nanoarray as an Efficient Bifunctional Electrocatalyst for Water Splitting in Acid. *Nat Commun* **2018**, *9* (1), 924. <https://doi.org/10.1038/s41467-018-03429-z>.
- (157) Kwong, W. L.; Lee, C. C.; Shchukarev, A.; Messinger, J. Cobalt-Doped Hematite Thin Films for Electrocatalytic Water Oxidation in Highly Acidic Media. *Chem. Commun.* **2019**, *55* (34), 5017–5020. <https://doi.org/10.1039/C9CC01369E>.
- (158) Mondschein, J. S.; Kumar, K.; Holder, C. F.; Seth, K.; Kim, H.; Schaak, R. E. Intermetallic Ni₂Ta Electrode for the Oxygen Evolution Reaction in Highly Acidic Electrolytes. *Inorg. Chem.* **2018**, *57* (10), 6010–6015. <https://doi.org/10.1021/acs.inorgchem.8b00503>.
- (159) Pan, S.; Li, H.; Liu, D.; Huang, R.; Pan, X.; Ren, D.; Li, J.; Shakouri, M.; Zhang, Q.; Wang, M.; Wei, C.; Mai, L.; Zhang, B.; Zhao, Y.; Wang, Z.; Graetzel, M.; Zhang, X. Efficient and Stable Noble-Metal-Free Catalyst for Acidic Water Oxidation. *Nat Commun* **2022**, *13* (1), 2294. <https://doi.org/10.1038/s41467-022-30064-6>.
- (160) Evans, T. A.; Choi, K.-S. Electrochemical Synthesis and Investigation of Stoichiometric, Phase-Pure CoSb₂O₆ and MnSb₂O₆ Electrodes for the Oxygen Evolution Reaction in Acidic Media. *ACS Appl. Energy Mater.* **2020**, *3* (6), 5563–5571. <https://doi.org/10.1021/acsaem.0c00526>.
- (161) A. Moreno-Hernandez, I.; A. MacFarland, C.; G. Read, C.; M. Papadantonakis, K.; S. Brunshwig, B.; S. Lewis, N. Crystalline Nickel Manganese Antimonate as a Stable Water-Oxidation Catalyst in Aqueous 1.0 M H₂SO₄. *Energy & Environmental Science* **2017**, *10* (10), 2103–2108. <https://doi.org/10.1039/C7EE01486D>.
- (162) Zhou, L.; Shinde, A.; Montoya, J. H.; Singh, A.; Gul, S.; Yano, J.; Ye, Y.; Crumlin, E. J.; Richter, M. H.; Cooper, J. K.; Stein, H. S.; Haber, J. A.; Persson, K. A.; Gregoire, J. M. Rutile Alloys in the Mn–Sb–O System Stabilize Mn³⁺ To Enable Oxygen Evolution in Strong Acid. *ACS Catal.* **2018**, *8* (12), 10938–10948. <https://doi.org/10.1021/acscatal.8b02689>.
- (163) Luke, S.; Chatti, M.; Yadav, A.; Kerr, B. V.; Kangsabanik, J.; Williams, T.; Cherepanov, P. V.; Johannessen, B.; Tanksale, A.; MacFarlane, D. R.; Hocking, R. K.; Alam, A.; Yella, A.; Simonov, A. N. Mixed Metal–Antimony Oxide Nanocomposites: Low PH Water Oxidation Electrocatalysts with Outstanding Durability at Ambient and Elevated Temperatures. *J. Mater. Chem. A* **2021**, *9* (48), 27468–27484. <https://doi.org/10.1039/D1TA07293E>.
- (164) Ifkovits, Z. P.; Evans, J. M.; Kempler, P. A.; Morla, M. B.; Pham, K. H.; Dowling, J. A.; Carim, A. I.; Lewis, N. S. Powdered MnSb₂O₆–YOx Catalysts for Cerium-Mediated Oxygen Evolution in Acidic Environments. *ACS Energy Lett.* **2022**, *7* (12), 4258–4264. <https://doi.org/10.1021/acseenergylett.2c01754>.
- (165) Shinde, A.; Jones, R. J. R.; Guevarra, D.; Mitrovic, S.; Becerra-Stasiewicz, N.; Haber, J. A.; Jin, J.; Gregoire, J. M. High-Throughput Screening for Acid-Stable Oxygen Evolution Electrocatalysts in the (Mn–Co–Ta–Sb)₂O₇ Composition Space. *Electrocatalysis* **2015**, *6* (2), 229–236. <https://doi.org/10.1007/s12678-014-0237-7>.
- (166) Mackus, A. J. M.; Schneider, J. R.; MacIsaac, C.; Baker, J. G.; Bent, S. F. Synthesis of Doped, Ternary, and Quaternary Materials by Atomic Layer Deposition: A Review. *Chem. Mater.* **2019**, *31* (4), 1142–1183. <https://doi.org/10.1021/acs.chemmater.8b02878>.

- (167) Yang, R. B.; Bachmann, J.; Reiche, M.; Gerlach, J. W.; Gösele, U.; Nielsch, K. Atomic Layer Deposition of Antimony Oxide and Antimony Sulfide. *Chem. Mater.* **2009**, *21* (13), 2586–2588. <https://doi.org/10.1021/cm900623v>.
- (168) McCrory, C. C. L.; Jung, S.; Ferrer, I. M.; Chatman, S. M.; Peters, J. C.; Jaramillo, T. F. Benchmarking Hydrogen Evolving Reaction and Oxygen Evolving Reaction Electrocatalysts for Solar Water Splitting Devices. *J. Am. Chem. Soc.* **2015**, *137* (13), 4347–4357. <https://doi.org/10.1021/ja510442p>.
- (169) Ilton, E. S.; Post, J. E.; Heaney, P. J.; Ling, F. T.; Kerisit, S. N. XPS Determination of Mn Oxidation States in Mn (Hydr)Oxides. *Applied Surface Science* **2016**, *366*, 475–485. <https://doi.org/10.1016/j.apsusc.2015.12.159>.
- (170) Biesinger, M. C.; Payne, B. P.; Grosvenor, A. P.; Lau, L. W. M.; Gerson, A. R.; Smart, R. St. C. Resolving Surface Chemical States in XPS Analysis of First Row Transition Metals, Oxides and Hydroxides: Cr, Mn, Fe, Co and Ni. *Applied Surface Science* **2011**, *257* (7), 2717–2730. <https://doi.org/10.1016/j.apsusc.2010.10.051>.
- (171) Militello, M. C.; Gaarenstroom, S. W. Manganese Dioxide (MnO₂) by XPS. *Surface Science Spectra* **2001**, *8* (3), 200–206. <https://doi.org/10.1116/11.20020401>.
- (172) Stranick, M. A. Mn₂O₃ by XPS. *Surface Science Spectra* **1999**, *6* (1), 39–46. <https://doi.org/10.1116/1.1247889>.
- (173) Nelson, A. J.; Reynolds, J. G.; Roos, J. W. Core-Level Satellites and Outer Core-Level Multiplet Splitting in Mn Model Compounds. *Journal of Vacuum Science & Technology A: Vacuum, Surfaces, and Films* **2000**, *18* (4), 1072–1076. <https://doi.org/10.1116/1.582302>.

